

Catalytic Reactions and Energy Conservation in the Cytochrome bc_1 and b_6f Complexes of Energy-Transducing Membranes

Marcin Sarewicz, Sebastian Pintscher, Rafał Pietras, Arkadiusz Borek, Łukasz Bujnowicz, Guy Hanke, William A. Cramer, Giovanni Finazzi, and Artur Osyczka*



Cite This: *Chem. Rev.* 2021, 121, 2020–2108



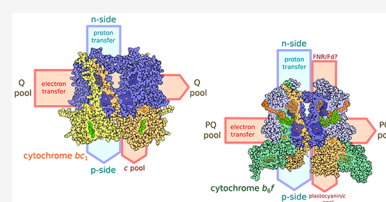
Read Online

ACCESS |

Metrics & More

Article Recommendations

ABSTRACT: This review focuses on key components of respiratory and photosynthetic energy-transduction systems: the cytochrome bc_1 and b_6f ($Cytc_{bc_1}/b_6f$) membranous multisubunit homodimeric complexes. These remarkable molecular machines catalyze electron transfer from membranous quinones to water-soluble electron carriers (such as cytochromes c or plastocyanin), coupling electron flow to proton translocation across the energy-transducing membrane and contributing to the generation of a transmembrane electrochemical potential gradient, which powers cellular metabolism in the majority of living organisms. $Cytc_{bc_1}/b_6f$ share many similarities but also have significant differences. While decades of research have provided extensive knowledge on these enzymes, several important aspects of their molecular mechanisms remain to be elucidated. We summarize a broad range of structural, mechanistic, and physiological aspects required for function of $Cytc_{bc_1}/b_6f$, combining textbook fundamentals with new intriguing concepts that have emerged from more recent studies. The discussion covers but is not limited to (i) mechanisms of energy-conserving bifurcation of electron pathway and energy-wasting superoxide generation at the quinol oxidation site, (ii) the mechanism by which semiquinone is stabilized at the quinone reduction site, (iii) interactions with substrates and specific inhibitors, (iv) intermonomer electron transfer and the role of a dimeric complex, and (v) higher levels of organization and regulation that involve $Cytc_{bc_1}/b_6f$. In addressing these topics, we point out existing uncertainties and controversies, which, as suggested, will drive further research in this field.



CONTENTS

1. Introduction	2021		
2. Energy Conserving and Regulatory Role of Intracellular Cytochromes bc	2023		
3. Overview of Structure and Function of Cytochromes bc	2025		
3.1. Catalytic Sites, Redox Cofactors, and Cofactor Chains	2025		
3.2. Brief Overview of Catalytic Cycle	2025		
3.3. H-Shaped Electron Transfer System in the Dimer	2026		
3.4. Large-Scale Movement of ISP-HD	2026		
3.4.1. First Structural Indications for ISP-HD Movement	2027		
3.4.2. Effects of the Q_o/Q_p Site Inhibitors	2028		
3.4.3. Constrained Diffusion or Allosteric Control	2028		
3.4.4. Structural Changes in Brief	2028		
3.4.5. Different Positions of ISP-HD in Crystal Structures	2028		
3.4.6. Structure–Function Relationships for the Neck Region of ISP-HD	2029		
3.4.7. Structure–Function Relationships for the Interaction of ISP-HD with Cytochrome b	2029		
		3.4.8. Effect of the Q_i Site Inhibitor, Antimycin	2030
		3.4.9. Effect of Movement on Redox Potential of the $2Fe_2S$ Cluster	2031
		3.5. Cytochrome bc_1 : Specific Structural and Functional Elements	2031
		3.5.1. Subunit Composition of Cytochrome bc_1	2031
		3.5.2. Structure and Spectral Properties of Hemes b , c_1 , and $2Fe_2S$ Cluster	2032
		3.6. Cytochrome b_6f : Specific Structural and Functional Elements	2034
		3.6.1. Comparison of Cytochromes f and c_1	2034
		3.6.2. Subunit Composition of Cytochrome b_6f	2034
		3.6.3. Structure and Spectral Properties of Hemes b , f , c_n , and $2Fe_2S$ Cluster	2035
		3.6.4. Lipid Content and Other Subunits	2037
		3.6.5. Q Cycle in Cytochrome b_6f : Mechanism and Controversies	2038

Received: July 7, 2020

Published: January 19, 2021



3.6.6. Additional Electron Path Related to Cyclic Electron Transfer in Photosynthesis	2039	7.6. Semiquinone Intermediate at the Q _o /Q _p Site	2074
4. Characteristics of Substrates for Cytochrome <i>bc</i> ₁ and <i>b</i> ₆ <i>f</i>	2039	8. Mechanistic Insights into the Catalytic Q _i /Q _n Site	2076
4.1. Basic Redox Properties of Quinones	2039	8.1. Overview of Structure of Q _i and Proton Paths	2076
4.1.1. Stability and Reactivity of Semiquinone Radical with Molecular Oxygen	2040	8.2. Catalytic Electron and Proton Transfers at the Q _i Site of Cytochrome <i>bc</i> ₁	2076
4.1.2. Stability Constant of Semiquinone	2041	8.3. Fast- and Slow-Relaxing SQ _i as Dominant Intermediates of Forward and Reverse Reactions at the Q _i Site, Respectively	2077
4.1.3. Chloroplast Photoactive versus Non-photoactive Plastoquinone Pools	2041	8.4. Charge Polarization of SQ _i Facilitates Electron and Proton Reactions at the Q _i Site	2077
4.2. Cytochrome <i>c</i> and Plastocyanin as Electron Acceptors	2042	8.5. Specific Residues Involved in PQ/PQH ₂ Binding to the Q _n Site of Cytochrome <i>b</i> ₆ <i>f</i>	2079
4.2.1. Redox Properties and Interaction of Cytochrome <i>c</i> with Cytochrome <i>bc</i> ₁	2042	9. Intermonomer Electron Transfer	2079
4.2.2. Redox Properties and Interaction of Plastocyanin with Cytochrome <i>b</i> ₆ <i>f</i>	2045	10. Higher Level of Organization and Regulation (Supercomplexes, State Transition, Kinase Activation)	2082
4.3. FNR/Fd Interactions with Cytochrome <i>b</i> ₆ <i>f</i>	2046	10.1. Role for Cytochrome <i>b</i> ₆ <i>f</i> in Regulation of Linear versus Cyclic Electron Flow?	2082
4.3.1. Potential <i>n</i> Side Donors	2046	10.2. The “Elusive” Cytochrome <i>b</i> ₆ <i>f</i> -PSI CET Supercomplex	2083
4.3.2. Direct Electron Donation from Fd to Cytochrome <i>b</i> ₆ <i>f</i>	2046	10.3. Role of Cytochrome <i>b</i> ₆ <i>f</i> in State Transitions	2084
4.3.3. Direct Electron Donation from FNR to Cytochrome <i>b</i> ₆ <i>f</i>	2047	11. Comments on the Nomenclature Used for Cytochrome <i>bc</i> ₁ and Cytochrome <i>b</i> ₆ <i>f</i>	2085
5. Inhibitors	2050	11.1. Complexes	2085
5.1. Cytochrome <i>bc</i> ₁ Specific Inhibitors	2050	11.1.2. Quinone Binding Catalytic Sites	2085
5.1.1. Inhibitors of the Q _i Site	2050	11.2. Cofactor Chains	2086
5.1.2. Inhibitors of the Q _o Site	2051	11.3. Protein Subunits	2086
5.1.3. Dual-Mode Inhibitors	2056	11.4. Cofactors	2086
5.2. Cytochrome <i>b</i> ₆ <i>f</i> -Specific Inhibitors	2058	11.5. Other	2086
5.2.1. Inhibitors of the Q _p Site	2058	Author Information	2086
5.2.2. Inhibitors of the Q _n Site	2060	Corresponding Author	2086
6. Thermodynamic Background of Cytochrome <i>bc</i> Catalysis	2060	Authors	2086
7. Mechanistic Insights into the Catalytic Q _o /Q _p Site	2061	Notes	2086
7.1. Overview of Structure of the Q _o Site	2061	Biographies	2086
7.2. Quinone Binding to the Q _o Site	2061	Acknowledgments	2087
7.3. Crucial Amino Acid Residues Involved in Binding and Catalysis of QH ₂ /PQH ₂ Oxidation at the Q _o /Q _p Site	2063	Abbreviations	2087
7.3.1. ^{Rh} H156 (^{Bt} H161) in Iron–Sulfur Protein and ^{Rh} E295 (^{Bt} E271) in Cytochrome <i>b</i>	2063	References	2088
7.3.2. Cyt ^{Rh} <i>b</i> : ^{Rh} Y147 (^{Bt} Y131) and Cyt ^{Rh} <i>b</i> : ^{Rh} Y302 (^{Bt} Y278)	2064		
7.3.3. Other Residues Involved in Substrate Binding to the Q _o Site	2065		
7.3.4. Specific Residues Involved in PQ/PQH ₂ Binding to the Q _p Site of Cytochrome <i>b</i> ₆ <i>f</i>	2065		
7.4. Catalytic and Side Reactions at the QH ₂ -Oxidation Site of Cytochromes <i>bc</i>	2065		
7.4.1. Forward, Reverse, and Short-Circuits Reactions at the Q _o /Q _p Site	2066		
7.4.2. Possible Physiological Meaning of Short-Circuits	2067		
7.4.3. Short-Circuit Suppression Mechanisms	2068		
7.5. Superoxide Generation at the Q _o /Q _p Site	2070		
7.5.1. Semiquinone at the Q _o /Q _p Site as Electron Donor to Molecular Oxygen	2070		
7.5.2. “Semireverse-Rieske off” Model of Superoxide Production	2071		
7.5.3. Other Postulated Reactions Involving Molecular Oxygen	2072		
7.5.4. Physiological Considerations	2073		

1. INTRODUCTION

Cytochromes *bc* (Cyt-*bc*) constitute one of the broadest groups of energy-transducing enzymes, present in almost every living cell. They are key components of both respiratory and photosynthetic electron transport chains and their function is often indispensable for the operation of these chains.

In this review, we focus on two important enzymes from that group: cytochrome *bc*₁ (Cyt*bc*₁), involved in respiration and bacterial photosynthesis and cytochrome *b*₆*f* (Cyt*b*₆*f*), involved in plant, algal, and cyanobacterial photosynthesis. We summarize a broad range of structural, mechanistic, and physiological aspects required for function of these enzymes, presenting both the textbook fundamentals based on the well-established ideas and the new intriguing concepts and attractive hypotheses emerging from more recent studies.

It is remarkable that the extensive knowledge gathered so far on Cyt*bc* has left many key issues not satisfactorily understood and opened new intriguing issues for consideration. Among subjects still intensely debated are the molecular mechanism of the catalytic electron bifurcation and the basis of high energetic efficiency of the enzyme, the mechanism of proton transfer to and from the catalytic sites, the role of dimer and the intermonomer electron transfer, and the role of Cyt-*bc* in regulation of electron flow and in redox or ROS signaling.

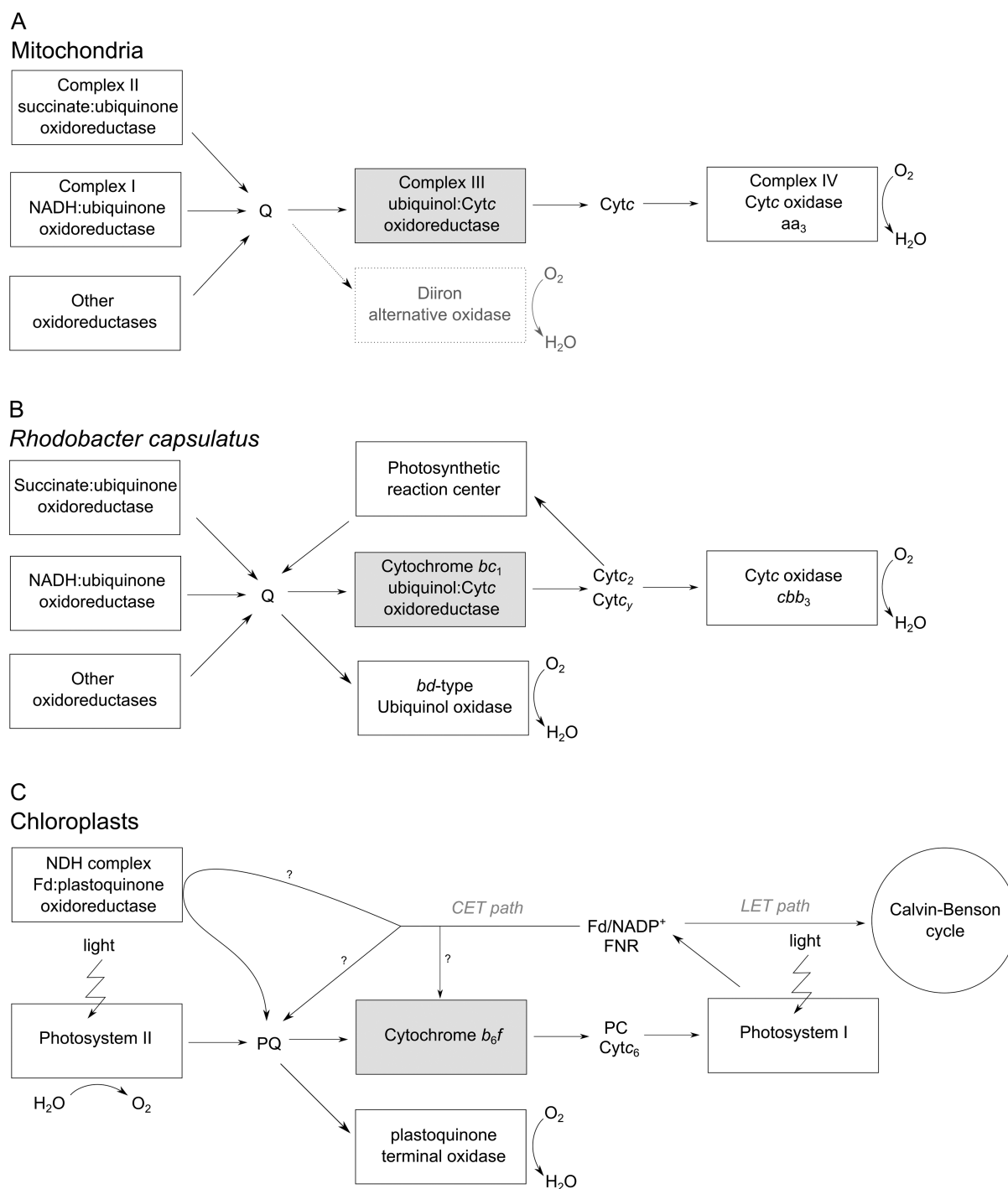


Figure 1. Overview of electron transfer paths involving Cyt-*bc* complexes: Cyt_{bc1} in (A) mitochondrial respiratory chain and in (B) anoxygenic photosynthesis or respiration of purple bacteria; (C) Cyt_{b₆f} in oxygenic photosynthesis in chloroplasts. Q and PQ denote ubiquinone and plastoquinone pool, respectively. PC, Fd, and FNR denote plastocyanin, ferredoxin, and ferredoxin/NADP⁺ oxidoreductase. LET depicts linear electron transfer in photosynthesis, while CET shows cyclic electron transfer path which recycles the electrons from Fd pool back to the PQ(H₂) pool. Scheme in A considers mitochondria of both plants and animals (the diiron alternative oxidase is not present in animal mitochondria except for rare cases such as in *Trypanosoma*).

It should be noted that in some cases there are questions about mechanisms of Cyt-*bc* structure–function which have been regarded as beyond doubt. Despite the fact that the catalytic Q cycle, the conceptual framework in which Peter Mitchell described principles of his chemiosmotic theory, is widely accepted for Cyt_{bc1}, its applicability to details of the function of Cyt_{b₆f} remain subject to some questions. Although the scheme showing cyclic electron transfer (CET) appears in

every textbook of photosynthesis, the actual pathway through which electrons recycle back to the main electron transport chain remains controversial. It is clear that all these and many other questions related to this important group of enzymes await resolution in future studies.

Even though our intention was to comprehensively cover the knowledge on Cyt-*bc*, the breadth of the subject makes it impossible to include all issues that relate to it. The reader is

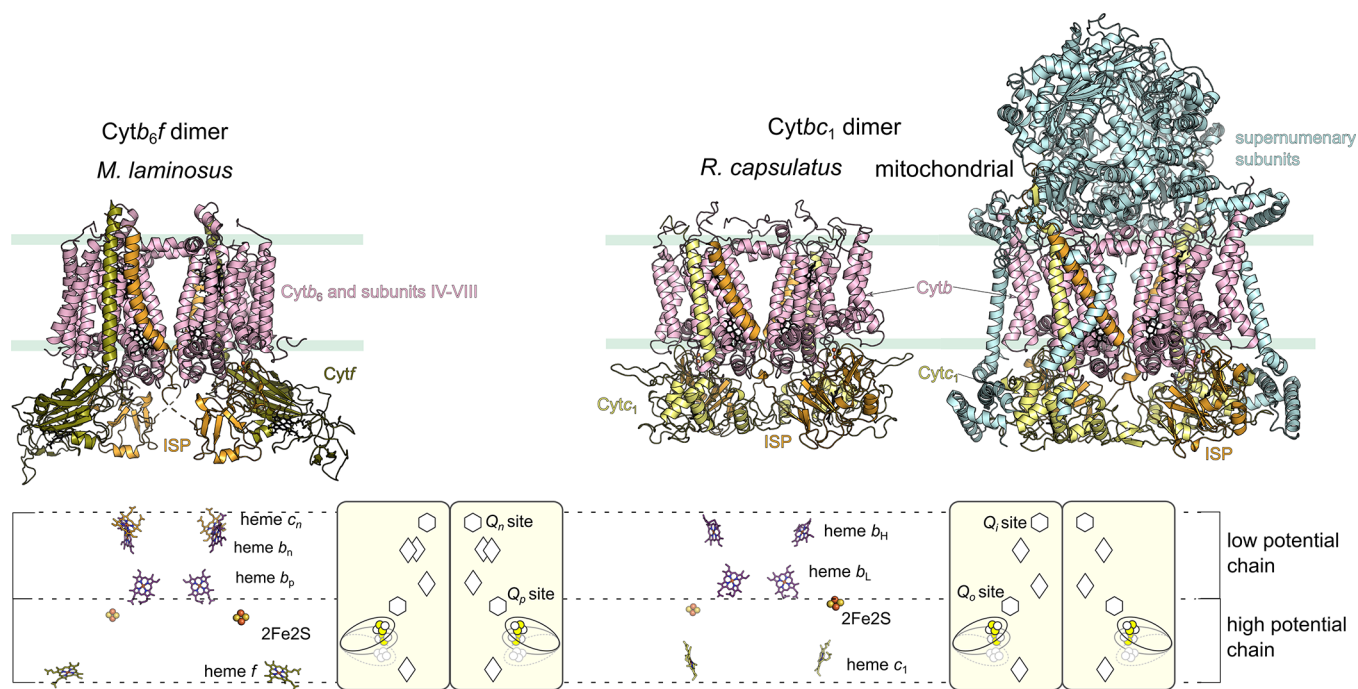


Figure 2. Overview of structures and cofactor chains in dimeric Cyt-*bc* complexes. Top: Crystal structure representations of *M. lamosus* Cyt_b₆f (left, PDB ID: 4H13), *R. capsulatus* Cyt_b_c₁ (middle, PDB ID: 1ZRT), and mitochondrial Cyt_b_c₁ (right, PDB ID: 1KYO). Bottom: Spatial arrangement of cofactors extracted from the structures above. The layout of cofactors in *R. capsulatus* and mitochondrial Cyt_b_c₁ is the same. The simplified cartoon models depict symbols for cofactors that are used throughout the figures.

referred to excellent reviews on this subject that have appeared in the literature.^{1–26}

2. ENERGY CONSERVING AND REGULATORY ROLE OF INTRACELLULAR CYTOCHROMES *bc*

Conversion of solar or chemical energy into a biologically useful form is one of the most fundamental processes of living organisms. As described by the chemiosmotic theory,^{27,28} this process involves generation of a transmembrane electrochemical potential gradient, $\Delta\tilde{\mu}_H^+$ (or proton motive force, pmf) by enzymes which use external sources of energy to couple electron transfer to proton translocation between cellular compartments separated by a membrane (termed energy-transducing membrane).²⁹ The pmf forces the ATP-synthase to convert ADP and P_i into ATP, and the energy is stored by maintaining the concentrations of ATP, ADP, and P_i far from their equilibrium values, thus providing the universal source of energy that powers cellular metabolism.²⁹

The enzymes that generate pmf are typically organized in chains, such as the mitochondrial and photosynthetic electron transfer chains, where the individual membrane-embedded electron transport protein complexes are linked functionally by components having diffusional freedom to move between complexes: hydrophobic low-molecular weight electron carriers and water-soluble protein electron carriers, respectively, inside and outside the membrane.^{30,31} These carriers shuttle electrons between complexes, which, overall, catalyze electron flow from a primary electron donor to a final electron acceptor, while the energy released in this process is used to transfer protons across the membrane.

There are two general mechanisms in electron transport chains by which protons are transferred across the energy-transducing membrane. In one mechanism, reduction of a quinone (coupled to proton uptake) occurs at one side of the

membrane while quinol oxidation (coupled to proton release) takes place at the opposite side of the membrane (Mitchell's redox loop^{27,32,33}). In the other mechanism, a series of protonation/deprotonation reactions taking place within the specific proton channels of an electron transfer complex (e.g., complex I and IV of mitochondrial electron transport chain) involving successive pK changes of amino acids in the transmembrane pathway, allow the pumping of protons between the two sides of the membrane without involvement of quinone molecules.

Cytochromes *bc* complexes comprise a set of the ubiquitous complexes contributing to the generation of pmf, through a mechanism involving quinone/quinol oxidation–reduction reactions. This superfamily of complexes includes cytochrome *bc*₁ (ubiquinol:cytochrome *c* oxidoreductase, EC 7.1.1.8) and cytochrome *b*₆*f* (plastoquinol:plastocyanin oxidoreductase, EC 7.1.1.6). Cyt_b_c₁ provides an electronic connection between quinone molecules and water-soluble electron carriers (such as cytochrome *c*, *c*₂) catalyzing a net reaction of oxidation of quinol (ubiquinol in mitochondria and several prokaryotic cells or menaquinol some bacteria, see section 4.1) and reduction of water-soluble electron carrier (section 4.2.1). Cyt_b₆*f* catalyzes an analogous reaction between membrane embedded plastoquinol molecules and the water-soluble plastocyanin (PC) of chloroplasts or Cyt_c₆ (in cyanobacteria and some microalgae) (section 4.2.2). In all cases, the energy released in these electron transfer reactions powers H⁺ translocation across the membrane according to the first mechanism described above.

Cyt_b_c₁ participates in respiration in oxygen-utilizing cells and also electron transfer in numerous bacteria, which utilize alternative terminal electron acceptors in addition to oxygen (Figure 1). In mitochondria, Cyt_b_c₁ (also referred to as mitochondrial complex III or respiratory complex III) is a confluence point for reducing equivalents from the various

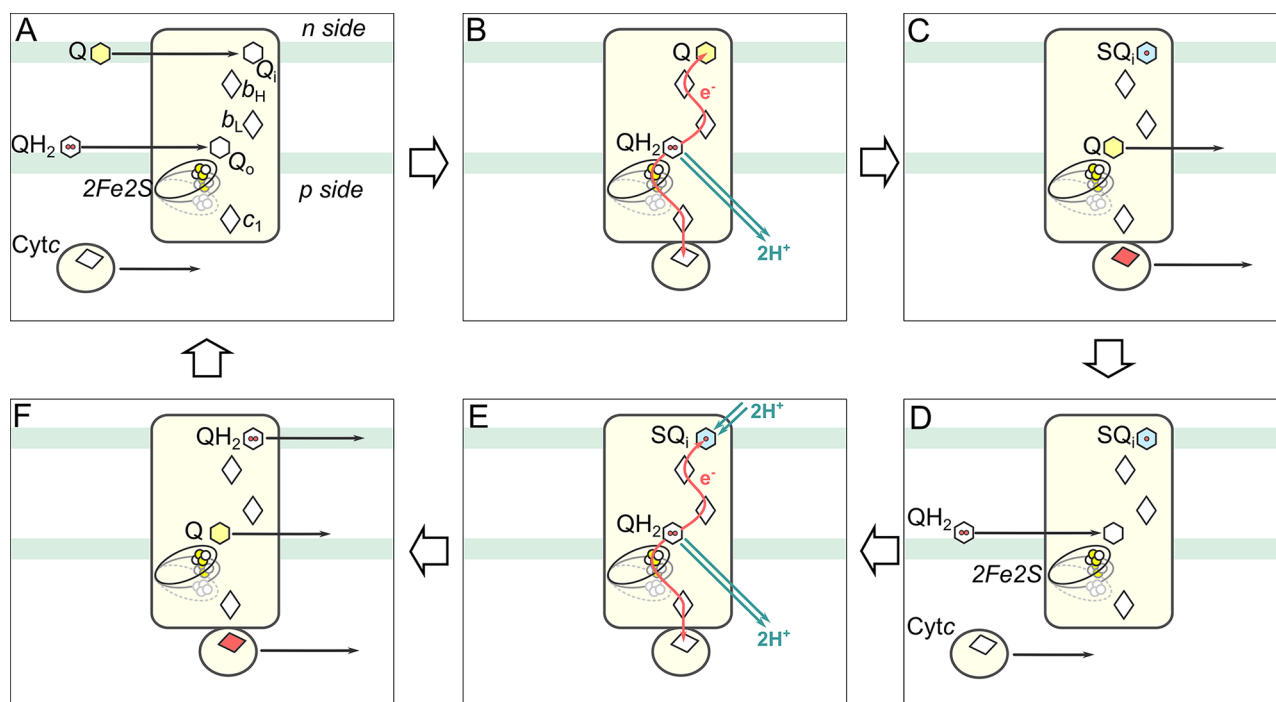


Figure 3. Simplified, static scheme, showing stepwise reactions taking place during the catalytic cycle of *Cytbc*₁. (A) Quinone (Q) and Quinol (QH₂) (yellow hexagon and white hexagon with 2 dots) bind to the Q_n and Q_o sites, respectively, while oxidized Cyt c (oval with white rhombus) binds to the Cyt c₁ domain. (B) After binding, QH₂ is oxidized, 2 protons are released (turquoise arrows) to the p side, one electron is transferred (red arrow) to Cyt c through the high-potential chain, while the second electron goes (red arrow), through the low-potential chain, to Q bound at the Q_n site. (C) Reduced Cyt c (oval with red rhombus) and Q diffuse out of the respective sites (black arrows), while SQ_n (blue hexagon with dot) stays stably bound at the Q_n site. (D) A second molecule of QH₂ and oxidized Cyt c bind to the Q_o site and Cyt c₁, respectively. (E) Oxidation of QH₂ takes place as in case B, but the electron from the low potential chain reduces SQ_n to QH₂, which is associated with uptake of two protons from the n side. (F) Q, QH₂, and reduced Cyt c diffuse out of the Q_n, Q_o, and Cyt c₁, respectively, and the cycle starts again. Hemes are shown as rhombuses; the 2Fe₂S is shown as yellow–white circles. Lipid bilayer is marked as green lines. For simplicity, only one monomer is shown and the motion of the head domain of iron–sulfur protein (ISP-HD) was not included. The scheme in general is believed to hold true also for *Cytbc*_{6f} with some modifications at the Q_n site associated with the presence of additional heme c_n and possible modifications to the electron transfer sequence associated with the involvement of this enzyme in CET (see Figure 4).

dehydrogenases (mitochondrial complexes I, II) (Figure 1A). In animal mitochondria, with the sole exception of some parasites, it is essential for mitochondrial respiration, as there is no alternative route to oxidation of ubiquinol by molecular oxygen. This enzyme is not essential in bacteria, where alternative mechanisms to oxidize ubiquinol usually exist in parallel to *Cytbc*₁. On the other hand, *Cytbc*₁ is an essential enzyme, in some photosynthetic bacteria such as *Rhodobacter sphaeroides* or *R. capsulatus* for cyclic, nonoxygenic, photosynthetic electron transfer in the absence of a terminal electron acceptor, but it is not essential when these organisms are grown heterotrophically (Figure 1B).³⁴

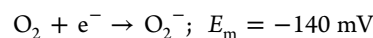
*Cytbc*_{6f} participates in oxygenic photosynthesis in cyanobacteria, plant and algal chloroplasts. It is a crucial component of the linear electron transfer (“Z scheme” or LET) linking photosystem I (PSI) with photosystem II (PSII) (Figure 1C). In addition, it also participates in cyclic electron transfer (CET) (Figure 1C) (see sections 3.6.6 and 10.1).

Apart from the involvement in generation of pmf, *Cyts-bc* are believed to be potential points of regulation of electron flow. This stems from the fact that their two quinone binding sites are directly connected with the two main redox pools (intra-membrane ubiquinone/plastoquinone and soluble cytochrome *c*/plastocyanin) of respiration/photosynthesis. Hence, by virtue of catalyzing opposite chemical reactions, these sites may influence one another (the product of one catalytic site becomes

a substrate for the second site and *vice versa*). Another regulatory function of *Cytbc*_{6f} is to trigger changes in the chloroplasts’ light harvesting capacity in response to changes in the ambient light intensity by sensing variations in the redox state of the plastoquinone pool. These changes modulate the interaction of *Cytbc*_{6f} with a kinase able to reversibly phosphorylate the light harvesting complexes, leading to their preferential association with one of the two photo centers (PSII and PSI) in a process called “state transitions” (section 10.3).³⁵

Moreover, although the activities of *Cytbc*₁ and *Cytbc*_{6f} complexes are different, because of the above reactions, they are also inferred to be involved in mitochondrial and chloroplast redox signaling.³⁶

Finally under specific conditions, *Cytbc* can generate a limited amount of superoxide as a side reaction of the catalytic cycle (section 7.5):³⁷



It is noted that the specific rate of superoxide (O₂⁻) production in purified active crystallizable *Cytbc*_{6f}, normalized to the rate of electron transport, is more than an order of magnitude greater than that of the yeast respiratory *Cytbc*₁.³⁸

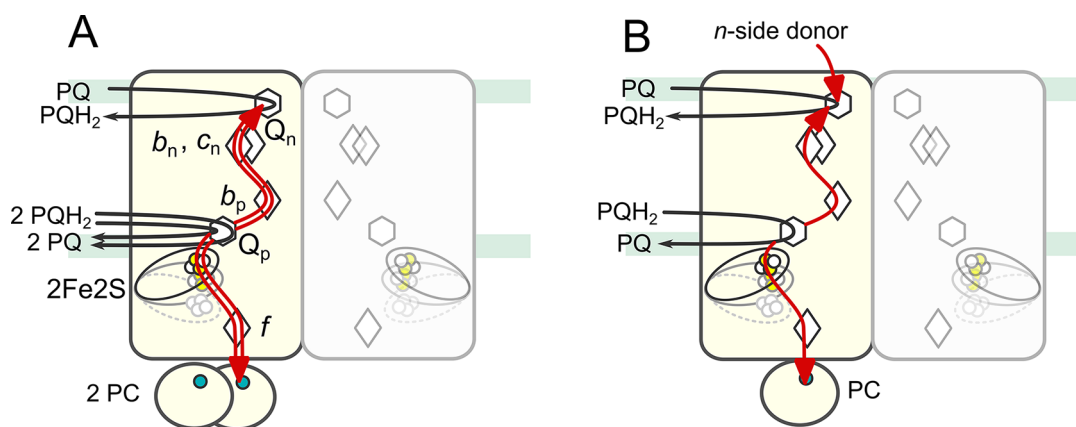


Figure 4. Two possible mechanisms of Q cycle in *Cytb_{6f}*. (A) The “modified Q cycle”,³⁹ which is similar to *Cytc₁*: two electrons are delivered to the Q_n site from Q_p site, which requires oxidation of 2 PQH_2 and reduction of 2 PC, per 1 reduced PQ at the Q_n site. (B) Original Mitchell Q cycle³² in which one electron delivered to the Q_n site comes from the PQH_2 oxidation at the Q_p site and the second electron comes from electron donors at the n side (Fd/FNR). According to the original Mitchell mechanism 1P PQH_2 , 1 PC, 1 PQ and 1 n side donor are needed to complete the cycle. Color code and symbols as in Figure 3. Copper in PC is marked as blue dot. For simplicity, proton paths are omitted and reactions in one monomer are shown while the second monomer is grayed out.

3. OVERVIEW OF STRUCTURE AND FUNCTION OF CYTOCHROMES BC

Cytc₁ and *Cytb_{6f}* share several structural and mechanistic features. Both are homodimers with each monomer containing a set of similarly arranged spatially separated quinone binding sites and redox active cofactors required for completion of the catalytic cycle (Figure 2). The general features common to both complexes are summarized in sections 3.1–3.4. Despite these similarities, several important differences exist between them. Therefore, the two following sections of this section, 3.5 and 3.6, discuss separately *Cytc₁*- and *Cytb_{6f}*-specific properties.

3.1. Catalytic Sites, Redox Cofactors, and Cofactor Chains

In each monomer of the Cyt-*bc* dimeric complex, the hemes and the iron–sulfur 2Fe–2S Rieske-type cluster (2Fe2S) assemble into two chains of cofactors designed to link the two catalytic quinone binding sites with diffusible pools of substrates (quinone and Cyt c /PC). The two quinone binding sites catalyze opposing reactions (quinol oxidation/quinone reduction) as integral parts of the catalytic cycle (see section 3.2).

In *Cytc₁*, the quinol oxidation site (the Q_o site) is linked with Cyt c by the *c*-chain composed of 2Fe2S and heme c_1 . The *b*-chain, composed of heme b_L and heme b_H , connects the Q_o site with the quinone reduction site (the Q_i site) located at the opposite side of the membrane. Considering the relative values of the redox midpoint potentials of cofactors, the *c*-chain and the *b*-chain are commonly named the ‘high-’ and ‘low-potential’ chain, respectively. A characteristic feature of this arrangement is that the Q_o site is located between the *c*- and *b*-chains, which has crucial consequences for the catalytic Q cycle mechanism (Figure 2).

In *Cytb_{6f}*, the high- and low-potential chains and the quinone catalytic sites (the Q_p and Q_n for quinol oxidation and quinone reduction, respectively, see section 11 for explanation on the usage of the names of the catalytic sites in this review and on other nomenclatural issues) are arranged in the similar manner, but some variation in the redox cofactor exists: heme f ($E_m = +370$ mV) is present in the high-potential chain in place of heme c_1 and the low-potential chain contains an additional and atypical heme c_n (not present in *Cytc₁*).

3.2. Brief Overview of Catalytic Cycle

The mechanism by which *Cytc₁* links electron transfer and proton translocation reactions is the proton motive Q cycle.^{33,39} It engages the high- and low-potential chains (*c*- and *b*-chains, respectively) and the Q_o and Q_i sites. Protons are taken up at the Q_i site, carried across the membrane by the quinol (QH_2), and released at the Q_o site. The Q_i site and the Q_o site are located toward the electronegative and electropositive sides of the membrane (n and p sides, respectively). For that reason, the Q_i site and Q_o site are alternatively named Q_n and Q_p , respectively. For the same reason, heme b_L and heme b_H are alternatively named b_p and b_n , respectively (see section 11).

The Q_o site, being positioned between the *c*- and *b*-chains, oxidizes QH_2 and passes its two electrons in a highly specific manner: one electron is delivered to the *c*-chain, while the other electron is delivered to the *b*-chain. This process occurs in a so-called bifurcation reaction in which QH_2 is oxidized by 2Fe2S of the *c*-chain and by the heme b_L of the *b*-chain. The reduced 2Fe2S passes 1 electron to heme c_1 , which subsequently reduces diffusible Cyt c . The reduced heme b_L passes 1 electron to heme b_H . The electron is then used for quinone (Q) reduction at the Q_i site. This way the Q_o -site-mediated oxidation of QH_2 delivers one electron to the Q_i site at the time, meaning that two cycles of the Q_o site are needed to fully reduce a Q to QH_2 at the Q_i site. Overall, the net oxidation of one QH_2 molecule and transfer of two electrons to two molecules of Cyt c leads to the uptake of two protons from the n side (mitochondrial matrix or bacterial cytoplasm) and the release of four protons on the p side (intermembrane space of mitochondria or bacterial periplasm). A stepwise scheme of the reaction taking place during the Q cycle in *Cytc₁* is shown in Figure 3.

In the case of *Cytb_{6f}*, although details of the Q cycle have been studied less completely and flash-induced reduction of heme b_n separate from that of heme b_p not defined experimentally,⁴⁰ the general principles of the Q cycle and proton translocation mechanism are believed by most researchers in the field to be essentially the same as for *Cytc₁* (see perspective on this issue in section 3.6.5). This includes the bifurcation reaction taking place at the PQH_2 oxidation site (Q_p site) with electrons delivered into the high- and low-potential chains. One of the main differences is the presence of an additional cofactor within

the low-potential chain. This is an atypical high-spin and relatively high-potential heme c_n covalently attached to the protein through a single thioether bond.^{41,42} The planes of hemes b_n and c_n are oriented perpendicularly and share electrons⁴³ with each other with the latter being close to the PQ binding niche. Although a role of this heme is still unknown, it was proposed that together with heme b_n it forms a pair of cofactors that can deliver two electrons to PQ to reduce it to PQH₂ in a virtually one-step event. This idea, however, has not been experimentally validated yet. Because the heme c_n is exposed to the stromal side of the thylakoids, this cofactor could provide an additional entry point for electrons at the level of the Q_n site, possibly triggering a different Q cycle mechanism, or providing an oxidant for stromal electrons in cyclic electron flow (see below and discussion in section 3.6.6). Another difference between Cytbc₁ and Cytb_{6f}, due to the variation in the composition of the high-potential chain, is the fact that electrons from the 2Fe2S are transferred to heme f , which further reduces diffusible PC or Cyt_c₆ (instead of Cyt_c interacting with Cyt_c₁).

The Q cycle originally proposed by Mitchell³² considered a mechanistic link between electron bifurcation at the Q_o site and electron confurcation at the Q_i site. As mentioned above, the bifurcation at the Q_o site results in one electron delivered to the Q_i site, implying that a completion of confurcation at the Q_i site requires the functional link with another redox-active enzyme/cofactor cooperating with Cytbc₁ and serving as an additional source of electrons for that site. The second electron to complete reduction of SQ at the Q_i site was initially proposed to originate from the activity of another dehydrogenase. Further studies revealed that Cytbc₁ does not need to be associated with any source of electrons but QH₂ to complete the cycle. Instead, Cytbc₁ must oxidize two QH₂ molecules at the Q_o site to sequentially deliver two electrons to the Q_i site.³⁹ On the other hand the idea that the complex interacts with another dehydrogenase could be relevant to account for the possible role of Cytb_{6f} in CET. Indeed, it has been proposed that electrons donated by PSI to the NADPH/ferredoxin pool could be reinjected into the PQ(H₂) pool by electron transfer to PQ or putative plastosemiquinone (PSQ) at the Q_n site. In such a case, the catalytic cycle of Cytb_{6f} under conditions favoring CET could operate according to the original Mitchell Q cycle (Figure 4).

The bifurcation reaction taking place at the Q_o/Q_p site is essential for the energetic efficiency of the catalytic cycle and has long been considered a unique feature of Cytbc. However, more recent findings indicate that bifurcation reaction may exist in other systems such as those utilizing flavins.⁴⁴

3.3. H-Shaped Electron Transfer System in the Dimer

Cytbc₁ complexes from mitochondria and bacterial cells have been crystallized and their structures solved to atomic resolution. The mitochondrial Cytbc₁ is a symmetrical, oligomeric homodimer in which each monomer encompasses the three catalytic subunits (Cytb, Cyt_c₁, and ISP) surrounded by a periphery of nonredox, supernumerary subunits. The bacterial enzyme is also dimeric and the overall structure of the catalytic subunits as well as the position of the redox cofactors are highly similar to the mitochondrial enzyme (Figure 5). The major difference is a general lack of the supernumerary subunits in the bacterial enzyme.

One unusual aspect of the dimeric structure is that ISP spans the dimer. This ISP subunit is anchored in one monomer by a single transmembrane helix, while the peripheral, hydrophilic

domain that contains 2Fe2S (ISP-HD) is located in the other monomer, where it forms part of the quinol oxidation Q_o site.^{20,21,45} A comparison of the structures of enzymes crystallized in the absence or presence of the Q_o site inhibitors indicated that the ISP-HD occupies different positions with respect to the other parts of the complex. This suggested that movement of ISP-HD between positions proximal to Cytb and Cyt_c₁ is necessary to transfer an electron between the Q_o site and heme c_1 in the c -chain. This hypothesis was confirmed by site-directed mutagenesis studies, which demonstrated that such movement was essential for enzyme activity. However, the mechanistic rationale behind the movement is not clear (see section 3.4).

In view of the topographic arrangement of ISP, the functional module at the level of the Cytbc₁ monomer consists of the Cytb and Cyt_c₁ and ISP linked to them through its ISP-HD, while also interacting with Cytb and Cyt_c₁ of the other monomer through its hydrophobic anchor. The same structure feature applies to Cytb_{6f} (see further).⁴⁶ The crystal structures of Cytbc₁ revealed that large distances separate the cofactors from different monomers, except for the two hemes b_L that are positioned close enough to allow electron transfer between the monomers (Figure 5). The capacity of this electron transfer bridge to connect the monomers on a catalytically relevant time scale was further proven in studies that exploited cross-inactivated forms of the enzyme.⁴⁷ The existence of the heme b_L – b_L electron transfer bridge implicates that cofactor chains in the dimer assemble into an H-shaped electron transfer system that connects the two Q_o sites with the two Q_i sites. Given that the functional module of each of the monomers provides all necessary elements to support the catalytic Q cycle (the c - and b -chains, the Q_o and Q_i sites), the mechanistic and physiological meaning of the H-shaped electron transfer system remains unclear but intriguing (see section 9 for details).

Cytb_{6f} is also a homodimer. The topographic arrangement of ISP that are intertwined with the dimer and the movement of ISP-HD are conserved, as is the distance between the two hemes b_p . In view of the general similarity of cofactor architecture between Cytbc₁ and Cytb_{6f}, it is reasonable to assume that the characteristic H-shaped electron transfer system is a shared feature of all Cyts- bc .

3.4. Large-Scale Movement of ISP-HD

The large-scale movement of the extrinsic domain of the iron–sulfur protein (ISP-HD) is an inherent part of the catalytic cycle of Cytbc₁ and Cytb_{6f}. The movement alternately brings the 2Fe2S either to the position close to the catalytic Q_o/Q_p site (referred to as the Q_o position or the b -position) or close to heme c_1/f (the c -position), separating in time and space the two electron transfers within the high potential chain: 2Fe2S at the b -position exchanges electrons exclusively with quinol bound at the site, while at the c -position it exchanges electrons exclusively with heme c_1/f . This movement was proven obligatory in many studies showing that impairment of the mobility of ISP-HD entails a severe limitation or complete loss of enzymatic activity.^{49–55} This is commonly explained considering the effect of changing in distance between cofactors on electron transfer rate:⁵⁶ the ISP-HD arrested at a specific position permanently (due to the presence of some inhibitors) or for prolonged period of time (due to specific mutations) cannot efficiently shuttle electrons between the Q_o/Q_p site and heme c_1/f as specific distances between the cofactors in a frozen configuration are not optimal for rapid electron transfer along the entire cofactor

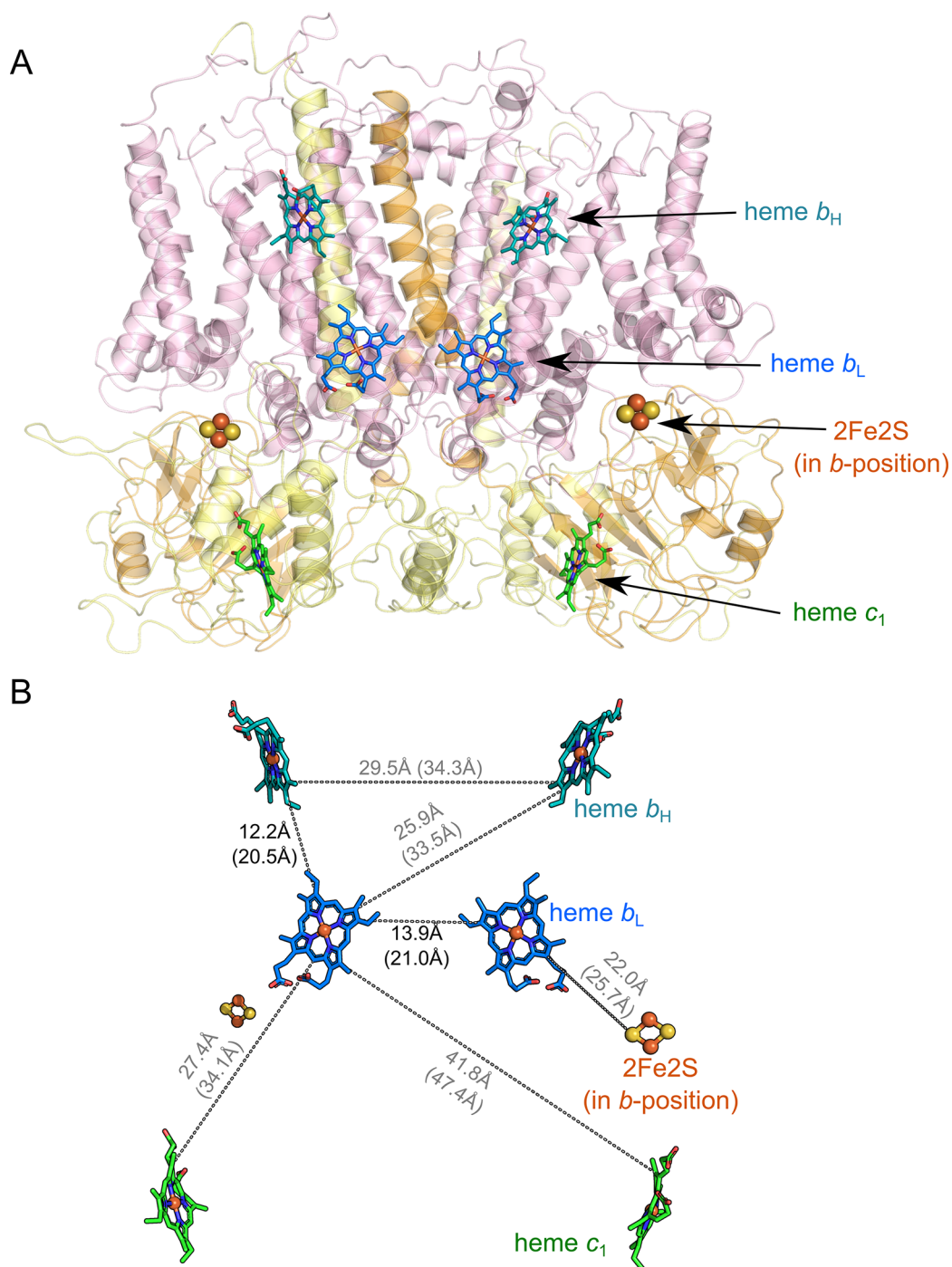


Figure 5. Crystal structure and spatial arrangement of electron-transfer cofactors in Cytbc₁ from *Rhodobacter capsulatus* (PDB ID: 1ZRT⁴⁸). (A) Ribbon structure showing all catalytic subunits in the dimer with the overlaid cofactors. (B) Redox-active cofactors in the dimer with edge-to-edge (numbers) and iron-to-iron distances (numbers in brackets).

chain. For example, in a configuration with the ISP-HD arrested at the Q_o site, a large distance between the 2Fe2S and heme c₁ prevents rapid electron transfer between these two cofactors and consequently enzymatic activity is lost.

3.4.1. First Structural Indications for ISP-HD Movement. The possibility that conformational changes might be associated with the catalytic reactions involving 2Fe2S was considered before the first crystallographic structures of Cytbc became available.^{57,58} Although the movement itself was not mentioned, a mechanism evoking a “catalytic switch” of 2Fe2S was formulated on the basis of different affinities of MOA-

stilbene and UHNQ (2-hydroxy-3-undecyl-1,4-naphtoquinone) inhibitors to the Q_o site that depended on the redox state of 2Fe2S. The concept of ISP-HD movement during the catalytic cycle was born soon after crystallographic structures with resolved ISP became available.^{59–61} Early structures of chicken Cytbc₁ revealed two conformations of ISP-HD,⁶¹ suggesting that it might switch between different positions during the catalytic cycle. This was further substantiated by the mammalian Cytbc₁ structures containing all 11 monomer subunits,⁶⁰ which clearly showed that ISP-HD can adopt different conformations for which 2Fe2S was found at the b-position, at the c-position, or

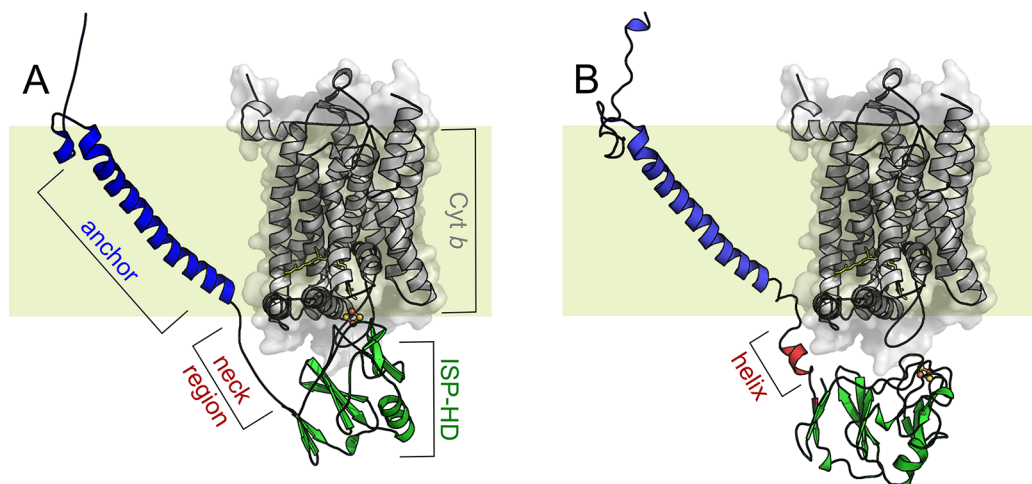


Figure 6. Structure of Cytb and two conformations of ISP in one monomer. (A) Structure based on PDB ID: 1sqx with ISP-HD at the b-position. (B) Structure based on PDB ID: 1be3 with ISP-HD being at the c-position. The hydrophobic anchor of ISP (blue helix) is embedded in the lipid membrane (pale green square). In A and B the neck region connecting ISP-HD (green) with the anchor has two different conformations. Cytb is shown in gray.

somewhere in between. Further crystallographic and cryo-EM structures of Cytbc originating from many different organisms: bacteria,^{42,48,62–67} chlorophyta,⁴¹ fungi,^{68–72} and plants⁷³ to avian^{74–76} and mammalian proteins,^{77–79} including humans,⁸⁰ were all consistent with the concept that ISP-HD must undergo a constrained diffusion to facilitate electron transfer between the Q_b/Q_p site and Cyt_c₁/Cyt_f. One recognized exception comes from recent analysis of the structure of Cyt-bc in supercomplex with cytochrome c oxidase from *Mycobacterium smegmatis*, which suggests that a globular domain of a diheme Cyt_c (equivalent of Cyt_c₁) might move instead of ISP-HD to support the catalytic cycle.^{81,82}

3.4.2. Effects of the Q_b/Q_p Site Inhibitors. It is recognized that two types of inhibitors exert opposite effects on the average position of ISP-HD seen in crystals.⁸³ The first group of inhibitors includes compounds, such as stigmatellin, famoxadone, *n*HDBT, atovaquone, and DBMIB in Cytb_{6f}, which fix ISP-HD at the b-position and thus are classified as P_f inhibitors (f for fixed). The second group includes compounds that do not arrest the ISP-HD at a single b-position, but, quite oppositely, expel ISP-HD from the Q_b/Q_p site forcing the domain to adopt positions remote from the Q_b/Q_p site, including the c-position.^{21,74,77,84} As they do not prevent the motion of ISP-HD, they are classified as P_m inhibitors (m- for mobile). Typical inhibitors of this group are myxothiazol, MOA-stilbene, and strobilurin derivatives (see section 5).

3.4.3. Constrained Diffusion or Allosteric Control. There are several mechanistic aspects of the movement of ISP-HD that remain the subject of discussion.²⁰ One of the most important and still unsolved issues concerns a fundamental question of whether the motion is simply a stochastic, thermally activated process or whether it is rather controlled by a particular state or states of the enzyme during the catalytic cycle.^{21,85–90} The simplest answer one may consider is that the motion represents a stochastic process of constrained diffusion,^{51,90–92} which is fast enough ($\sim 80\,000\text{ s}^{-1}$)⁹³ not to limit the overall rate of catalysis.⁹⁴ The stochastic diffusion, in contrast to any mechanism that would rely on a specific element or elements of control imposed on the ISP-HD movement, has the clear advantage of not requiring energy expenditure for “information

gain” needed to control the cycle. This seems important given that the primary function of the enzyme is to conserve energy.

However, the general difficulty with understanding the high energetic efficiency of bifurcation taking place at the Q_b/Q_p site and associated with it, efficient suppression of side reactions (see section 7.4) prompted a search for structural factors responsible for controlled docking/release of the ISP-HD from the b-position during the catalysis. This seemed additionally justified by the specific effects of the P_f and P_m inhibitors on modulation of the position of ISP-HD and on interactions of ISP-HD with Cytb. None of the available structures succeeded in resolving the position of natural substrates, UQ/PQ or UQH₂/PQH₂, bound at the Q_b/Q_p site,²⁰ which left room for interpretation of any observed structural effects in the context of possible effects of the presence of Q or QH₂ at the catalytic site on the ISP-HD motion. Some additional clues have been drawn from MD simulations.^{95–97}

3.4.4. Structural Changes in Brief. Prior to discussions on the mechanisms of the ISP-HD motion, it is necessary to briefly describe key structural elements of ISP. The ISP subunit can be divided into three domains:⁹⁸ (a) ISP-HD harboring the redox-active [2Fe-2S] Rieske cluster (2Fe2S), (b) the membranous anchor, consisting of a single hydrophobic helix (residues^{Rh}1–38, ^{Bt}1–61), and (c) the neck or hinge region (residues^{Rh}39–48 or ^{Bt}62–74) containing highly conservative amino acid sequence⁹⁹ connecting the anchor with the ISP-HD (see Figure 6). The two ISPs interwind the dimer in such a way that each ISP-HD, interacting with Cyt_c₁ or Cytb of one monomer, has its anchor associated with Cytb of the second monomer (see Figure 5). The movement of ISP-HD is associated with conformational change within the flexible neck region (described below), rotation of the domain by approximately 57 to 65°,^{92,100} and displacement of the domain by approximately 2 nm.

3.4.5. Different Positions of ISP-HD in Crystal Structures. Comparing different crystal structures, Berry et al.²⁰ proposed that the observed populations of ISP-HD fall into four main groups if one considers differences in distances and angles of the position of the 2Fe2S in the structure relative to the stigmatellin bound at the Q_b site (Figure 7). The first group encompasses a population of ISP-HD in “b-positions” or “fixed positions” with the distances of up to $\sim 0.15\text{ nm}$ and the angles

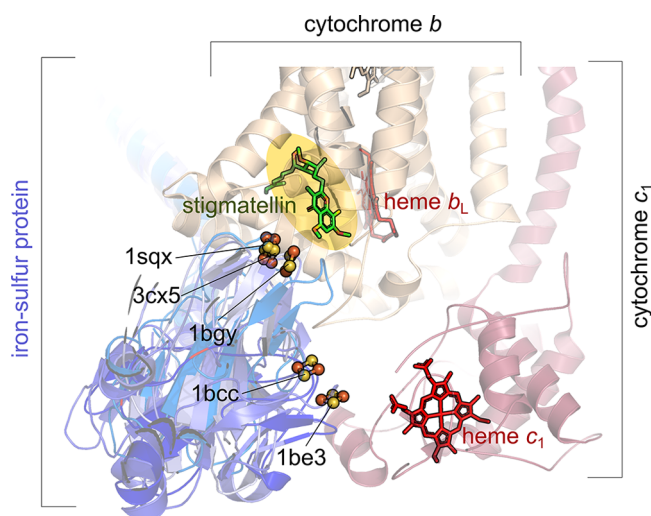


Figure 7. Several crystal structures of $\text{Cyt}bc_1$ monomers with different conformations of ISP-HD. The figure shows positions of $2\text{Fe}2\text{S}$ clusters (yellow and orange spheres) from the overlaid positions from bovine (PDB IDs: 1sqx, 1bgy, and 1be3), mouse (PDB ID: 3cx5), and chicken (PDB ID: 1bcc) crystallographic structures of ISP. Blue, ochre, and red ribbons represent ISP, $\text{Cyt}b$, and $\text{Cyt}c_1$, respectively. Hemes are shown as red sticks. Green sticks show the stigmatellin from 1sqx structure bound at the Q_o site (yellow oval).

up to 7° . The second group gathers “famoxadone-positions” for which the distance is between ~ 0.15 and ~ 0.2 nm with the angle $\sim 10^\circ$. The third group encompasses “low-affinity fixed positions” at distances ~ 0.4 to 0.45 nm and angles ~ 17 to $\sim 20^\circ$. The last group considers ISP-HD at the “c-positions” for which angles fall between 55 and 60° and distances ~ 1.5 to ~ 2.0 nm. It is of note that the diagram by Berry et al.²⁰ includes a structure originally resolved by Iwata et al.,⁶⁰ which was not classified to the group of c-positions and for which distance is ~ 2.3 nm and angle $\sim 65^\circ$. For this structure, the distance between $^{\text{Bt}}\text{H}161$ ($^{\text{Rh}}\text{H}156$) of ISP and heme c_1 is short enough to allow the formation of a H-bond between this histidine N_ϵ atom and the propionate group of heme c_1 indicating the most probable conformation predisposed to fast electron exchange between the cluster and heme c_1 .

3.4.6. Structure–Function Relationships for the Neck Region of ISP-HD. While detailed comparisons of structures revealed several elements that might undergo specific conformational changes upon the motion of ISP-HD, the cause–effect relationships of these elements in the context of the mechanism are not fully understood. The most evident structural change concerns the neck region, which, depending on the position of ISP-HD, adopts conformations differing in length.^{21,51} When the ISP-HD is at the c-position, the neck forms a small helical structure, whereas docking the domain to the Q_o site coincides with the “melting” of this small helix, thus lengthening the connection between the anchor and the ISP-HD (Figure 6). However, helix formation was seen upon transition of ISP-HD from the “low-affinity fixed position” (group 3) to the b-position (group 1).²⁰

The first evidence for the involvement of the neck region in ISP-HD mobility can be found in studies showing that mutations in the conserved fragment of the *Box 1* sequence of the ISP (ISP: $^{\text{Rh}}\text{L}136$), that destroy sensitivity of $2\text{Fe}2\text{S}$ to UQ at the Q_o site, were mitigated by mutations in the hinge region (ISP: $^{\text{Rh}}\text{V}44$ or ISP: $^{\text{Rh}}\text{A}46$).^{101,102} Further mutational studies

systematically investigated the effects of changing the length and amino acid composition of the neck region on movement of ISP-HD. Elongating the neck by insertion of 1, 2, or 3 alanine residues (+1Ala, +2Ala, or +3Ala mutants, respectively) was found to decrease overall electron transfer through the high-potential chain and the magnitude of this decrease depended on the length of the insertion. In +1Ala, the electron transfer to heme c was found to occur within the millisecond time scale, while in +2Ala and +3Ala on the second time scale, which is orders of magnitude slower than in the native enzyme (micro to milliseconds). Apparently ISP-HD movement, which in the native enzyme is fast and not rate-limiting, becomes rate-limiting in the mutants.^{51,93,103,104}

Interestingly, +1Ala is still functional *in vivo*, while +2Ala and +3Ala are not, indicating that some level of functional tolerance to restrictions of the ISP-HD movement exists. Detailed analysis of the kinetic data led to the proposal that these mutants progressively restrict the movement in such a way that the ISP-HD gets arrested for a prolonged period of time at the b-position (for milliseconds in +1Ala or seconds in +2Ala or +3Ala).^{50,52,90,105–107} Also, replacement of the neck-region residues with 6 prolines^{50,106} abolished helix formation and precluded the release of the domain from the b-position. Surprisingly, shortening of the neck region by 1 to 5 amino acids did not lead to loss of catalysis and the EPR spectra obtained for deletion mutants still reflected the ability of $2\text{Fe}2\text{S}$ to interact with the UQ and UQH_2 bound at the Q_o site, albeit with stoichiometry of ISP to $\text{Cyt}b$ progressively decreasing to 0.2 in 5-residue deletion mutant.⁵⁰

The conclusion reached from analysis of kinetic data that the alanine insertions arrest the ISP-HD at the b-position was confirmed by EPR studies with oriented membranes^{88,100,108–111} and pulse EPR with isolated $\text{Cyt}bc_1$.^{90,107,112,113} The latter studies allowed direct monitoring of changes in the average position of the ISP-HD with respect to heme b_L by measuring the distance-dependent enhancement of reduced $2\text{Fe}2\text{S}$ relaxation by oxidized heme b_L . The average distance between these two cofactors was found to increase in the following order +2Ala mutant, +1Ala mutant, WT.¹⁰⁷ These measurements also revealed that the position of ISP-HD in +2Ala is no longer influenced by P_m inhibitors but remains sensitive to the addition of stigmatellin.⁹⁰ This suggests that conformational changes at the neck region can be overwhelmed by the energy of stigmatellin binding, with a large contribution coming from H-bond formation (typical value of energy required to break an H-bond is ~ 21 kJ/mol).²⁰

3.4.7. Structure–Function Relationships for the Interaction of ISP-HD with Cytochrome b. Given that the P_f and P_m inhibitors exert different effects on the position of ISP-HD, the question arises as to how the P_f inhibitors fix the domain at a position close to the Q_o site. One of the most obvious structural effects of the presence of stigmatellin, *n*HDBT, atovaquone, crocacin D, and ascochlorin (group-1 of P_f inhibitors) at the Q_o site is formation of the H-bond between $^{\text{Rh}}\text{H}156$ ($^{\text{Bt}}\text{H}161$ or $^{\text{Sc}}\text{H}181$) of the ISP subunit and the inhibitor. Formation of this bond is not only associated with docking of ISP-HD to the Q_o site but also stabilizes the reduced state of $2\text{Fe}2\text{S}$ by significantly raising its redox potential.^{114–116} This suggests stabilization of the reduced cluster under conditions when it forms the H-bond with a molecule occupying the Q_o site. Indeed, the observation that the reduced cluster is detected by EPR at the b-position in membranes indicates that interactions of the reduced $2\text{Fe}2\text{S}$ and the natural quinone at the Q_o site are also stabilized. On the

other hand, ISP-HD appears to favor the *c*-position when the cluster is oxidized.¹⁰⁰ This difference in affinity to quinones at the Q_o site between the reduced and oxidized cluster may be one of the elements contributing to the mechanism that diminishes the risk of energy-wasting short-circuits (see section 7.4.1). It should be noted, however, that some inhibitors (famoxadone, fenamidone, or JG144 inhibitors, all belonging to the group 2 of P_f inhibitors) hold the domain at the *b*-position without creating an H-bond to $^{Rh}H156/^{Bt}H161$.¹¹⁷ This indicates that factors other than the H-bond between $^{Rh}H156/^{Bt}H161$ of ISP and the occupant of the Q_o site can also stabilize binding of ISP-HD to *Cytb*. While formation of this bond would be expected to significantly strengthen the interaction, it is clearly not an absolute requirement for the domain fixation to *Cytb* or *Cytb₆*.

It seems reasonable to assume that some changes in conformation on the surface of *Cytb* or *Cytb₆* contribute to the process of fixing to or release of the domain from the *b*-position.^{20,21,78,85} The potential “holding and release lever”, if it exists, would be expected to localize to the part of the *Cytb/b₆*, which remains in close contact with the surface of ISP-HD. These regions encompass small helices that are connected to the transmembrane ones by loops: *cd1*, *cd2*, and *ef* loop.^{18,20,55,64,118} However, when structures containing P_f and P_m inhibitors are compared, there is no significant change in the position of helices in *Cytb*, except for the *cd1* helix, which seems to be slightly pushed inside *Cytb* by ISP-HD upon interaction of stigmatellin with 2Fe2S.²⁰ Furthermore, a comparison of the structures of intermediate positions (group 3) and the *c*-position (group 4) reveals no changes in the *cd1* and *cd2* helices, suggesting that the motion of ISP-HD between “low-affinity fixed positions” (group 3) and the *c*-position (group 4) is a free diffusional process constrained by the neck region of the ISP acting as a peptide tether.

It is not clear if the shift of the *cd1* helix upon docking ISP-HD at the Q_o site is an effect of the inhibitor itself, allowing the 2Fe2S cluster to “come closer” or if the H-bond between the inhibitor and $^{Rh}H156$ induces “pressure” of ISP-HD on the structure forcing *cd1* to move. Such a pressure could be an element of the “spring-loaded” mechanism, which proposes that H-bond formation between ISP-HD and a substrate present in the Q_o site stores some energy, which is released after the reaction and facilitates the dissociation of ISP-HD from the *b*-position.¹¹⁹

The involvement of the *cd1* helix in binding of ISP-HD to the Q_o site is also implicated by mutation studies in which $^{Rh}G167$, located at the end of the *cd1* and before the *cd2* helix, was replaced by proline. This significantly perturbed the docking of ISP-HD to *Cytb*, which was reflected in an observed shift in the equilibrium distribution of the ISP-HD toward the *c*-position.^{120,121} As a result, the interaction of 2Fe2S with UQ or UQH₂ at the Q_o site was broken and the enzymatic activity of the $^{Rh}G167P$ mutant dramatically decreased, abolishing the functionality of the enzyme *in vivo*. Also superoxide generation by the Q_o site increased in this mutant (see section 7.5 for details). Despite these effects, the mutant remained sensitive to stigmatellin. Interestingly, addition of the +1Ala or +2Ala mutation to the $^{Rh}G167P$ mutant was found to mitigate the inhibitory effects of $^{Rh}G167P$ mutation to various extent. A remarkable example was the double $^{Rh}G167P/+2Ala$ mutant in which the equilibrium distribution of ISP-HD was similar to that of the single +1Ala mutant, partially restoring sensitivity of the reduced 2Fe2S to UQ at the Q_o site. This brought back some level of functionality to the enzyme *in vivo* even though both

single mutations were nonfunctional. Clearly, the opposite effects of $^{Rh}G167P$ mutation (“pushing” ISP-HD away from the *b*-position) and the alanine insertions (arresting ISP-HD at the *b*-position) can partly compensate one another, establishing that dynamics of the docking/release of ISP-HD to/from cytochrome *Cytb* can be effectively coinfluenced by the specific interactions at the ISP-HD-*Cytb* interface and the conformational changes taking place within the neck region. A functional link between these two distinct structural domains was also documented in other mutational studies.¹²²

Another eye-catching structural element that may somehow influence the ISP-HD movement is the region of the *ef* loop (*Cytb*: $^{Rh}286-292$, $^{Bt}262-268$), a small peptide fragment connecting the transmembrane E helix, the conserved PEWY sequence and the transmembrane F helix.^{20,55,60} It is considered to be the main “obstacle” that forms a barrier to ISP-HD on its trajectory from the *b*- to *c*-position. The role of the *ef* loop was proposed following the finding that mutations in this region can compensate the effect of +1Ala.^{51,53} Further mutational studies revealed that bulky side chains located in the middle part of the loop limit the ability of ISP-HD to move outside the Q_o site.¹²² This led to the proposal that the *ef* loop acts as a switch increasing or decreasing the rate of electron transfer between the Q_o site and heme *c*₁,^{55,103} which together with the *cd1* helix constitutes the mechanism of binding and release of ISP-HD depending on the redox state of hemes *b*.^{78,86,88,89} However, as demonstrated by mutational studies, amino acid side chains such as $^{Rh}L286$, $^{Rh}I292$ on the *ef* loop in fact may serve to resist in transitions between *b*- and *c*-position.⁵⁵ The control mechanisms steering this loop during the catalytic cycle are a matter of discussion. The observed effect of modifications on the motion caused by mutations in the *ef* loop does not preclude a simple stochastic model for the movement of ISP-HD in which the mobile loop regions undergo random thermal fluctuations rather than specifically controlled motion.

Not only the redox state of hemes *b* but also specific events taking place at the Q_i site have been considered as potential factors that influence the mobility of ISP-HD. In view of topographical arrangement of ISP-HD in the dimer, this would imply a highly ordered communication between monomers, which would allow transfer of information over ~4 nm across *Cytb*, possibly through the membranous anchor of ISP that ends in proximity to the Q_i site. Most of the proposals on this type of allosteric influence are derived from analysis of the effects of antimycin bound at the Q_i site. However, as we discuss further, the interpretation of these effects needs to be treated with caution.

3.4.8. Effect of the Q_i Site Inhibitor, Antimycin.

Evaluating the influence of antimycin on the basis of crystallographic structures containing antimycin bound at the Q_i site is difficult as the majority of the antimycin-containing structures were obtained with stigmatellin bound at the Q_o site, which overrides any possible structural effects of antimycin on the Q_o site. To our knowledge, until now, there are two PDB crystallographic structures in the database, containing antimycin bound at the Q_i and no other inhibitor at the Q_o site.^{117,123} As discussed by Berry and Huang (*ibidem*), antimycin does not seem to change the ground state of the structure but might change dynamics of the structure.¹¹⁷ The dynamic change was considered to accommodate several biochemical studies suggesting that antimycin induces effects that might be associated with changes to the different mobility of the domain.

The first series of experiments was based on the susceptibility to proteolytic cleavage of the neck region (between residues ^{Rh}46 and 47) as a sensor of conformational changes taking place in this region. It was found that the cleavage was substantially limited by fixing of ISP-HD at the b-position by P_f inhibitors, when compared to the enzyme with P_m or without any bound inhibitors.¹²⁴ On the other hand, the addition of antimycin increased proteolysis, suggesting that this inhibitor induced changes that increased accessibility of this fragment for thermolysin.

The second series of experiments focused on various EPR methods to monitor the 2Fe2S. Continuous wave (CW) EPR spectra of microscopically disordered samples containing antimycin- or HQNO-supplemented membranes did not show any significant changes in the spectra when compared to the noninhibited samples.¹¹¹ However, analysis of the samples containing ordered layers of membranes revealed that after addition of antimycin, the angular-dependent amplitudes of g_x and g_y transitions of the 2Fe2S cluster are different from those detected in samples not containing antimycin.^{88,111} Pulse EPR measurements with isolated Cytbc₁ showed that the presence of antimycin at the Q_i site caused an increase in distance between the reduced 2Fe2S and oxidized heme b_L⁹⁰ and an increase in the efficiency of spin–lattice relaxation of the 2Fe2S cluster via two-phonon Raman process. All recognized changes associated with the presence of antimycin at the Q_i site consistently indicate that this inhibitor induces some structural changes that modify the average position of ISP-HD. This effect was interpreted by some authors as evidence for allosteric inter- or intramonomer interactions between the Q_i/Q_n and Q_o/Q_p site that lead to specific sequences of a “duty cycle” of Cytbc₁/b_{6f} during the catalysis.^{86–88,125,126}

In our view, the observed effects of antimycin on the ISP-HD are associated with a decrease in the rigidity of the Cytbc₁ structure, which decreases the energetic barrier for moving from b- to c-positions. This simple concept assumes that the population of ISP-HD domains is distributed over different conformations and various inhibitors, including antimycin, just modify a barrier for this movement.⁹⁰ In fact, pulse EPR measurements revealed that the average position of ISP-HD can be effectively modified by mutations or inhibitors and the observed shifts in this position can be placed in the following order (starting from b-position and going further toward the c-position): +2Ala mutant > stigmatellin > Cytb:^{Rh}G167P/ISP: +2Ala double mutant > +1Ala mutant > Cytb:^{Rh}G167P/ISP: +1Ala double mutant > no-inhibitor WT > WT + myxothiazol ≈ Cytb:^{Rh}G167P ≈ WT + antimycin > WT + antimycin + myxothiazol.^{90,120} In all cases, addition of stigmatellin overrides any other effect, which suggests that the energy of H-bonding between the inhibitor and ISP:^{Rh}H156 exceeds the energy associated with changing the structure of the neck region. Although stigmatellin is able to overcome the effects of alanine insertion into the neck region, neither P_m inhibitors (myxothiazol) nor antimycin influences the ISP-HD position in +2Ala mutations.⁹⁰ Gathering all these observations, we can propose that the strength of factors that influence the ISP-HD mobility can be put in the following order: P_f inhibitors that form H-bonds > conformation of *cd1* helix (^{Rh}G169P mutation) > increase in the length of the neck region > P_m and Q_i inhibitors (myxothiazol, antimycin). The *ef* loop was not included in this list since no direct spectroscopic measurements of distance distribution of ISP-HD were done for mutants in this particular region. However, by comparing the kinetics data and the effect

of the redox potential of 2Fe2S, it may be suggested that the energetic barrier of crossing the *ef* loop by ISP-HD is lower than the barrier imposed by +2Ala, comparable with the effect of +1Ala insertion and higher than the barrier imposed by P_m-type or Q_i inhibitors.^{53,55}

We note that most of the structural studies involving EPR spectroscopy have been performed under conditions for which 2Fe2S was reduced. Although no changes on the surface of the ISP-HD associated with the changes in the redox state of the cluster were observed,²⁰ the domain with a reduced 2Fe2S appears to show a greater tendency to occupy the b-position compared to the domains with the oxidized 2Fe2S. This is in line with the observation that E_m of 2Fe2S depends on the position of ISP-HD.¹⁰⁶

3.4.9. Effect of Movement on Redox Potential of the 2Fe2S Cluster. There are numerous studies showing that the E_m of 2Fe2S depends on interaction between ISP-HD with the Q_o site.^{50,52,53,106,109,113,114,116} In general, the greater the tendency for ISP-HD to be at the b-position, the more positive the redox potential of 2Fe2S. For the mutants +1Ala, +2Ala, and 6Pro, that were discussed earlier, the E_m values of 2Fe2S were found to increase by the same order. This could suggest a decrease in water accessibility, which changes pK of ^{Rh}H156 (^{Rh}H161). However, the position of the ISP-HD is not alone in influencing the redox potential of 2Fe2S. Another important factor is the interaction of the domain with the occupant of the Q_o site. The most prominent effect is formation of a H-bond with stigmatellin, which increases the midpoint potential by more than 200 mV. Other inhibitors that form a H-bond with ^{Rh}H156 of the ISP-HD, such as tridecylstigmatellin or UHDBT, exert a weaker effect on the rise in the redox potential.¹⁰⁶ Also, the presence of Q bound at the Q_o site appears to slightly contribute to a slight increase in the redox midpoint potential of 2Fe2S.¹⁰⁹ However, it should be noted that the effect of Q bound at the Q_o site has been recognized in +nAla mutant but not in WT¹⁰⁹ (see Table 1 in ref 127). On the other hand, P_m inhibitors such as myxothiazol or MOA-stilbene slightly decrease the E_m value of the 2Fe2S.¹²⁸ Thus, it was proposed that H-bonding is the factor that controls the redox potential and stabilizes binding of substrate and enzyme.¹²⁸

3.5. Cytochrome bc₁: Specific Structural and Functional Elements

3.5.1. Subunit Composition of Cytochrome bc₁. All Cyts bc₁ contain three protein subunits per monomer with redox prosthetic groups: the diheme Cytb, the monoheme Cytc₁ and the ISP (Rieske iron–sulfur protein). Cytb is built of 8 transmembrane helices and contains a relatively high-potential heme b_H and a lower potential heme b_L. Cytc₁ and the ISP are membrane-anchored and their water-soluble, globular domains contain prosthetic groups (high-potential heme c₁ and 2Fe2S, respectively). All these three subunits are necessary for the catalytic function of Cytbc₁. In some bacteria, such as *Paracoccus denitrificans*, *Rhodospirillum rubrum*, or *Rhodobacter* (*R.*) *capsulatus*, Cytbc₁ contains only these three subunits. Other bacteria, including *R. sphaeroides*, contain a fourth subunit of unknown function that lacks prosthetic groups.¹²⁹

In addition to the catalytic subunits, Cytsbc₁ of mitochondria contain as many as seven (in some yeast) or eight (in bovine and human) supernumerary subunits. The largest supernumerary subunits associate to the catalytic subunits from the mitochondrial matrix side. The functions of the supernumerary subunits are not known, except for the established mitochondrial

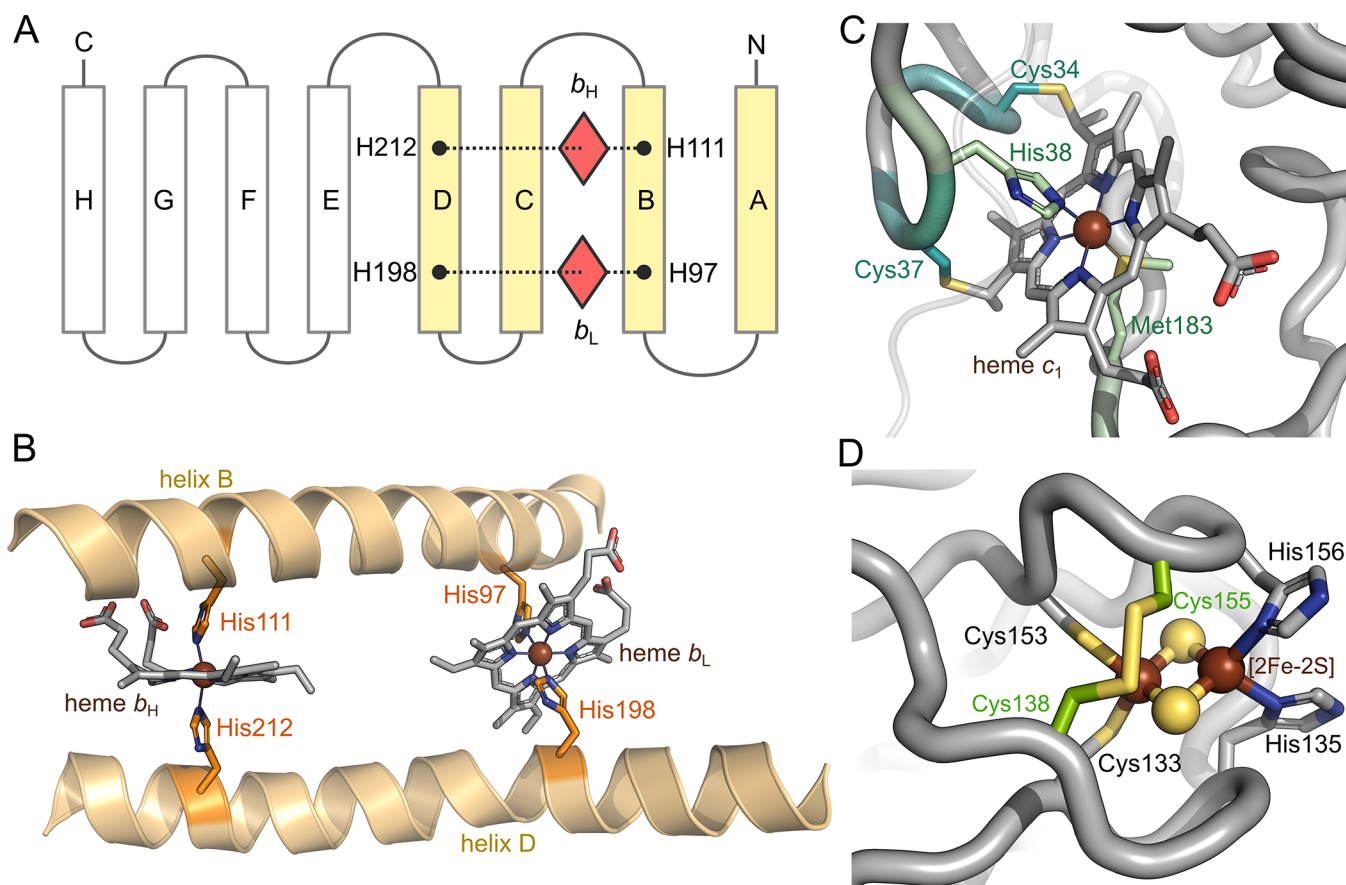


Figure 8. Structure features and binding motifs of metallic cofactors of *Cytbc₁*. (A) Schematic representation of the transmembrane part of *Cytb*, showing helices involved in formation of the heme-bearing 4-helix bundle (A–D, pale orange rectangles). Hemes are shown as orange polyhedrons, positions of axial ligands of hemes are marked by black dots, *R. capsulatus* residue numbering is used. (B) Structural model showing hemes *b* orientation within the transmembrane bundle and orientation of their axial ligands. Helices providing axial ligands are shown in pale orange cartoon, ligating histidines are colored orange. (C) Structural model showing heme *c₁* binding site in the globular domain of *Cyt c₁*. Cysteines of the binding motif are colored light blue, axial ligands are colored pale green. (D) Structural model showing the [2Fe-2S] cluster binding site in ISP. Coordinating residues are labeled in black, cysteines that form the disulfide bridge are colored and labeled in green. All representations are based on PDB ID: 1ZRT entry.

processing peptidase activity of large subunits, as discussed by Berry et al.²⁰ The supernumerary subunits are believed to contribute to the increased stability of mitochondrial complexes but are not required for the electron transfer and proton translocation activities of the enzyme; the three-subunit bacterial enzymes have the same electron transfer and proton translocation functionality as the mitochondrial enzymes.

3.5.2. Structure and Spectral Properties of Hemes *b*, *c₁*, and 2Fe2S Cluster. The redox-active components of *Cytbc₁* in all organisms are evolutionary conserved within the catalytic core.¹ Remarkably, as shown by the crystal structures of *Cytbc₁* from various organisms, the positions of the stationary cofactors, hemes *b* and *c₁*, are unchanged among them.^{21,48,60}

The two *b*-type hemes, (heme *b_L* and *b_H*) of *Cytb* subunit are embedded within the four-helix-bundle, assembling in what appears to be a common (evolutionary conserved) structural motif of many bioenergetic complexes.^{130–132} In the *Cytb* subunit, helices named A–D are involved in bundle formation (Figure 8A), with helices B and D providing axial ligands for the heme iron of both hemes (Figure 8A,B).¹³³ Both hemes *b* are axially coordinated by the two conserved histidines (referred to as a bis-His ligation pattern) via bonds between the heme iron and N_τ atom of the respective imidazole ring (Figure 8B).^{48,132}

The heme *c₁* is a *c*-type heme attached to the globular head of *Cyt c₁* (Figure 8C). It is covalently bound to the apoprotein via

thioether linkers formed by its two vinyl side chains and two cysteine residues,^{48,60} belonging to a characteristic CXXCH motif.¹³⁴ The iron of heme *c₁* is axially coordinated by N_τ of the conserved histidine from this motif and S_δ of the conserved methionine (referred to as a His-Met ligation pattern).^{48,135} Interestingly, in some bacterial species, the ligation of heme *c₁* is secured by an additional pair of cysteines that form a disulfide bond to stabilize the distant loop of the globular part of *Cyt c₁*.¹³⁵ However, the freedom retained for conformational rearrangement results in a partial weakening of the methionine ligation when the cytochrome is in its oxidized form, which is reflected in an ability to bind small exogenous ligands such as cyanide.¹³⁶ Removing the disulfide by mutations was found to significantly perturb the conformational stability and further weaken the methionine ligation. As a result, the potential of the heme dropped dramatically (more than 300 mV) and the reduced cytochrome showed a capability to bind carbon monoxide, all of which imply change in the heme ligation pattern.¹³⁵ In other *Cyt c₁*, such as mitochondrial *Cyt c₁*, the disulfide is not present. Instead, the βXM structural motif (where β stands for the β-branched amino acid located one residue away from the methionine axial ligand) appears to restrict the conformational flexibility of the domain of the methionine axial ligand to the point that the binding of external

ligands is not observed.¹³⁶ Some bacterial Cyt_c₁ have both the disulfide and the β XM motif.^{135,137}

Similarly to the heme *c*₁, 2Fe2S is attached to ISP-HD and situated between the two loops of the protein backbone that are hooked by a disulfide bridge formed between two cysteine residues.¹³⁸ The cluster is coordinated by the thiolate side chains of the two conserved cysteine residues, acting as ligands for one Fe ion, and N π atoms of the two conserved histidine residues, acting as ligands for second Fe ion (Figure 8 D).^{48,138} This type of [2Fe-2S] cluster coordination by two Cys and two His residues is almost exclusive to ISP of Cyt-*bc* and aromatic ring-hydroxylating monooxygenases and dioxygenases.^{139,140}

Iron atoms in all the hemes of Cyt_{bc}₁ are hexa-coordinated and have strong axial ligands (with bis-His and His-Met ligation pattern for hemes *b* and heme *c*₁, respectively). Therefore, they all exist in low spin states. In the reduced (ferrous) state, the hemes exhibit partially overlapping α/β absorbance bands in the visible region of the UV-vis spectrum (Figure 9A), with α -band maxima at 560–562 and 552–553 nm for hemes *b* and *c*₁, respectively.^{141–144} The spectral resolution of heme *b*_H and heme *b*_L by optical spectroscopy is difficult. In the bacterial Cyt_{bc}₁, a deconvolution of the spectra obtained upon redox titration implicates a dominant contribution from the heme *b*_H at 562 nm and a significantly smaller contribution from heme *b*_L, which has a split α -peak spectrum with maxima at 564–566 and ~558 nm.^{39,145,146} On the other hand, the heme *c*₁, due to its much higher redox midpoint potential and α -band maximum at a lower wavelength, can be easily isolated spectrally from hemes *b* in the partially reduced enzyme (Figure 9A, in orange).¹⁴¹ In their oxidized (ferric) state, hemes *b* and *c*₁ are paramagnetic (*S* = 1/2),¹⁴⁷ thus detectable by electron paramagnetic resonance (EPR) spectroscopy at low temperatures (<20 K). All three hemes fall into the HALS (highly axial/anisotropic low spin) hemes category, with only their *g*_z (often called *g*_{max}) transition being observable by EPR.¹³² In general, the bis-His coordinated hemes *b* exhibit a HALS signal when the imidazole rings of the two His residues are nearly perpendicular to each other.¹⁴⁸ In the case of hemes *b*_L and *b*_H, the angles between the two imidazole ring planes are ~84° and ~58°, respectively,¹³² which translates into the two separate EPR transitions at *g* = 3.78 and *g* = 3.44, respectively (Figure 9B).^{149,150} Thus, EPR, unlike optical spectroscopy, offers a full spectral separation of the two hemes *b*. It is of note that the *g*_z transition of heme *b*_H is sensitive to Q_i site occupancy: when the site is occupied by antimycin A (a specific Q_i site inhibitor) or semiquinone radical (SQ_i), the *g*_z value is shifted to *g* = 3.47 or 3.42, respectively (Figure 9B).^{149,151} In *R. capsulatus* Cyt_{bc}₁, the *g*_z transition of heme *c*₁ occurs at *g* = 3.16.¹⁵² The exact *g*-values for *g*_z transitions of each heme may differ among organisms. Some of them were included in Table 1.

It is difficult to use optical spectroscopy in studies on the 2Fe2S, as it has no prominent spectrum¹⁵⁷ and its transitions are dominated by the spectra of hemes. The one-electron reduced form ([2Fe-2S]¹⁺) is paramagnetic (due to its ground state with *S* = 1/2 resulting from the antiferromagnetic spin coupling between Fe³⁺ (*S* = 5/2) and Fe²⁺ (*S* = 2) ions) and can only be detected by EPR at temperatures <50 K. The fully oxidized ([2Fe-2S]²⁺) cluster is in the EPR-silent (*S* = 0) ground state (the spins of the two Fe³⁺ ions are spin-coupled).^{140,158} The EPR spectrum of the reduced cluster ([2Fe-2S]¹⁺) exhibits a unique rhombic symmetry (Figure 9C), with transitions at *g*_z = 2.03, *g*_y = 1.90 and *g*_x between 1.78 and 1.76, resulting in the average *g* value of approximately 1.9.¹⁵⁷ In bacterial Cyt_{bc}₁, the shape and the position of the *g*_x transition was found to be sensitive to the

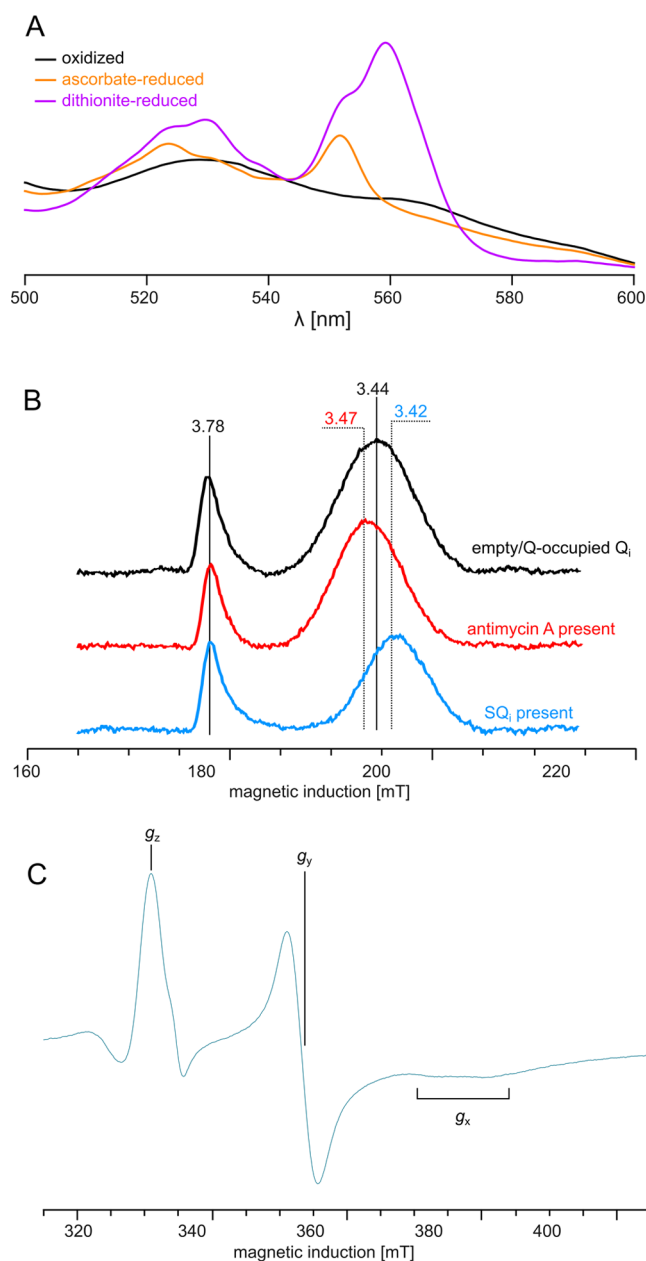


Figure 9. Spectral features of Cyt_{bc}₁ redox cofactors. (A) Optical spectra of α/β -band region of hemes. Spectrum of the fully oxidized enzyme is shown in black, spectrum after reduction with sodium ascorbate is shown in orange (showing prominent contribution from heme *c*₁), and spectrum of the fully reduced enzyme (with dithionite) is shown in magenta. (B) EPR spectra of *g*_z transitions of hemes *b*_L and *b*_H in an air-oxidized sample (top), sample of the enzyme inhibited with antimycin A (middle) and a sample with generated SQ_i (bottom). Numbers indicate *g* values. (C) EPR spectrum of a one-electron reduced [2Fe-2S] cluster in isolated Cyt_{bc}₁.

occupant of the Q_o site (whether it is occupied by substrate, or inhibitor or remains empty), the redox state of quinone (whether quinone or quinol are present), and the size of the quinone pool/potential number or quinone molecules at the Q_o site (see section 7.2). For those reasons, EPR analysis of the cluster has proven to be a convenient spectroscopic tool for monitoring the status of the Q_o site.^{50,159}

The midpoint redox potentials (*E*_m) of hemes *b*, heme *c*₁, and 2Fe2S may vary in different systems, depending on the quinone

Table 1. g_z Values Measured for Hemes in Selected *Cytc₁*

organism (reference)	g_z value (concerns <i>Cytc₁</i>)		
	heme b_L	heme b_H	heme c_1
<i>Rhodobacter capsulatus</i>			
153	3.78	3.45	n.d.
151	3.78	3.44 (3.47/antimycin) (3.42/SQ _i)	n.d.
152, 150	3.78	3.44	3.16
<i>Rhodobacter sphaeroides</i>			
153	3.78	3.49	3.36
<i>Saccharomyces cerevisiae</i>			
141	3.76	3.60	3.49
<i>Bos taurus</i>			
155	3.79	3.43	3.37
153	3.78	3.45	3.35
154	3.78	3.44 (3.47/antimycin)	n.d.
<i>Aquifex aeolicus</i>			
156	3.70	3.45	3.55

derivatives employed by the organism to serve as electron/proton carriers. In organisms using menaquinones, they are usually lower than in organisms that employ ubiquinones.¹⁶⁰ However, a general rule can be drawn, that the hemes b have much lower E_m 's than 2Fe2S and heme c_1 . For this reason, the chain of cofactors built by hemes b is referred to as a low-potential chain, while that formed by the 2Fe2S and heme c_1 is a high-potential chain. The large gap in potential between components of the high- and low-potential chains is crucial for electron bifurcation and efficiency of the catalytic cycle (see section 7.4). Among the hemes b , heme b_L has lower E_m (−290 to −50 mV) than heme b_H (−160 to 100 mV).^{21,160} This difference in E_m values of the hemes b is evolutionary conserved.^{149,160} It is generally assumed to facilitate cross-membrane electron transfer and assist in overcoming the barrier of membrane potential.^{161,162} However, such a function becomes less obvious in light of recent studies demonstrating that the difference in E_m values of the hemes b is not required to support the *in vivo* and *in vitro* functionality of the enzyme.¹⁴⁹ Interestingly, E_m of heme b_H depends on the occupant (and the redox state) of the Q_i site. When the Q_i site is occupied by Q_i , heme b_H has a higher potential than when the site is occupied by SQ_i. This results in a biphasic titration of the heme.¹⁶³ However, when the Q_i site is occupied by an inhibitor, the b_H titrates as a single species.^{163,164} The 2Fe2S and the heme c_1 usually have close values of E_m , both falling in range of 100 to 350 mV.^{21,160} Some of the known values of E_m for each of cofactors in various organisms were included in Table 2.

3.6. Cytochrome b_6f : Specific Structural and Functional Elements

The discussion of structure–function of *Cytc₁* is based on a high resolution (2.50 Å) crystal structure (PDB ID: 4OGQ) of the complex.¹⁷⁴ The complex consists of a 250 kDa heterooligomeric intramembrane lipo-protein complex containing, per monomer, 13 transmembrane α -helices and seven prosthetic groups, the latter consisting of four hemes, one chlorophyll a molecule and one β -carotene. In addition, each monomer contains 23 lipid binding sites, the function of which involves a new area of research into the structure–function of intra-

Table 2. E_m Values of Redox Cofactors in Selected *Cytc₁*

organism (reference), [pH]	E_m value [mV] (concerns <i>Cytc₁</i>)			
	[2Fe2S]	heme c_1	heme b_L	heme b_H ^a
<i>Rhodobacter capsulatus</i>				
150 [7.0]		+295	−138	+43, +134
163 [7.0]			−137	+35, +202
104 [7.0]		+335		
135 [7.0]		+320		
51 [7.0]	+310			
<i>Rhodobacter sphaeroides</i>				
143 [7.0]	+280/+325	+240	−100	+48
170 [7.0]		+237	−87	+41
<i>Rhodospirillum rubrum</i>				
142 [7.4]		+320	−90	−30
<i>Paracoccus denitrificans</i>				
165 [n.d.]	+265	+190	−95	+30, +120
<i>Aquifex aeolicus</i>				
156 [7.0]	+210	+160	−190	−60
<i>Saccharomyces cerevisiae</i>				
166, 167 [7.0]	+285		−60	+82
168 [7.4]	+286	+270	−20	+62
<i>Bos taurus</i>				
21 [7.0]		+238	−83, −60	+26, +85
169 [7.0]	+250	+230	−30	+100

^aTwo values of E_m for heme b_H result from two-component fit to data obtained for *Cytc₁* without antimycin.

membrane proteins, both for *Cytc₁* and the entire field of membrane proteins.

3.6.1. Comparison of Cytochromes f and c_1 . In contrast to the conserved nature of *Cytc₁*, for the *Cytc₁* and *Cytf*, except for the single transmembrane helix (TMH), which binds the subunit to the membrane, the structures are different. The only conserved sequence segment is the CXXCH motif, responsible for covalent binding of the c -type heme. The p side heme binding domain has a completely different secondary structure, β sheet and α -helical, respectively, in *Cytf* and *Cytc₁*.^{171,172} In fact, all three of the p side electron transfer proteins which are part of *Cytc₁*, or interact with it, the ISP, *Cytf*, and PC, which mediate electron transfer between the quinol hydrogen donor and the P700 PSI reaction center are predominantly in the β -conformation. Both *Cytf* and *Cytc₁* have a relatively positive potential, +370 mV and +260 mV, respectively, sufficient to provide an oxidant for the ISP.

3.6.2. Subunit Composition of Cytochrome b_6f . Crystal structures have been obtained for the *Cytc₁* from the green alga, *Chlamydomonas reinhardtii*,⁴¹ and cyanobacteria.^{42,46,65–67,173,174}

The crystal structures of the mitochondrial and bacterial *Cytc₁* contain 11 and 3 or 4 polypeptide subunits, respectively, compared to 8 in the *Cytc₁* from cyanobacteria^{42,174} and the green alga, *C. reinhardtii*.⁴¹ This subunit count refers to those which remain after the purification and crystallization procedures and does not include relatively weakly bound peptides, which may be important for function but are lost during purification and crystallization. Molecular weights (MW) and pI values for the 8 core subunits of *Cytc₁* are summarized in Table 3.

Subunits containing redox prosthetic groups with a high degree of conservation between *Cytc₁* and *Cytc₁* are (i) *Cytc₁* in the *Cytc₁*, which is equivalent in many structure–function

Table 3. Parameters of Subunits of Cyt_b₆f

subunit	MW (kDa)	pI
Cyt ^f ^a	30.9	4.7
Cyt ₆ ^a	24.7	8.5
ISP ^a	19.3	5.3
SubIV ^a	17.5	7.8
PetG ^a	3.9	8.1
PetL ^a	3.2	9.9
PetM ^a	3.5	4.3
PetN ^a	3.3	9.5
FNR ^b	35.4	6.3
PetO ^c	15.1	9.6
PetP ^d	7.4	8.2

^aFrom cyanobacterium *Nostoc* sp. PCC 7120. ^bPetH; resolved on SDS-PAGE, spinach prep; MW, *A. thaliana*. ^cPetO, *C. reinhardtii*. ^dPetP, *Arthrospira platensis*.

aspects to Cyt₆ and subunit IV in the Cyt_b₆f;¹⁷⁵ and (ii) the high potential ($E_{m,7} = +300$ mV) 2Fe2S, often called the “Rieske” protein because of the origin of its discovery.¹⁷⁶ The protein subunit containing the covalently bound *c*-type cytochrome, Cyt^f and Cyt_c₁, respectively, is not conserved between Cyt_b₆f and Cyt_b_c₁ complexes.

3.6.2.1. Four Small Peripheral Subunits, Pet G, L, M, and N.

A unique lattice of four short (3.3–4.1 kDa), single TMH “hydrophobic sticks,” denoted as PetG, PetL, PetM, and PetN (Table 3), provides a hydrophobic lattice, or “picket fence,” around each monomer, a structure that is unique among all known integral membrane protein structures. Of these four subunits, PetM,¹⁷⁷ along with the ISP, is the only subunit among the 13 in the complex that are nuclear-encoded. Specific functions of these four subunits are not defined, although PetL interacts sterically with the TMH of the ISP and may provide a constraint on the membrane-spanning orientation of the latter. The position of much of the lipid in the complex between the Pet picket fence and the conserved Cyt₆-subIV core of the complex suggests a “boundary lipid” function and that the “picket fence” may have been added to the core of the complex relatively late in the evolution of the complex (see section 3.6.3).

3.6.3. Structure and Spectral Properties of Hemes b_p, f, c_n, and 2Fe2S Cluster. High-resolution structures of a C-terminal soluble domain of the 250 residue extrinsic C-terminal domain of Cyt^f,^{171,172} and of the N-terminal soluble domain of the ISP,¹⁷⁸ were obtained prior to their determination in the intact multisubunit complex. The crystallized complex is a symmetric (C₂ symmetry) dimer that consists of eight transmembrane polypeptide subunits in plants, green algae, and cyanobacteria.⁴² The analogous Cyt_b_c₁ consists of eleven subunits in the yeast, PDB ID: 1KYO⁶⁸ and bovine, PDB ID: 1QCK, 1BE3⁶⁰ complex, and three in the complex from the photosynthetic bacterium, *Rhodobacter sphaeroides*.⁶³ In all cases, the dimeric structure of the complex is required for a physiologically significant electron transfer activity, 250–400 electrons transferred (Cyt^f/sec)⁻¹.^{179–181} This is possibly because of a defined intermonomer quinol entry pathway.

A ribbon diagram of Cyt_b₆f (PDB ID: 2ZT9, 4H44, 4OGQ) derived from crystal structure analysis of the cyanobacterium *Nostoc* sp. PCC 7120,^{65,66,174} the latter study at 2.5 Å resolution, is shown in 2 views differing by a 180° rotation to display more clearly the arrangement of the 8 subunits that span the membrane with 13 TMH per monomer containing 7 prosthetic groups, including 5 with redox function consisting of 4 hemes,

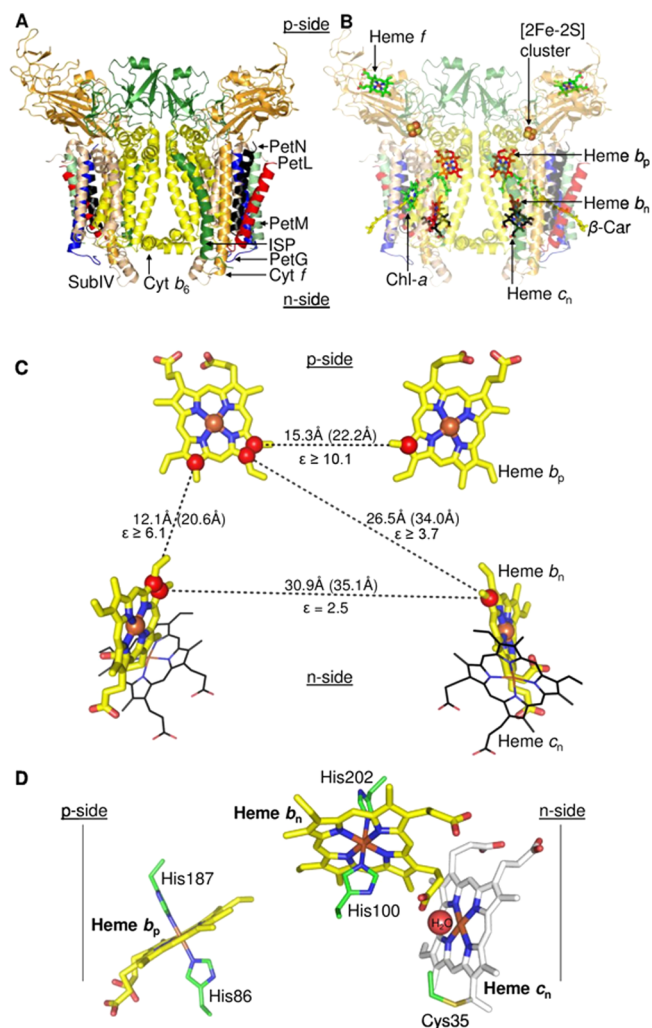


Figure 10. Dimeric cytochrome *b*₆*f* complex. (A) Polypeptide subunits from the cyanobacterium *Nostoc* sp. PCC 7120 (PDB ID: 4OGQ) are shown in ribbon format: Cyt_b₆ (yellow), subIV (light brown), Cyt^f (orange), ISP (dark green), PetL (red), PetM (light green), PetG (blue), PetN (black). (B) Prosthetic groups of Cyt_b₆*f*. Transmembrane hemes *b*_p, *b*_n (red/blue), and *c*_n (black/blue) are shown as sticks. On the *p* side, heme *f* (green/blue) is shown as sticks, the [2Fe-2S] cluster as spheres (brown/yellow), and the Chl-*a* (green/blue) and β -car (yellow) as sticks. (C) Heme-heme distances within the transmembrane domain of the complex (PDB ID: 4OGQ). Distances shown as black dashes. Heme edge-edge and center-center (Fe-Fe) distances are shown, respectively, outside and inside parentheses (selected atoms shown as spheres). The dielectric constant, ϵ_{ij} , between each pair of hemes, $\epsilon_{n1,p1}$, $\epsilon_{n1,p2}$, $\epsilon_{n2,p1}$, etc.,¹⁸⁴ is shown. (D) Transmembrane heme ligation in Cyt_b₆*f*. The central Fe atom of heme *b*_p and *b*_n is axially ligated, respectively, by residues His86/His187 and His100/His202 which bridge the B and D TMH of Cyt_b. Heme *c*_n is covalently attached to the protein via Cys35. Heme *c*_n is unique as it lacks an amino acid axial ligand, and the central Fe-atom is penta-coordinated. The sole ligand of heme *c*_n is provided by H₂O or OH⁻ on the heme *b*_n side. Fe of heme *c*_n is separated by 4.0 Å from a propionate oxygen of heme *b*_n, which results in electronic coupling, a high spin $g = 12$ EPR signal,^{43,185} and an oxidase-like reaction with nitric oxide.¹⁸⁶ Electrochemically positive, negative sides of membrane labeled *p*, *n*. Reprinted with permission from ref 17. Copyright 2016 Springer Nature.

one 2Fe2S, one chlorophyll *a*,¹⁸² and one β -carotene¹⁸³ (Figure 10A,B and Figure 11). These features were confirmed in a lower resolution (3.6 Å) cryo-EM structure of the spinach Cyt_b₆*f*.⁷³

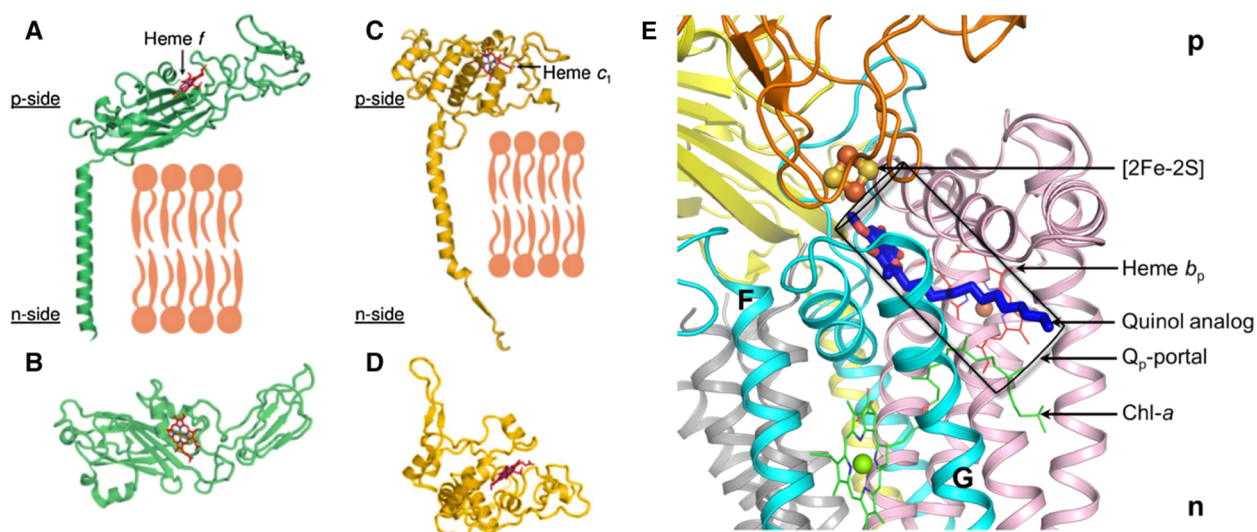


Figure 11. High potential electron acceptor of Cyt-*bc*: (A, B) Cyt f of Cyt b_6f and (C, D) Cyt c_1 of Cyt bc_1 complex. Cyt f and Cyt c_1 are attached to the respective complexes and membrane through one TMH. Cyt f binds *c*-type heme (heme f , red/blue sticks) in the β -sheet extrinsic domain. Cyt f extrinsic domain of Cyt c_1 , with *c*-type heme (heme c_1 , red/blue sticks) is mostly α -helical. B and D rotated 90° about horizontal axis relative to A, C. (E) Tridecyl-stigmatellin (TDS, blue sticks), bound in an 11 Å long channel of Cyt b_6 (purple) terminating proximal to the 2Fe2S cluster. The Q_p -portal in Cyt b_6f is marked as the black rectangle. ISP-HD is shown as orange ribbons. A chlorophyll molecule (Chl a), inserted between F and G helices of subunit IV (cyan), using its phytyl tail, functions as a gate for quinol/quinone traffic in the Q_p -portal. Drawing by S. Saif Hasan.

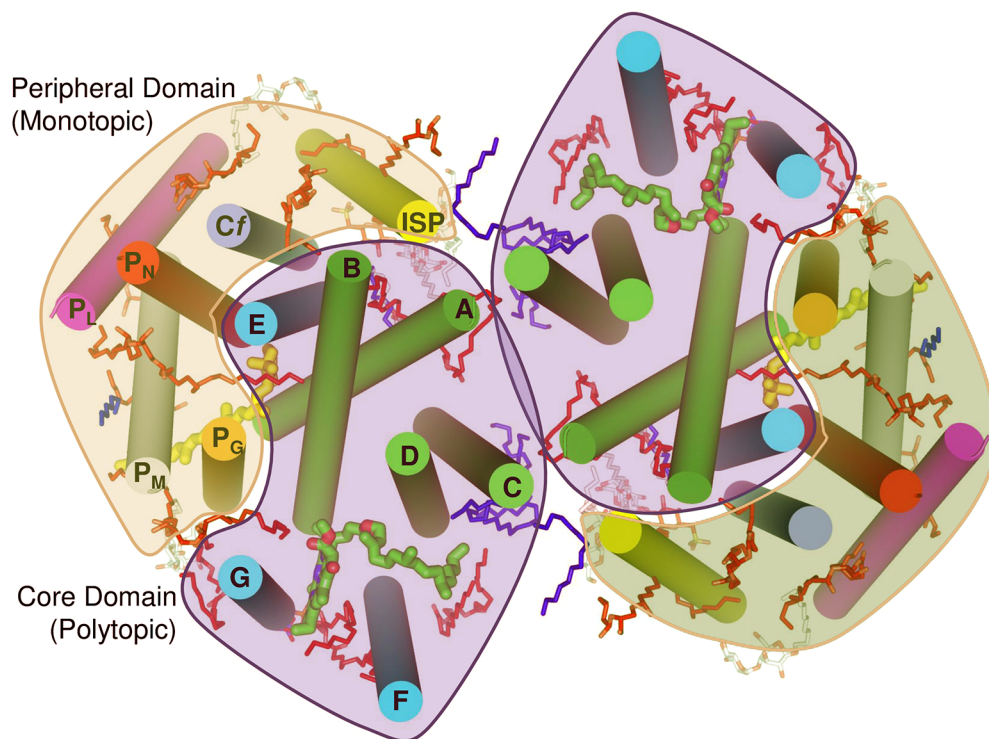


Figure 12. Transmembrane helices and distribution of lipid in Cyt b_6f complex (Figure drawn by S. Saif Hasan). Reprinted with permission from ref 17. Copyright 2016 Springer Nature.

3.6.3.1. Unique Chlorophyll *a* and β -Carotene. The presence of a single chlorophyll a ^{182,187,188} and β -carotene¹⁸³ in each monomer of Cyt b_6f is enigmatic. The β -carotene is separated by 14 Å from the chlorophyll,^{41,42} too large to allow β -carotene to quench a chlorophyll excited triplet state.¹⁸⁹ (ii) The β -carotene protrudes by approximately 11 Å from the complex between the TMH of PetG and PetM.

3.6.3.2. Transmembrane Hemes, b_n and b_p . The four TMH of the Cyt b_6 are connected by loops at the p and n side

membrane interfaces. SubIV (~ 17 kDa) has three TMH (E–G) that form a p side saddle around the four helix bundle of Cyt b_6 . Helix E of SubIV is located in proximity to the A- and B-helices of Cyt b_6 , while the F- and G-TMH span the four helix bundle, close, respectively, to the C-, D-, and B-TMH (Figure 12). The C-terminus of the E-TMH is separated from the N-terminus of the F-TMH by a distance of ~ 40 Å, which is bridged by the p side *ef*-loop. This seven TMH assembly forms the conserved

core of Cytb_{6f} , which is bounded in each monomer by the four subunit hydrophobic “picket fence”.

The arrangement of the two pairs of transmembrane b -hemes, b_p and b_n , with interheme edge–edge and center–center (Fe–Fe) distances (in parentheses) is shown (Figure 10C), along with the heterogeneity of the interheme dielectric constants,¹⁸⁴ and the complex of heme b_n with a skeleton of the covalently bound c -type heme c_n .^{43,185,186,190,191} The heme b_n – c_n complex, a unique feature of the Cytb_{6f} compared to the Cytbc_1 , in which the close proximity of the two hemes results in sharing of the 3d electronic shells is displayed in a $g = 12$ EPR signal.^{43,185}

3.6.3.3. Hemes, b_n and b_p , Oxidation–Reduction Potentials. Determination of the oxidation–reduction potentials of these hemes in Cytbc_1 is consistent in showing a separation of 100–150 mV between the E_m values of the two hemes, which are thus often labeled b_H and b_L (high and low potential hemes). For the two hemes in the Cytb_{6f} , there is disagreement as to whether the E_m values of the two hemes are¹⁹¹ or are not^{40,192} separable in a redox titration of thylakoid membranes. A simulation shows that a midpoint potential difference of 50 mV or less of a one electron titration cannot be resolved. For the isolated complex, the midpoint potentials of the two hemes in the Cytb_{6f} are separated by approximately 90 mV.

3.6.3.4. Reducibility of b Hemes: Heterogeneity of Internal Dielectric Constants. Excitonically split circular dichroism (CD) spectra of the Cytbc_1 ¹⁹³ and the Cytb_{6f} ^{184,194} arise from interactions of the reduced hemes. Determination of the time course of heme reduction and the onset of the split CD spectra for the isolated complex shows that the heme pair that is preferentially reduced is the intramonomer pair, b_p and b_n . This result contrasts with that which is expected. If heme b_n , whatever its exact redox potential, has a more positive potential in isolated Cytb_{6f} than heme b_p , the two hemes b_n should be preferentially reduced under equilibrium conditions. The straightforward explanation is that the protein medium between hemes b_p and b_n is more polarizable, that is, has a higher dielectric constant, than the medium between the two hemes b_n ¹⁸⁴ implying that the dielectric constant in the complex is heterogeneous and anisotropic.

The unique heme c_n at the n side quinone (Q_n) binding site of Cytb_{6f} ,^{173,191} located in close (4 Å) proximity to heme b_n , constitutes a major structure difference between Cytbc_1 and Cytb_{6f} complexes. Consequently, it would also imply a difference, compared to the mitochondrial and bacterial Cytbc_1 , in the details of the involvement of heme b_n in the transmembrane electron transport pathway [*n.b.*, heme c_n is designated heme c_i in the *C. reinhardtii* crystal structure, which first emphasized its unique existence in the structure of Cytb_{6f} ⁴¹].

Heme c_n has no axial ligand on the heme surface facing the intermonomer cavity. As shown by EPR studies, which document its open axial ligand position,¹⁸⁶ and cocrystallization of the Cytb_{6f} complex with quinone analog inhibitors,¹⁷³ it has been inferred that heme c_n serves as the n side quinone binding site (Q_n site). The Q_n site is located closer to the membrane–water interface in Cytb_{6f} complex than in the respiratory Cytbc_1 , as noted in the original crystal structure.⁴¹ This surface-proximal location of the Q_n site implies that a short pathway may suffice for proton conduction to the n side bound quinone from the n side aqueous phase. The crystal structure of Cytb_{6f} from the filamentous cyanobacterium *Nostoc* PCC 7120, revealed a unique anhydrous Asp20 → Arg207 (Cytb_6) pathway for proton

conduction from the n side aqueous phase to the Q_n site for reduction and quinone protonation.⁶⁶

3.6.3.5. ISP Electron Transfer: A p Side Conformation/Mobility Problem. A remaining structure–function problem is that the closest approach distance of the Cytf heme to 2Fe2S in Cytb_{6f} is 28 Å, which is much too large to support physiologically meaningful millisecond electron transfer rates.^{195,196} How, then, does 2Fe2S of ISP transfer electrons to Cytf ? A major gap in understanding of the p side electron transfer reactions for the Cytb_{6f} results from the absence of the structure data that would allow kinetically competent electron transfer from 2Fe-2S to the heme of Cytf . Given the documented conformation change determined from crystal structure data for the avian mitochondrial Cytbc_1 (see section 3.4 for details), electron transfer from 2Fe2S to the Cytf heme must involve a rotational–translational conformational change in the ISP.⁶⁶

3.6.4. Lipid Content and Other Subunits. 3.6.4.1. Lipids in the Cytb_{6f} Lipoprotein Complex. ‘Boundary lipids’ define a domain structure (Figure 12). Because the conserved Cytb_6 -SubIV core of the complex is separated by a lipid layer from the “picket fence”, it is implied, as noted earlier, that the “picket fence,” was added to the core structure at a later stage in the evolution of the Cytb_{6f} , perhaps to facilitate interaction with the reaction center complexes. As noted earlier, the β -carotene, which protrudes from the surface of the picket fence, may act as a “latch” to facilitate supercomplex formation with the PSI reaction center complex.¹⁹⁷

3.6.4.2. Lipid Content. The dominant lipid species in plant Cytb_{6f} are monogalactosyl-diacylglycerol (MGDG), digalactosyl-diacylglycerol (DGDG), phosphatidyl-glycerol (PG), and sulfoquinovosyl diacylglycerol (SQDG). The galactolipids (MGDG, DGDG, and SQDG) and phospholipids dilinolenoyl-, phosphatidyl glycerol (DLPG), 1,2-dioleoylphosphatidyl-glycerol (DOPG), and 1,2-dioleoyl-*sn*-glycerol-3-phosphatidylcholine DOPC) stabilize the Cytb_{6f} to a varying extent.¹⁹⁸

3.6.4.3. PGR1 Components. A 35.7 kDa ($pK = 5.2$) protein, “PgrL1”, is present at unknown stoichiometry in the PSI supercomplex *C. reinhardtii*,¹⁹⁷ and at a stoichiometry comparable to, although smaller (0.5:1), that of ISP in *Arabidopsis thaliana*, and has been inferred to be the ferredoxin-quinone reductase.¹⁹⁹ The absence of the protein results in a partial decrease of the chlorophyll fluorescence yield that results from reduction of the quinone pool. The redox function is believed to be derived from the six cysteine residues in the protein, perhaps in conjunction with iron that is present in the preparation. PgrL1 is also inferred to be able to bind to the Cytb_{6f} ,¹⁹⁹ although it has not been detected in mass spectroscopic analysis of isolated Cytb_{6f} .²⁰⁰ In addition, it is noted: (a) the fluorescence yield effects ascribed to PgrL1 are perhaps not quantitative indicators of an obligatory function in the ETC, as they involve changes of a factor of 2–3 on a time scale of 10 s, approximately a factor of 1000-times slower than the rate-limiting step of electron transport in this region of the ETC; (b) the rate of P700 reduction, a standard kinetically competent assay for cyclic electron transport, in the presence and absence of the peptide has not been reported; (c) details of the chemical nature and quantitative properties of the hexaCys-Fe redox moiety in PgrL1, proposed to serve as the redox group responsible for ferredoxin-quinone reductase (FQR) activity, are not presently available. The significance of the PgrL1 components may need to be re-evaluated in light of the recent information on their very diminished stoichiometry relative to the known electron transport components.²⁰¹

3.6.5. Q Cycle in Cytochrome b_6f : Mechanism and Controversies. The observation of oxidant-induced reduction²⁰² in $Cytc_1$ (see details in section 7), and measurement of a greater than unity ratio of coupled protons translocated to electrons transferred, $H^+/e^- > 1$, were important in the formulation of the “modified Q cycle” mechanism,³⁹ whose general formulation and application to photosynthetic membranes²⁷ followed 15 years after the original inference of the chemiosmotic concept of membrane energization.²⁸ The demonstration of oxidant-induced reduction of $Cytb$ heme in the mitochondrial $Cytc_1$ and the requirement in this electron transfer reaction for the high potential (ca. + 0.25 V) $2Fe_2S$ was elucidated in studies by B. Trumpower.²⁰³ An apparently anomalous reduction of the $Cytb$ component was observed in a preparation of mitochondrial membrane protein “complex III”. Support for the Q cycle model of proton translocation in the mitochondrial $Cytc_1$ was provided in studies by Wikstrom and Saraste,²⁰⁴ and Rich.²⁰⁵

Support for the application of Q cycle model to $Cytc_1$ has been well documented and discussed extensively in refs.^{1,2,13,39,117,118,206,207} Studies on function and, lately, also the structure of the related $Cytb_6f$ functioning in chloroplasts, green algae, and cyanobacteria have been reviewed in the past decade.^{17,19,22,184,209–216}

While there is a general consensus on the occurrence of the “modified Q cycle” in the case of $Cytc_1$ (see section 3.2 for details), experimental evidence exists that is not completely in agreement with this hypothesis in the case of $Cytb_6f$. In the following, we summarize this evidence, compare contrasting results, and summarize different interpretations of the results.

Arguments that imply that the PQ/PQH₂ cycle in $Cytb_6f$ is different from the “modified Q cycle” proposed for regeneration of UQH₂ through function of $Cytc_1$ in the respiratory chain and photosynthetic bacteria are:

- (i) The presence of an additional heme c_n , which could act as a PQ reductase. On the basis of its redox properties and location within the complex, this heme could catalyze the injection of an electron into the quinone binding side using stromal reductants as a donor (i.e., the presence of ferredoxin:NADP⁺ reductase (FNR) bound to purified plant (spinach) $Cytb_6f$, see further). The electronic coupling between hemes b_n and c_n would imply that PQ reduction need not proceed through a semiquinone intermediate but perhaps cooperatively through hemes b_n and c_n , providing protection against the formation of superoxide and other reactive oxygen species. This mechanism is not compatible with the modified Q cycle mechanism, but, as introduced in section 3.2, it is actually consistent with the original mechanism of the Q cycle as proposed by Mitchell (see Mulikidjanian¹⁹ for a discussion) (see also Figure 4). The possibility of direct injection of stromal electron in the b hemes could also account for another observation that is not entirely compatible with the modified Q cycle in $Cytb_6f$.
- (ii) The “slow” electrochromic phase attributed to oxidation of the PSQ in the Q_p site and transfer of its electron across part of the low dielectric membrane to reduce the intramembrane b hemes is also observed when the hemes were chemically reduced and therefore not able to function as an electron acceptor.¹⁹² In principle, injecting 1 electron into the stromal site via the heme c_n would allow oxidation of one b heme, generating 1 PQH₂ and

regenerating the Q cycle (the so-called “activated” Q cycle mechanism¹⁹). Note, however, that another explanation has been proposed by Joliot and Joliot, who suggest that the slow electrochromic phase observed under reducing condition could reflect the transmembrane movement of a charged SQ (the SQ cycle hypothesis,²¹⁷ see ref 218 for a different view). This mechanism may represent an adaptation to reducing conditions when no Q is available at the Q_n site. Note, however, that some inhibitors of $Cytb_6f$ (NQNO, stigmatellin and MOA-stilbene) act on the n side at the side of heme c_n that faces the quinone-exchange cavity, as shown in crystal structure¹⁷³ and prevent oxidant-induced reduction in $Cytb_6f$, in agreement with the modified Q cycle hypothesis.

- (iii) The initial slope of the “slow” electrochromic phase shows a pronounced isotopic effect, being slowed 4-fold by a H₂O/D₂O substitution, in contrast to the redox-reactions of $Cytf$ and $Cytb_6$ that were only slightly affected.²¹⁹ These findings have led to the hypothesis that proton pumping across $Cytb_6f$ could be triggered by the oxidation of PQH₂,²²⁰ an idea that is not conceived in the frame of the “modified” Q cycle, but that is supported by the analysis of $Cytb_6f$ mutants of *Chlamydomonas*.²²¹
- (iv) One component of the “driving force” for the Q cycle in mitochondria and the purple photosynthetic bacteria is the pronounced difference (>100 mV) in the redox potentials of the two b-type hemes, (i.e., b_L and b_H), which span the membrane. However, it has not been possible, in redox titrations done *in situ*, that is, in thylakoid membranes to define through anaerobic redox titrations a difference in midpoint redox potentials of the two b hemes, b_p and b_n .^{40,192,222} More recently, however, Alic and colleagues used a different approach for redox titrations and found E_m differences between the two b hemes of isolated $Cytb_6f$ from *Chlamydomonas* (−130 mV and −35 mV),¹⁹¹ which are closer to those predicted by the “modified” Q cycle. Thus, an E_m difference is seen for the isolated $Cytb_6f$ complex, but this difference is not clear in titrations done *in situ*, in membrane preparations.
- (v) Studies on the kinetics of heme b reduction show that an intramonomer pair (hemes b_n and b_p) is reduced first, rather than the two hemes b_n being preferentially reduced as implied by the Q cycle.¹⁸⁴ Moreover, reduction of the two b hemes is not observed with repetitive laser flashes.⁴⁰
- (vi) The existence of CET in oxygenic photosynthesis could help to maintain a high H^+/e^- ratio, as required for proper CO₂ assimilation, thereby making the occurrence of a Q cycle less stringent in oxygenic photosynthesis than in respiration. One of the main purposes of the Q cycle is to couple electron and proton transfer generating a H^+/e^- ratio = 2 for proton translocation across the complex. Thus, the transfer through the high potential chain of the $Cytb_6f$ of the 4 electrons arising from water splitting and oxygen evolution can result in the translocation of 8 protons into the chloroplast lumen which, together with the 4 translocated protons released into the lumen with each O₂ molecule, would provide 12 of the 14 H⁺ needed to drive a full rotation of the rotatory c-ring of the chloroplast ATP synthase and therefore the synthesis of the three ATP molecules needed to fix a CO₂ molecule. In plants, the additional 2 H⁺ could be generated by CET, assuming that it runs at a prescribed rate of 25% of the linear noncyclic pathway. Applying the same reasoning to

the cyanobacterium, *Arthrospira platensis*, where the ATP synthase *c*-ring contains 15 subunits, implies that CET would have to run at 3/8 or 37.5% of the rate of the linear pathway to generate the additional three H^+ needed to drive a complete rotation. However, no such percentage of CET is observed in most photosynthetic organisms, at least under steady state conditions (see section 10). This suggests that CET alone is not sufficient to provide the “extra” H^+ for ATP synthesis. Consistent with this conclusion, Kramer and colleagues measured the H^+/e^- ratio illumination in intact tobacco leaves and found that it was constant under low to saturating illumination. Therefore, they inferred that this ratio was maintained by a continuously engaged, proton-pumping Q cycle at *Cytb₆f*.²²³

Although the Q cycle mechanism has a readily conceived role in contributing to the transmembrane proton flux required to provide ATP levels commensurate with the need for CO_2 assimilation, it may be suggested that the Q cycle mechanism applied to *Cytb₆f* is not obligatory (see however Cape et al.²²⁴ for a different conclusion). An alternative mechanism is a membrane Bohr effect, a mechanism that is prominent in the description of the mechanism of proton pumping in the classical bacteriorhodopsin system,²²⁵ and which has been applied to the problem of proton translocation in the mitochondrial cytochrome *c* oxidase.²²⁶

3.6.6. Additional Electron Path Related to Cyclic Electron Transfer in Photosynthesis. Electrons generated at the PSI reducing side can be reinjected into its donor side via the CET pathway. Discovered by Arnon in the 50s,²²⁷ this process is now considered as a relevant mechanism to counterbalance over-reduction of the PSI acceptor side²²⁸ and to inject “extra” protons into the thylakoid lumen, to adjust the ATP/NADPH ratio for CO_2 assimilation. Although the ratio of ATP/NADPH generated by LET is still uncertain,²²⁹ it could be insufficient to fuel CO_2 accumulation in chloroplasts and its assimilation via the Calvin, Benson, and Bassham cycle (see Allen²³⁰ for a discussion). In *viridiplantae* (including green algae and higher plants), CET could be the main route to optimize this process by bypassing NADPH production while permitting the formation of the pmf and therefore ATP synthesis.

Two main pathways have been proposed for CET (see section 10 for further details). The first one involves the activity of a chloroplast NAD(P)H dehydrogenase (NDH) complex (review in Peltier et al.²³¹). In plants, this enzyme has similar characteristics to the mitochondrial complex I, while mainly sharing features with bacterial complex one in algae.²³² The plant complex would mainly use Fd as an electron donor, while the algal counterpart (Nda2 complex) uses NADPH as a source of electrons in the green alga *Chlamydomonas reinhardtii*.²³¹

The second CET pathway would correspond to the so-called ferredoxin-quinone reductase complex (FQR), the existence of which was proposed by Bendall and co-workers in the 90s,²³³ based on the effect of antimycin, a putative inhibitor of this complex, on photosynthetic electron flow. An alternate target of antimycin in the chloroplast has been proposed by Sugimoto and colleagues as Pgr5, a thylakoid protein²³⁴ previously identified as a component of the CET pathway by a genetic screening or the *Arabidopsis thaliana*.²³⁵ The FQR complex itself has been putatively identified as a membrane complex,¹⁹⁹ containing Pgr5 as well as PgrL1, another protein previously invoked as an essential component of the CET machinery in

plants.²³⁶ However, see the critique of these studies in section 3.6.4.

Alternatively, the FQR may correspond to *Cytb₆f* itself, mediating electron flow from reduced Fd to the $PQ(H_2)$ pool through the additional *c* heme in the stromal pocket.^{41,42} This process could take place if there is a significant interaction allowing electron transfer between the cytochrome complex and the ferredoxin-NADP reductase (FNR) enzyme (see section 4.3).

4. CHARACTERISTICS OF SUBSTRATES FOR CYTOCHROME *BC₁* AND *B₆F*

As a main function of *Cyt-bc* is the generation of proton motive force utilizing energy associated with electron transfer from low-potential electron donors (membranous pool of quinone derivatives) to water-soluble *c*-type cytochrome (*c*, *c₂*, *c₆*) or plastocyanin, it is worth introducing basic information on the substrates that are used by these enzymes. A brief summary on structure and redox properties of quinones is especially important as proton translocation and electronic bifurcation is largely associated with quinone chemistry.

4.1. Basic Redox Properties of Quinones

A role of quinones in electron transfer between membranous respiratory complexes was first proposed by Crane et al. in 1957.^{237,238} It was shown that extraction of relatively low-weight molecules, ubiquinones, from the membrane completely abolished the process of electron transfer within the mitochondrial respiratory chain.²³⁹ In biology, the most widespread quinones belong to a family of 1,4-benzoquinone derivatives. While in eukaryotic cells, quinones are generally restricted to ubiquinones (in mitochondria) and plastoquinones (in chloroplasts), prokaryotic organisms can use several other quinone derivatives as membranous electron carriers. Besides ubiquinones and plastoquinones that are commonly found in bacteria or cyanobacteria, respectively, there is a relatively large group encompassing naphthoquinone derivatives, menaquinones.²⁴⁰ In some bacteria, there are numerous, less common quinones that are based on other chemical structures of the redox-active rings. These are not discussed in this review. Interested readers are referred to a comprehensive review on biological quinones.²⁴¹

Despite differences in chemical structure of the redox-active quinone rings, a common feature shared between of mena-, ubi-, and plastoquinones is a relatively long hydrocarbon chain consisting of several isoprenoid fragments. This imposes a high level of hydrophobicity on natural quinones. The number of isoprenoid fragments in the chains is usually given by a number put after the name of the respective quinone.²⁴¹ For example, UQ-10 means that the ubiquinone possess the tail built of 10 isoprene molecules. The extent of hydrophobicity of quinones is expressed by a large partition coefficient ($\log_{10}P$) for organic/water mixtures such as octanol and water.²⁴² Quinol forms are generally slightly more hydrophilic than the respective quinone forms. In case of ubiquinone-1 or plastoquinone-1, $\log_{10}P$ exceeds 3 and further increase in the length of isoprenoid tail increases the hydrophobicity, forcing quinone molecules to be constrained to a lipid environment.²⁴² The natural quinones engaged in electron transfer usually have the hydrophobic tail built of 7–10 isoprenoid moieties, depending on the organism and very rarely exceeds 10. In plastoquinones, the number of isoprenoids is usually 9, while in mammalian mitochondria, ubiquinones usually have 9 or 10. For menaquinones, the length

of the chain most often varies between 7 and 8.²⁴¹ Comparison of the chemical structure of menaquinone-7, ubiquinone-10, and plastoquinone-9 is presented in Figure 13.

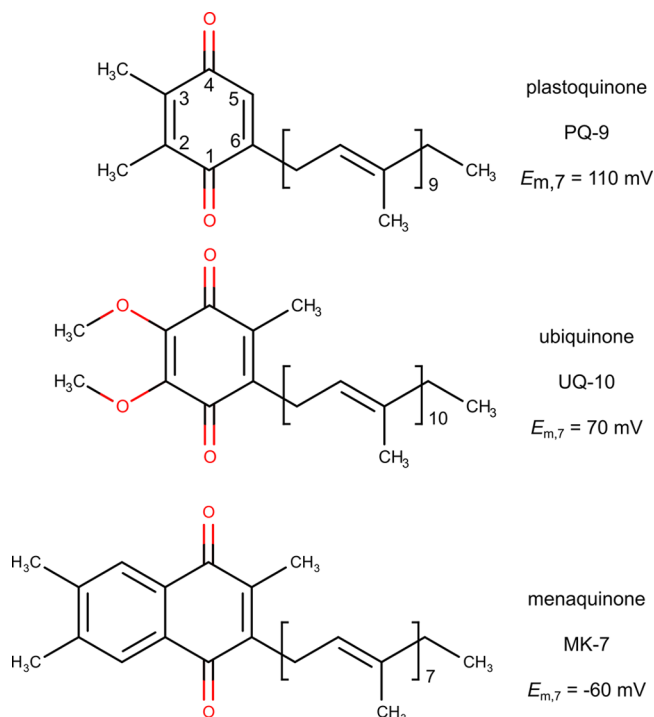


Figure 13. Chemical structures of biologically important quinones with a different number of isoprenoid molecules comprising the hydrophobic side chains. From top to bottom there are plastoquinone-9 (PQ-9), ubiquinone-10 (UQ-10), and menaquinone-7 (MK-7). The $E_{m,7}$ values corresponds to the average redox midpoint potentials at pH 7 for the respective Q/QH₂ couples.

Another common feature that makes quinones important members of nearly all enzymatic processes of electron exchange between the membranous enzymes is their ability to undergo reversible two-electron, two-proton reactions of oxidation or reduction without damaging the chemical structure of the redox-active ring.²⁴³ This reaction can be generally described as



where Q stands for quinone (fully oxidized form) and QH₂ for quinol or hydroquinone (fully reduced form).

The complete oxidation/reduction reaction of eq 1 can be divided into two, one-electron steps involving a semiquinone (SQ) intermediate:



Eqs 2 and 3 assume that reduction of quinone leads to the semiquinone anion, and further reduction of SQ⁻ is coupled to the protonation of the reduced quinone. This particular proton/electron sequence is supported by the fact, that pK of neutral semiquinone (SQH) is significantly lower than the first pK (pK₁) of the first proton dissociation of QH₂.²⁴⁴

The average redox midpoint potential (E_m) of Q/QH₂ couple is equal to the arithmetic mean of redox midpoint potentials of the Q/SQ⁻ and SQ⁻/QH₂ couples:²⁴⁵

$$E_m(Q/QH_2) = 0.5(E_1 + E_2) \quad (4)$$

where E_1 and E_2 represent E_m values of Q/SQ⁻ and SQ⁻/QH₂ couples, respectively.

The average redox potential of the Q/QH₂ couple depends on the type of the redox-active ring of a particular quinone molecule and it generally decreases upon substituting the 2,3 and 5,6 positions of the ring with a methyl group.²⁴⁶ Conversely, when the ring is substituted with a group that has high electronegativity such as chlorine or bromine, the E_m of Q/QH₂ rises considerably.^{246–248} For example, when one considers a simple case of 1,4-benzoquinone, its average redox midpoint potential at pH 7 ($E_{m,7}$) is approximately +300 mV and decreases to +230 and +176 mV upon attachment of one or two methyl groups to the ring at position 2 and 2,3, respectively.²⁴⁶ On the other hand, substituting the ring with chlorine at position 2 and 5 increases the E_m to approximately +540 mV. Attachment of methoxy groups to the ring also increases the measured E_m in relation to 1,4-benzoquinone. For example, the E_m of 2,6-dimethoxy-1,4-benzoquinone is approximately +340 mV, which is higher by about 200 mV than the E_m of 2,6-dimethyl-1,4-benzoquinone. The redox midpoint potentials of quinones belonging to the family of menaquinones are significantly lower than those of benzoquinone derivatives, for example the $E_{m,7}$ of 2-methyl-1,4-naphthoquinone (menadione) is only -5 mV, which is much lower than +230 mV of methyl-1,4-benzoquinone. Because of such a low redox midpoint potentials of menaquinones, they are considered as “ancient devices” for electron transport in living organisms recruited at early stages of evolution by some eubacteria or archaeobacteria, at a time, when the atmosphere on Earth was anaerobic.^{160,241}

This general rule of changes in the E_m values of quinones containing different groups substituted to the ring holds true for natural, biologically active quinones that are used by living organisms as substrates for Cyt-*bc*. It means that the E_m of Q/QH₂ couples increases in the order: menaquinone/menaquinol ($E_{m,7}[MK/MKH_2] = -60$ mV), ubiquinone/ubiquinol ($E_{m,7}[UQ/UQH_2] = 70$ mV), and plastoquinone/plastoquinol ($E_{m,7}[PQ/PQH_2] = 110$ mV) (see Figure 13).

As the redox reactions of quinones involve 3 electron and 3 protonation states, the theoretical number of possible states is 9. However, from all these possible states (electrons and protons), QH⁺ (protonated quinone), QH₂²⁺ (doubly protonated quinone), and SQH₂⁺ (doubly protonated semiquinone) are not possible since their expected pK values are less than 0.^{244,249} The typical pK₁ and pK₂ values for the first deprotonation of QH₂, leading to QH⁻, and the second deprotonation, leading to Q²⁻ are separated by 2, thus pK₂ = pK₁ + 2. Interestingly, pK₁ and pK₂ are inversely correlated with the redox midpoint potential of Q/SQ⁻ couples. For mena-, ubi-, and plastoquinone pK₁ is in the range 9–11.²⁴⁶ For semiquinone, the pK value also depends on the E_m of Q/SQ⁻ couple with typical values falling in the range 4–5.²⁴⁴

4.1.1. Stability and Reactivity of Semiquinone Radical with Molecular Oxygen. A potential danger associated with quinone redox reactions, not only those catalyzed by enzymes, is the possibility of reaction of SQ with molecular oxygen:^{248,250–254}

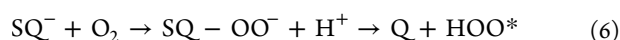


Although this reaction is reversible, occurrence of superoxide dismutation or superoxide scavenging by, for example, Cyt_c or PC, will shift the equilibrium to the right side.²⁴⁶ A superoxide

release during the enzymatic catalysis by *Cytc₁* or *Cytc_{6f}* is considered deleterious and leads to a decrease in energetic efficiency of the enzyme, as generation of superoxide decouples the oxidation of QH₂ at the Q_o/Q_p site with Q reduction at the Q_i/Q_n site. Thus, this side reaction decreases the number of protons translocated across the membrane during the catalytic cycle. However, in living cells, some portion of O₂^{•-} can be scavenged by electron donation from the radical to the oxidized Cyt^c²⁵⁵ or PC²⁵⁶ with a relatively large second order rate constant. Such scavenging of superoxide can be considered as a protection and partial remedy to energy-wasting side reactions, as the electrons that leak to oxygen can be subsequently used to generate pmf at the level of cytochrome *c* oxidase (CcO) (complex IV).²⁵⁷

The second-order reaction rate constant for the reaction of SQ⁻ with O₂ depends on the E_m value of the Q/SQ⁻ couple and generally increases when the potential of the E_m of the Q/SQ⁻ couple decreases. When E_m(Q/SQ⁻) is more negative than -200 mV, the reaction of SQ⁻ with dioxygen becomes diffusion-limited.²⁴⁶

The mechanism of reduction of O₂ to O₂^{•-} by the SQ⁻ radical is generally viewed as electron transfer process that follows the Marcus theory of electron transfer.²⁵² An alternative mechanism proposes a chemical reaction of addition of oxygen to the SQ⁻ ring followed by release of the superoxide anion, which after protonation changes to the neutral, peroxy radical.²⁵³



Valgimigli et al. showed evidence that reaction 6 is significantly slower in solutions in which a semiquinone can form H bonds with molecules of the solvent.²⁵³ Therefore, it can be supposed that formation of a hydrogen bond to the SQ⁻ may be protective against superoxide formation in catalytic sites of enzymes (see section 7.5).

4.1.2. Stability Constant of Semiquinone. Under equilibrium conditions, Q, QH₂, and SQ are linked by a reaction of comproportionation (or in reverse direction by disproportionation):²⁴⁶



The equilibrium constant of this reaction defines the stability constant (K_s) of SQ⁻, which depends on the difference in E_m values of Q/SQ⁻ (E₁) and SQ⁻/QH₂ (E₂), couples:^{258–260}

$$\begin{aligned} K_s &= \frac{[\text{SQ}^-]^2 [\text{H}^+]^2}{[\text{Q}][\text{QH}_2]} = 10^{(E_m(\text{Q}/\text{SQ}) - E_m(\text{SQ}/\text{QH}_2))/59.1} \\ &= 10^{(E_1 - E_2)/59.1} \end{aligned} \quad (8)$$

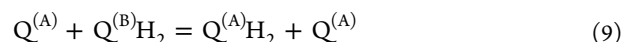
The stability constant for SQ defines the equilibrium between concentrations of Q/SQ⁻/QH₂ in this triad. It means that in equimolar mixtures of Q and QH₂, some SQ⁻ is also present but its relative amount depends on the equilibrium constant K_s. For some chlorine substituted quinones, K_s can be higher than 1.²⁴⁷ However, for biologically important quinone derivatives, the E_m of the Q/SQ⁻ couple is more negative than SQ⁻/QH₂; thus, the exponent in the eq 8 is always less than zero (and therefore K_s < 1). Any further increase in the split between the E_m values of these two couples (E₁ - E₂) leads to a decrease in the equilibrium concentration of SQ⁻ in solutions containing a mixture of Q and QH₂ forms. This, on one hand, increases the rate of reaction of SQ⁻ with O₂ but on the other hand decreases

the probability of superoxide generation as the concentration of SQ⁻ decreases.

Despite the fact that K_s for SQ⁻ is used in chemistry of quinones under equilibrium conditions, it is also widely used to describe the properties of semiquinones that are generated at catalytic sites of enzymes such as the Q_o/Q_p and Q_i/Q_n site of *Cytc* during catalysis.^{261–264}

The concentration of quinones within the membrane is usually expressed as the number of molecules (Q and QH₂) versus the number of CcO molecules. In mammal and plant mitochondria the number of quinones per CcO is around 6–8, while it is much larger in yeast mitochondria (~38 per CcO). In purple bacteria the estimated number of quinone molecules per reaction center (RC) is also quite large, in the order of 15–30. The number of quinones in humans depends significantly on the tissue and the age. The content of Q in mitochondria increases during the first 20 years and after that time gradually decreases to the level even lower than after birth (see discussion in ref 13).

A significant content of the quinone molecules in the membrane may suggest that the comproportionation reactions should be very efficient leading to generation of a significant amount of SQ, which after dismutation would lead to the process of electron self-exchange:



However, such a reaction is very unlikely in membranes as it requires at least two steps that involve reactions of protonation and deprotonation,^{243,265} which is difficult in the lipid environment.

4.1.3. Chloroplast Photoactive versus Nonphotoactive Plastoquinone Pools. The concepts discussed above apply to quinol or quinone (Q(H₂)) in bioenergetic membranes in ideal conditions. However, due to crowding of both the photosynthetic and respiratory membranes, differences exist between Q(H₂) located in different lipid environments. In the case of photosynthetic membranes (the thylakoids), the proportion of Q(H₂) that participates in electron transport (i.e., that feeds the *Cytc_{6f}*) does not correspond to the entire population of PQ(H₂). This fraction (the photoactive PQ(H₂) pool) makes up a relatively small percentage of the entire PQ(H₂) pool because 60–70% of the total PQ(H₂) is nonphotoactive, being stored inside thylakoid-associated lipid droplets known as plastoglobules.^{266–268} There is increasing evidence that the size of this photoactive PQ(H₂) pool is tightly regulated in response to environmental cues, for example changes in light intensity.^{269,270} This homeostasis is necessary because the PQ(H₂) pool fulfills multiple functions *in vivo*. First, it shuttles electrons within the crowded thylakoid membranes,²⁷¹ probably via percolation through the lipid environment between other membrane complexes.^{272,273} Moreover, its redox state controls physiological processes in response to environmental changes, such as changes in the PSII and PSI antenna size via state transitions²⁷⁴, as well as gene expression and pigment biosynthesis.²⁷⁵

Recent results suggest that the amount of PQ(H₂) active in electron transport is mainly regulated through exchanges between the photoactive pool (in the thylakoids) and the nonphotoactive pool (in the plastoglobules). Homeostasis of photoactive PQ(H₂) abundance seems to be under the control of ABC1 (Activity of *Cytc₁*), typical kinases.²⁷⁶ Knocking out a member of this family (*pgr6*),²⁷⁷ where the ABC1K1 kinase is inactivated (*abc1k1*) prevents changes in the size of the photoactive PQ(H₂) pool, that would otherwise occur in

response to high light, facilitating increased electron flow and replacing photo oxidized plastoquinones. Thereby, *abck1* mutants display decreased electron flow and photoacclimation responses in high light.²⁷⁸ ABC1K1 acts in tandem with ABC1K3, another member of the ABC1 family, and the push pull relationship between these two kinases provides a fine-tuning mechanism to control the size of the PQ(H₂) pool in response to high light.²⁷⁹

This tight control of the size of the photoactive PQ(H₂) pool *in vivo* likely explains the phenotype of the *menD1* mutant of *Chlamydomonas reinhardtii*. This mutant is deficient in MenD, the enzyme catalyzing the first step of phyloquinone biosynthesis.²⁸⁰ Therefore, the phyloquinones playing the role of electron acceptors within PSI are replaced by PQ in this mutant, making PSI less active. However, the *menD1* mutant has another phenotype: its photoactive PQ(H₂) pool is decreased by 20–30%. This can be explained by assuming that the size of the photoactive PQ(H₂) pool is constant between the WT and the mutant. Therefore, the overall number of diffusing PQ(H₂) molecules would decrease from around 6 per *Cytb₆f* in the WT to around 4 per *Cytb₆f* complex in *menD1*.²⁸⁰ On the basis of this result, it is tempting to propose that the mechanism by which ABC1K1/ABC1K3 maintains a constant photoactive PQ(H₂) pool size depends on “quantification” of the total number of PQ(H₂) molecules available per electron flow chain. If this were the case, the size of the pool would be unresponsive in *menD1*, as the ABC1K1/ABC1K3 machinery will not deliver two additional PQ(H₂) per chain to the thylakoid membrane from the plastoglobuli to replace the PSI bound PQ.

4.2. Cytochrome *c* and Plastocyanin as Electron Acceptors

Electron donation from both *Cytb_{c1}* and *Cytb₆f* to soluble proteins at the p side has been extensively studied. These molecular events have often served as pioneering models for electron transfer between different proteins and reflect the development of techniques and theories of how such processes occur. In both cases, a single electron passes from a cytochrome in the complex (*Cyt_{c1}* in *Cytb_{c1}* or *Cytf* in *Cytb₆f*) to a small, soluble redox protein that is specifically but transiently bound. Once reduced, the electron carrier protein must rapidly dissociate (so as not to block the catalytic cycle) and diffuse through the p side space to another large membrane bound protein complex. In mitochondrial respiration, this is cytochrome *c* oxidase (CcO, complex IV),²⁸¹ while in plant photosynthesis, this is photosystem I.²⁸²

Protein acceptors vary between *Cytc₁* and *Cytf*. In the case of the respiratory complex, the acceptor is a c-type heme containing protein, cytochrome *c* (*Cytc*),²⁸³ perhaps one of the most studied of all redox proteins. *Cytb_{c1}* in purple bacteria uses a homologue of *Cytc*, soluble *Cytc₂*, or membrane-anchored *Cytc_y*^{284,285} as an electron acceptor, although this organism is photosynthetic and the final electron acceptor for the soluble electron carrier is a photosynthetic reaction center.²⁸⁶ In the case of *Cytb₆f*, the dominant electron acceptor is a copper-containing protein called plastocyanin (PC).^{287,288}

It is generally accepted that PC has evolved to replace a *Cytc* homologue, *Cytc₆*, the primordial acceptor for electrons coming from the *Cytf* subunit of *Cytb₆f* (see De la Rosa et al., and references therein²⁸⁹). Following oxygenation of the atmosphere, oxidation of Fe²⁺ to Fe³⁺ in the ocean would have made it considerably less bioavailable, while oxidation of Cu to Cu¹⁺ would correspondingly have made it more soluble and therefore bioavailable. Interestingly, some prokaryotic photosynthetic

organisms retain a cytochrome, *Cytc₆*, as their *Cytf* electron acceptor, and in primitive oxygen evolving cyanobacteria this can be the only electron acceptor from *Cytf*. Where both genes are present, *Cytc₆* replaces PC under conditions of limiting copper.²⁹⁰ *Cytc₆* also occurs in some algae where it is also upregulated to act as an electron acceptor of the *Cytb₆f* under copper limiting growth conditions.²⁹¹ A *Cytc₆* homologue gene is present in plant genomes.²⁹² However, despite initial reports, the surface charge distribution on higher plant *Cytc* precludes its function as an effective *in vivo* electron acceptor from *Cytf*.²⁹³

The basic pattern of interaction is thought to be the same for electron transfer processes between *Cytb_{c1}:Cytc* and *Cytb₆f:PC*. The redox centers are oriented for optimal electron transfer by long distance charge effects in an encounter complex, before formation of a transiently stabilized productive complex, dominated by hydrophobic interactions. Mismatched surfaces between the partners, along with the retention of some water molecules at the interface, prevents interaction being so strong that it inhibits dissociation following the electron transfer event. The following subsections will describe the soluble electron carrier proteins in more detail, and outline the mechanisms by which soluble electron carriers interact with, and oxidize the *Cytb_{c1}* and *Cytb₆f* complexes.

4.2.1. Redox Properties and Interaction of Cytochrome *c* with Cytochrome *bc₁*. Cytochrome *c* is a small globular heme protein (90–120 amino acids, 10–13 kDa), which in bioenergetic systems serves as a water-soluble electron carrier. This definition encompasses the representatives found in eukaryotic (mitochondrial *Cytc*, yeast iso-*Cytc*) and prokaryotic (*Cytc₂*, present in several bacteria species) respiratory chains. A more distinct relative, *Cytc₆*, is also a member of this category. However, due to its occurrence in plant-related systems, *Cytc₆* is discussed in the chapter devoted to plastocyanin. For the scope of this review, we will briefly go through the most important properties of *Cytc* with respect to its function and research in bioenergetic systems. More detailed information about the c-type family of cytochromes can be found in reviews on cytochromes.^{294,295}

In the *Cytc* molecule, the heme is bound via two thioether linkages to the peptide. The covalent attachment of heme is a distinctive property of all c-type family cytochromes.²⁹⁶ The bond is formed between a cysteine residue (C) and the penultimate carbon of a vinyl side-group of the heme moiety. Comparison analyses revealed a specific heme binding motif, CXXCH (present also in *Cytc₁* and *Cytf*, see sections 3.5.2 and 3.6.3, respectively). The cysteine residues (C) involved in thioether bonds are separated by any two residues (XX). This four amino acid subsequence is immediately followed by a histidine residue, which is an axial ligand to the heme iron. The second axial ligand is the sulfur atom of a methionine residue, which together with four pyrrole nitrogen atoms of porphyrin completes the octahedral ligand geometry of the heme iron.

Redox properties of *Cytc* are related to the ability of heme iron to undergo reversible oxidation and reduction of ferrous (Fe²⁺) and ferric (Fe³⁺) states, respectively. The presence of a methionine ligand significantly elevates the redox potential of *Cytc* compared to bis-His coordination.²⁹⁷ Thus, among biological compounds the redox midpoint potential of *Cytc*, and its counterparts, is considered high, in the range of +260 mV for horse heart *Cytc*²⁹⁸ and bacterial *Cytc₂* + 360 mV.²⁹⁹ This is consistent with a location of *Cytc* in electron transport chains as an acceptor of electrons from quinol oxidizing membrane

complexes (i.e., Cyt_c–Cyt_bc₁; Cyt_c–Cyt_bc₂; Cyt_c–Cyt_bc₆).^{2,13,211}

Upon reduction, Cyt_c donates electrons to a terminal oxidase of the mitochondrial electron transport chain, CcO. In related systems, cytochrome *c*-type electron carriers are oxidized by photosynthetic complexes of high oxidizing power, that is, the bacterial photosynthetic reaction center in case of Cyt_c³⁰⁰ or PSI for Cyt_c in the case of cyanobacteria and some algae.³⁰¹ Beyond its primary role as a carrier shuttling electrons between membrane complexes, mitochondrial Cyt_c is also involved in the process of cellular apoptosis in higher organisms.³⁰²

The amino acid sequence of Cyt_c varies between different organisms. The degree of identity spans quite high values (70%) among vertebrates³⁰³ to low values (20%) when mitochondrial and prokaryotic Cyt_c are compared.³⁰⁴ Nevertheless, general structural features are evolutionarily conserved: the number of helices (5) and their general spatial arrangement.³⁰⁵ The heme is buried in a hydrophobic pocket within the apoprotein with only one edge being exposed to the surface of the protein. Such an asymmetric cover insulates most of the heme moiety from the water environment and only exposes the heme to the area where the binding occurs with physiological partners.

Cyt_c, as for other hemeproteins, absorbs strongly in the visible spectrum of electromagnetic radiation, in the range of 500–600 nm and the Soret band (around 400 nm). Reduced Cyt_c (Fe²⁺) shows a sharp peak at 550–556 nm (α band) and a slightly broader peak around 520 nm (β band). A unique feature of ferriheme *c* (Fe³⁺) is the presence of a weak absorbance band around 700 nm due to interaction with the sulfur of the methionine ligand. The peak in the Soret band (γ band) of Cyt_c shifts slightly when the redox state of heme *c* changes. The Soret peak is often used as a mark of the protein condition because when the protein denatures, significant changes in the γ band peak are observed. This was exploited in studies of Cyt_c folding stages and its stability.^{306,307} The heme *c* also possesses peaks in the UV region around 320 and 280 nm (δ and ϵ band, respectively),³⁰⁸ which are, however, of little use due to overlapping signals from aromatic amino acids residues.

Octahedral heme iron in Cyt_c is in a low-spin configuration, hence, the reduced Cyt_c (Fe²⁺) is diamagnetic ($S = 0$) while oxidized (Fe³⁺) is paramagnetic ($S = 1/2$). Oxidized Cyt_c molecules from different organisms are the source of the EPR spectrum with significant *g*-factor anisotropy that usually exhibit rhombic symmetry with well resolved *g*-tensor principal values.³⁰⁹ In some cases, the EPR spectrum of Cyt_c is a HALS type.³¹⁰ These differences originate from structural changes in the mutual orientation of the His and Met ligands. However, no simple rules have been found so far which allow prediction of the type of EPR spectrum.¹⁴⁸ Such peculiarities are assigned to rather weak interaction with Met that under some circumstances can be disrupted. It was shown that pH changes, denaturation stress, or interaction with lipids (cardiolipin) can lead to the breakage of the coordination bond changing heme *c* from hexa- to pentacoordinated high-spin geometry.^{311–313}

Several studies involving measurement of the Cyt_c reduction rate by Cyt_bc₁ and kinetics of electron transfer showed sensitivity to ionic strength.^{314–319} This led to the notion that electrostatics is a key player in a “find-and-bind” game between the two protein contenders.

Chemical modification and site directed mutagenetic studies allowed identification of the crucial amino acid residues responsible for Cyt_c–Cyt_bc₁ interaction. Indeed, it was established that the interaction is possible due to electrically

charged surfaces. The surface of the Cyt_c molecule around the heme pocket has a net positive charge due to the presence of basic amino acid residues (mostly lysine residues), while the binding domain on the Cyt_c surface includes complementary (negative) charges of acidic residues.^{320–325} These long-range interactions are thought to orient the Cyt_c molecule in an encounter complex which enables the maintenance of an electron-transfer-productive orientation at the early stages of interaction. Additionally the Cyt_c molecule itself possesses negatively charged residues on the side opposite to the interaction domain. This spatial separation of charges makes the Cyt_c molecule an electric dipole. It was shown that the presence of a dipole moment further facilitates the orientation of Cyt_c in the Cyt_c–Cyt_bc₁ complex that is proper for physiologically efficient electron transfer.³²⁶

Following initial orientation, the proteins form a productive complex, the knowledge of which is based on the structure of cocrystallized yeast proteins, either both in the oxidized, or both in the reduced state.^{72,327} Only subtle differences in structure are observed between the different redox states. In these complexes, the oppositely charged side-chain pairs on Cyt_c and Cyt_bc₁ do not directly interact, being 4 to 9.6 Å apart and therefore beyond the Debye length in physiological salt concentrations. Rather, the interface is dominated by nonpolar interactions. The core surface area of interaction is 880 Å² around the heme clefts and contains a core of 4 pairs of amino acids in nonpolar interactions including a cation– π interaction between a Cyt_c Phe residue and a Cyt_bc₁ Arg residue. The interface contains 30 water molecules, only 2 of which coordinate H-bonds between the proteins. This highly solvated surface aids rapid dissociation of the complex. The two heme cofactors have an interplanar angle of 55° and are very close, only 4.1 Å between the closest thioester bonded carbons of the tetrapyrrole rings, and 17.4 Å between the Fe centers. This short distance means that, in principal, electron transfer could already occur when Cyt_c is approaching the Cyt_bc₁. Many other less stable, productive complexes are also possible aside from those in the crystallized structure. A molecular dynamics approach has attempted to rationalize the apparent importance of charged side chains in mutational studies with the dominance of nonpolar interactions in the crystal structures.³²⁸ This analysis indicates that many of the lysine side chains on Cyt_c, which surround the hydrophobic interface, are highly dynamic, and capable of forming H-bonds or even salt bridges with Cyt_bc₁. On the basis of this finding, the authors suggest a more dynamic mixture of interaction modes between Cyt_c and Cyt_bc₁.

No significant structural changes seem to occur between noncomplexed and complexed proteins in the crystal structures, although one loop region that is poorly resolved in the crystal structure does change orientation in the molecular dynamics experiments.³²⁸ This, in combination with the small surface area of interaction and short distance between the cofactors probably contributes to the rapid rate of electron transfer by the complex. Interestingly, only one Cyt_c site in the dimer is occupied by Cyt_c in the crystal structures (Figure 14A), and this coincides with an increase in Q_i site occupancy in the same monomer, indicating binding of the substrates could be coordinated.³²⁷ Indeed, a change in the conformation of ISP-HD headgroup is observed upon Cyt_c binding to the Cyt_bc₁. The molecular dynamics studies on Cyt_c–Cyt_bc₁ interaction show that Cyt_c binding to one monomer induces structural changes at the Cyt_c binding site of Cyt_bc₁ in the other monomer.³²⁸ Co-crystallization of yeast Cyt_c with a second yeast isoform of Cyt_c (Cyt_c isoform

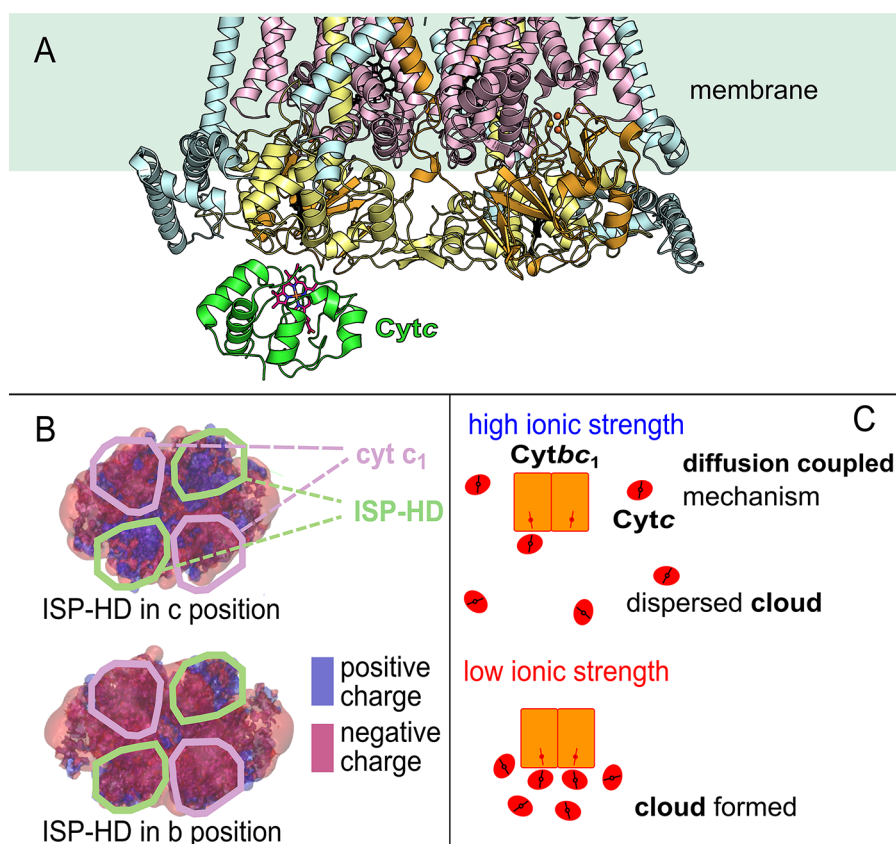


Figure 14. Binding of Cyt *c* to Cyt *bc*₁. (A) Fragment of the structure of Cyt *bc*₁ cocrystallized with Cyt *c* (PDB ID: 1KYO). (B) Comparison of electrostatic potential of the surface of Cyt *bc*₁ accessible to Cyt *c* in two different positions of ISP-HD. (C) Schematic representation showing different molecular organization of Cyt *c* near the binding domain of Cyt *bc*₁ at low and high ionic strength.

2) showed a nearly identical structural arrangement, although some of the charged pairs vary slightly.⁷²

Interestingly, an inspection of the electrostatic surface potential of crystal structures with different ISP-HD positions indicates that a negatively charged area accessible to Cyt *c* is significantly larger when ISP-HD is in the b-position compared to the case when it is in the c-position (Figure 14B). This could potentially influence the molecular organization of Cyt *c* near the binding domain.

The idea of one Cyt *c* per dimer stoichiometry has been experimentally tested. On one hand, this idea suggested that binding of Cyt *c* to the one monomer disables the binding site in the other monomer was explored in the context of half-of-the-site activity model of Cyt *bc*₁ regulation. It was proposed that during enzyme turnover only one monomer of Cyt *bc*₁ is active at a time.³²⁹ On the other hand it inspired other authors to investigate the stoichiometry issue by other experimental approaches. Titration data obtained by plasmon resonance spectroscopy suggested that Cyt *c*₂ interacts with the Cyt *bc*₁ dimer in a biphasic manner which was interpreted as a modulating effect of ISP-HD on the binding.³³⁰ The data obtained by NMR and ITC for Cyt *c* interaction with the soluble Cyt *c*₁ head domain in low ionic strength (both in plant and bovine system) revealed two binding sites of different affinity on Cyt *c*₁.³³¹ The authors proposed that Cyt *c*₁ exposes a proximal site at which electron transfer takes place, and the distal site, which is too far for electron transfer, but keeps molecule close, prior to electron transfer. In this way a subpool of Cyt *c* is trapped close to the surface of the Cyt *bc*₁–C*c*O supercomplex. This restricts diffusion of Cyt *c* in the vicinity of the Cyt *bc*₁–C*c*O

complex leading to the enhancement of electron flow rate between the two complexes. The Cyt *c* then does not need to return to the intermembrane bulk phase. A somewhat similar finding was revealed by experiments in which titration of Cyt *bc*₁ binding sites was done by means of spin-labeling and pulse EPR.³³² Titration curves obtained at low ionic strength (no NaCl in buffer) were explained by a multiple-site-binding model. When electrostatic interactions are strong, Cyt *c*₁ attracts many Cyt *c* molecules which organize in a molecular cloud near the Cyt *c*₁ binding surface (Figure 14C).

The putative presence and a role of such supramolecular structures in the Cyt *c* pool are intriguing. However, as the authors state in both cases (NMR, ITC) and (pulse EPR) the titration curves at higher ionic strength (25–50 mM NaCl) could be readily explained with one binding site per Cyt *c*₁.^{332,333} This means that binding of Cyt *c* to the proposed additional sites under physiological conditions is much weaker than binding to the primary (electron transfer relevant) site on Cyt *c*₁. Hence in order for these additional collective interactions in the Cyt *c* subpool to be physiologically relevant, other factors including macromolecular crowding, may be involved. This matter remains to be determined.

All available titration data report dissociation constants in the range of several to tens of μM , indicating that the Cyt *c*–Cyt *bc*₁ affinity is not very strong.^{330–332} What is even more striking is that EPR data indicates that when the ionic strength is increased to the physiological levels (100–150 mM NaCl) binding of Cyt *c* to the primary interaction site is not even detectable.³³⁴ Even though the stationary concentration of stable long-lived Cyt *c*–Cyt *bc*₁ complex is low, the proteins do interact because the

electron transfer between them is not stopped.³¹⁴ Therefore, this interaction is transient and the lifetime of the complex is much shorter than the time scale of electron transfer. This would also explain the discrepancy between the measured rate of Cyt_c–Cyt_c₁ electron transfer that turned out to be several orders of magnitude lower³¹⁴ than the calculated electron transfer rate based on crystallographic data.³²⁷ This finding supports a diffusion-coupled (in contrast to diffusion limited) mechanism of electron transfer between Cyt_c and Cyt_b_c₁, in which the proteins constantly collide and several collisions are needed before one ET event occurs (Figure 14C).^{332,334} This dynamic aspect of the Cyt_c–Cyt_b_c₁ interaction has tremendous impact on the flow of electrons from Cyt_b_c₁ to Cyt_c pool and it cannot be neglected.

4.2.2. Redox Properties and Interaction of Plastocyanin with Cytochrome *b*₆*f*. A structure of cocrystallized Cyt_f and PC is lacking, and so our understanding of their interaction is based on a combination of mutagenesis studies, nuclear magnetic resonance (NMR), and molecular dynamics. Knowledge has recently been augmented with atomic force microscopy (AFM) and 2D infrared spectroscopy (2D-IR) experiments, meaning that although we lack a perfect snapshot of any one interaction mode, we do have an excellent understanding of the dynamic events that occur during oxidation of Cyt_f.

While the C-terminal domain of Cyt_f forms a membrane spanning domain, the soluble, N-terminal portion contains the heme group. The heme lies below the surface for interaction with PC or Cyt_c₆.¹⁷¹ This is composed of a hydrophobic surface with a ridge of associated charged residues. The hydrophobic surface is highly conserved between Cyt_f proteins from different species, while there is great variation in the ridge residues, and even their charge, between different groups of photosynthetic organism.^{335–337} In higher plants and algae, the ridge is functionalized by basic residues, and mutation of these disrupts interaction with PC.^{171,338–340} The charged residues on the Cyt_f ridge in cyanobacteria are by contrast usually acidic.^{341,342}

The secondary structure of PC is fundamentally different from Cyt_c. It is an 11 kDa protein composed of eight β strands and a small α -helix.^{343–346} It contains a single copper center, coordinated by one cysteine, one methionine and two histidine residues. There are two areas on the surface of PC involved in association with Cyt_f.^{171,342,347–350} The first (site 1) is a hydrophobic patch over the copper-His ligand, while the second (site 2) is functionalized by charged residues complementary to those on the Cyt_f. These therefore vary between photosynthetic organisms, being predominantly acidic in plants and algae, but basic in cyanobacteria. Long distance attraction between the charged residues on the surface of Cyt_f and PC is proposed to orient the molecules for optimal electron transfer, prior to formation of the catalytic complex. This is supported by the observation that low ionic strength results in a strongly bound complex incapable of turnover, while high ionic strength disrupts complex formation.³⁵¹ In addition, AFM experiments, with the Cyt_b₆*f* complex tethered to the surface and PC attached to the tip, indicate that ionic strength strongly impacts both frequency of initial interactions and unbinding forces.³⁵² Despite this evidence supporting the importance of electrostatics for Cyt_f:PC interaction *in vitro*, the only *in vivo* analysis to date, on the alga *Chlamydomonas reinhardtii*, indicates that mutation of the basic ridge residues on Cyt_f has little impact on its oxidation rate.^{339,340}

While a recent molecular dynamics study supported a role for the charged amino acid side chains at site 2 in the initial complex

formed between higher plant Cyt_f and PC,³⁵³ it also found no evidence for electrostatic preorientation in the cyanobacterium *Nostoc*. Moreover, there is little impact of electrostatics on formation of the Cyt_f:PC complex from the thermophilic cyanobacterium *Phormidium laminosum*, where nonpolar interactions appear to both orient the complex and stabilize it.³⁴² Recent 2D-IR experiments on cyanobacterial (*Nostoc*) PC:Cyt_f interaction used site specific labeling of PC with cyanophenylalanine probes to measure very fast changes in conformation and orientation.³⁵⁴ This indicated that a wide variety of initial encounter complexes are formed, with rapid (1–2 ps) changes in orientation. It should be noted that this experiment was performed with the proteins in redox states opposite to that expected in electron flow (oxidized Cyt_f and reduced PC).

Following correct orientation of the electron transfer partners, interaction occurs mainly through nonpolar interactions, with exclusion of some water from the interface. Chemical shift perturbation experiments indicate that in plants and cyanobacteria, the surface area of interaction is around 600–850 Å², with the Cu-His ligand close to the Fe coordinating Tyr residue in Cyt_f.^{349,350,355,356} Different plants appear to have the PC rotated slightly relative to Cyt_f, although the distance between the two redox centers remains around 11–14 Å. Although the surface charge distributions are reversed in cyanobacterial complexes, the orientation of PC relative to Cyt_f is conserved between higher plants and the cyanobacterium *Nostoc*.³⁴⁷ However, NMR studies³⁴⁷ and modeling approaches^{353,357} indicate that other cyanobacteria show different patterns of interaction: in *Phormidium laminosum*, where Cyt_f lacks the charged ridge, computer modeling indicates that PC is highly mobile, with only the site 1 hydrophobic patch interacting. This also seems to be the case for *Prochlorothrix hollandica*, where NMR studies show that although electrostatics make a modest contribution, site 1 dominates the interaction, although PC is oriented slightly differently.³⁵⁸ On binding to Cyt_f, X-ray absorption spectroscopy indicates that the geometry of the coordination sphere around the Cu ligand changes dramatically.³⁵⁹ This may be responsible for the –30 mV negative shift in PC redox potential of PC on Cyt_f binding,³⁶⁰ which counterintuitively makes electron transfer to PC less energetically favorable. Nevertheless, electron transfer is rapid, on the order of 104 k_{et} s⁻¹.^{361,362} It appears that the relative charge of the interaction partners also plays a large role in interaction, presumably in terms of the electrostatics of initial interaction. AFM experiments show a 5-fold increase in interaction frequency between the two proteins when redox states are opposite (irrespective of whether Cyt_f or PC is reduced or oxidized).³⁵² This suggests that the rate of PC dissociation might be enhanced by rapid rereduction of Cyt_f.

Cyt_b₆*f* also uses the Cyt_c homologue, Cyt_c₆ as an electron acceptor in cyanobacteria and algae grown under copper deficiency condition.²⁹⁰ It is reported to show a faster rate of electron transport between Cyt_f and terminal oxygenases than does PC.³⁶³ Intriguingly, Cyt_c₆ is also the principle electron acceptor in the heterocysts of the cyanobacterium *Anabaena*, even when Cu is replete.³⁶³ These cells are specialized for N-fixation, a process dependent on an O₂ sensitive enzyme (nitrogenase), and so PSII activity is very low and the environment anaerobic.³⁶⁴ In heterocysts, the majority of electron transport is therefore thought to result in oxygen reduction or in cycling between PSI and Cyt_b₆*f* via PQH₂ and Cyt_c₆. *Anabaena* could no longer grow under diazotrophic

conditions (obligatory N-fixing) when the gene for $Cytc_6$ was knocked out.³⁶³

$Cytc_6$ is a 10 kDa single c-heme type cytochrome bound by a typical CXXCH motif, where the His and a Met act as axial coordinators.³⁶⁵ The protein has a midpoint potential of +335 mV,³⁶⁶ close to that of PC. In cyanobacteria, $Cytc_6$ has a hydrophobic surface area around the heme, and a positively charged surface patch of amino acid side chains analogous to sites 1 and 2 in PC.³⁶⁷ Although modeling of the *Chlamydomonas* $Cytf:Cytc_6$ complex indicates that a charged patch on the $Cytc_6$ is important, many orientations are possible for the encounter complex.³⁶⁸ A combination of NMR and molecular dynamics^{367,369} has shown that the heme edge region (where the cofactor breaks the surface of the protein) is critical for interaction with $Cytf$, and long distance charge interactions approximately orient the two proteins in an encounter complex, as for PC. Many orientations of $Cytc_6$ result in cofactor–cofactor distances that are close enough for electron transfer, and thus, no specific interaction complex is expected.³⁶⁹

Our knowledge of the interactions between $Cytc_1$ and $Cytc_6$ carriers and their p side electron carrier is not equivalent; in the case of the respiratory complex, cocrystallization has given a wealth of molecular detail about one particular productive complex. The absence of such a structure for the photosynthetic complex has led to the innovative use of NMR and molecular dynamics, along with other recent techniques to provide abundant information on dynamic events. It is to be hoped that we will reach an equivalence of knowledge between these two fascinating systems soon so that more detailed comparisons can be made.

4.3. FNR/Fd Interactions with Cytochrome b_6f

4.3.1. Potential n Side Donors. In the initial model of the Q cycle proposed by Mitchell, one of the electrons reducing the heme b_H site in the $Cytc_1$ complex came from a soluble n side electron donor.³³ He revised this idea not long after proposing the classical model of the Q cycle,³² and more recent studies have given us a much firmer grasp on the classical Q cycle mechanism (see refs 216 and 259 for detailed reviews). However, solution of the crystal structure of $Cytc_6f$ complexes^{41,42} prompted reassessment of whether an n side soluble electron donor might contribute to a modified Q cycle. The discovery of an additional heme group, named heme c_n , or heme c_m , 6 Å closer than heme b_n to the n side solute interface and in contact with the Q_n site has reignited the debate as to whether the $Cytc_6f$ might indeed receive electrons from a soluble, n side source. By contrast, the $Cytc_1$ lacks heme c_n , and it is reasonable to assume that such a mechanism is precluded. This may be a reflection of the different bioenergetic environments of the two complexes, where the $Cytc_1$ can rely on consistent availability of quinols, while the $Cytc_6f$ is maintaining a proton gradient in the face of variable quinone reduction by PSII, due to fluctuations in light intensity.

Therefore, where could such n side soluble reductant come from? In photosynthetic systems, the final steps in electron transport involve the donation of electrons from photoexcited PSI to the soluble, single electron carrier protein ferredoxin (Fd), and subsequent oxidation of Fd by the Fd:NADP(H) reductase (FNR).³⁷⁰ In turn, FNR transfers these electrons over a flavin moiety (flavin adenine dinucleotide, FAD) to the 2 electron carrier NADP⁺, making NADPH (see refs 371 and 372 for a detailed description of the reaction mechanism). Both Fd and NADPH are used as electron donors by multiple enzymes,

supplying the cytosol (bacteria) or stroma (chloroplasts) with reducing equivalents. Crucially, the FAD in FNR enables the relatively safe storage of a single electron from Fd before a second reduced Fd can donate the second electron necessary for NADP⁺ reduction. The injection of these electrons back into the quinone pool from soluble, n side carriers in CET therefore depends upon events involving Fd and FNR.

The two dominant mechanisms of CET have been historically separated on the basis of their sensitivity to the inhibitor antimycin A. Curiously, despite the sensitivity of the $Cytc_1$ to this inhibitor, the $Cytc_6f$ was until recently thought to be insensitive,³⁷³ and linear electron transport to NADPH was not found to be impeded by antimycin A. For many years, it proved extremely difficult to identify the proteins involved in quinone reduction by the antimycin A sensitive CET pathway. Three independent mechanisms have been proposed: (1) direct electron donation from Fd to the $Cytc_6f$;^{19,374,375} (2) electron donation from FNR to the $Cytc_6f$;^{180,376} (3) electron donation from Fd via $Cytc_6f$ associated Pgr5 and PgrL1 pathways.¹⁹⁹ It remains a possibility that all three of these pathways occur depending on the bioenergetic situation. Although robustly debated,^{234,377–380} it has been the consensus among many researchers that a pathway involving Pgr5/PgrL1 catalyzes the bulk of CET in most algae and higher plants.^{197,381–385} However, results in *Arabidopsis*³⁸⁶ and the green algae *Chlamydomonas reinhardtii*³⁸⁷ lead the authors to propose that the role of these proteins is regulatory rather than mechanistic.^{374,377,386,387} Moreover, the PgrL1 protein appears to be significantly substoichiometric to the $Cytc_6f$ and would therefore only be able to drive electron flux into a small proportion of $Cytc_6f$ complexes present in the membrane.²⁰¹ Finally, it has recently been reported that antimycin A can indeed act as an inhibitor of the Q_n site on $Cytc_6f$ in conditions of highly reduced PQ pool, dependent on the presence of the Stt7 kinase and Pgr5.³⁸⁸ Given the controversy, it is timely to discuss how the relationship between these different candidates and the $Cytc_6f$ might help to resolve this question.

4.3.2. Direct Electron Donation from Fd to Cytochrome b_6f . As mentioned previously, the original Q-cycle proposed by Mitchell involved a single electron from the soluble n side,³² and if this were to be the case for the $Cytc_6f$, Fd would be an obvious candidate for such a donor. The advantages of such a system in amplifying the proton motive force (pmf) are evident, with additional electrons from the n side enabling immediate quinone reduction at the Q_n site on oxidation of a single quinone at the Q_p site, and also providing the means to close “incomplete” catalytic cycles in the $Cytc_6f$ that would otherwise leave $Cytc_6$ in a reduced state.¹⁹ It is possible that this could be automatically poised by the redox state of the quinone and stromal electron carriers, but seems more likely that some regulation would be required, particularly in the dark, when reduced Fd is required for multiple other metabolic reactions³⁸⁹ and continuous input of n side electrons to the $Cytc_6f$ undesirable.

Nearly all photosynthetic organisms possess a suite of Fd proteins that are presumed, and in some cases proven, to have variable affinity for different electron acceptors.^{390–395} Such a system means that, depending on the relative abundance of these Fd iso-proteins, electron flux into different pathways could either be increased or decreased. There is abundant evidence that Fd iso-proteins specific for CET exist (see ref 396 for a full discussion). For example, maize plants perform an adapted photosynthetic pathway known as C4, in which one cell type has

a greatly increased ATP demand and low PSII activity, a situation that demands high CET. A specific Fd iso-protein (FdII) is exclusively present in this ATP demanding cell type³⁹⁷ and when this is used to replace the native Fd in cyanobacteria it prompts massive CET.³⁹⁸ Pea plants also possess an Fd iso-protein that is expressed only in times of high ATP demand^{399–401} and when this is overexpressed in tobacco it also results in elevated CET.⁴⁰² At this point, it is not clear whether these CET specific Fds operate in the antimycin A sensitive or insensitive pathways.

After the characterization of Fd-dependent CET by Arnon and colleagues,⁴⁰³ the possibility of direct electron donation from Fd to the *Cytb₆f* was investigated in isolated spinach thylakoids.⁴⁰⁴ The authors showed that although *Cytb₅₆₃* (heme *b_n*) is only slowly reduced by dithionite, addition of hydrophobic quinone mediators accelerated this reduction, while Fd had no effect. Moreover, the addition of NADPH and Fd in the dark had little effect on the redox state of the cytochrome. In these experiments, rapid rereduction of the oxidized P700 center of PSI was measured in the presence of Fd and NADPH, indicating that Fd-CET was operating very efficiently. This result indicates that, in this system at least, Fd is a poor direct electron donor to the *Cytb₆f*. It remains possible that direct electron donation from Fd to heme *c_n* is downregulated in the dark adapted membranes used in this experiment or that it might not result in reduction of the heme *b_n*. Interestingly, the broken chloroplast assay, used extensively to characterize the *pgr5* and *pgrL1* mutant *Arabidopsis* plants,^{235,236} does not work if attempted on washed thylakoid membranes (personal observation, GH). The possibility therefore also remains that components only weakly associated with the *Cytb₆f* complex are required to regulate direct Fd:*Cytb₆f* interaction, and the obvious candidates for such proteins are *Pgr5* and *PgrL1*, although documentation of the role of these proteins in competent electron transport reactions is minimal and their presence substoichiometric.²⁰¹ If this is not the case, then further experiments are necessary to identify (1) the interaction partners and (2) their mechanism of function.

As part of a possible model involving direct electron donation from Fd to the *Cytb₆f*,³⁷⁴ one can propose a docking model of Fd binding to the n side of the *Cytb₆f*. Although binding sites are notoriously difficult to predict, interactions between Fd and Fd-dependent enzymes are characterized by charge interactions between the proteins, whose purpose is to optimally orient the redox centers for electron transfer.^{405–407} For example, Figure 15 shows the Fd-binding sites (highlighted in black) on two classical Fd-dependent enzymes (C, nitrite reductase; D, FNR). There is an obvious ring of basic charges around the active center to which Fd can dock. When the n-facing surface of the *Cytb₆f* is examined, such a patch does appear to exist on the *C. reinhardtii* complex, used in the model proposed by Nawrocki et al.,³⁷⁴ highlighted with a hashed circle (Figure 15B). However, such a mechanism would be expected to be universal throughout CET performing organisms, and when the same surface of the cyanobacterial *M. laminosus* complex is examined (Figure 15A), the location of such a binding site is much less clear, although coevolution of Fd iso-proteins with the *Cytb₆f* complex and auxiliary subunits could result in differences in Fd–*Cytb₆f* interactions.

4.3.3. Direct Electron Donation from FNR to Cytochrome *b₆f*. Involvement of the FNR enzyme in reinjection of electrons into the quinone pool from the n side of the membrane has long been debated, and there is plenty of circumstantial

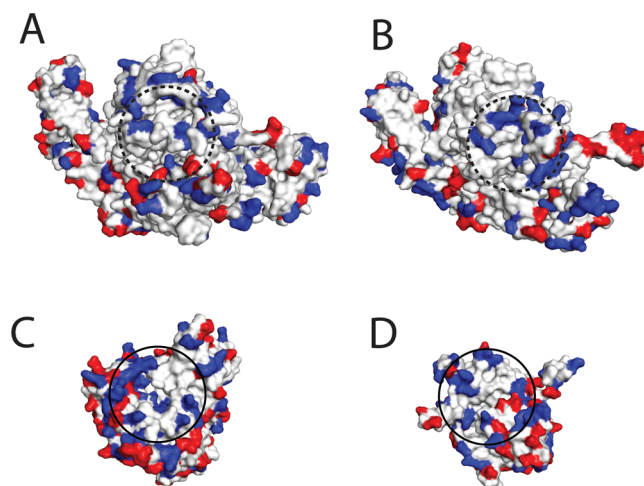


Figure 15. Comparison of charge distribution on the n side surface of the *Cytb₆f* with known Fd-binding sites. (A) *Cytb₆f* monomer from *M. laminosus* (taken from 2D2C), seen as looking down from the n side. (B) *Cytb₆f* monomer from *C. reinhardtii* (taken from 1Q90), seen as looking down from the n side. (C) Fd-dependent nitrite reductase (2AKJ), looking down on the Fd binding site, as defined by site directed mutagenesis studies. (D) Fe:NADP(H) oxidoreductase (FNR, 1GAW), looking down on the Fd binding site, as defined by site directed mutagenesis studies and cocrystallization. Known Fd binding sites are highlighted with a black circle. The putative Fd binding site on *Cytb₆f* suggested by Nawrocki et al.³⁷⁴ is indicated by a hashed line. Positively charged groups in blue, negatively charged groups in red.

evidence to suggest that this is the case. For example, CET appears inhibited in cyanobacteria when FNR is no longer tethered to the membrane,⁴⁰⁸ FNR is more strongly membrane bound in higher plant cells performing enhanced CET,⁴⁰⁹ and plants with diminished FNR content also show perturbed CET.⁴¹⁰ Moreover, FNR has been consistently colocalized with *PgrL1*,^{197,236} and FNR is no longer recruited efficiently to the membrane in the classic *pgr5* mutant of the alga *C. reinhardtii*.⁴¹¹ Inhibitors of FNR indicate that the enzyme is essential to some CET pathways,^{233,375,412–416} although FNR does not bind antimycin A in solution²³³ and is relatively insensitive to this CET inhibitor.⁴¹⁷ Immuno-inhibition studies show that blocking Fd to NADP(H) electron transfer by FNR does not affect CET activity,^{414,418} indicating that any CET role for FNR does not involve the NADP⁺ binding site. On the other hand, It has been reported that *Cytb₆f* complexes purified from spinach and incorporated into liposomes are only capable of NADPH mediated quinone reduction if the purification method is mild enough to preserve FNR binding.⁴¹⁹ It should be noted that the severe washes employed to remove FNR in this paper may also have removed other proteins important for this function such as Fd or *PgrL1*. Importantly, addition of NADPH to the purified FNR:*Cytb₆f* complex only results in reduction of *Cytb₆* in the presence of Fd.¹⁸⁰

Mutant studies on FNR would provide a definitive answer but are lacking due to the difficulty in fully knocking out the gene for a protein that is essential for photoautotrophic growth. Plants with minimal FNR downregulate the entire electron transport chain to compensate, leaving an extremely severe phenotype,⁴²⁰ making interpretation of CET measurements problematic.

The discovery that FNR is copurified with the *Cytb₆f* complex^{180,421,422} prompted the suggestion that FNR could act as a conduit of electrons from Fd into the *Cytb₆f*, potentially via the heme *c_n*.^{180,376} As with Fd, the absence of information

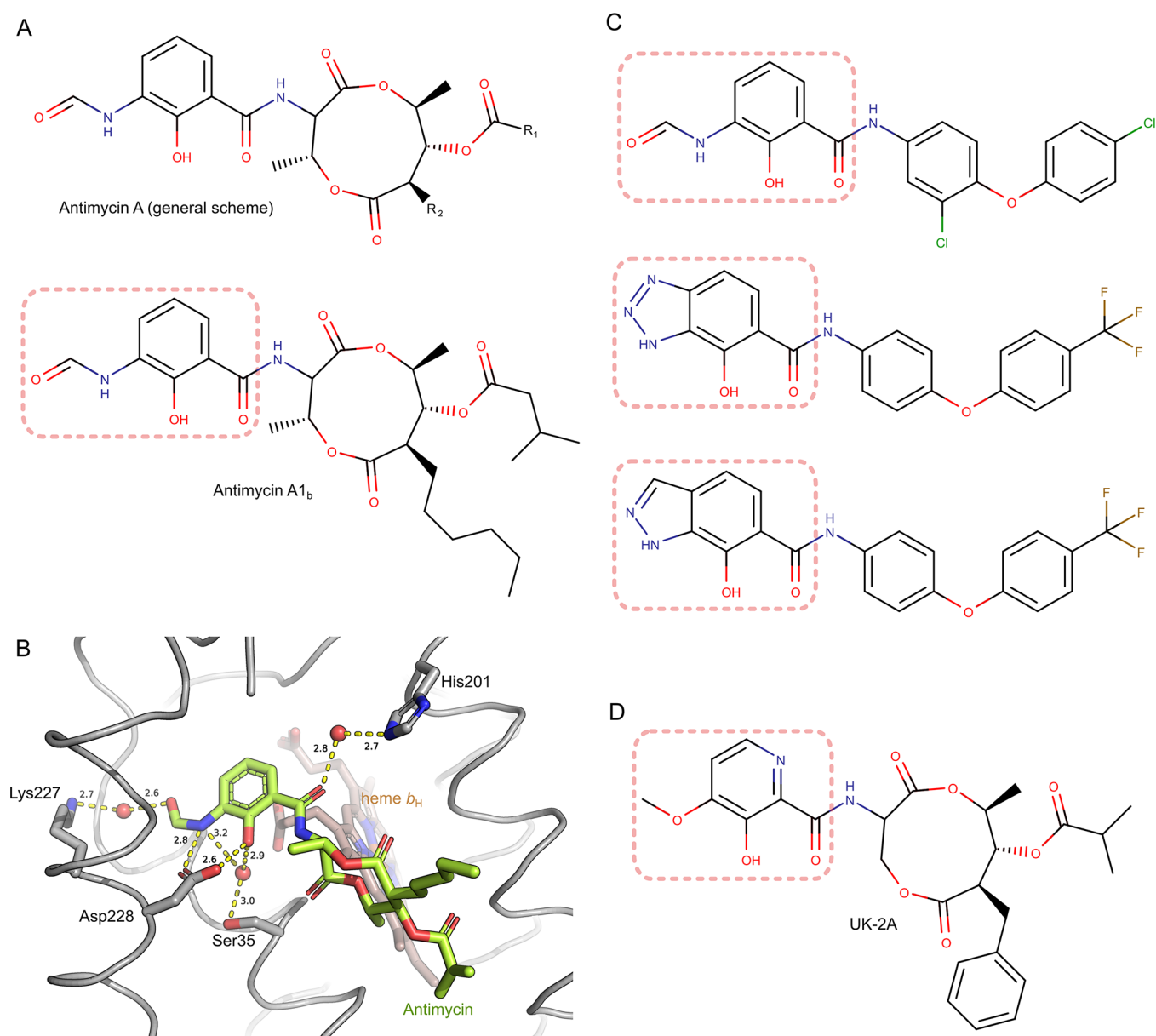


Figure 16. Structural features of antimycin and related compounds. (A) Structural formulas of compounds belonging to the antimycin A family. The upper formula represents the general structural elements of antimycins A, the lower is a formula of antimycin A_{1b}. (B) Stick/ribbon representation of binding of antimycin A in the Q_c site, as revealed by X-ray crystallography. Antimycin A (pale green sticks) forms a direct hydrogen bond to ^{Bt}Asp228 and additional, water-bridged bonds to ^{Bt}Lys227, ^{Bt}His201 and ^{Bt}Ser35 (gray sticks). Oxygen and nitrogen atoms are colored red and blue, respectively. Heme *b_H* shown in brown. The model is based on PDB entry 1PPJ. (C) Structural formulas of synthetic antimycin analogues. (D) Structural formula of UK-2A. In A, C, and D, pale-red, dotted frames indicate the toxophore moiety of each compound.

about where and how FNR docks to the *Cytb_{6f}* is currently the major impediment to our understanding of a functional mechanism of electron transfer from FNR to the complex. It seems clear that the PgrL1 and PgrS proteins are involved in FNR recruitment to the membrane (and therefore probably the *Cytb_{6f}*), at least in algae,⁴¹¹ but in higher plants, FNR is recruited to the membrane by two tether proteins, Tic62⁴²³ and TROL.⁴²⁴ On the basis of blue native PAGE analysis, it has been suggested that these are the only sites of FNR interaction.^{424,425} However, this is likely a function of detergent disruption of interactions between FNR in complex with its tether proteins and other thylakoid membrane components such as the *Cytb_{6f}*. Indeed, in a blue native PAGE experiment using different solubilization conditions, FNR comigrated with several

complexes including the *Cytb_{6f}*.⁴²⁶ It remains unknown whether the tethering proteins Tic62 and TROL also play a role in FNR association with the *Cytb_{6f}* or whether release of FNR from these tethers (which happens in response to the generation of Δ pH across the membrane) might prompt association with the *Cytb_{6f}*. Interestingly, only FNR iso-proteins capable of binding to the TROL tether were found copurified with the *Cytb_{6f}* from maize.⁴²²

If FNR acts as a conduit of electrons from Fd into the heme *c_{1v}*, it prompts some energetic questions. The FAD moiety of FNR can be reduced by one electron from Fd to the flavin radical state (FNR_{ox} to FNR_{sq}), and a second electron can then fully reduce the FAD (FNR_{sq} to FNR_{red}), with redox midpoint potentials of -338 mV and -312 mV, respectively, measured at pH 8,⁴²⁷ or

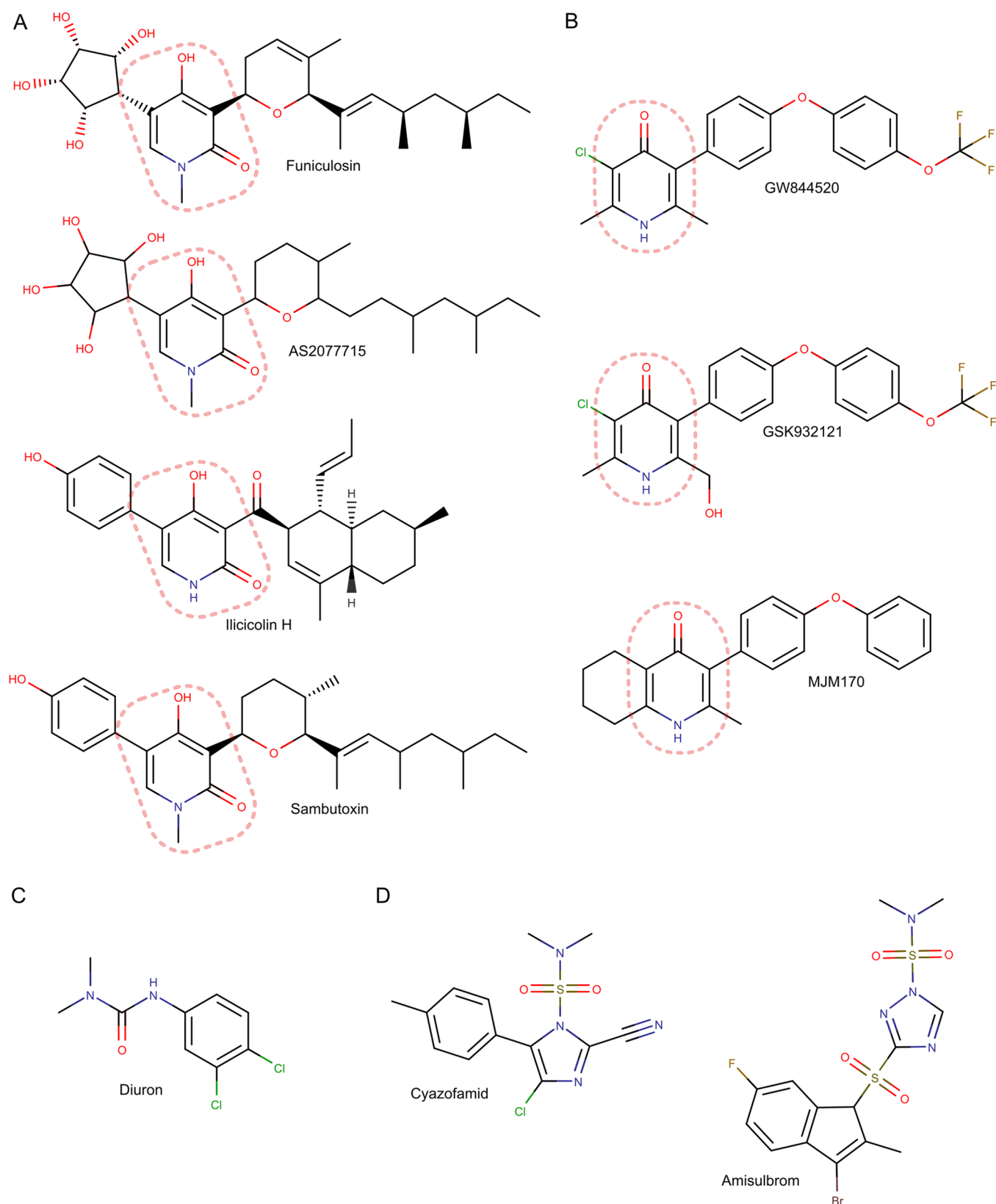


Figure 17. Structural formulas of Q_1 site inhibitors. (A) Naturally occurring 4-hydroxy-2-pyridone derivatives. (B) Synthetic 4-pyridone-based antimalarial drugs. (C) Diuron. (D) Sulfonamide-based commercial fungicides. Pale-red, dotted frames indicate the toxophore moiety of each compound.

NADPH can directly donate two electrons to fully reduce the FAD (FNR_{ox} to FNR_{red}), with a redox midpoint potential around -380 mV.^{428,429} Any of these reduced centers would be

adequate to reduce heme c_n , irrespective of whether or not the quinone site was occupied.⁴³⁰ Therefore, is the mechanism of FNR to $\text{Cyt}b_6$ reduction a single or double electron transfer to

the Q_n site from FNR? The dependence on Fd of NADPH mediated reduction of Cytb,¹⁸⁰ and the seeming independence of CET on the NADPH binding site of FNR^{414,418} implies that single electron reduction and oxidation of the FNR FAD moiety is sufficient for CET. It has also been suggested that rather than having an electron transfer function, FNR could simply act as an Fd recruiting module, providing a site for Fd to bind on the Cytb_{6f} complex before transfer of electrons directly to heme c_n or via PgrL1.¹⁹⁹ A number of experiments are required to clarify the role of FNR recruitment to Cytb_{6f} in CET, principally: (1) more information is needed regarding the binding site of FNR on Cytb_{6f}, and its orientation; (2) the capacity for CET has to be correctly measured in membranes or cells where the FNR protein has no capacity to interact with the Cytb_{6f} or is missing. Finally, if electron donation from Fd or FNR directly to Cytb_{6f} is the major route of antimycin A sensitive CET, rates of electron transfer for this complex close to those estimated for the CET pathway, in the range of $10 \text{ e}^{-1} \text{ s}^{-1} \text{ PSI}^{-1}$ to $130 \text{ e}^{-1} \text{ s}^{-1} \text{ PSI}^{-1}$,⁴³¹ would be the final proof.

5. INHIBITORS

5.1. Cytochrome bc_1 Specific Inhibitors

Microorganisms often produce and secrete chemical substances to restrain or kill other species or strains. As Cytbc₁ is a crucial component of the respiratory chain in many bioenergetic systems, its quinone binding catalytic sites have become a critical target in this chemical warfare. Indeed, many compounds that bind to the catalytic sites and act as Cytbc₁ inhibitors can be found in bacteria and fungi. Over the past few decades, these naturally occurring toxins became popular templates for man-made chemicals, with many proposed functions, from medicinal drugs and treatments for parasitic infections to fungicides in agriculture.

Depending on the site of action, the Cytbc₁ inhibitors are often divided into two groups. The first group is considered to be small and consist of compounds with the ability to inhibit the Q_i site. The second group consists of the Q_o site inhibitors and is considered to be much larger, with numerous synthetic compounds developed over the years of research. Moreover, with recent developments, dual-mode inhibitors, capable of binding to both active sites, have been found or synthesized. It is important to note that this classification excludes the inhibitors that do not act on the quinone-binding sites, such as cyanide, which has been shown to inhibit bacterial Cytbc₁¹³⁶ or 2,3-dimercaptopropanol (also known as BAL or British anti-Lewisite), which is known as a respiratory inhibitor since the early studies on mitochondrial material⁴³² and later has been shown to destroy the Rieske cluster.⁴³³

5.1.1. Inhibitors of the Q_i Site. The best known compound that inhibits the Q_i site is antimycin A. However, this group consists also of naturally occurring ilicicolin H, funiculosin, funiculosin-related compounds, and various synthetic inhibitors (Figures 16 and 17).

Antimycin A (Figure 16A) is a depsipeptide with an acyl- (R_1) and alkyl-substituted (R_2) dilactone ring with an amide linkage to a 3-formamidosalicylate moiety. In fact, antimycin A is a whole family of compounds (about 29),⁴³⁴ produced by actinobacteria from the *Streptomyces* genus, with the first members isolated and identified in 1948.^{435,436} Antimycin A1 has a high binding affinity to the Q_i site, with a dissociation constant (K_d) of 32 pM in bovine Cytbc₁.⁴³⁷ It has been shown that antimycin is able to displace quinones and even other

inhibitors from the active site.^{438–440} On the basis of the crystal structures,^{63,79,123} it is known that the 3-formamidosalicylate group acts as the toxophore and forms hydrogen bonds with highly conserved residues of Q_i (Figure 16B), including the His, Asp, and Lys, that serve as proton donors in Q reduction,¹⁶³ and a Ser (^{Bt}S35). The dilactone ring of antimycin appears to control its solubility and hydrophobicity.⁴⁴¹ There have been attempts to create synthetic analogues (example in Figure 16C, top) with the dilactone replaced by various other moieties,^{442–444} with promising *in vitro* results for biphenyl and biphenyl ether groups.⁴⁴⁴ Some of synthetic inhibitors where the 3-formamidosalicylate moiety is replaced with benzazoles and the dilactone rings are replaced with a trifluoromethyl-substituted biphenyl ether moiety (Figure 16C, middle and bottom) were shown to be almost as potent as the natural antimycin A in *in vitro* inhibitor assays. However, they exhibited a negligible *in vivo* activity because of low uptake into the living cell.⁴⁴² Recently, UK-2A (Figure 16D), which belongs to a group of dilactone compounds isolated from *Streptomyces* sp. S17–02,^{445,446} has been revisited and shown to bind to the Q_i site in a similar mode to antimycin A.⁴⁴⁷ In contrast to antimycin, UK-2A comprises a 4-methoxypyridin-3-ol moiety as its toxophore. Its inhibitory potency was estimated to be about 3-fold lower than that of antimycin.⁴⁴⁸

Funiculosin (Figure 17 A top) is an *N*-methyl-4-hydroxy-2-pyridone derivative, substituted with a cyclopentanetetrol moiety. It is a natural compound with antifungal properties, isolated from *Penicillium funiculosum*.^{449,450} Funiculosin was shown to inhibit Cytbc₁ by a similar mechanism to antimycin A.^{164,451,452} However, there is no structural data on funiculosin binding mode to the Q_i site. It is speculated that it binds in close proximity to heme b_H , as a rise in E_m of this heme by about 100 mV was observed in the inhibited enzyme.¹⁶⁴ Moreover, studies on yeast mutants of ³⁵Asp208 revealed that this residue can possibly be involved in funiculosin binding, which distinguishes it from antimycin.⁴⁵² Recently, funiculosin analogues were shown to be produced by other microorganisms, for example, the compound AS2077715 (Figure 17A, upper middle), isolated from fungal strain *Capnodium* sp. 33985. AS2077715 has been shown to exhibit selective and highly inhibitory properties toward *Trichophyton mentagrophytes* Cytbc₁ while being a weak inhibitor of the mammalian counterpart. Therefore, it has been proposed as a potential drug for *Trichophyton* infections.⁴⁵³

Another 2-pyridone derivative, ilicicolin H (Figure 17A, lower middle), was isolated from *Cylindrocladium ilicicola*⁴⁵⁴ and *Gliocladium roseum*.⁴⁵⁵ Despite some structural differences to funiculosins, ilicicolin was shown to act in similar way, being a potent and broad-spectrum antifungal agent,⁴⁵⁶ inhibiting yeast and fungal Cytbc₁ with high selectivity.^{439,456} Thus, a 2-pyridone moiety is the suggested toxophore in both funiculosins and ilicicolins.⁴³⁹ However, a closer examination of the influence of antimycin A, funiculosin and ilicicolin H on Cytbc₁ isolated from distinct organisms and yeast Q_i -site mutants, reveals some differences in sensitivity between the enzymes, which suggests that there is some variation in the binding mode of these inhibitors.⁴⁵⁷

The same 2-pyridone moiety as in funiculosin and ilicicolin H can be found in sambutoxin (Figure 17A, bottom) and related compounds isolated from *Fusarium sambucinum*^{458,459} and other strains of *Fusarium*.^{460,461} Sambutoxins have been also shown to be toxic to mitochondrial respiration and specific toward Cytbc₁.⁴⁵⁹ Although their binding mode was not specified, they can be expected to bind to the Q_i site as well. More recently,

several synthetic antimalarial compounds comprising a 4-pyridone ring with a biphenyl ether tail were also shown to inhibit the Q_i site, for example, GSK932121, GW844520 (Figure 17B, top and middle),⁴⁶² or MJM170 (Figure 17B, bottom).⁴⁶³ The cocrystal structures of bovine enzyme with these three novel inhibitors indicate that they all bind close to heme b_H , with the carbonyl group of the pyridone toxophore in a direct contact to the Bt Ser35.^{462,463}

Diuron (Figure 17C), 3-(3,4-dichlorophenyl)-1,1-dimethylurea, is a relatively simple synthetic compound that was shown to have strong inhibitory properties in photosynthesis and weak in mitochondrial respiration.⁴⁶⁴ No structural data is available for its binding mode. The mechanism of action, through inhibition of the Q_i site, is known from genetic analysis of diurone- and antimycin-resistant mutations in the yeast model^{465,466} and comparative kinetic studies.⁴⁶⁷

Cyazofamid (Figure 17D, left) and amisulbrom (Figure 17D, right) are commercial, synthetic compounds that are imidazole and triazole sulfonamides, respectively. Both are fungicides with high selectivity toward oomycetes.^{468–470} Cyazofamid was shown to be almost inactive toward yeast, rat and potato *Cytc₁*,⁴⁷⁰ and a weak inhibitor of porcine *Cytc₁* Q_i site when compared to antimycin A.⁴³⁷ Little is known about the binding mode of these inhibitors to the Q_i site. However, based on computational docking studies, it has been suggested that cyazofamid forms a hydrogen bond to Bt Asp228.⁴³⁷

5.1.2. Inhibitors of the Q_o Site. They are commonly divided into two subclasses. The compounds belonging to the first subclass, of which stigmatellin is the best known example, are capable of immobilizing the ISP-HD in a position near the Q_o site (in the b -position). The inhibitors belonging to the second subclass, such as myxothiazol or MOA-type compounds, bind deeper in the Q_o site cavity and do not fix the ISP-HD position. Therefore, these two subclasses are often referred to as P_f (with f originating from “fixed”) and P_m (with m originating from “mobile”) inhibitors, respectively. The influence of these inhibitors on movement of ISP-HD is explained in detail in section 3.4.

Stigmatellin A (Figure 18A, upper) is a natural compound isolated from the myxobacterium *Stigmatella aurantiaca*⁴⁷¹ and the inhibitor of Q_o site exhibiting the lowest K_d (<0.01 nM).⁴⁷² It consists of a chromone moiety, acting as its toxophore, substituted with a lipophilic alkenyl chain. Crystallographic studies have revealed that stigmatellin fixes the position of the ISP-HD near the Q_o site by formation of hydrogen bond between carbonyl oxygen of chromone ring and one of the His residues acting as a ligand to the 2Fe2S (Figure 18B).^{61,63,123,473} The second hydrogen bond is formed between the phenolic hydroxyl group of the compound and the carboxylate side chain of a conserved Glu residue (belonging to the PEWY motif) of the *Cytc₁*.^{63,474} The alkenyl tail of stigmatellin is not involved in any specific interactions, but studies on synthetic analogs indicate that modification of this tail can decrease the inhibitory potency of the compound.⁴⁷² However, such a modification was also made in the case of tridecyl-stigmatellin (Figure 18A, lower), which has the native tail replaced with tridecyl chain but retains its potency. It was developed as a stigmatellin replacement and a potential inhibitor of *Cytc₁*.⁴⁷⁵ Tridecyl-stigmatellin has been shown to bind to the *Cytc₁* at both active sites⁶⁶ and also to inhibit the Q_o site of the bacterial *Cytc₁*^{151,263,472} in similar way to the natural compound.

Atovaquone (Figure 18C, left) is 2-hydroxynaphthoquinone substituted with a cyclohexyl-chlorophenyl moiety, which was

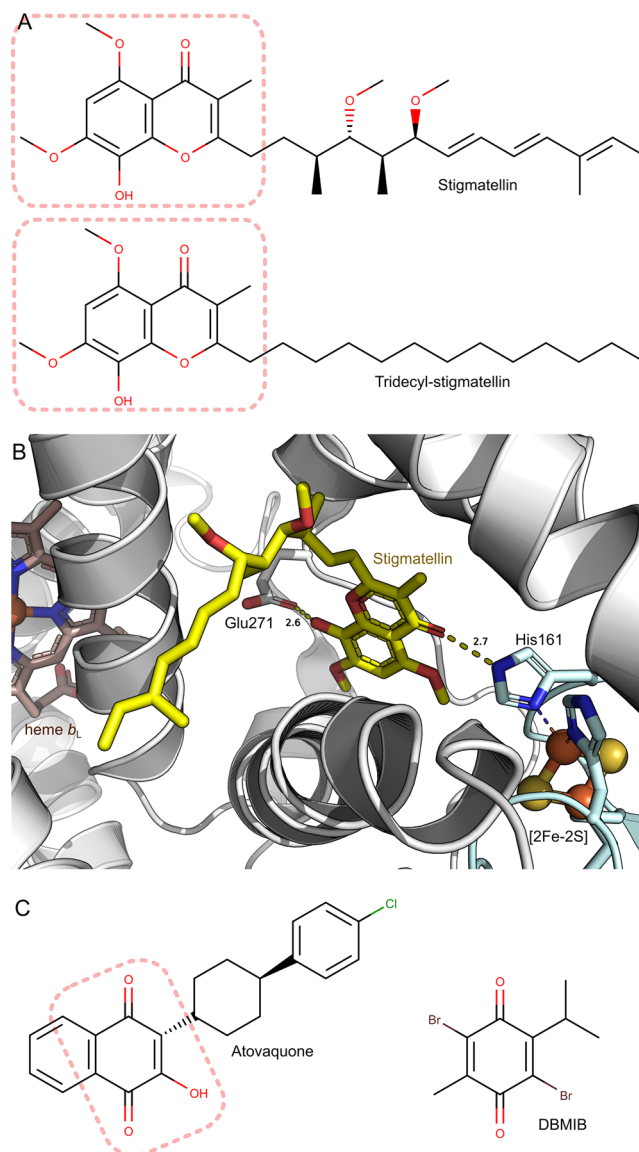


Figure 18. Q_o site inhibitors that fix ISP-HD at b -position. (A) Structural formulas of natural stigmatellin A and synthetic tridecyl-stigmatellin. Pale-red, dotted frames indicate the toxophore moiety of each compound. (B) Stick/cartoon representation of binding of stigmatellin A in the Q_o site, as revealed by X-ray crystallography. Stigmatellin A (yellow sticks) forms hydrogen bonds to Bt Glu271 of *Cytc₁* (gray sticks) and to Bt His161 of ISP (pale cyan sticks). Oxygen and nitrogen atoms are colored red and blue, respectively. Heme b_L is shown in brown. Model is based on PDB entry 1PPJ. (C) Structural formulas of atovaquone (left) and DBMIB (right). The toxophore of atovaquone is marked with a frame.

developed as a drug for malaria in 1990s.⁴⁷⁶ Among numerous other naphthoquinone derivatives created at the time, it was shown to be the most active against apicomplexan parasites including several species of *Plasmodium*.^{441,476–478} It is the only drug against *Cytc₁* currently in clinical use.⁴⁴¹ Atovaquone inhibits the enzyme of *P. falciparum* with nanomolar affinity,^{476,479,480} and has much lower toxicity to the human counterpart.⁴⁸⁰ The results of early studies, based on EPR and redox potentiometry, indicated that atovaquone has a similar binding mode to stigmatellin, and also arrests ISP-HD at b -position.⁴⁷⁹ Moreover, based on the complementary molecular modeling studies, atovaquone was suggested to bind within the

Q_o site, forming a hydrogen bond between its hydroxyl group and the 2Fe2S cluster-ligating His residue, and a water bridge between the carbonyl oxygen at position 1 of naphthoquinone ring and the conserved Glu of PEWY motif.⁴⁷⁹ However, crystallographic studies on yeast showed that the only hydrogen bond is formed between the ionized hydroxyl group of the inhibitor and the N_r atom of $^{Sc}His181$. The $^{Sc}Glu272$ residue side chain was shown to face the opposite direction with respect to the carbonyl oxygen, and does not appear to be involved in atovaquone binding.⁷¹

DBMIB (Figure 18C, right), 2,5-dibromothymoquinone, is a halogenated benzoquinone derivative. Although DBMIB is known more as a *Cytb_{6f}* inhibitor¹¹⁰ (see section 5.2), it has been shown to exhibit similar potency against *Cytb_{c1}*.⁴⁸¹ DBMIB should not be considered as a regular inhibitor competing with QH_2 , as has been commonly assumed. Rather, it binds to the Q_o site in the form of a semiquinone and there forms a spin-coupled state with 2Fe2S, which leads to locking of the ISP-HD at *b*-position⁴⁸² (see section 7.6). The spin-coupled state can be detected in EPR experiments as the prominent $g = 1.94$ EPR signal in X-band at low temperatures.^{84,108,110,483}

UHDBT and HHDBT (Figure 19A) are both 6-hydroxy-4,7-benzothiazolediones (HDBT) with undecyl and heptyl tails, respectively. HDBT compounds are synthetic inhibitors capable of binding to the Q_o site.^{70,116,484,485} As they comprise the hydroxybenzoquinone moiety, they exist as a mixture of ortho- and para-quinone tautomers (Figure 19B). The 6-hydroxy

group is ionizable, with a pK_a of 6.5, which is reflected in a distinctive color change from yellow to violet when pH changes from acidic to alkaline.⁴⁸⁶ These compounds are also redox active and, as is typical for quinones, the E_m exhibits a pH dependence with a slope of about 60 mV/pH unit.⁴⁸⁶ Thus, HDBTs may be regarded as substrate analogues. However, the E_m value of UHDBT was shown to be about -40 mV at pH 7,⁴⁸⁶ thus much lower than the ubiquinone pool (about 100 mV).^{487,488} Cytochrome *b_{c1}* inhibition by UHDBT was found to be pH dependent, with a 10-fold decrease in the binding rate constant at more alkaline pH.⁴⁸⁵ This had been initially associated with ionization of the hydroxyl moiety. This effect was also noted for 6-bromo substituted UHDBT.⁴⁸⁴ As indicated by the results of X-ray crystallography, HDBT compounds immobilize the ISP-HD in the *b*-position via formation of a hydrogen bond with one of His ligands of the 2Fe2S cluster.^{70,77,474} However, there is no agreement on the detailed mode of hydrogen bonding for HHDBT and UHDBT within the Q_o site. On the basis of the structure of yeast *Cytb_{c1}* cocrystallized with HHDBT, hydrogen bonds are proposed to form between (1) the oxygen from the ionized hydroxyl group of HHDBT and the protonated N_r of $^{Sc}His181$ of the ISP; and (2) the carbonyl O4 atom and the water molecule that is itself bonded to the backbone nitrogen of the Glu within the PEWY motif.⁷⁰ A slightly different model has been proposed in the case of bovine *Cytb_{c1}* interaction with UHDBT. It was suggested that the protonated His of ISP interacts with the carbonyl O7, while its deprotonated form interacts with the hydroxyl group of the inhibitor. Moreover, the carbonyl O4 and N3 of UHDBT were suggested to form a hydrogen bond with the hydroxyl group of the conserved $^{Bt}Tyr131$ of the *Cytb* ($^{Sc}Tyr132$).⁷⁷

Crocacin A and D (Figure 20A, upper and middle) are naturally occurring dipeptide derivatives, comprising a Z-enamide moiety of glycine and either a aminohexadienoic or aminohexenoic acid (respectively), substituted with a polyketide acyl tail. They belong to a whole family of compounds isolated from the myxobacterium *Chondromyces crocatus*.^{489–491} Some of the crocacin exhibit inhibitory properties against many strains of bacteria, yeasts, and fungal plant pathogens, with (+)-crocacin D recognized as the most potent compound of the family.^{75,491} In studies on bovine *Cytb_{c1}* in SMPs, it has been shown that the inhibitory mechanism of crocacin is based on binding to the Q_o site.⁴⁸⁹ The model for binding of crocacin A and D was developed based on EPR studies and crystallographic analysis of the crocacin D analogue (Figure 20A, bottom) bound to the avian *Cytb_{c1}*, combined with molecular modeling and docking studies. Crocacin were shown to immobilize the ISP-HD in the *b*-position, with the Z-enamide carbonyl forming a hydrogen bond to N_r of the 2Fe2S-ligating His. Moreover, it was suggested that the glycine residue of crocacin can form hydrogen bonds to the backbone nitrogen with the PEWY motif Glu and to the carbonyl group of the conserved Met ($^{Bt}Met138$) of *Cytb*. However, the existence of a hydrogen bond to the Met residue is not supported by the crystal structure. Interestingly, the Z-enamide seems to adopt a hairpin conformation, with an intramolecular hydrogen bond between the two amide groups.⁷⁵

Because natural crocacin have been shown to exhibit a photostability of minutes under field conditions,⁷⁵ they are not suitable for use in agriculture, despite their inhibitory potency. However, in recent years, several methods for synthesis of crocacin^{491,492} and their simplified, more stable analogues have been developed.⁴⁹³

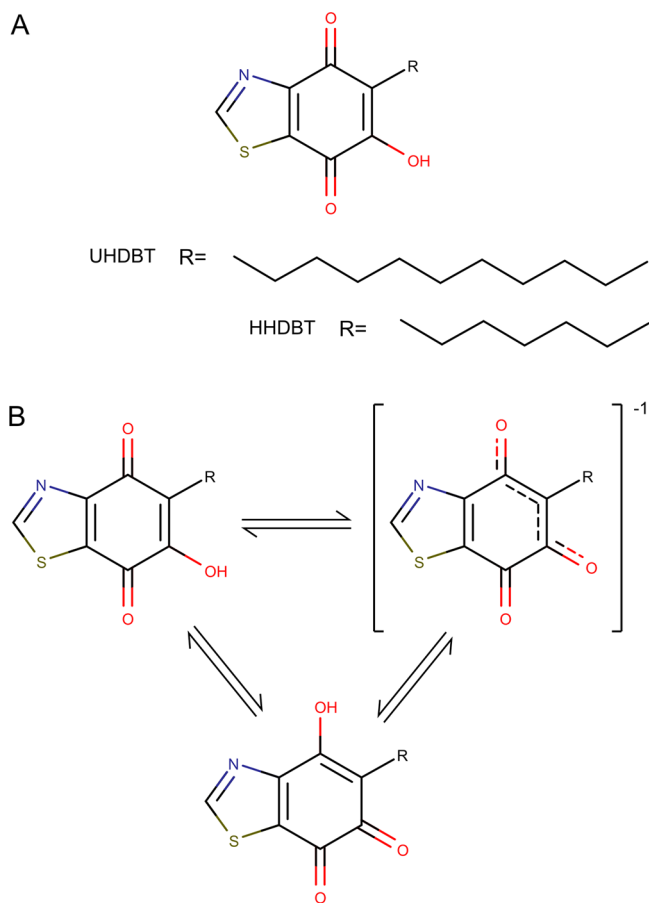


Figure 19. Structural features of 6-hydroxy-4,7-benzothiazolediones. (A) General structural formulas of *n*HDBT compounds. (B) Possible tautomeric states of *n*HDBT compounds.

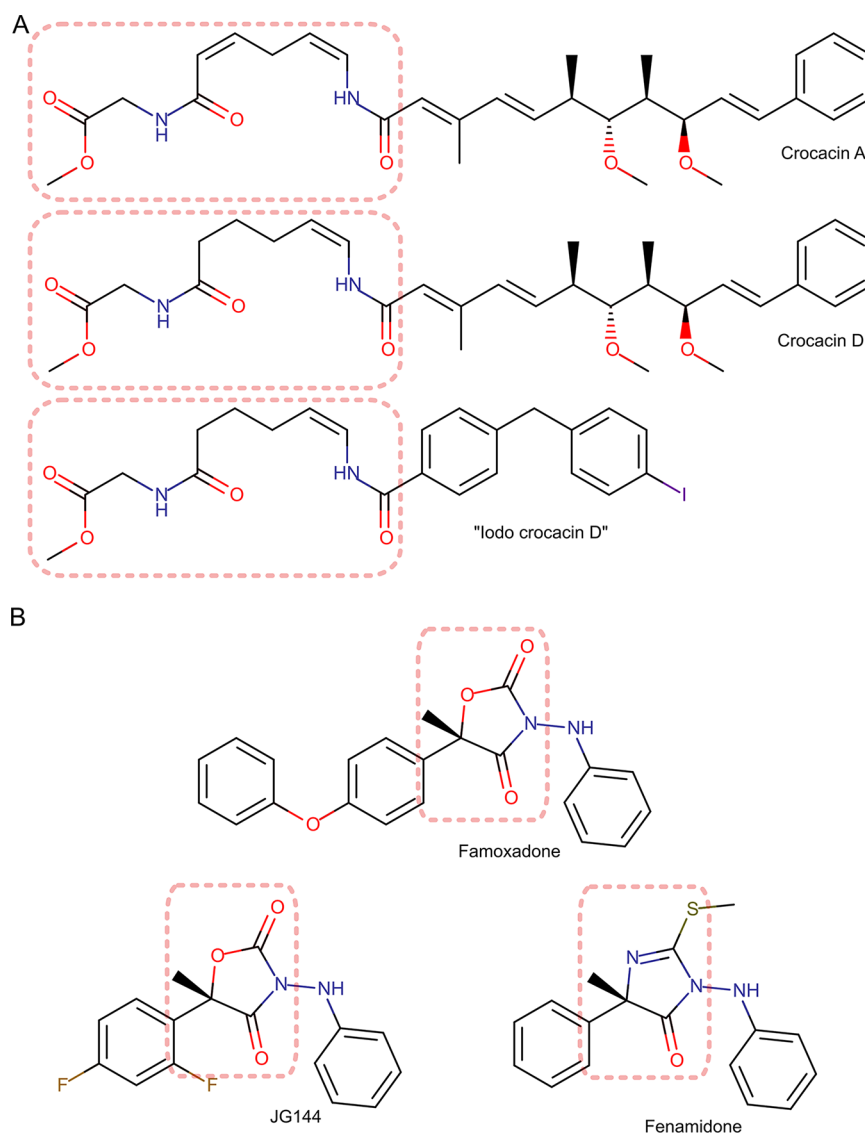


Figure 20. Crocacin and famoxadone-like compounds. (A) Structural formulas of natural crocacin A and D (top and middle, respectively) and synthetic derivative of crocacin D (bottom). (B) Structural formulas of famoxadone (upper), JG144 (lower, left), and fenamidone (lower, right). Pale red, dotted frames indicate the toxophore moiety of each compound.

Famoxadone, JG144, and fenamidone (Figure 20B) are synthetic fungicides. The toxophores of famoxadone and JG144 comprise 1,3-oxazolidine-2,4-dione, and those of fenamidone comprise imidazol-4-one.^{78,117,494,495} The famoxadone molecule is chiral, and the *S*-(-)-enantiomer has been shown to be active against *Cytc₁*.⁴⁹⁶ The crystal structures of famoxadone^{78,117,495} and its analogs^{78,117,495} indicate that these inhibitors bind to the Q_o site in the same fashion, with carbonyl oxygen at ring position 4 forming a hydrogen bond to the backbone nitrogen of the PEWY motif Glu. This resembles the binding mode of MOA-like inhibitors, but in contrast to those, famoxadone-like inhibitors are capable of immobilizing the ISP-HD near the Q_o site, close to *b*-position (P_f inhibitors subclass).⁴⁷⁴ However, famoxadone and its analogs do not form a hydrogen bond with the His of the ISP as in the case of other ISP-fixing compounds.^{78,117} Rather, the inhibitor binding is thought to induce conformational changes, which result in formation of a hydrogen bond between the 2Fe2S His ligand and a highly conserved Tyr residue of the *ef* α -helix of *Cytc₁*, thus immobilizing the ISP-HD in the near *b*-position.¹¹⁷

Myxothiazol A (Figure 21A, top) is a natural compound obtained from the predatory bacterium, *Myxococcus fulvus*.^{497,498} It is the best known representative of the thiazole-based bacterial toxins that possess a β -methoxyacrylamide or β -methoxyacrylate (MOA) toxophores.^{474,499,500} Myxothiazol is considered a classic P_m type Q_o inhibitor: its binding does not involve the immobilization of the IPS-HD in the *b*-position. On the basis of the structure of the bovine *Cytc₁* cocrystallized with myxothiazol,⁷⁷ it has been proposed that the inhibitor molecule is bound to the Q_o pocket, mostly through interactions of the dithiazole moiety with aromatic residues in the binding site and by a characteristic hydrogen bond formed between the amide oxygen atom of myxothiazol and the backbone amide of the conserved Glu in the PEWY motif. Moreover, the amide nitrogen of myxothiazol can form a hydrogen bond with the conserved Tyr of the PEWY motif. It was also suggested that the C18 methyl group of myxothiazol can serve as an unusual hydrogen bond donor to the sulfur atom of ^{Bt}Met124. It is worth mentioning that myxothiazol-related compounds that demonstrate inhibitory properties toward the Q_o site are more

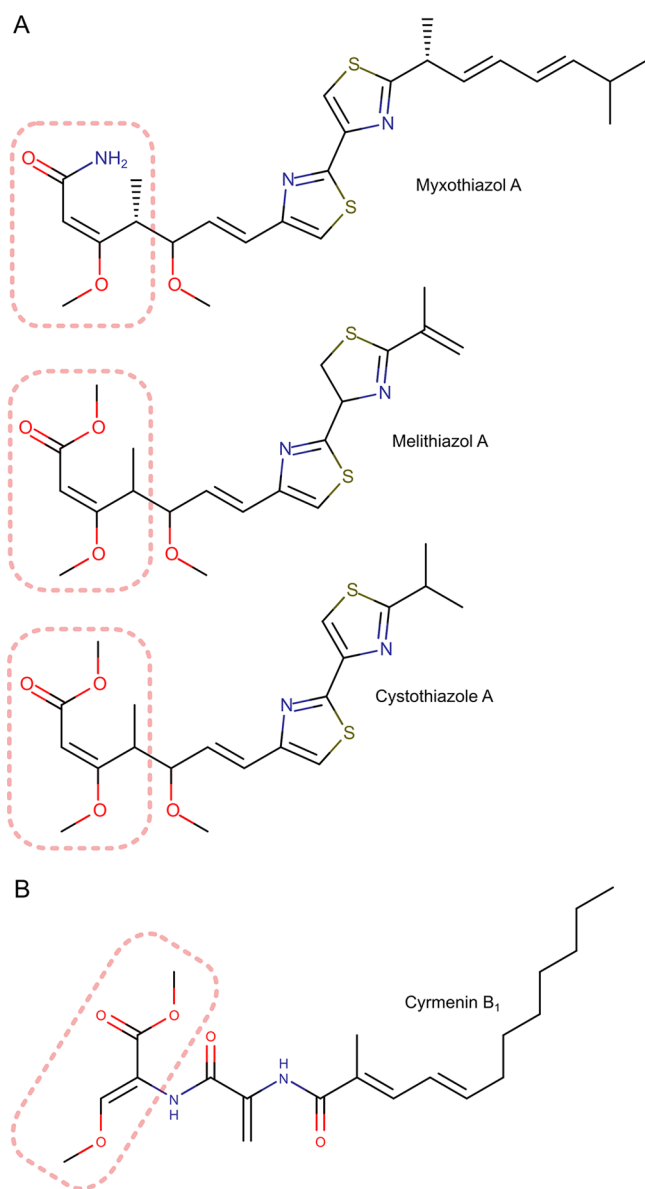


Figure 21. MOA-comprising myxobacterial toxins. (A) Structural formulas of natural Q_o site inhibitors with dithiazole moieties: myxothiazol A (top) comprising β -methoxyacrylamide toxophore and two others, comprising the β -methoxyacrylate toxophore, melithiazol A (middle) and cystothiazole A (bottom). (B) Structural formula of cyrmenin B₁. Pale-red, dotted frames indicate the toxophore moiety of each compound.

abundant. In the case of *M. fulvus* toxins, myxothiazol Z, which comprises a β -methoxyacrylate moiety, has also been shown to exhibit antifungal properties *in vivo*.⁵⁰¹ This group also includes the melithiazols (Figure 21A, middle) isolated from *Melittangium lichenicola* and several other strains⁵⁰² and cystothiazoles (Figure 21A, bottom) from *Cystobacter fuscus*,⁵⁰³ which were shown to exhibit antifungal properties *in vivo*.^{502,503} In the enzymatic assays with bovine SMPs, melithiazol A was shown to exert a similar spectroscopic effect on redox cofactors to that of myxothiazol.⁵⁰² Therefore, it can be expected that these inhibitors have a similar mode of binding to the Q_o site.

Another group of myxobacterial compounds, cyrmenins (Figure 21B), was obtained from *Cystobacter armeniaca* and *Archangium gephyra*. Cyrmenins are distinct from myxothiazol-

related compounds and comprise a MOA moiety substituted at the α -position.⁵⁰⁴ Cyrmenin B₁ has been shown to inhibit Cytbc₁, but the binding mode was not investigated in detail.⁵⁰⁵ The presence of the MOA toxophore suggests that cyrmenin targets the Q_o site as well.

Strobilurins (Figure 22) are currently recognized as a large group of synthetic P_m class Cytbc₁ inhibitors with various structures and toxophore moieties. However, such generalization can be confusing, and in fact they were all designed using natural fungal poliketides as a template. These compounds were isolated from several species of large, wood-decaying Basidiomycetes, and initially named strobilurins, for example, strobilurin A (also known as mucidin⁵⁰⁶) (Figure 22A, left) from *Strobiluris tenacellus*⁵⁰⁷ and oudemansin A (Figure 22A, right) from *Oudemansiella mucida*.⁵⁰⁸ Later an Ascomycete, *Bolinea lutea*, was also reported to produce strobilurins and their derivatives.⁵⁰⁹ Natural strobilurins possess the β -methoxyacrylate (MOA) toxophore^{499,510} (Figure 22, 1 in red frames), which targets the heme b_L proximal part of the Q_o site.^{511,512} In contrast to myxothiazol-like inhibitors, the β -methoxyacrylate moiety of strobilurins is substituted with a tail at the α -position, not the β -position. Because of this difference, their distinct origin, and their separate paths of biosynthesis,⁵¹³ myxothiazol and other myxobacterial compounds should not be referred to as “strobilurins”. The presence of MOA in both groups of compounds should be rather taken as a biochemical example of evolutionary convergence. Natural strobilurins exhibit a low photostability.⁵¹⁰ Therefore, various synthetic compounds (Figure 22B) with differently substituted MOA toxophores (Figure 22, 1 in red frames) have been created such as MOA-stilbene,⁵⁷ azoxystrobin,⁷⁷ or picoxystrobin.^{510,514} Several derivatives of classic MOA toxophore were developed (Figure 22B, 2–8 in red frames) such as oximino-acetate (2), e.g., kresoxim-methyl^{510,514} and trifloxystrobin,^{510,514} oximino-acetamide (3), e.g., dimoxystrobin,⁵¹⁰ methyl *N*-methoxycarbamate (4), e.g., pyraclostrobin,^{514,515} triazolone⁵¹⁶ (5), e.g., JZZ,¹¹⁷ tetrazolinone (6), e.g., metyltetraprole,⁵¹⁷ dihydro-dioxazine (7), e.g., fluoxastrobin⁵¹⁰ and the methyl-carbamate (8), e.g., pyribencarb.⁵¹⁸ Such diversity of synthetic strobilurin analogues is mostly a result of “patent wars” between agrochemical companies, driven by a large demand from the global fungicidal market.⁵¹⁴ Despite apparent differences in structure, man-made strobilurins are expected to share the same binding mode to the Q_o site as the classic MOA inhibitors. This has been partially confirmed by the results of X-ray crystallographic studies on Cytbc₁ with bound MOA-stilbene,^{77,83} azoxystrobin,⁷⁷ trifloxystrobin,⁴⁷⁴ iodinated derivative of kresoxim-methyl,⁴⁷⁴ and JZZ (PDB ID: 3L73),⁵¹⁹ showing that the toxophores of these inhibitors superimpose within the binding site, with formation of a hydrogen bond to the backbone amide of the conserved PEWY motif Glu residue. Among the synthetic strobilurin-like inhibitors mentioned here, pyribencarb has been suggested as a novel, “benzylcarbamate” type of Q_o inhibitor.⁵¹⁸ Indeed, it has been shown to possess a higher selectivity than other MOA analogues. However, neither its methyl-carbamate toxophore nor binding mode is unique as has been claimed because methyl-carbamate moiety is present in previously described natural crocacin, and also in macrolides isolated from sponges such as neopeltolide (Figure 23A, upper) from unidentified *Daedalopelta* sp.^{520,521} and leucascandrolide A (Figure 23A, lower) from *Leucascandra caveolata*.⁵²² Enzymatic assays confirmed that these compounds also exhibit inhibitory properties toward Cytbc₁.⁵²³ Moreover, the recent molecular modeling docking

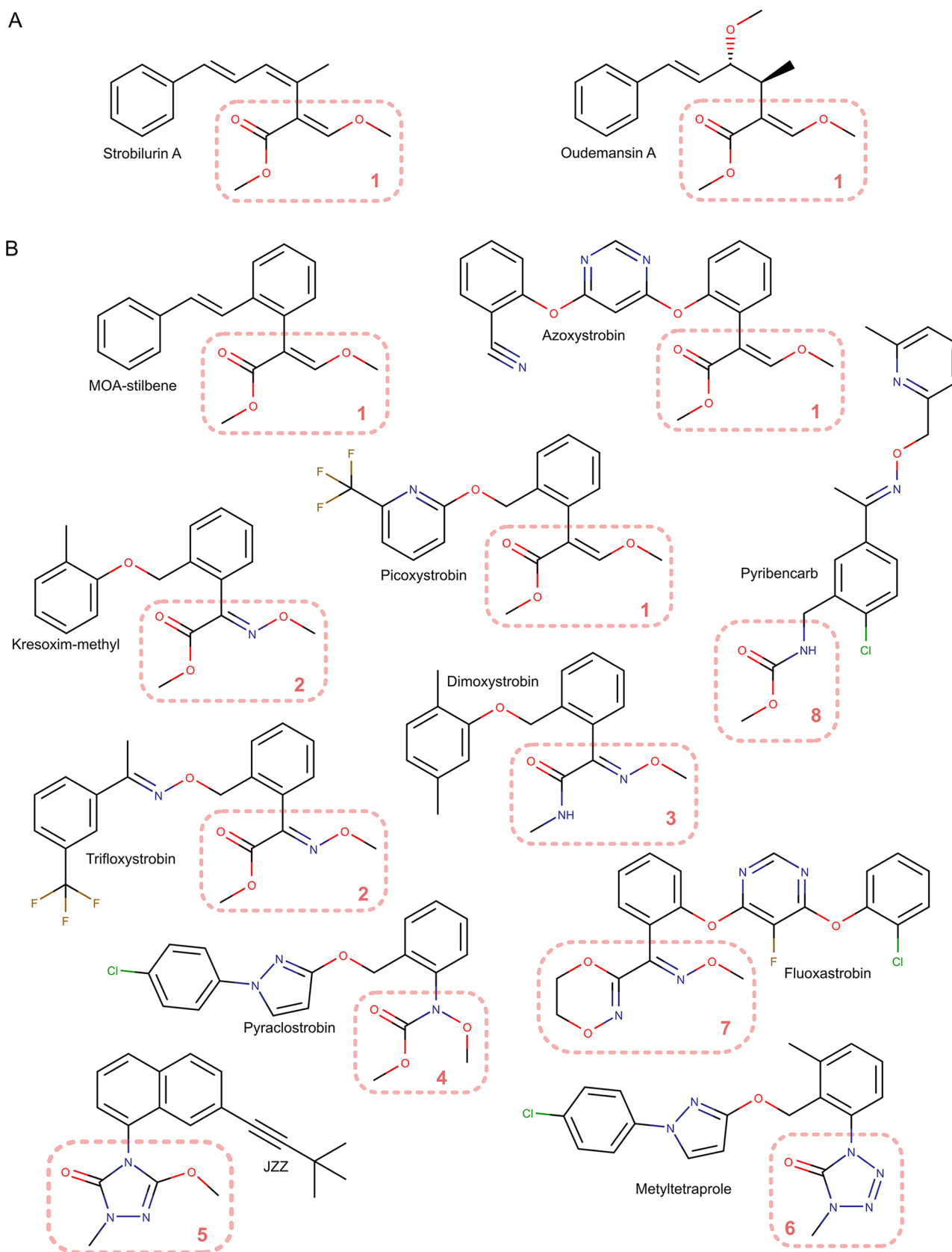


Figure 22. Structural formulas of selected (A) natural and (B) synthetic strobilurins. Pale-red, dotted frames indicate the toxophore moiety of each compound. Numbers within frames indicate the type of toxophore (explained in text).

studies revealed that pyribencarb, crocacin, and neopeltolide all bind to the Q_D site through their methyl-carbamate moieties, in a

way similar to the MOA moiety of azoxystrobin, forming a hydrogen bond to the backbone amide group of B^T Glu271.⁵²⁴

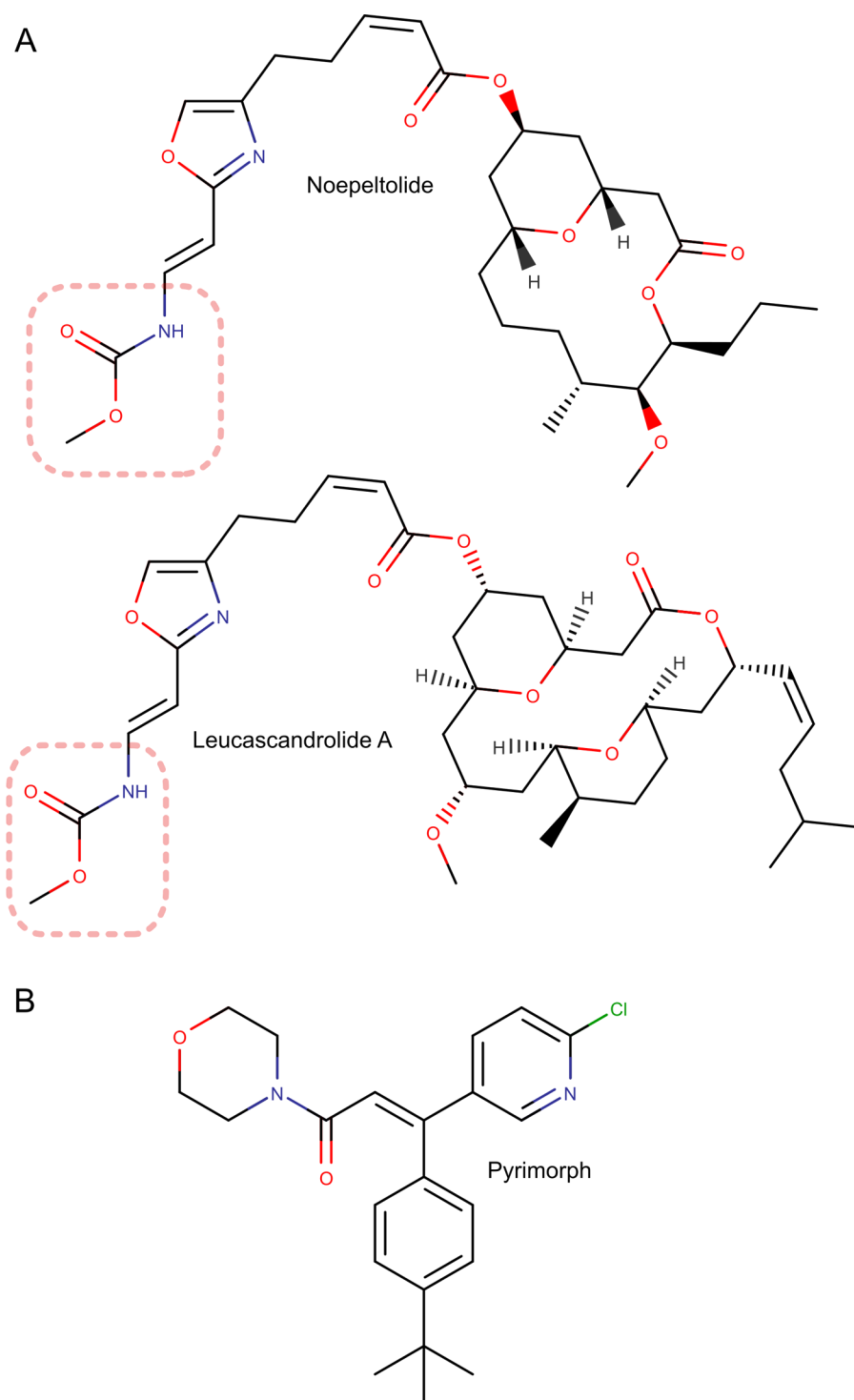


Figure 23. Structural formulas of (A) macrolides isolated from sea sponges, with their methyl-carbamate toxophores marked with frames, and (B) pyrimorph. Pale-red, dotted frames indicate the toxophore moiety of each compound.

Pyrimorph (Figure 23B) is a synthetic morpholine derivative, already in use as a fungicide against pathogens of plants.^{525–527} It has been shown to exhibit inhibitory activity toward multiple targets, including cellulose synthase A⁵²⁶ and *Cytc*₁.⁵²⁷ Results of enzymatic assays indicate that pyrimorph acts as a noncompetitive inhibitor of the *Q*_o site. Moreover, complementary molecular modeling studies showed that pyrimorph docks in the central cavity between *Cytc*₁ monomers, at the entrance of the *Q*_o site, and thus blocks access of the substrate.

The binding mode of pyrimorph has no resemblance to any other *Q*_o site inhibitor. It was found that it does not form hydrogen bonds within the *Q*_o site but instead it is held in place by hydrophobic and van der Waals interactions.⁵²⁷ Thus, pyrimorph should be considered a unique inhibitor type, distinct from MOA-related compounds.

5.1.3. Dual-Mode Inhibitors. Some inhibitors are capable of binding to both *Q*_i and *Q*_o catalytic sites; therefore, they should be considered as a third, dual-mode class of *Cytc*₁

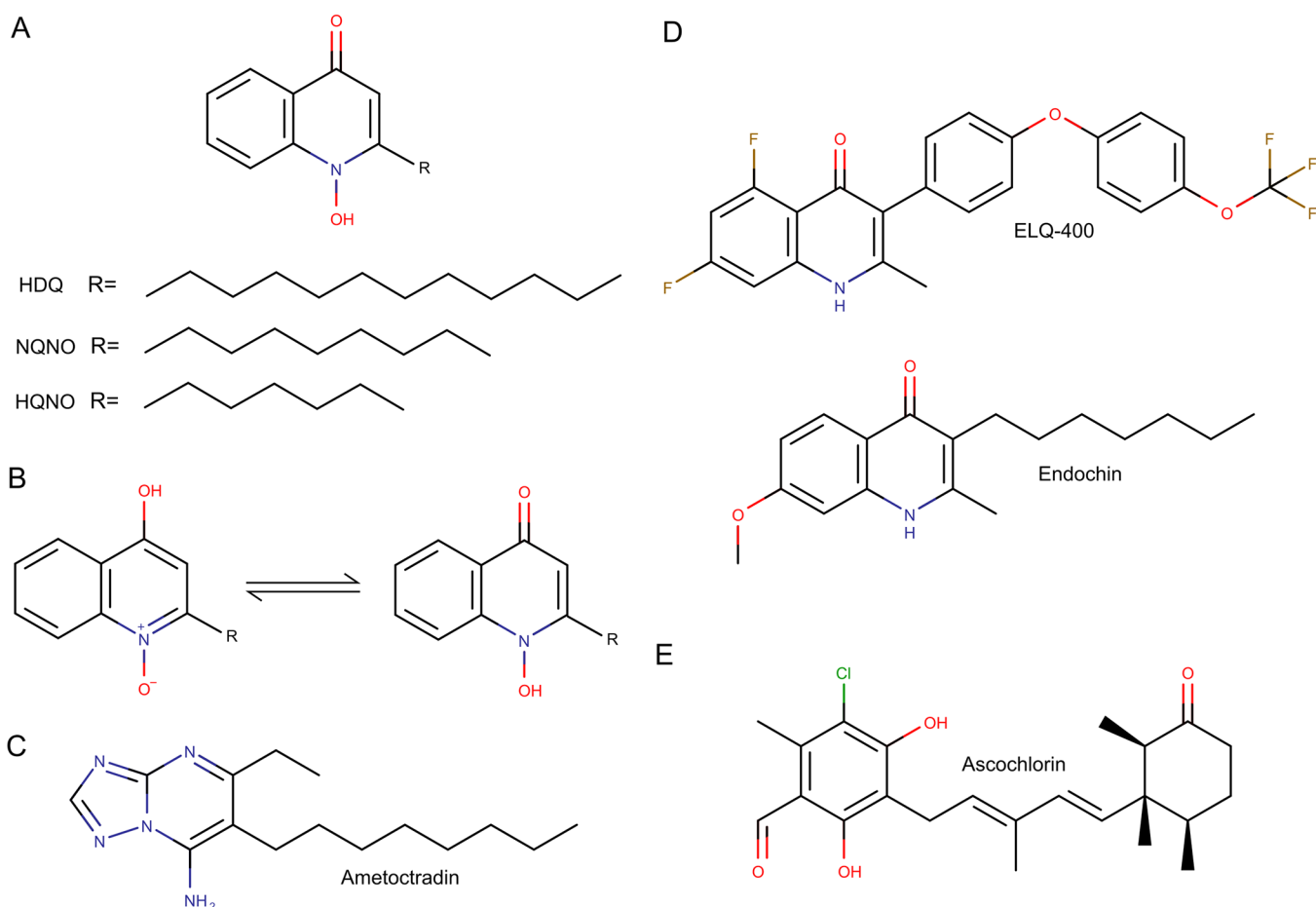


Figure 24. Structural formulas of dual-mode inhibitors of *Cytbc*₁. (A) 1-Hydroxyquinolin-4-ones. (B) Tautomeric states of 1-hydroxyquinolin-4-one. (C) Ametotradin. (D) Quinolones. (E) Ascochlorin.

inhibitors. They are often quinone analogues or compounds semi-isosteric with quinones and therefore able to mimic the natural substrate within both sites.

The 2-alkyl derivatives of 1-hydroxyquinoline-4-one, such as HQNO, NQNO, or HDQ (Figure 24A), are usually considered *Q*_i site inhibitors, with a mechanism of action similar to that of antimycin A.^{111,438,528} Some early reports suggested that HQNO and NQNO bound to *Cytbc*₁ can be displaced by both antimycin A and UHDBT.^{529,530} This effect was explained as a possible result of allosteric interactions between the two binding sites.⁵³⁰ However, more recent crystallographic analysis has shown that NQNO is indeed capable of binding to both *Q*_i and *Q*_o sites. It has been proposed that in solution, NQNO most likely exists as a mixture of two tautomers (Figure 24B), which is likely a determinant factor in this dual mode of binding. At the *Q*_i site, the NQNO tautomer with its hydroxyl group protonated (Figure 24B, left) can form a hydrogen bond to ^{Bt}Ser205, while the form with *N*-oxide protonated (Figure 24B, right) can hydrogen bond with ^{Bt}Asp228. In the structural model obtained in these studies, the ^{Bt}His201 imidazole ring was not in the correct orientation for hydrogen bonding. At the *Q*_o site, the *N*-oxide protonated form of NQNO can form two hydrogen bonds. The *N*-oxide oxygen forms a water-mediated hydrogen bond with ^{Bt}Glu271 of the PEWY motif, and the 4-carbonyl oxygen forms a hydrogen bond with the His (^{Bt}His161) ligand of 2Fe2S cluster, immobilizing the ISP-HD in *b*-position.⁷⁹ However, there is no data to confirm the dual-mode binding for other 1-hydroxyquinoline-4-ones. Recent studies suggest that HQNO

induces changes in the environment of the *Q*_o site, but not due to binding in the site.¹¹¹

ELQ-400 (Figure 24D, upper) is a 4(1H)-quinolone, one among a large number of derivatives of the antimalarial drug, endochin (Figure 24D, lower).^{441,531} Most of ELQs (endochin-like quinolones) are expected to inhibit the *Q*_i site of apicomplexan *Cytbc*₁.^{441,531,532} Thus, it was proposed that they be used in combination with the *Q*_o site-targeting atovaquone.⁵³² However, it has recently been suggested that the binding mode of ELQ-400 is more complex, with the inhibitor targeting both active sites.⁵³³ This proposal was strongly supported by mutational analysis and molecular modeling studies. At the *Q*_i site, ELQ-400 was predicted to bind in a similar manner to the substrate or pyridone inhibitors (mentioned earlier). At the *Q*_o site, it was predicted to bind similarly to atovaquone or stigmatellin, with a hydrogen bond formed by the NH group of the quinolone to the His ligand of 2Fe2S cluster.⁵³³

Ametotradin (Figure 24C) is a triazolopyrimidine derivative, acting as a highly selective inhibitor against the *Cytbc*₁ of oomycetes.^{469,534,535} It has been shown to be active against mammalian (porcine),⁴⁶⁸ but inactive toward yeast⁵³⁵ *Cytbc*₁. Ametotradin is commonly used in agriculture and available under trade name Initium.⁵³⁴ No cross-resistance of ametotradin with MOA-like inhibitors has been observed, so it is speculated to bind in the *Q*_o site in a manner similar to stigmatellin.⁵³⁵ However, the molecular modeling docking studies have shown that although ametotradin binds in roughly

the same part of Q_o pocket as stigmatellin, and forms a hydrogen bond to the carboxylate side chain of the conserved PEWY motif Glu residue, the distance to the 2Fe2S-ligating His residue is too far to expect formation of a strong hydrogen bond.⁴⁶⁸ In addition, there is no experimental indication that ISP-HD is immobilized by ametoctradin in the b -position, as in the presence of stigmatellin. More recent studies suggest that ametoctradin is a dual-mode inhibitor, targeting both the Q_i and Q_o site.⁵³⁶ This model seems to be supported by the observation that ametoctradin is inactive toward the wild-type strain of *Saccharomyces cerevisiae* and active toward a mutant with an altered Q_i site. On the basis of this finding, it was suggested that, like NQNO, ametoctradin can bind to both active sites.

Ascochlorin (Figure 24E) is an isoprenoid compound, which was independently isolated from four distinct fungal strains (*Ascochyta viciae*,^{537,538} *Cylindrocladium ilicicola*,⁴⁵⁴ *Fusarium* sp. LL-Z 1272,⁵³⁹ and *Acremonium luzulae*⁵⁴⁰) and described by four different research groups at about the same time. Because of this remarkable coincidence, it can be found in the literature and databases under three different names: ascochlorin, LL-Z 1272 γ , and ilicicolin D.⁵⁴¹ In the recent comprehensive biochemical, spectroscopic, and crystallographic studies, ascochlorin has been shown to bind to both Q_i and Q_o sites of bacterial, yeast, mammalian, and avian *Cytc₁*.⁵⁴² At the Q_i site, the position of the aromatic ring of bound ascochlorin overlaps with the position of the bound ubiquinone aromatic ring. Moreover, at the Q_i site, it has been proposed that ascochlorin forms a halide bond between the Cl atom and the conserved His (the proton donor in Q reduction) and a hydrogen bond between its hydroxyl group in the para position to Cl and the conserved Asp (the second proton donor in Q reduction). At the Q_o site, ascochlorin occupies a position similar to stigmatellin. A hydrogen bond is formed, possibly from both the hydroxyl group and the C=O group to the His ligand of 2Fe2S cluster, immobilizing ISP-HD at the b -position. On the other side of the aromatic ring, the Cl atom is suggested to form a halide bond with Glu in the conserved PEWY motif. However, as it has been pointed out that a mixture of conformations may exist, this remains uncertain. The dual mode of action can be explained in terms of ascochlorin and related compounds being in general, ubiquinone analogs, as they can mimic natural substrates also in other ubiquinol oxidoreductases.⁵⁴³

The inhibitors of *Cytc₁* already comprise numerous groups of compounds, both natural and synthetic, with new ones being discovered or developed almost every year.^{524,544} Many were omitted in this section, as little is known about their mechanism of action, and any attempt to deduce it would go beyond the scope of this review. Some recent discoveries in the field are rather unexpected, for example, the recent findings with karrikinolide (Figure 25, upper), a naturally occurring by-product from the combustion of plant material, which earlier had been shown to stimulate plant seed germination.⁵⁴⁵ Karrikinolide itself exhibits almost negligible inhibitory properties toward *Cytc₁*. However, some of its synthetic derivatives, such as 4-*n*-butylphenyl-substituted variant (Figure 25, lower), have been shown to inhibit porcine *Cytc₁* with efficiency comparable to commercially available inhibitors.⁵⁴⁶

5.2. Cytochrome b_6f -Specific Inhibitors

Several inhibitors have been employed to characterize the functional and structural features of the *Cytc_{6f}*. These compounds act on both the Q_p and the Q_n sites similarly to the situation described above for the *Cytc₁*.

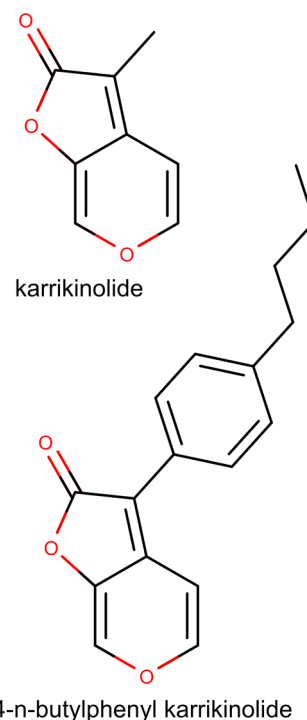


Figure 25. Structural formulas of karrikinolide (upper) and its 4-*n*-butylphenyl derivative (lower panel).

5.2.1. Inhibitors of the Q_p Site. Typical inhibitors of this site are DNP-INT, stigmatellin, and DBMIB.

(2,4-Dinitrophenylether of 2-iodo-4-nitro-thymol) (Figure 26) belongs to the family of dinitrophenyl ethers,⁵⁴⁷ that is,

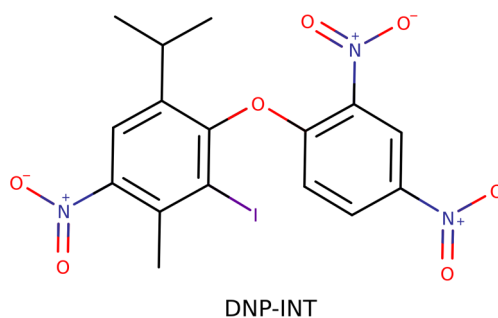


Figure 26. Chemical structure of DNP-INT inhibitor.

compounds that compete with plastoquinol for its oxidizing pocket without having redox properties. These compounds do not act as electron donors or redox mediators, unlike DBMIB (see further). DNP-INT inhibits photosynthetic electron flow *in vitro*, where its activity can be circumvented by addition of TMPD (N-tetramethyl-*p*-phenylenediamine), an artificial electron carrier able to mediate electron flow from PQH₂ to the *Cytc₆*.⁵⁴⁷ DNP-INT is also active *in vivo* as demonstrated by the work of Delosme and colleagues in *Chlorella sorokiniana*.⁵⁴⁸ In this organism, DNP-INT lowers the rate of *Cytc₆* oxidation and of PC reduction under single turnover flash conditions. Furthermore, DNP-INT diminishes the amplitude of the slow phase of the electro-chromic band shift (ECS), a modification of the absorption spectrum of intramembrane pigments in response to the transmembrane electrical field (ca. 3×10^5 V/cm) an expression of the quantum-mechanical Stark effect, following the establishment of the pmf across the thylakoid

membrane.⁵⁴⁹ The ECS slow phase (phase b) has been proposed to be a consequence of the transfer of an electron across the low potential chain of the cytochrome complex.⁵⁵⁰ A study by Fitzpatrick and colleagues⁵⁵¹ challenged the efficiency of DNP-INT as an inhibitor of photosynthetic electron flow. A possible explanation for this finding is that DNP-INT would be a poor inhibitor in continuous light, while efficiently blocking *Cytb₆f* under single turnover illumination, as previously reported.⁵⁵²

Stigmatellin (Figure 18A) is a potent antibiotic obtained from the myxobacterium *Stigmatella aurantiaca*, which inhibits both the *Cytc₁* and *Cytb₆f*.⁵⁵³ This compound binds to the PQH₂ oxidizing site, as shown by crystallographic studies in cyanobacteria and green algae,^{41,42} although not in the same position in the two organisms. Stigmatellin interacts with the 2Fe2S, raising its midpoint potential (in isolated *Cytb₆f*) from 320 to about 460 mV.⁵⁵⁴ This increase in potential is accompanied by changes in the EPR spectrum of the 2Fe2S cluster. *In vivo*, its action mechanism is similar to that DNP-INT.⁵⁵² Under single turnover flash illumination, stigmatellin reduces, in parallel, the rate of *Cytf* and of *Cytb₆* reduction in a concentration-dependent manner.

In *Cytc₁*, stigmatellin has been extensively used to probe conformational changes related to the moment of ISP-HD from a proximal site, that is, close to the quinol, to a distal site, close to *Cytc* (reviewed in Berry et al.¹). This movement is required to facilitate electron flow in the high potential chain, and to promote electron bifurcation, as predicted by the Q cycle mechanism.¹ In *Cytb₆f*, the transition between these two positions has not been resolved by X-ray crystallography in the same clear-cut manner as in *Cytc₁*. Nonetheless, electron crystallography⁵⁵⁵ has underlined movements of the ISP-HD in the *Cytb₆f* via the comparison of projection maps of thin three-dimensional crystals of *Cytb₆f* prepared with or without stigmatellin. The 2D crystallography has also suggested possible conformational changes in the transmembrane region of the complex, upon stigmatellin binding.

Unlike other inhibitors of *Cytb₆f*, stigmatellin binds not only to the luminal but also to the stromal side of the *Cytb₆f*.^{66,173} The Q_n site has a lower affinity for stigmatellin than does the p-side luminal site. In the Q_n site, stigmatellin faces the quinone exchange cavity, being in interaction with Arg 207 of the *Cytb₆* and the supplementary heme c_n (see also section 3.6.3).

DBMIB (2,5-dibromothymoquinone) (Figure 18 C) is probably the most representative of a class of inhibitors based on halogenated or hydroxylated lipophilic benzoquinones.⁵⁴⁷ DBMIB has been extensively used as a specific inhibitor of PQH₂ oxidation. Early results by Haehnel indicate that it does not affect PQ reduction by PSII while blocking its reoxidation by PSI.⁵⁵⁶ The number of DBMIB molecules required for inhibition is one per 300 chlorophylls, that is, one per electron-transport chain. This would argue in favor of a 1 to 1 binding stoichiometry with *Cytb₆f*. However, studies of the consequences of DBMIB on the EPR spectrum of the 2Fe2S by Roberts and Kramer led to the conclusion that two molecules of DBMIB bind to each monomer of the spinach *Cytb₆f*, both in the isolated form and in intact thylakoid membranes.⁵⁵⁷ Binding likely occurs in two sites: a high affinity one, where DBMIB binding would cause small shifts in the EPR spectrum of the 2Fe2S similar to those induced by stigmatellin, and a low-affinity site, where binding was induced by superstoichiometric amounts of the inhibitor. DBMIB binding is accompanied by the appearance of a new EPR signal (*g* = 1.94). The binding of

two molecules of DBMIB to the Q_p pocket would be consistent with the so-called “double-occupancy” models proposed in the case of *Cytc₁* (see section 7.2). However, crystallographic data unambiguously showed that only one molecule of DBMIB can bind to the PQH₂ oxidation site.⁶⁷ To reconcile these findings, Roberts and co-workers repeated the EPR spectra with oriented *Cytb₆f*⁴¹⁰ and found that DBMIB affects the orientation of the ISP-HD within *Cytb₆f* depending on the stoichiometry of the inhibitor at the Q_p site. With a single DBMIB, the EPR signatures of the ISP-HD are consistent with this protein being in the proximal position (close to the Q_p pocket), similar to the orientation observed in the X-ray crystal structure of the *Cytb₆f* in the presence of DBMIB.⁶⁷ With ≥2 equiv. of DBMIB bound, the ISP-HD would be in a position resembling the one observed in the *Chlamydomonas reinhardtii*, *Cytb₆f* in the presence of tridecylstigmatellin (TDS),⁴¹ suggesting that the low-affinity DBMIB site is at the distal niche. This conclusion is consistent with earlier EPR measurements of isolated *Cytb₆f* poisoned with DBMIB⁸⁴ and can explain the peculiar mechanism of inhibition of PQH₂ oxidation by this compound observed *in vitro* and *in vivo*.

Early studies by Rich and colleagues⁵⁵⁸ showed that reduced DBMIB (DBMIBH₂) does not block the *Cytb₆f* activity during its first turnover. Thus, DBMIB would bind the complex in its reduced form but only become inhibitory upon its oxidation. The inhibitory complex would thus involve a semiquinone or a quinone form of DBMIB. This hypothesis was subsequently confirmed *in vivo*.⁵⁵² The authors found that DNP-INT affects equally the low- and high-potential chain of *Cytb₆f* decreasing the rates of both *Cytf* reduction and *Cytb₆* turnover. Conversely, DBMIB inhibits only the rate of *Cytf* reduction while reducing, at the same time, the amplitude of *Cytb₆* redox signals. The accessibility of DNP-INT to the Q_p site was unaffected by preillumination, while that of DBMIB was greatly enhanced, even after a single turnover. Overall, the authors propose that oxidation of DBMIBH₂ by a single turnover flash would trigger the same conformational changes of the ISP-HD that occurs during oxidation of PQH₂ in unpoisoned *Cytb₆f*. This would allow transferring one electron to the high-potential chain and generating at the same time the inhibitory DBMIB species.⁵⁵² Slow reduction of DBMIB inside the Q_p pocket (see Rich et al.⁵⁵⁸) would regenerate DBMIBH₂, which would diffuse out of the quinol binding pocket, unslashing the inhibition. A relatively recent study by Sarewicz/Bujnowicz et al. revealed that the EPR spectrum of 2Fe2S in DBMIB-supplemented spinach *Cytb₆f* is frequency-dependent, which is a strong indication that DBMIB semiquinone at the Q_p site is spin–spin coupled to the reduced 2Fe2S.⁴⁸²

Besides being extensively used to characterize electron flow in the photosynthetic chain, DBMIB has also been largely employed to study cell biological responses in photosynthetic organisms. Combining DBMIB with the PSII specific inhibitor DCMU allows the PQ(H₂) pool to be either reduced (DBMIB) or oxidized (DCMU) in the light. On the basis of this approach, it was proposed that the redox state of the PQ(H₂) pool regulates the transcription of a subset of chloroplast genes to adjust the relative stoichiometric amounts of the two reaction centers (PSII and PSI) (see, e.g., reviews by^{559–561}). These findings have led to the concept of redox mediated plastid retrograde signaling that orchestrates the expression of genes by the plastid and nuclear genomes, a concept that is still discussed (review in refs.^{562,563}).

5.2.1.1. Ions. Divalent cations also inhibit the catalytic cycle of the Cytb_{6f} in concentration-dependent manner. Inhibition was first reported for Cu^{2+112} and then for Zn^{2+108} . Both metals were proposed to hamper the movement of the ISP-HD. On the basis of EPR data, it was proposed that binding of the two ions in proximity of His143 in the ISP would induce the inhibition. Later crystallographic studies with Cd^{2+} poisoned Cytb_{6f}^{173} provided a structural confirmation of this hypothesis, showing the existence of two Cd^{2+} binding sites, the strongest one being mediated by Cd–H143 interactions.

5.2.2. Inhibitors of the Q_n Site. Typical inhibitors of this site are N(H)QNO, MOA stilbene and, to a lower extent, stigmatellin.

NQNO (2-n-nonyl-4-hydroxy-quinoline *N*-oxide) was first investigated by Jones and Whitmarsh⁵⁶⁴ *in vitro* and by Joliot and Joliot⁵⁶⁵ in *Chlorella sorokiniana* cells. Jones and Whitmarsh⁵⁶⁶ used single turnover and steady state absorption spectroscopy to show that NQNO binds to the stromal quinone site, thereby inhibiting the oxidation of the Cytb_6 heme, and slowing down electron transfer between the two *b*-hemes. On the basis of the effect of NQNO on the ECS kinetics, the authors concluded that (i) the slow phase of the ECS under single turnover flash (phase b, see above) is due to electron transfer between the two *b* hemes, followed by a reaction associated with PQ reduction; and (ii) the two quinone binding sites would be separated by 70% of the dielectrically weighted distance across the membrane.

Joliot and Joliot further explored the relationship between this inhibitor, redox changes of Cytb_6 , and changes in the kinetics and amplitude of phase b of the ECS. On the basis of the consequences of NQNO poisoning of phase b, the authors proposed that reduction of the quinone occurring at the stromal site (Q_n) would be coupled to protonation, implying that this site is connected to the outer face of the thylakoid by a proton channel. Recent crystallographic studies have provided a molecular interpretation for these findings, showing that at least two residues (Asp20 and Arg207) form a H^+ wire connecting the stroma to the quinone binding pocket.⁶⁶

NQNO binds in close proximity to the heme c_n , acting as a direct axial ligand of the heme. This interaction explains why NQNO binding to the Cytb_{6f} leads to a strong modification of the properties of heme c_n .¹⁹¹ This heme titrates as a one-electron Nernst curve with a E_m value of +100 mV in unpoisoned complexes. Its reduced minus oxidized spectrum displays a broad absorbance increase peaking at approximately 425 nm. Upon binding of NQNO two heme c_n titration waves are visible: one with an E_m value similar to that observed in noninhibited enzyme and the other with a midpoint shift by about –225 mV.¹⁹¹ Moreover, the Soret spectrum of the heme is shifted by 1 nm to longer wavelengths upon NQNO binding.¹⁷³

MOA-stilbene (Figure 22, 1 in red frames) was first studied by Rich and colleagues,⁵⁶⁷ who showed that at variance with Cytbc_1 , MOA-stilbene does not affect quinol oxidation but instead quinone reduction. Its binding to Cytb_{6f} induces a red-shift of the Soret and visible absorbance bands of the *b* hemes, enhancing their “oxidant-induced reduction” and slowing down their subsequent dark reoxidation at the same time. Its effect is therefore similar to that of NQNO.

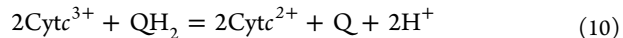
Later, Kramer and Crofts²¹⁸ confirmed these results, showing that MOA-stilbene increases the reduction of the high potential form of Cytb_6 by ~45%, and reduced the amplitude of the ECS signal by about 25%, again in agreement with results obtained with NQNO.

Stigmatellin (Figure 18A) also binds to the Q_n site with very similar features as NQNO. However, due to its higher affinity for the Q_p site, this inhibitor cannot be used to test the mechanism of electron and proton transfer to PQ.

6. THERMODYNAMIC BACKGROUND OF CYTOCHROME BC CATALYSIS

This section covers the thermodynamic principles behind operation of Cyt_{bc} , using the reactions characteristic for Cytbc_1 . If the Cytb_{6f} were to operate according to a “modified Q cycle”, as described for Cytbc_1 , then the equations below would be equally applicable to both complexes, simply by exchanging the parameters for PC/ Cytc_6 and PQ(H_2) with those of Cytc and UQ(H_2) respectively. However, as described in detail in section 3.6.5, some doubts remain about the operation of a Q cycle at Cytb_{6f} , with the possibility that additional electrons may be added to the Q_n side from soluble components. In this case, the stoichiometry of the equations below will clearly be altered for the Cytb_{6f} .

In aqueous solutions, the quinone-dependent enzymatic reaction of Cytbc_1 can be summarized as^{1,568}



where Cytc^{3+} and Cytc^{2+} stand for ferri- and ferro- Cytc , respectively.

In this case, the change in ΔG associated with reaction of electron transfer from quinone molecules to Cytc molecules after mixing UQH₂ derivatives with Cytc can be estimated using the relationship:⁵⁶⁹

$$\Delta G = -nF\Delta E_h \quad (11)$$

where ΔE_h is the difference in the actual redox potential between the couples of the donor ($E_{h(D)}$ of UQ/UQH₂) and acceptor ($E_{h(A)}$ of $\text{Cytc}^{3+}/\text{Cytc}^{2+}$) and n is the number of electrons in the reaction (here $n = 2$) and F is the Faraday constant:

$$\Delta E_h = E_{h(A)} - E_{h(D)} \quad (12)$$

The corresponding $E_{h(A)}$ and $E_{h(D)}$ can be calculated using the Nernst equation, which takes into account the redox midpoint potentials at pH 7 (E_{m7}^Q and E_{m7}^{Cyt}) and actual concentrations of reduced and oxidized form of UQ/UQH₂ and $\text{Cytc}^{3+}/\text{Cytc}^{2+}$, the temperature (T), and the gas constant (R):⁵⁶⁹

$$E_{h7(A)} = E_{m7}^{\text{Cyt}} + RT/nF \ln([\text{Cytc}^{3+}]/[\text{Cytc}^{2+}]) \quad (13)$$

$$E_{h7(D)} = E_{m7}^Q + RT/nF \ln([\text{UQ}]/[\text{UQH}_2]) \quad (14)$$

During a typical measurement of Cytbc_1 turnover rate, the substrates are added to the solutions in total concentrations that should exceed Michaelis–Menten constants, while proportions of oxidized to reduced substrates are approximately 0.05 and 0.95 for $[\text{UQ}]/[\text{UQH}_2] + [\text{UQ}]$ and $[\text{Cytc}^{3+}]/([\text{Cytc}^{2+}] + [\text{Cytc}^{3+}])$, respectively.⁵⁷⁰

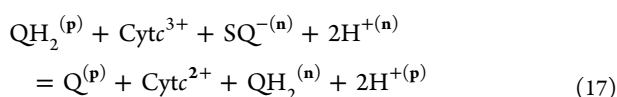
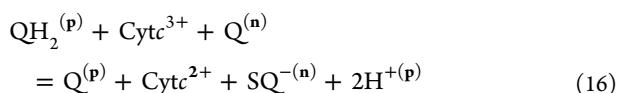
Taking +260 mV as the E_m at the physiological pH of 7 (E_{m7}) of $\text{Cytc}^{3+}/\text{Cytc}^{2+}$,⁵⁷¹ +70 mV as the E_{m7} of Q/QH₂,⁴⁸⁸ and the number of electrons $n = 2$, one may calculate the energy released during the oxidation of 1 mol of QH₂ and reduction of 2 mol of Cytc :

$$\Delta G = -nF\Delta E_h = -66 \text{ kJ/mol} \quad (15)$$

For comparison, the ΔG of oxidation of 1 mol of NADH in complex I and reduction of O₂ in complex IV in the

mitochondrial respiratory chain is approximately -224 kJ/mol.¹⁶²

However, for the enzyme operating in living cells, eq 11 is too simple by far and ignores an important fact that Cyt c reduction by Cyt bc_1 is associated with the coupling of two oppositely directed redox reactions taking place at the Q_o/Q_p and Q_i/Q_n catalytic sites. Moreover, these reactions are coupled to the release of protons to the p side, and uptake of protons from the n side of membrane. Therefore, the simple eq 10 should be split into two equations to account for this spatial separation of the two different quinone redox reactions in Cyt bc_1 :



Superscripts (p) and (n) denote that the respective reaction takes place at the Q_o/Q_p and Q_i/Q_n site, respectively.

These reactions lead to proton transfer across the membrane in which Cyt- bc is embedded. Four protons are released (from Q_o/Q_p site) to the positive side (p side), while two protons are taken (at the Q_i/Q_n site) from the n side of the membrane. In this way, the proton transfer catalyzed by the enzyme contributes to an increase of the transmembrane electrochemical potential gradient ($\Delta\psi$), which is used to drive the energetically uphill reaction of ADP to ATP conversion in cells.¹⁶² However, it is worth mentioning here that the protons are transferred across the membrane by coupling deprotonation of QH_2 at p side with protonation of Q at n side, according to Mitchelian redox loop mechanisms. This is different from other complexes such as CcO , for example, which catalyzes active pumping of protons through specific proton channels.

Proton motive force is a value expressed as the sum of two components: difference in proton concentration between two sides of membrane (ΔpH) and the electric potential difference ($\Delta\psi$) between the two sides of membrane. However, for simplicity, Δp is commonly converted to equivalent differences in electric potential expressed in millivolts.

In mitochondria, ΔpH is usually small, and thus, Δp is largely dominated by $\Delta\psi$, which is on the order of 150–200 mV,¹⁶² depending on the actual state of mitochondria (ADP/ATP ratio, oxygen tension, and the activity of decoupling proteins). The architecture of Cyt- bc imposes an additional energetic barrier to electron transfer from the Q_o/Q_p site through heme b_L/b_p and b_H/b_n to the Q_i/Q_n site as the electrons must be transferred against $\Delta\psi$, when the enzyme is embedded in the coupled membrane.^{161,572–574} Therefore, eq 15 must take into account this additional energetic barrier:

$$\Delta G = -nF(\Delta E_h - \Delta\psi) \quad (18)$$

Under conditions in which the $\text{Q}(\text{H}_2)$ pool and Cyt c /PC pool are half reduced, the driving force is significantly lowered. As a result, increasing $\Delta\psi$ influences the ET process, hence increasing the probability of reduction of heme b_L/b_p at the expense of heme b_H/b_n . Under extreme conditions, $\Delta\psi$ can be high enough to impair the QH_2 oxidation at the Q_o/Q_p site leading to an increase in superoxide generation during the catalysis.⁵⁷³

7. MECHANISTIC INSIGHTS INTO THE CATALYTIC Q_o/Q_p SITE

7.1. Overview of Structure of the Q_o Site

Cyt b of Cyt bc_1 is built of 8 transmembrane helices arranged in two helical bundles with the first bundle (helices A to E) incorporating both hemes b (b_L and b_H) (Figure 8A). The second bundle (helices F to H) is located in the vicinity of heme b_L and together with the large helix-connecting loops at the intermembrane (periplasmic) side of the membrane, forms the Q_o site binding pocket.^{20,21,79,132} This pocket is highly hydrophobic and contains many highly conserved residues. The major loop regions that participate in formation of the Q_o site include the two helices $cd1$ and $cd2$ of the CD loop and the ef helix of the EF loop. The helices $cd1$ and $cd2$ cap the pocket from the intermembrane (periplasmic) space where Cyt b interacts with the ISP-HD. Transient binding of the ISP-HD to Cyt b brings the 2Fe2S cluster into proximity with the substrate occupying the Q_o site pocket, which means that in this pocket the substrate can be flanked by two redox active cofactors: the 2Fe2S and heme b_L . This corresponds to the state when the two cofactors required for electron bifurcation are present close enough to the substrate bound at the Q_o site for fast electron transfer to occur (the exact distance is not known but approximated from the crystal position of the Q_o site inhibitors, see further). Because of the large-scale oscillatory movement of the ISP-HD between the Cyt b and Cyt c_1 (see section 3.4), there are states of the Q_o site with 2Fe2S not present at the site and therefore unable to interact with the bound substrate (precluding the bifurcation reaction). The movement itself is an inherent part of the catalytic cycle as it connects the Q_o site with heme c of Cyt c_1 : transient binding of the ISP-HD away from Cyt b to Cyt c_1 brings the 2Fe2S and heme c_1 close enough for fast electron transfer between these two cofactors.

7.2. Quinone Binding to the Q_o Site

Binding of the QH_2 molecule to the Q_o site is an obvious requirement for initiating the catalytic QH_2 oxidation. Despite many years of study, the way in which Q or QH_2 are bound to this site is still not fully understood. A major part of what is known about these interactions comes from investigation of site-directed mutants of bacterial Cyt bc_1 , usually of conserved residues at the Q_o site, in spectroscopic studies, mainly EPR spectroscopy and X-ray crystallography. The latter method has always been considered as the most promising tool for detection of specific chemical interactions between substrates and the protein. However, soon after solving the first structures of Cyt bc_1 , it became clear that in the case of this protein (as in some other quinone-binding proteins), the crystallography failed to show natural substrate bound at the Q_o site and neither Q nor QH_2 has been resolved within this site.²⁰ It has been proposed that this failure is due to the Q molecules at the Q_o site being in a very dynamic state. However, a simple loss of the substrate during the isolation and crystallization of the protein also cannot be ruled out, in particular in the light of spectroscopic observations that samples of isolated Cyt bc_1 tend to have an empty Q_o site.^{59,127,260}

In the absence of structures containing natural substrate at the Q_o site, structures obtained with many different site-specific inhibitors have served as a starting point for the construction of models for Q binding to Q_o . Several of these proposals, including the most recent ones, considered specific interactions derived

after substituting the chromone ring of stigmatellin with the natural quinone ring.^{91,95,96,575,576}

In studying the binding of QH₂ and Q to the Q_o site, EPR spectroscopy of the reduced 2Fe2S has been one of the most widely used methods. It has benefited from the observation that, for Cytbc₁, the continuous wave EPR (CW-EPR) spectra of 2Fe2S is highly sensitive to variation in the type of molecule occupying the Q_o site and its redox state, providing a convenient means to monitor the status of the site in the native membranes. This approach seems to also be applicable for detection of PQ or PQH₂ bound to the Q_p site of Cytb_{6f}.⁵⁷⁷ From the very beginning it became apparent that CW-EPR spectra of 2Fe2S could not be simulated by modeling a single EPR component for the 2Fe2S¹⁵⁹ nor by using a statistical theory of *g* strain that has previously worked for other iron–sulfur clusters.⁵⁷⁸

The sensitivity of the CW-EPR spectra of the reduced 2Fe2S to the occupant of the Q_o site is best documented for bacterial Cytbc₁. It was observed that the shape of the spectrum differed depending whether Cytbc₁ was embedded in native membranes or isolated and solubilized in detergent micelles.¹²⁷ It was also observed that the shape of the spectrum in the membranes was sensitive to the total quinone content in the membrane^{109,260,579,580} as well as being a convenient tool for discriminating between Q or QH₂ occupancy of the Q_o site.⁵⁸¹

In bacterial chromatophores, the most characteristic spectral feature of 2Fe2S is the *g_x* transition, which equals 1.800 when UQ bound to the Q_o site interacts with the cluster.⁵⁸⁰ Among all the transitions of the 2Fe2S spectrum, the *g_x* component appears the most influenced by the occupant of the Q_o site. When the site contains UQH₂, *g_x* broadens significantly and shifts to approximately 1.777.^{109,579,580} Other transitions (*g_z*, *g_y*) are also relatively narrow when UQ is bound to the Q_o site, suggesting a relative small *g*-strain of the cluster.^{90,111,113,580,582} These transitions also broaden, although less significantly compared to *g_x* when UQ exchanges with UQH₂.

Careful analysis of the *g_x* transition has established that measurements of relative proportions of *g_x* at 1.800 versus *g_x* at 1.777 signal can be used to monitor the redox state of the Q(H₂) pool in the membrane. Most probably the *g_x* = 1.800 transition results from interaction of the 2Fe2S environment with the carbonyl group of UQ, while the *g_x* = 1.777 results from interaction with the hydroxyl group of UQH₂.⁵⁷⁹ However, this sensitivity of the 2Fe2S spectrum to UQ or UQH₂ is completely abolished when low-molecular-weight alcohols, such as methanol, ethanol, or glycerol (a common cryoprotectant), are present.⁵⁸³ This most likely results from interaction of the hydroxyl group with the ^{Rh}H156 ligand of 2Fe2S (^{Bt}H161). It follows that measurements of the redox state of the Q(H₂) pool by CW-EPR spectra of 2Fe2S (which must be performed at low temperatures) must avoid cryoprotective agents as they usually contain hydroxyl groups.⁵⁸⁴ On the other hand, the absolute necessity of using cryoprotectants in low-temperature pulse EPR measurements compromises sensitivity of the 2Fe2S spectra to UQ and UQH₂. Otherwise, formation of ice may cause aggregation and denaturation and may significantly increase the efficiency of paramagnetic relaxation distorting the results, which are dependent on spin–lattice relaxation rates.

For the empty Q_o site, the *g_x* transition is very broad and its *g* value approaches 1.765.⁵⁸¹ A similar shape and *g* value for the *g_x* transition is detected when the Q_o site is occupied by the inhibitor myxothiazol or MOA-stilbene.⁵⁷⁹

Interestingly, the experiments on partial extraction of UQ from purple bacteria membranes (chromatophores) revealed

that when the ratio of the number of Q molecules per Q_o sites is between 2:1 and 1:1, the *g_x* value changes to approximately 1.78 and its line width lies in-between *g_x* = 1.800 (for UQ) and 1.777 (for UQH₂).⁵⁸⁵ Furthermore, this 1.78 transition could not be reproduced by a linear combination of “UQ *g_x* 1.800” and “empty-site *g_x* 1.765” lines. To explain these observations, Ding et al. proposed that there are two niches, strong and weak quinone binding at Q_o: Q_{os} and Q_{ow}, with dissociation constants (*K_d*) of approximately ~0.05 and ~1 mM, respectively.²⁶⁰ Taking these *K_d* values and assuming that, under normal conditions, the effective concentration of UQ in the membrane is ~30 mM,²⁶⁰ it was concluded that the Q_o site should be occupied by two molecules of UQ at the same time. This led the authors to formulate a “double-occupancy” model, according to which the Q_o site can accommodate two UQH₂ molecules simultaneously.^{260,579,581} Further support for the double occupancy model has come from determination of the stoichiometry of UQH₂ binding to Cytbc₁ by NMR-based analysis of inhibitor displacements. With this approach, two molecules of UQ(H₂) were shown to bind specifically to the Q_o site.⁵⁸⁶ This observation was incorporated into a model that aimed to explain the mechanism of bifurcation. It was proposed that UQH₂ and UQ binds at the same time in the Q_o site and undergo a comproportionation reaction according to eq 7, resulting in formation of two SQ molecules, each donating one electron to the *c*- or *b*-chain.^{586,587} However, this concept has not been verified with other, more direct studies.

In the opinion of the authors of this review, the double-occupancy model remains problematic and it was previously the subject of debate.⁹¹ When measuring the redox state of the Q(H₂) pool in samples poised at ambient redox potentials (*E_h*) equal to or lower than the *E_m* of the UQ/UQH₂ couple, the Q_o site would be occupied by UQ at the Q_{os} niche with an increasing population of UQH₂ at the Q_{ow} niche as *E_h* shifts negatively. If this happened during redox titration of the membranous UQ(H₂) pool, as monitored by EPR measurements of the 2Fe2S spectrum, the *g_x* would likely be different from the observed experimentally linear combination of *g_x* = 1.800 (corresponding to UQ^{Qos}UQ^{Qow}) and 1.777 (corresponding to UQH₂^{Qos}UQH₂^{Qow}) transitions. Such a titration should also reveal a separate component corresponding to the unique UQ^{Qos}UQH₂^{Qow} state or respective molecules after comproportionation. Alternatively, the presence of two nonequivalent sites for UQ(H₂) at the Q_o site would very likely lead to a non-Nernstian shape of the redox titration curve for the UQ/UQH₂ couple, detected in the *g_x* transition of 2Fe2S. However, none of these observations can be made, and the titration curve in such experiments closely follows the Nernst equation with *n* = 2.^{109,580} In addition, the *E_m* values of UQ/UQH₂ obtained from EPR measurements of the 2Fe2S spectra remain consistent with spectrophotometric measurements of the redox midpoint potential of this couple.⁵⁸⁸ This suggests that UQ and UQH₂ at the Q_o site are in dynamic equilibrium with UQ and UQH₂ of the membranous pool. Going further, one may conclude that if changes in EPR spectra follow the redox state of the UQ(H₂) pool, UQ is not favorably bound to the site over UQH₂ and *vice versa*.

The first step of the QH₂ oxidation at the Q_o site involves binding of QH₂ and association of the ISP-HD with an oxidized 2Fe2S to the Q_o site. Thus, the initial step of the reaction is formation of the enzyme–substrate (ES) complex, which depends on equilibrium constants describing the ratio between the population of Q_o sites with QH₂ bound and those that are

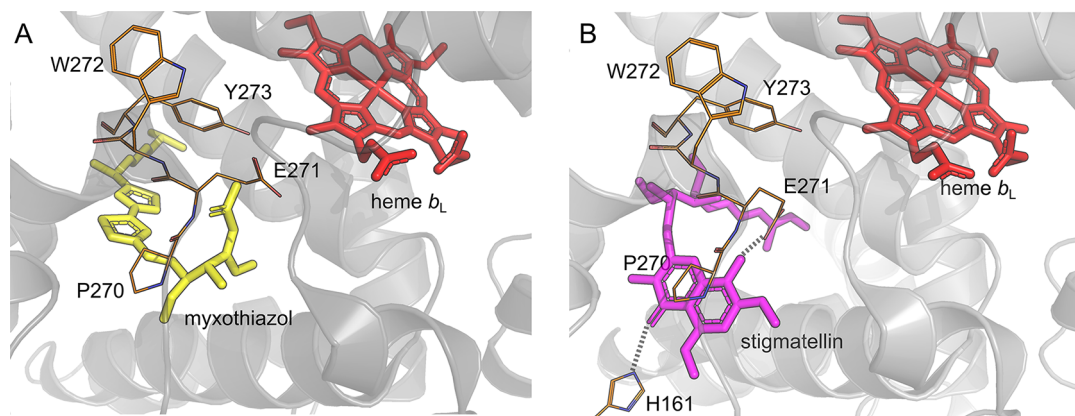


Figure 27. Comparison of structure of the Q_o site from *Bos taurus* with bound (A) myxothiazol or (B) stigmatellin. Prepared on the basis of 1SQP⁷⁷ and 1PP9,¹²³ respectively. Amino acids of ISP are not shown in A since myxothiazol induce c-position of ISP-HD. The imidazole ring of the 2Fe2S ligand–histidine 161 is shown in B as a structure forming an H-bond to stigmatellin.

empty ($K_{QH_2-Q_o}$). Additionally, the association constant of ISP-HD containing oxidized 2Fe2S with the Q_o (K_{ISPox}) site is also a crucial parameter defining the probability of ES complex formation. While direct designation of $K_{QH_2-Q_o}$ and K_{ISPox} is not experimentally possible, the respective values for *Cytc₁* were approximated by Crofts et al.²³ who considered the following states:

$$K_{QH_2-Q_o} = [Q_o - QH_2] / [Q_o - \text{empty}] = \sim 10 \quad (19)$$

$$K_{ISPox} = [Q_o - QH_2 - ISP - HD_{Q_o}] / [Q_o - ISP - HD_{\text{remote}}] = \sim 10 \quad (20)$$

where $[Q_o-QH_2]$ and $[Q_o-\text{empty}]$ are the concentrations of QH_2 at the Q_o site and empty Q_o site, respectively, at the time when ISP-HD containing oxidized 2Fe2S cluster is in position close to the Q_o site. $[Q_o-QH_2-ISP-HD_{Q_o}]$ and $[Q_o-ISP-HD_{\text{remote}}]$ denote relative concentrations of ISP-HD containing oxidized 2Fe2S at position close to the Q_o site with bound QH_2 and remote from the site, respectively.

From eq 19, it can be concluded that both QH_2 and oxidized 2Fe2S have a tendency to form the ES complex to initiate the first step of electronic bifurcation. Unfortunately, a direct observation of the interaction of QH_2 with oxidized 2Fe2S has not yet been made, as such a state can be generated only under nonequilibrium conditions, which would make the 2Fe2S diamagnetic and therefore not detectable by EPR spectroscopy. The EPR spectroscopy performed with cryoreduction of the 2Fe2S cluster in oriented membranes is also not informative. Although it can detect the position of ISP-HD with oxidized 2Fe2S, the Q_o site contains only UQ , not UQH_2 .¹⁰⁰

7.3. Crucial Amino Acid Residues Involved in Binding and Catalysis of QH_2/PQH_2 Oxidation at the Q_o/Q_p Site

This paragraph focuses on some of the crucial amino acid residues of the Q_o site that are thought to be involved in $Q(H_2)$ binding, and of the Q_p site, involved in $PQ(H_2)$ binding. At a general level, understanding how individual structural elements contribute to $Q(H_2)$ or $PQ(H_2)$ binding is challenging because of the difficulty in defining specific and universal $Q(H_2)$ binding motifs in proteins⁵⁸⁹ and the possibly related observation that many protein- $Q(H_2)$ interactions involve atoms of the main polypeptide chain.

Nevertheless, extensive mutational studies targeting residues of the Q_o site have identified those that affect catalysis, although

some of these mutations were found to primarily affect the stability or assembly of the whole protein complex. It is of note that, despite a large number of mutations that have already been tested in the region of the Q_o site, relatively few were able to completely abolish enzymatic activity, implying significant robustness and tolerance for structural change of both $Q(H_2)$ binding and Q_o site catalysis.

Current models of Q and QH_2 binding to the Q_o site are derived from crystallographic structures of *Cytc₁* with bound inhibitors replacing the natural substrate (structures with the substrate have not been solved yet). The models consider both P_m and P_f inhibitors, that is, inhibitors exerting different effects on the motion of ISP-HD as well as those occupying different niches of the Q_o pocket, (see sections 3.4 and 5 for details). The latter difference is visualized by a comparison of the structures shown in Figure 27, which compares binding of myxothiazol (representative of P_m group) at a position closer to heme b_L and further from ISP-HD with binding of stigmatellin (representative of P_f inhibitors), at a position closer to ISP-HD and further from heme b_L .

7.3.1. ^{Rh}H156 (^{Bt}H161) in Iron–Sulfur Protein and ^{Rh}E295 (^{Bt}E271) in Cytochrome *b*. The two most prominent, and thus most frequently discussed, candidates for residues that directly participate in binding of substrate are histidine ^{Bt}H161 (^{Rh}H156), one of the ligands of the 2Fe2S, and glutamate ^{Bt}E271 (^{Rh}E295) from conserved PEWY motif of *Cytc₁*. A binding mode for substrate involving these two residues is thought to be equivalent to the configuration of stigmatellin in the crystal structure. Stigmatellin forms two strong H-bonds in the Q_o site (Figure 27B): one between the $>C=O$ group of the inhibitor and N_τ atom of ^{Bt}H161 of ISP-HD and second between $-OH$ group and carboxylic group of ^{Bt}E271 residue.¹²³ Interestingly, myxothiazol crystallized in the Q_o site does not form specific hydrogen bonds to either of these groups. A comparison of the two structures reveals variable positions for the ^{Bt}E271 side chain: it rotates further toward the chromone ring of stigmatellin to create a hydrogen bond with the $-OH$ group at the C8 atom of the ring. It is highly unlikely that Q or QH_2 molecules at the Q_o site simultaneously form H-bonds to ^{Bt}H161 and ^{Bt}E271 as stigmatellin does. Therefore, it was proposed that during the oxidation QH_2 undergoes a rapid movement between the two niches within the Q_o site filled by stigmatellin and myxothiazol.^{23,576,590,591} According to this mechanism, QH_2 binds to the Q_o via ^{Bt}H161 (^{Rh}H156) and the first electron

transfer to the oxidized 2Fe2S takes place. The first proton is released and then the neutral SQH moves to form a hydrogen bond to ^{Bt}E271. The Glu residue promotes deprotonation of SQH, which then donates an electron to heme *b_L*. After formation of Q_o it shifts back to the position that allows interaction with ^{Bt}H161 and then it can be replaced with another QH₂. This mechanism has not been proven yet, and it is still a matter of debate.²⁵⁹ While the SQ moving between the two niches should be trappable, the experiments generally fail to detect such an intermediate of reaction (see section 7.6). Importantly, it remains an open question as to whether stigmatellin is actually a good model for Q(H₂) binding. The spatial separation of the two –OH groups differs between the QH₂ and the chromone ring of stigmatellin, with consequences for the capacity to form H-bonds. Comparing structures crystallized with different inhibitors, it seems that binding of UHDBT⁷⁷ or atovaquone⁷¹ at the Q_o site might more closely reflect binding of QH₂ as the structures of these inhibitors are more similar to natural quinones, (menaquinone and sulfolobus- or caldariellaquinone for example⁵⁹²), than the chromone ring of stigmatellin.

The idea that ^{Bt}H161 might participate in binding of Q and QH₂ to the Q_o was proposed after ENDOR measurements revealed that the 2Fe2S is coordinated by 2 Cys and 2 His side chains,⁵⁹³ which was later confirmed by crystallographic structures.⁵⁹⁴ Electrochemical studies revealed that the *E_m* value of 2Fe2S is pH dependent, and therefore, dependency requires two different p*K* values.⁵⁹⁵ It was estimated that the p*K_a* for oxidized 2Fe2S is ~7.5 and increases to more than 10 upon reduction of the 2Fe2S. This suggests that the protonation of ^{Bt}H161 is tightly coupled to the redox state of the 2Fe2S.²⁰⁸ Such an increase in p*K* means that the energy of hydrogen bond formation between an occupant of the Q_o and ^{Bt}H161 is larger when 2Fe2S is reduced compared to when the 2Fe2S is oxidized. Stabilization of the ISP-HD by the reduced 2Fe2S through interaction with Q(H₂) occupying the Q_o site is also inferred from EPR measurements. Typically, the EPR spectra of the reduced 2Fe2S in chromatophore membranes reflect close interactions with the Q(H₂), revealing that the reduced state of 2Fe2S promotes ISP-HD occupancy of a position close to the Q_o site (see section 3.4). On the other hand, experiments in which *Cytc₁* containing oxidized 2Fe2S was frozen before the cluster was reduced for detection by EPR showed that the ISP-HD with oxidized cluster tends to occupy a position remote from the Q_o site.¹⁰⁰

The 2Fe2S coordinating ^{Bt}H161 is well established as a crucial amino acid residue for the activity of all *Cyt-bc*. Its role in formation of initial ES complex is supported by many biochemical and computational studies. However, all mutational studies aimed at replacing this residue result in loss of the whole ISP subunit,¹³⁸ making definitive proof elusive.

The majority of the models describing formation of the initial ES complex assume that ^{Bt}H161 must be deprotonated before binding the QH₂, whereas Q can bind to the Q_o site when it is already protonated.^{596–598} In some models, this His residue has therefore been proposed as the first proton acceptor during the oxidation of QH₂. However, MD simulations indicate that QH₂ can also form a stable H-bond to the His, even when it has already been protonated.^{95,96}

The role and significance of the conserved PEWY domain Glu residue in binding substrate and catalytic reaction are less understood.^{23,118,580,599} In several models ^{Bt}E271 is considered to directly accept the second proton from QH₂ upon its

oxidation. However, mutational studies of this residue (^{Rh}E295) in the bacterial enzyme revealed only a modest impact on turnover rate and no significant changes in the estimated binding affinity of QH₂ to the Q_o site.⁵⁸⁰ On the other hand, mutation of the same residue in yeast (^{Sc}E272Q or ^{Sc}E272D) induced stigmatellin resistance.⁵⁹⁹ These two observations suggest that ^{Bt}E271 may not be directly involved in either binding of Q or QH₂ to the Q_o site or be critically required for proton uptake from QH₂ during the bifurcation reaction. Rather, it may be residue that increases stability of the water network at the Q_o site, which is necessary to create an appropriate environment for efficient and fast proton removal from the Q_o site. Clearly, further studies are needed to clarify the role of this residue in binding or proton events taking place at the site.

Interesting evolutionary aspects of the PEWY motif are beyond the scope of this review, but interested readers will find a discussion on this subject in an appropriate reference.¹¹⁸

7.3.2. *Cytc₁*:^{Rh}Y147 (^{Bt}Y131) and *Cytc₁*:^{Rh}Y302 (^{Bt}Y278). The Y147 residue is conserved among all *Cytc₁* complexes. Its importance in the activity of the Q_o site was postulated before crystallographic structures were available.⁶⁰⁰ Mutations of this residue to Phe, Val, Ser or Ala have a dramatic effect on the activity of bacterial *Cytc₁*.⁶⁰⁰ This significant impairment of catalysis is not associated with a change in the redox potentials of heme *b_L* or 2Fe2S. MD studies imply that Y147 can rotate to form a hydrogen bond between the –OH group at position 4 of UQH₂ and the –COO[–] group of ^{Rh}E295,⁹⁶ suggesting that this residue might play an important role in formation of the ES complex and the process of proton uptake during the bifurcation reaction. Quantum mechanics calculations performed on MD optimized structures indicate that when UQH₂ interacts with protonated ISP:^{Rh}H156, proton transfer from the hydroxyl group of ^{Rh}Y147 to the carboxyl group of ^{Rh}E295 takes place, creating a negative ^{Rh}Y147 and neutral ^{Rh}E295. At the same time, the deprotonated hydroxyl of ^{Rh}Y147 forms a hydrogen bond to the O1 atom of the hydroxyl group of UQH₂. When similar calculations were performed using the structure in which the hydroxyl O4 atom of UQH₂ forms a hydrogen bond to the already protonated ^{Rh}H156 of ISP-HD, and the H atom of the ubiquinol –OH group interacts with water molecules, this proton transfer from ^{Rh}Y147 to ^{Rh}E295 was not observed, despite the fact that ^{Rh}Y147 could still perform a relay function between UQH₂ and ^{Rh}E295.⁹⁶ Other MD simulations on the binding of UQH₂ to the Q_o site did not show involvement of ^{Rh}Y147 hydroxyl in interaction with UQH₂. Instead, a hydroxyl group at the C1 atom of UQH₂ formed a hydrogen bond with a network with water molecules.⁹⁵

Although a possible role of ^{Rh}Y147 and ^{Rh}E295 in binding and proton uptake from UQH₂ during the bifurcation reaction was proposed on the basis of biochemical and mutational studies,^{591,600} the concept of H-bond network formation between UQH₂-^{Rh}Y147-^{Rh}E295 clearly needs further investigation.

An important role for *Cytc₁*:^{Rh}Y302 (^{Sc}Y279) in the binding and oxidation of QH₂ by the Q_o site emerged from several studies on bacterial and mitochondrial *Cytc₁*. Mutating this residue to Leu, Gly, or Glu in *R. sphaeroides* *Cytc₁* was found to decrease catalytic rates by a factor between 3-fold and 50-fold^{590,601} and to increase ROS generation.⁶⁰² These effects were also reported for ^{Sc}Y279C, a mutation associated with mitochondria-related diseases.⁶⁰³ The g_x transition of the EPR spectra of 2Fe2S in this mutant suggested that the Q_o site was “partially empty”.⁶⁰¹ Furthermore, the spectrum of 2Fe2S with

bound stigmatellin differed from the equivalent spectrum for typical wild-type enzymes, indicating much stronger binding of the chromone than the benzoquinone ring to the Q_o site of *Cytbc₁*. Analysis of the structure of yeast *Cytbc₁* with the inhibitor HHDBT bound suggested that ^{Sc}Y279 might contribute to the binding of UQH₂ by creation of a H-bond to the =O atom of the main chain of ^{Sc}C180 in ISP-HD.⁷⁰ Such a hydrogen bond is expected to stabilize UQH₂ binding with ^{Sc}H181 (^{Rh}H156 and ^{Bt}H161) of the ISP-HD.

In *Rhodobacter capsulatus*, the ^{Rh}Y302C mutation exerted a deleterious effect on stability of 2Fe2S due to disruption of a disulfide bridge in ISP-HD and resulting cross-linking between the *Cytb* subunit and ISP-HD (^{Rh}Y302C-^{Rh}C155). This made the 2Fe2S more sensitive to oxidative damage.^{602,604}

In *Plasmodium falciparum*, ^{Pf}Y268S (equivalent ^{Sc}Y279S and ^{Rh}Y302S) was identified as a mutation responsible for resistance of the parasite to the antimalarial drug, atovaquone.⁶⁰⁵ This potent inhibitor of the Q_o site was found to completely block activity of the yeast *Cytbc₁* ($IC_{50} = 5$ nM).⁶⁰⁶ Atovaquone arrests the ISP-HD at the Q_o site in a similar way to stigmatellin, despite the fact that unlike stigmatellin it does not form a direct H-bond with the conserved PEWY sequence Glu residue.^{71,607} The crystal structure revealed that ^{Sc}Y279 forms hydrogen bond to Cys180 in the ISP but it also interacts weakly with ionized hydroxyl group at C3. The loss of this Tyr residue in *Plasmodium* is not lethal to the parasite, but significantly slows its *Cytbc₁* activity, thus slowing the parasite growth rate.⁶⁰⁵

7.3.3. Other Residues Involved in Substrate Binding to the Q_o Site. Besides the amino acid side chains discussed above, it is expected that the binding of substrate to the Q_o site also engages other residues in the site including atoms of the main polypeptide chain of *Cytb* and ISP. Indeed, MD simulations investigating possible structures of bound UQH₂ and UQ at the Q_o site identified the =O atoms of ^{Rh}I292 (*Cytb*) and ^{Rh}C155 (ISP) as potential residues participating in binding of UQH₂ and UQ through water molecules.

Another residue important for binding of the substrate to the Q_o site is conserved Gly ^{Rh}G158 (^{Sc}G143 and ^{Bt}G142) in the WGA sequence.^{260,570,608} Mutagenesis studies have revealed that its replacement with residues that have bulkier side chains, particularly tryptophan, prevents binding of either UQ(H₂) or inhibitors such as stigmatellin. This effect is most probably due to a steric hindrance at the Q_o site, preventing catalytic activity of the enzyme.

It should be noted that the isoprenoid chain of UQ also constitutes an important part of the Q binding interface. Indeed, several hydrophobic residues of *Cytb* interact with this tail. In *R. capsulatus*, they are F144, F166, F298, F337, I162, I169, V333, M336, L165, V161, F298, G141, M140, L201, L178.⁹⁵

7.3.4. Specific Residues Involved in PQ/PQH₂ Binding to the Q_p Site of Cytochrome *b₆f*. Studies to characterize residues of *Cytb₆f* involved in PQ(H₂) binding at the Q_p site are more limited than in the case of the *Cytbc₁* counterpart. These studies have been mainly performed in *Chlamydomonas* and have revealed strong similarities between the Q_p and Q_o sites of *Cytb₆f* and *Cytbc₁*, a concept that was later confirmed by crystallographic studies.

The first characterized mutant (FUD50) bears a 36 base pair duplication in the chloroplast *petB* gene, leading to a 12 amino acid duplication in the CD loop of *Cytb₆*. This modification decreases the affinity of the Q_p site for PQ(H₂),⁶⁰⁹ likely by increasing the size of the Q_p site itself. Subsequent studies have also focused on this region of the Q_p site, revealing the essential

role of the PEWY sequence in Q(H₂) binding and proton release. Later on, this concept that has been rationalized based on the structures of the *Cytb₆f* in this alga and cyanobacteria.^{41,42,66}

Additional mutants have been made in *Chlamydomonas* to study the role of the ISP flexible hinge in catalytic turnover of the complex. Six Gly residues in the flexible hinge critical for domain movement in the *Cytbc₁* (section 3.4) were replaced by alanine residues (6G6A). Moreover, substitutions were created near 2Fe2S (S128 and W163), and seven C-terminal residues were deleted (G171och). The 6G6A and G171och mutations affect highly conserved segments in the chloroplast ISP, but no phenotype was found in these lines. Although extensions of up to five residues or deletion of one residue in the flexible hinge had no significant effect on complex accumulation or electron transfer efficiency, deletion of just three residues (Δ 3G) dramatically decreased reaction rates by a factor of \sim 10. Overall, these findings indicate that the chloroplast ISP hinge is also very flexible⁶¹⁰ and its movement is not limiting for catalysis, consistently with previous conclusions in the case of *Cytbc₁* (see section 3.4).

Only one mutant has so far been reported to affect PQ(H₂) binding to the Q_p site in plants. This mutant (pgrl1)⁶¹¹ was obtained by random mutagenesis and bears a point mutation in the ISP (P194L). Although the mutation does not affect photosynthetic electron transport at low light intensities, it drastically affects thermal dissipation of absorbed light energy in high light, suggesting that Pro194 may affect H⁺/e⁻ coupling in the *Cytb₆f*. Single amino acid substitutions in *Cytb₆* at the positions D148, A154, and S159 were generated in the cyanobacterium *Synechococcus* sp. PCC 7002. Mutant phenotyping revealed increased resistance to DBMIB in the mutants A154G and S159A, increased resistance to stigmatellin in A154G, and induction of myxothiazol sensitivity in the D148G mutant, confirming the role of these residues in PQ(H₂) binding and inhibitor sensitivity of the complex.⁶¹²

7.4. Catalytic and Side Reactions at the QH₂-Oxidation Site of Cytochromes *bc*

The oxidant-induced reduction of *b* hemes in submitochondrial particles is an intriguing phenomenon first reported by Chance in 1952 during II International Congress of Biochemistry in Paris (see ref 613 and citations therein). This phenomenon was difficult to explain until a concept of a semiquinone-mediated electronic bifurcation was introduced by Wikström and Berden in 1972.²⁰² The central role of a semiquinone in the mechanism of bifurcation was further developed by Peter Mitchell in the frames of his original idea of so-called proton-motive Q cycle mechanism.³² This groundbreaking concept of electronic bifurcation, inherent to this mechanism, postulated that QH₂ at the Q_o / Q_p site undergoes two-electron oxidation reaction but routes for these two electrons are obligatorily different and very efficient. This entails the first electron being transferred to the oxidized 2Fe2S center (the first cofactor of the high-potential chain), while the second electron is transferred exclusively to heme *b₁/b_p* (the first cofactor of the low-potential chain) see section 3.2.

It is assumed that the mechanism of electron bifurcation is sequential and involves formation of a transient semiquinone intermediate. While the time between the first electron transfer from QH₂ to 2Fe2S and the second electron transfer from SQ to heme *b₁/b_p* remains unknown, it seems reasonable to assume

that it is not shorter than the time required for electron tunneling from the SQ to heme b_L/b_P .

According to Mitchell's principles, QH_2 must donate its two electrons to two different chains of cofactors and the two redox couples involved in the first and the second electron transfer; SQ^-/QH_2 and Q/SQ^- couples, respectively, must therefore possess different redox midpoint potentials,³² as originally discussed by Wikström and Berden in 1972.²⁰² It has been proposed that the E_m of the SQ^-/QH_2 redox couple is very positive, and comparable to the high potential acceptor (2Fe2S and heme c_1/f), while the Q/SQ^- is expected to be a more reducing couple and therefore able to donate electrons to the low-potential chain (hemes b_L/b_P and b_H/b_N). This separation of E_m values (the split) of the two redox couples implies that the stability constant for the SQ^- intermediate at the Q_o/Q_p site must be very low, and hence detection of such an intermediate by spectroscopic methods might be difficult, especially under equilibrium conditions.^{487,488} Indeed, until recently, the semiquinone intermediate state associated with the operation of the Q_o/Q_p site could not be experimentally detected (see section 7.6).

7.4.1. Forward, Reverse, and Short-Circuits Reactions at the Q_o/Q_p Site. A simple diagram of E_m values taken from *Rhodobacter capsulatus* $Cytc_1$ with associated ΔG changes due to electron transfer through the cofactor chains is shown in Figure 28. As originally proposed by Mitchell, there is a large, albeit unknown, split between E_m values (here ~ 800 mV) of the Q/SQ^- and SQ^-/QH_2 couples, and this split depends on the stability constant of the SQ^- . This makes the first electron transfer from QH_2 to 2Fe2S essentially endothermic and requires an energy debt for electron transfer to the acceptor of

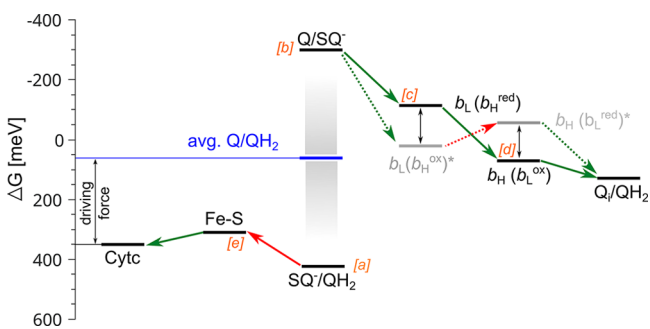
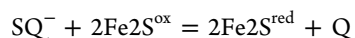
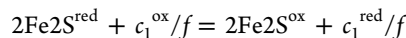


Figure 28. Energy diagram of electron transfer through cofactor chains in $Cytc_1$. Horizontal black lines mark E_m values at pH 7 of the respective oxidized/reduced couple and are labeled with an orange letter in bracket. Gray gradient denotes a split in potentials between Q/SQ^- and SQ^-/QH_2 couples at the Q_o site. The average E_m value at pH 7 of membranous Q/QH_2 pool is shown in blue. Red and green solid arrows show endothermic and exothermic reactions, respectively. Green dashed arrows show exothermic reaction to the heme states for which E_m s are not directly measurable by equilibrium redox titration. Gray horizontal lines show a possible E_m values of hemes b_L and b_H modified by Coulombic interactions between the hemes (assuming the same energy of interactions ~ 80 mV for b_L and b_H ^{133,206}) that are not accessible for direct measurement. Vertical double arrows denotes the changes in E_m depending on the redox state of the coupled heme. $Cytc$ and $Fe-S$ denote oxidized/reduced couples of $Cytc_2$ and 2Fe2S; $b_L(b_H^{ox})$ and $b_L(b_H^{red})$ denote oxidized/reduced couple of heme b_L , at a time when heme b_H is oxidized and reduced, respectively; $b_H(b_L^{red})$ and $b_H(b_L^{ox})$ redox couple of heme b_H at a time when heme b_L is reduced or oxidized, respectively. Note that this scheme does not necessarily apply for $Cytc_{\delta f}$.

a more negative redox potential (2Fe2S) than the donor (QH_2). This energetic debt is repaid during the second electron transfer from SQ^- to heme b_L/b_P . The forward reactions, meaning the net electron transfer from QH_2 to $Cytc$, are continued as long as there is a difference (driving force) between the E_h of membranous Q/QH_2 , the p side acceptor pools ($Cytc$, PC or $Cytc_6$) and all the cofactors of $Cytc-bc$ complexes. Nevertheless, it has been shown by several experiments that under specific conditions $Cytc_1$ has the capacity to catalyze a fast, reverse reaction of reduction of Q to QH_2 at the Q_o site. Such a process was observed in *in vitro* studies of $Cytc_1$ reconstituted into liposomes⁶¹⁴ and also proposed to occur *in vivo* to support the growth of the chemolithotrophic bacteria *Thiobacillus ferrooxidans* using Fe^{2+} ions as a source of electrons.⁶¹⁵ This suggests that the reactions at the Q_o site are rapidly and efficiently reversible, where "efficient" means that these reactions do not lead to significant energy-wasting side reactions (short-circuits or leaks). Indeed, light-induced electron transfer measurements using cofactor knockouts of bacterial $Cytc_1$ to dissect out individual electron transfer steps, demonstrated that the reactions of the Q_o site are reversible on a catalytically relevant time scale (milliseconds).⁶¹⁶ Fast reversibility of these reactions makes an understanding of the energetic efficiency of electronic bifurcation conceptually challenging. As long as one forgets the reversibility, the diagram in Figure 28 simply explains the energetic efficiency of electron transfer onto two different chains of cofactors. However, the fast reversibility of reactions at the Q_o/Q_p site means that the enzyme can potentially catalyze energy-wasting short circuit reactions.^{259,616} Four possible short-circuit reactions of the Q_o/Q_p site are shown in Figure 29.

The first type of short circuit (SC1) is a reaction in which two electrons from QH_2 are transferred to the high potential chain according to the following reaction sequence:



SC1 would be very exothermic since the electron transfer would be associated with a large potential energy change due to the transition from state [b] to [e] in Figure 28. Despite the fact that SC1 is thermodynamically very favorable, it is avoided relatively easily, due to the requirement for the movement of ISP-HD (see section 3.4) during transfer of electrons from 2Fe2S to heme c_1 or f . Through this constrained diffusion of ISP-HD, the distance between SQ^- and the cluster increases significantly, slowing down any possible second electron transfer from the semiquinone to 2Fe2S. In the absence of ISP-HD in close proximity, the unstable SQ^- therefore pushes the second electron onto heme b_L/b_P . SC1 decreases the proton transfer efficiency across the membrane: it yields $+2H^+_p/OH^+_n$ per oxidation of one QH_2 , while an energy-conserving Q cycle yields $+4H^+_p/-2H^+_n$ per 1 QH_2 .

In contrast to SC1, the second type of short-circuit reaction (SC2) is extremely difficult to suppress without involvement of any additional mechanisms to lower the probability that it occurs. SC2 is a mixture of partial reactions of the forward and the reverse catalysis performed by the Q_o/Q_p site and is a result of the following reactions (for simplicity in the following schemes b_L and b_H also represent hemes b_p and b_n , respectively):



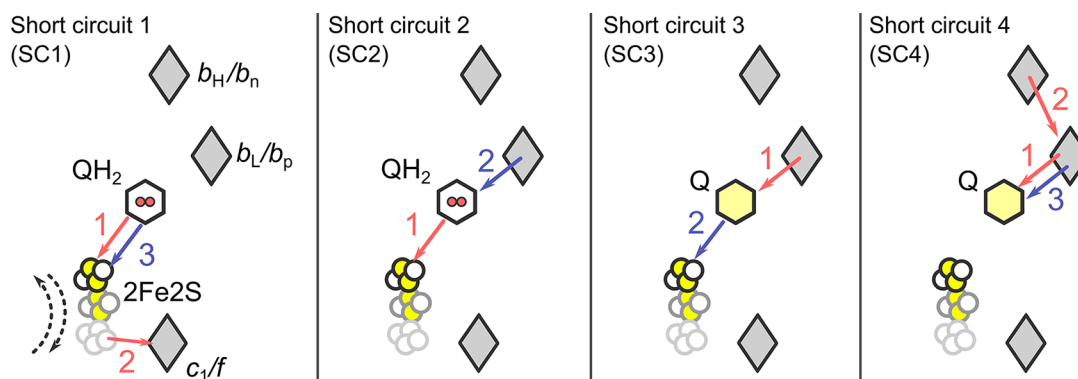


Figure 29. Scheme showing 4 types of short circuit reactions that are theoretically possible during the catalytic cycle of Cytbc₁ and Cytb_{6f}.²⁵⁹ Red arrows show energy conserving ET while blue arrows shows energy-wasting short circuiting ET. Numbers denote the order of ET events. Short circuits start with QH₂ (SC1 and SC2) or Q (SC3 and SC4) present at the Q_o/Q_n site. Gray rhombuses denote hemes, and white–yellow circles show 2Fe₂S. Scheme does not consider redox states of cofactors. Dashed arrows and 3 positions of 2Fe₂S denote movement of the ISP-HD (necessary to complete SC1). See text for details.

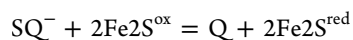
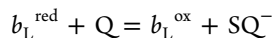


SC2 may take place when QH₂ undergoes oxidation by 2Fe₂S as a part of the chemistry of the normal forward reaction, while heme b_L/b_p is reduced and unable to accept electron from SQ[−]. In this situation, heme b_L/b_p can then donate an electron to SQ[−], reforming QH₂, as this reaction is also much more energetically favorable than any possible forward electron transfer from heme b_L/b_p to heme b_H/b_n (compare the difference in energy associated with [b] to [a] and [b] to [c] transition in Figure 28).

Energy conversion of this process is compromised as this short circuit gives the same stoichiometry as SC1 (+2H_p⁺/0H_n⁺ per 1 oxidized QH₂), assuming that every SC2 is preceded by QH₂ oxidation.

Conditions in which SC2 could take place are created not only when an inhibitor such as antimycin, blocks electron transfer from heme b_H to Q at the Q_i/Q_n site, but also during reverse electron transfer from QH₂ bound at the Q_i/Q_n site, which is a natural consequence of the physiological reverse catalysis of Cytbc. It has been demonstrated (see section 8) that electrons from the Q_i site of one monomer can be transferred through the heme b_L to the other monomer, creating the possibility that heme b_L is already reduced when SQ[−] is generated during oxidation of QH₂ by 2Fe₂S at the Q_o site.

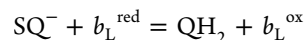
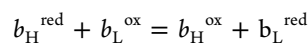
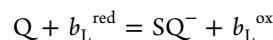
The third type of short circuit (SC3) is electron transfer from reduced heme b_L/b_p to Q that is bound concurrently with QH₂ to the Q_o/Q_p site, when the oxidized 2Fe₂S is close to the Q_o/Q_p site. SC3 consists of two sequential reactions: first uphill (transition from states [c] to [b]), followed by downhill ET (transition from [b] to [e] in Figure 28), which can be summarized as follows:



SC3 is quite similar to SC2 and the proton transfer efficiency is the same. The only difference is the fact that SC3 should be favored over SC2 when concentrations of Q in the Q(H₂) pool are higher. However, in the absence of an inhibitor blocking the Q_i/Q_n site or mutation retarding electron transport from heme b_H/b_n to the Q_i/Q_n site, SC3 seems to be less probable than SC2.

The last type of short circuit (SC4) is the two-electron reduction of Q at the Q_o/Q_p site by the hemes b_L/b_p and b_H/b_n

of the low-potential chain without involvement of the 2Fe₂S. SC4 can be summarized as follows:



According to the modified Q cycle,³⁹ SC4 is obviously considered as the energy-wasting reaction since it diminishes the number of protons transferred across the membrane. However, calculations of the number of protons that are transferred per oxidized QH₂ under condition in which SC4 takes place is more complex than in the case of SC1, SC2, and SC3.

Let us first consider 4 cycles of QH₂ oxidation steps according to the energy-conserving Q cycle. If the modified Q cycle is operating, this will lead to 8H⁺ released to the p side, 4H⁺ taken from the n side and the net consumption of 2 QH₂ molecules from the Q(H₂) pool. The overall stoichiometry of this modified Q cycle is +8H_p⁺/−4H_n⁺ and −2QH₂/+2Q in the Q(H₂) pool.

Now consider a similar sequence of 4 QH₂ oxidation reactions but with a single SC4 reaction occurring in the middle of the process: 2 QH₂ oxidations, SC4 reaction, another 2 QH₂ oxidations. For clarity, let us divide the process into three parts. In the first part, 2 QH₂ oxidations yield +4H_p⁺/−2H_n⁺ and −1QH₂/+1Q. During the second part, SC4 gives −2H_p⁺/+2H_n⁺ and +1QH₂. During the third part, another 2 QH₂ oxidations take place yielding the same +4H_p⁺/−2H_n⁺ and −1QH₂/+1Q as in the first part. Addition of all products from these three parts gives a net stoichiometry of +6H_p⁺/−2H_n⁺ and −2QH₂/+2Q in the Q(H₂) pool, which means that 1 occurrence of SC4 per 4 oxidized QH₂ decreases the number of protons released to the p side from 8 to 6. This would give an average +3H_p⁺/−1H_n⁺ per 1 QH₂ oxidized during this sequence versus +4H_p⁺/−2H_n⁺ per 1 QH₂ in the Q-cycle.

7.4.2. Possible Physiological Meaning of Short-Circuits. In general, short-circuit reactions decrease the efficiency of energy conversion by Cytbc and the probability of their occurrence should be minimized or slowed down by two or 3 orders of magnitude in comparison to the productive forward and reverse reactions. It must be emphasized, however, that it is still possible for some of the SC reactions to be catalyzed under specific conditions, such as severe mutation or presence of

inhibitors, which preclude normal catalysis. In fact, it has been proposed that the reactions of SC2 could be a potential mechanism to support photosynthetic growth of green alga *Chlamydomonas reinhardtii* strains, in which normal function of *Cytb₆f* is disabled by mutation to replace the heme *b_H* ligand, histidine 202 with glutamine.⁶¹⁷

The reactions of SC4 could also be potentially considered as desirable for electron recirculation back to the PQ(H₂) pool in, for example, photosynthetic CET at the level of *Cytb₆f* (see section 4.3). Assuming alternating reactions of oxidation of PQH₂ and reduction of PQ at the Q_p site, using electrons delivered through the low-potential chain from the Fd/NADP⁺ pool, the overall proton pumping efficiency would be significantly increased yielding +6H⁺_p/−4H⁺_n, −1PQH₂ in the Q(H₂) pool and −2 Fd from the Fd/NADP⁺ pool. This would contribute to a much higher proton gradient per oxidized PQH₂ than +4H⁺_p/−2H⁺_n per 1 PQH₂ resulting from the modified Q cycle mechanism. However, a possible involvement of SC4 in the mechanism of CET around *Cytb₆f* and PSI has not been proposed earlier and thus has never been tested experimentally.

Another potential physiological implication of short-circuits relates to the concept of kinetic competition between short-circuits and the leak of electrons (i.e., reactions that may lead to superoxide production). The completion of any type of short-circuit reaction retains electrons within the enzyme, therefore diminishing the probability of leaks. Thus, this could be considered as a possible means of protection against unwanted release of superoxide, which might be of importance in the context of a postulated signaling role for superoxide release from the Q_o/Q_p site (see section 7.5).

7.4.3. Short-Circuit Suppression Mechanisms. As indicated in section 7.4.1, understanding the fast reversibility of electron transfer in *Cyt-bc* and the efficient suppression of short circuit reactions is conceptually challenging.^{259,616,618,619} Direct electron transfer between the low- and high-potential chains is significantly limited by the 2.3 nm distance between 2Fe2S and the ring of heme *b_L/b_p*.²⁵⁹ Such a large spatial separation slows down electron transfer to a time scale of seconds, minimizing the probability of its occurrence on a catalytic time scale. However, the problem appears when a redox active molecule such as quinone (QH₂, Q or SQ[−]) is bound at the Q_o/Q_p site and cuts the 2.3 nm distance into two much shorter distances, each being well below the 1.4 nm limit.⁵⁶ This means that any type of quinone molecule bound in the site (whether it is the substrate, product or intermediate of the QH₂ oxidation) can in principle act as mediator to significantly enhance electron transfer between the low- and high-potential chains.

To explain the general lack of experimentally detected short circuits, several “gating” mechanisms were constructed. The problem is, however, that in most cases the gating mechanisms are either very effective at suppressing short-circuits, therefore sacrificing reversibility, or if they allow reversibility, they are prone to some short circuits.^{259,616} It appears that to explain how the *Cytbc* can accomplish full and rapid reversibility and short circuit suppression while limiting superoxide production, elaborate mechanisms involving more than a single gating factor are needed.

The necessity for elaborate gating is a consequence of the sequential mechanism that is considered to drive the reaction at the Q_o/Q_p site, which is obliged to form SQ[−] as a true intermediate of the two-electron reactions of bifurcation. This mechanism assumes formation of SQ[−] at the Q_o/Q_p site, albeit

at low occupancy.²²⁴ It is generally in line with many observations that the Q_o/Q_p site can, under specific conditions, generate superoxide and also with recent experiments reporting detection of a SQ[−] intermediate at this site (see sections 7.5 and 7.6 and references therein). The sequential mechanism is also in agreement with the chemical properties of quinones and their ability to take part in single-electron redox reactions. However, the major problem with sequential electron transfer is its susceptibility to short-circuiting.

As an attractive alternative and seemingly the simplest solution to the short-circuit problem, a concerted reaction was also proposed for the Q_o/Q_p site. This reaction, based on a fundamentally different mechanism, assumes that the reaction takes place through a transition state devoid of semiquinone character. In the following sections, we will first reflect on the concerted mechanism before discussing the various possible gating mechanisms related to the sequential mechanism of the bifurcation.

7.4.3.1. Short-Circuit-Proof and Leak-Proof Concerted Reaction. The “concerted” reaction initially proposed for the Q_o/Q_p site is “thermodynamic” cooperativity of the bifurcation reaction, in which electron transfer is sequential, but with a transient semiquinone state that never accumulates enough to be observable (i.e., reduction and oxidation of reaction partners may appear concurrent).^{155,620,621} Together with the kinetic resolution of millisecond reversibility of all electron transfer steps within *Cytbc₁*, including the reactions at the Q_o/Q_p site, the “concerted” reaction was introduced as one of the possible mechanism allowing reversible operation of this site while preventing all short-circuits (the other mechanism introduced in parallel was a “double-gating”, as described below).^{259,616} The term “concerted” was regarded as a “kinetic” definition of two events taking place without time for significant atomic rearrangement. This concept recognized that all short-circuits would be efficiently suppressed if QH₂ oxidation (forward catalysis) and Q reduction (reverse catalysis) took place as a virtually single step involving 2 electron and 2 proton transfers. Suppression would then simply be a consequence of forbidding one-electron transfer reactions, of which all short-circuits are composed (see Figure 29).^{155,259,616,620,621}

It follows that if the concerted reaction is the catalytic mechanism at the Q_o/Q_p site, the SQ[−] intermediate would not be formed at all during either QH₂ oxidation or Q reduction as its lifetime is shorter than the time needed for nuclei reorganization of molecules taking part in the electron transfer reactions.²⁵⁹ This mechanism elegantly explains the energetic efficiency of the reversible catalysis of *Cytbc₁*, but it remains hypothetical. While theoretical and experimental descriptions of kinetically concerted two-electron transfer reactions do exist,^{622,623} the chemical and physical details of the any concerted reaction at the Q_o/Q_p site remain unknown, as is the mechanism that would explain how SQ[−] formation is forbidden.

The concerted mechanism becomes difficult to reconcile with recent experiments reporting the detection of transient SQ[−] intermediates in the Q_o/Q_p site (see section 7.6). As the concerted reaction is by definition short-circuit-proof and leak-proof, it eliminates entirely the possibility of superoxide generation. It follows that another mechanism of SQ[−] formation by *Cytbc* would therefore have to be envisaged to explain this activity of *Cyt-bc*, such as electron transfer from reduced heme *b_L/b_p* to O₂, for which there is no evidence.

7.4.3.2. Gating Mechanisms of Sequential Reaction. (i) Catalytic switch and $\text{QH}_2/\text{SQ}/\text{Q}$ mobility-driven gating at the Q_o site. The “catalytic switch”, proposed by Brandt et al. before the discovery of 2Fe2S motion, can be considered the first gating model.^{57,58} This model pointed to a key role of the redox state of the 2Fe2S on the bifurcation reaction. It was formulated based on the difference between the binding constants of two types of inhibitors, stigmatellin and MOA-stilbene to $\text{Cyt}b_{c1}$, caused by changes in the reduction state of the 2Fe2S cluster and the discovery that ISP-HD can be found at two different positions. The model assumed that QH_2 and Q can interact with oxidized 2Fe2S while SQ^- interacts with an oxidized heme b_L but not with the reduced 2Fe2S cluster. Thus, electron transfer to 2Fe2S or heme b_L strictly depends on the redox state of these two cofactors forcing the forward bifurcation reaction at the Q_o site.⁵⁷

A somewhat similar model was proposed recently to explain the forward electron transfer in bifurcation through the movement of SQ^- at the Q_o site to drive electrons to the correct chain. This model was also based on structural studies of stigmatellin binding to the Q_o site.⁹¹ It predicts that reduction of the 2Fe2S cluster and formation of semiquinone leads to disruption of the H-bond between $^{\text{Rh}}\text{H156}$ ($^{\text{Bt}}\text{H161}$), which favors the movement of ISP-HD to the c-position (see section 3.4 for details) and a rapid movement of the benzoquinone ring toward the $^{\text{Rh}}\text{E295}$ ($^{\text{Bt}}\text{E271}$).^{119,576} The latter movement facilitates the deprotonation of the semiquinone and therefore increases the rate of electron transfer from SQ^- to heme b_L by shortening the distance between the reagents.^{23,597} After the second oxidation, Q returns to the niche that is close to the 2Fe2S cluster. In this way, the redox state of Q and heme b_L determine the direction of electron transfer at the Q_o site. These two mechanisms, termed “catalytic switch” and “ SQ motion”, do not protect the enzyme from performing SC2 or SC4. Furthermore, they do not describe the proton/electron sequence of the reverse direction and, as discussed in the literature,^{259,616} they are not easily reversible.

(ii) Surface-modulated motion switch of $\text{Cyt}b_{c1}$. Another gating mechanism proposes that the movement of ISP-HD (after the 2Fe2S cluster is reduced) is coupled to the oxidation of heme b_L by heme b_H .^{21,78,89,624} The authors proposed that electron transfer from heme b_L to heme b_H triggers some conformational changes in the region of $\text{Cyt}b$ ⁸⁹ responsible for docking the ISP-HD, releasing this domain from the Q_o site and then releasing Q and binding QH_2 .⁷⁸ Although this mechanism allows the reversible reactions at the Q_o site, some short-circuit reactions (SC2, SC3, and SC4) are still possible. Furthermore, this model predicts that the presence of Q at the Q_o site would favor occupation of positions remote from the Q_o site by the ISP-HD. However, this seems at odds with the experimental observation that when Q is bound at the Q_o site it leads to EPR spectra typical of 2Fe2S interacting with Q for the whole population of the reduced 2Fe2S (see section 3.4 for details).

(iii) Proton gated affinity change and proton gated charge-transfer mechanisms. The “proton gated affinity change” mechanism was formulated on the basis of the electrochemical properties of 2Fe2S, in particular the difference between the pK value of the $^{\text{Rh}}\text{H156}$ ($^{\text{Bt}}\text{H161}$) for the reduced and oxidized 2Fe2S.⁵⁷⁵ According to this mechanism, either QH_2 binds to the deprotonated histidine or QH^- binds to the protonated histidine. The first electron transfer to 2Fe2S then drastically increases affinity of SQ^- for the reduced 2Fe2S, leading to a positive shift in the redox potential of the 2Fe2S in the

$2\text{Fe}2\text{S}^{\text{red}}-\text{H}^+-\text{SQH}$ complex. Such a stabilization should lead to a relatively large occupancy of SQ^- at the Q_o site. However, when this proposal was framed, experiments failed to detect any SQ^- at the Q_o site. This discrepancy was explained on the ground of strong antiferromagnetic coupling between SQ^- and $2\text{Fe}2\text{S}^{\text{red}}$ leading to disappearance of the EPR signal.

Evoking antiferromagnetic coupling as a reason for the failure to detect an EPR signals implies that the energy of such interactions must be very high to depopulate the paramagnetic, excited state at temperatures >10 K (typical experimental conditions). However, this kind of strong spin–spin exchange is very unlikely for most bonds through which SQ^- could interact with 2Fe2S, including a single H-bond. Interestingly, experiments performed 16 years after the initial formulation of the “proton gated affinity change” mechanism established that a spin–spin exchange interaction between SQ^- and reduced 2Fe2S does occur but that the energy of such coupling is very low in comparison to the thermal energy of experimental EPR conditions and that this state can be detected by EPR (this is described in detail in section 7.6).

As described in section 7.2, several experimental results have been interpreted as being indicative of binding two substrate molecules to the Q_o site at the same time. This concept was also used to formulate a “proton gated charge-transfer mechanism” in which a QH_2/Q pair must first undergo two deprotonation steps followed by electron transfer to 2Fe2S and heme b_L .⁵⁸⁷ The two proton-gated mechanisms allow reversibility of the Q_o site but do not prevent SC2, SC3 nor SC4.

(iv) Double-gating mechanism. More recent models of bifurcation take into account the fact that a single gating step is generally not sufficient to suppress all types of short-circuits for reversible sequential bifurcation.

The first model of this type was the “double gating” mechanism, introduced as an alternative to the concerted mechanism in providing a means for short-circuit-proof and efficient reversible operation of the Q_o site. It evoked the concept that changes in protonation/deprotonation of water molecules or amino acid side chains near the Q_o site occur upon changes to the redox state of immediate cofactors, 2Fe2S and heme b_L , to specifically modulate barriers in the sequential reaction.^{259,616} Double gating allows QH_2 oxidation only when both 2Fe2S and heme b_L are oxidized and allows Q reduction only when both 2Fe2S and heme b_L are reduced. This would be accomplished by raising the barrier for SQ^- formation when QH_2 is bound at the Q_o site (involving a SQ^-/QH_2 couple) when heme b_L is reduced and the 2Fe2S cluster is oxidized, or by lowering that barrier when both cofactors are oxidized. This would prevent SC1 and SC2 (Figure 29). On the other hand, the barrier for SQ formation when Q is bound at the Q_o site (involving Q/SQ^- couple) would be raised when heme b_L is reduced and the 2Fe2S cluster is oxidized, or the same barrier is lowered when both cofactors are reduced. This would prevent SC3 and SC4.

(v) Logic-gating mechanism. A “logic-gating” mechanism is quite similar to the “double gating” mechanism. It also evokes a concept of changes in protonation/deprotonation of water molecules or amino acid side chains near the Q_o site upon changes in the redox state of the immediate cofactors 2Fe2S and heme b_L . The model proposes that crucial elements for energy-conserving redox reactions depend on specific H-bond formation in the Q_o site.⁵⁹⁸ Binding of QH_2 requires $^{\text{Rh}}\text{H156}$ ($^{\text{Bt}}\text{H161}$) and $^{\text{Rh}}\text{E295}$ ($^{\text{Bt}}\text{E271}$) to be in deprotonated states, which is possible when 2Fe2S and heme b_L are oxidized.

Otherwise, reduction of 2Fe2S and heme b_L induces protonation of the N_τ atom of the histidine and the carboxyl group of the glutamate, allowing binding of Q to the Q_o site. Such a mechanism imposes constraints on the direction of reaction, as QH_2 binds predominantly when both 2Fe2S and heme b_L are oxidized and Q binds predominantly when both 2Fe2S and b_L are reduced. This mechanism, like the double-gating mechanism, protects against all short-circuits while still allowing reversibility.²⁵⁹ It is also generally consistent with the fact that reduction of 2Fe2S is associated with a shift in the pK value of the 2Fe-2S protein from about 7.6 to more than 10^{595} and is in line with the observation that Q bound at the Q_o site strongly influences EPR spectra of the 2Fe2S (see section 7.2 for details). In this model, a tentative coupling between hemes b_L and the Glu residue exists, and thus, the reduction of heme b_L would be associated with protonation of the Glu carboxylic group while oxidation of the heme would induce deprotonation of the same side chain. However, experimental results on a series of mutants that replace $^{Rh}E295(^{Bt}E271)$ with other amino acids revealed only minor effects on the redox midpoint potential of heme b_L .^{580,599} Also, equilibrium redox titrations of the bacterial chromatophore $Q(H_2)$ pool, made by monitoring changes in the g_x EPR transition of the 2Fe2S, showed that the reduced cluster is still able to interact with QH_2 under conditions in which heme b_L remains oxidized. The experimental detection of Q bound to the Q_o site under conditions of reduced heme b_L is not feasible due to large difference in E_m values of the Q/ QH_2 couple and heme b_L .

In this mechanism, water dipoles are proposed to be the crucial elements that stabilize Q or QH_2 binding when 2Fe2S and heme b_L are either both reduced or both oxidized, respectively.

(vi) Coulombic gating. When the rapid reversibility of reactions at the Q_o site was established,⁶¹⁶ it became clear that the “ SQ^- movement” mechanism (see above) does not explain gating, nor does it prevent all types of short-circuit. In an attempt to modify this mechanism to accommodate reversibility and the prevention of all short-circuits, “Coulombic gating” was proposed.⁵⁹⁷ The crucial element of this model is an assumption that SQ^- is attracted by Coulombic interactions and thus moves toward the oxidized heme b_L , therefore increasing the electron transfer rate. On the other hand, when SQ^- is formed while heme b_L is reduced, then it is repelled, moving toward the 2Fe2S and decreasing the probability of electron transfer from heme b_L to SQ^- . Although this mechanism seems to explain the limited efficiency of short-circuit SC2, it is still not clear how it would allow rapid reversibility of the Q_o site.

7.4.3.3. Current Status and Emerging Concepts of Short-Circuit Suppression. Despite many proposals and the various models outlined above, the exact mechanism of gating and reversibility at the Q_o site that minimizes energy-wasting reactions is still not known. It appears that each of the mechanisms presented is able to explain the bifurcation reaction under certain specific conditions, but at the same time, they may not be sufficient to explain observations under other conditions, or to provide a detailed molecular basis, or be fully consistent with the ensemble of existing experimental data. Our intention in this review is not to favor any particular mechanism. Rather, in view of their diversity and general complexity, and also given that no obvious elements unifying them into one common mechanism can be proposed, we argue that the bifurcation at Q_o site is far from being satisfactorily understood and still deserves extensive experimental and theoretical exploration.

This is particularly the case for the $Cytb_{6f}$, where the situation is further complicated by the possible injection of an additional electrons from the n side through heme c_n to heme b_n .

It is worth hypothesizing that the “true” mechanism of energy-conserving reversible bifurcation could be a process to which several of the many different gating mechanisms proposed by different authors could contribute, depending on the starting conditions. We also anticipate that the transition from forward to reverse electron transfer at the Q_o site may not be a simple reversal of the proton/electron transfer and that dynamic events that start the reverse reaction may differ from the final step of forward reaction. It could very well be that the stability constant of the SQ^- formed during oxidation of QH_2 is different from the stability constant of SQ^- formed by reduction of Q. We believe that the key players are likely to be protons, as different proton configurations could favor different stabilities of the SQ^- formed during forward and reverse reactions. However, the proton events and paths for uptake and release have not been resolved yet.

7.5. Superoxide Generation at the Q_o/Q_p Site

The operation of any electron transfer chain (ETC) in the presence of oxygen is connected to the generation of superoxide radical. *In vivo*, superoxide is quickly converted into H_2O_2 in a reaction catalyzed by superoxide dismutase. This is presumably why first mentions of ETC-derived radicals were related to H_2O_2 and not superoxide. Indeed, the first information about reactive oxygen species (ROS) in mitochondria showed mitochondrial levels of H_2O_2 at 1–2% of total O_2 uptake in state 4 of respiration (the state not coupled to ATP synthesis), while the rate of H_2O_2 generation in state 3 of respiration (the state associated with ADP to ATP conversion) was negligible.^{625,626} It was also noticed that antimycin enhances production of H_2O_2 in intact mitochondria.^{627,628}

7.5.1. Semiquinone at the Q_o/Q_p Site as Electron Donor to Molecular Oxygen. The first reports on superoxide production in antimycin-treated submitochondrial particles to suggest that ROS are $Cytc_1$ -derived appeared in Boveris and Cadenas work in 1975.^{629–631} Over the next few years, it was established that the origin of ROS in antimycin-inhibited $Cytc_1$ of submitochondrial particles is the redox reaction in the UQH_2 oxidation site.^{254,632} Using $Cytc_1$ isolated from yeast, it was also shown that inhibition with antimycin A as well as with myxothiazol which binds to the proximal niche of the Q_o site leads to production of ROS at the Q_o site.^{633,634} The link between superoxide production and the action of Q_o/Q_p site is consistent with the widely accepted notion that a highly unstable SQ^- at the Q_o site (SQ_o^-) is a direct one-electron donor to oxygen.²²⁴

In view of the reversibility of the catalytic reactions in the Q_o site, there are two possible reactions that can lead to the formation of semiquinone at this site: one electron oxidation of QH_2 by the oxidized 2Fe2S cluster (the “semiforward” reaction)^{633,635} or one electron reduction of quinone by heme b_L (the “semireverse” reaction).^{636,637} It therefore follows that there are two possible reaction sequences leading to ROS production by the Q_o site. These sequences involve either semiforward or semireverse reaction followed by electron transfer from the formed SQ^- to molecular oxygen. Both sequences require the initial presence of reduced heme b_L , which either blocks the heme b_L from accepting an electron from SQ^- formed via the semiforward reaction or donates an electron back to Q bound at the Q_o site, forming SQ^- via the semireverse

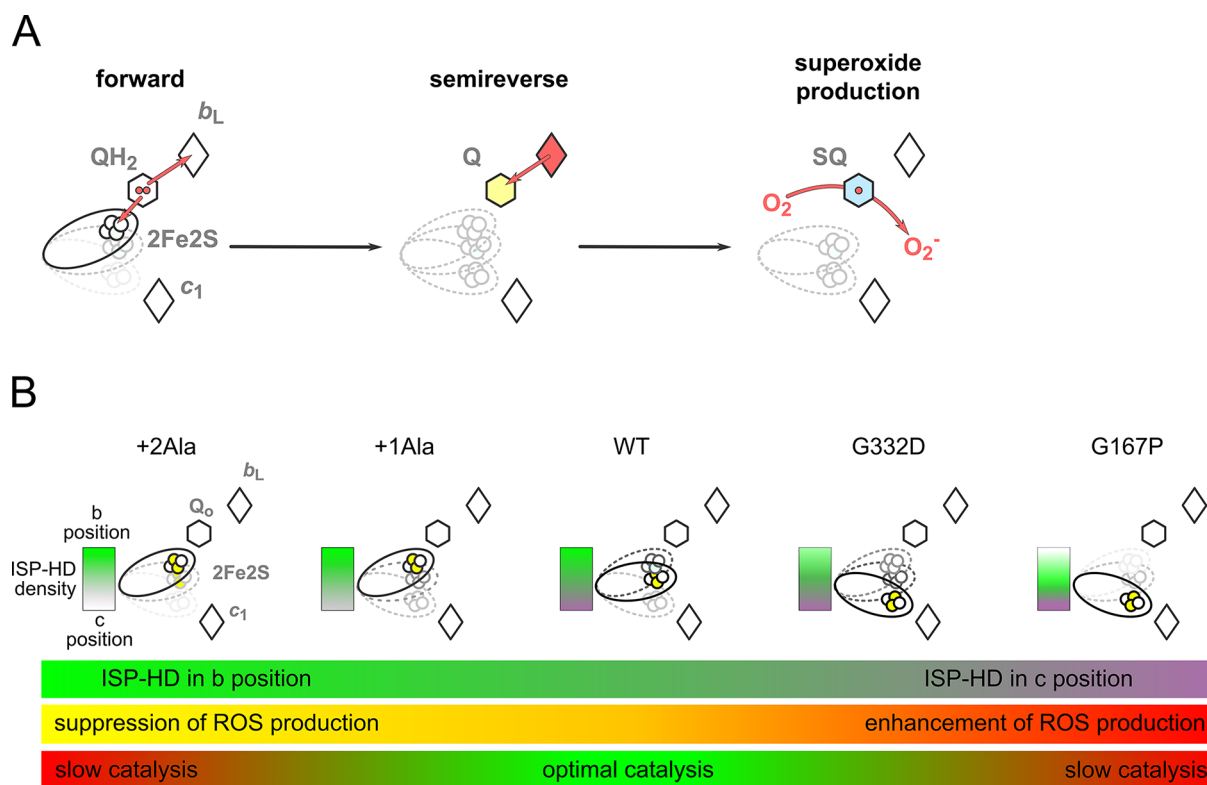


Figure 30. “Semireverse-Rieske off” model of ROS generation in the Q_o site. (A) Simplified static scheme showing one of the possible sequences of reactions leading to ROS formation at the Q_o site: oxidation of QH_2 (“forward” box), electron transfer from heme b_L to Q (“semireverse” box), electron transfer from SQ to molecular oxygen (“superoxide production” box). In the “forward”, and “semireverse” box, white and red rhombus correspond to the redox state of heme b_L before the reaction (oxidized and reduced, respectively). The reduced heme b_L necessary to start the semireverse reaction can also be a product of electron transfer from heme b_H (reaction 2 in SC4 in Figure 29). Note that the semireverse reaction corresponds to reaction 1 in SC3 and SC4 or reaction 2 in SC2 in Figure 29. (B) Scheme illustrating that a shift in the equilibrium distribution of the ISP-HD positions from the b-position toward the c-position (from left to right) induced by specific mutations correlates with an increase in the ability of the Q_o site to generate ROS.

reaction. This requirement is generally consistent with the observation that ROS are detected when electron transfer between heme b_L and heme b_H is impeded by blocking the Q_o site with antimycin A or by an increase in membrane potential.^{573,638}

In the currently discussed mechanisms of ROS production by the Q_o/Q_p site, both reaction sequences (i.e., involving semiforward or semireverse reaction for semiquinone formation) are taken into account. Some models propose that only one from these two sequences is responsible for ROS production, while other models consider a contribution from both. Indeed, it seems plausible that the detected ROS may be a combined product of both mechanisms but that their relative contributions change depending on the experimental conditions or introduced electron transfer barriers within cofactor chains.

The specific rate of superoxide production in $Cytb_{6f}$, normalized to the rate of electron transport, is more than an order of magnitude greater than that measured in isolated yeast respiratory $Cytc_1$.³⁸ The higher rate of superoxide production in $Cytb_{6f}$ could be a consequence of an increased residence time of plastoquinone/plastoquinol in its binding niche near ISP-HD, resulting from (i) occlusion of the quinone portal by the phytol chain of the unique bound chlorophyll, (ii) an altered environment of the proton-accepting glutamate believed to be a proton acceptor from semiquinone, or (iii) a more negative redox potential of the heme b_p on the electrochemically positive side of the complex.³⁸

7.5.2. “Semireverse-Rieske off” Model of Superoxide Production. The mechanism involving the semireverse reaction (heme b_L to Q electron transfer) is a relatively new concept that emerged from the initial observation that ROS production exhibits a bell-like shape dependence on the redox state of the $Q(H_2)$ pool. This means that maximal production of ROS occurred when the pool was partially oxidized, which was taken as an indication that the semireverse reaction, for which the substrate is Q (not QH_2) is involved in superoxide generation.^{120,637}

A contribution of the semireverse reaction in ROS generation was also established in studies using mutated forms of the bacterial $Cytc_1$, which introduced limitations in electron transfer at the level of different cofactors within the low and high potential chains.^{107,120,636} Furthermore, these studies revealed an important constraint associated with the kinetic effects of the motion of ISP-HD. In the proposed model, production of radicals depends on the position of the ISP-HD with respect to the Q_o site. Mutants with the insertion of a single or two alanine residues (+1Ala, or +2Ala, respectively) at the neck region of ISP, which increases the probability of ISP-HD being located in close proximity to the Q_o site,^{90,107} were found to be less prone to ROS production in antimycin A inhibited $Cytc_1$.^{107,636} (Figure 30). To explain this observation, it was proposed that molecular oxygen competes kinetically for electrons with cofactors of the Q_o/Q_p site. When ISP-HD is present at the Q_o/Q_p site during SQ^- formation, the probability

of electron transfer between the 2Fe2S and SQ^- is high. The reduced 2Fe2S can then reduce the SQ^- , reforming QH_2 and completing the reverse reaction, while the oxidized cluster can accept an electron from SQ^- and completing short-circuit reaction (SC3 in Figure 29). However, when ISP-HD occupies positions remote from the Q_o/Q_p site at the time of SQ^- formation, the rate of the electron transfer between SQ^- and the 2Fe2S decreases. Under these circumstances, the probability that molecular oxygen outcompetes 2Fe2S for electrons from the SQ^- increases, which leads to the release of detectable levels of superoxide from the Q_o/Q_p site.

Initial studies on the +2Ala mutant were not able to discriminate between the possible contributions of semiforward or semireverse reactions in ROS generation.⁶³⁶ In addition to the suppression of ROS generation in the +2Ala mutant, this study examined another mutant, $Cyt c_1$:^{Rh}M183L, that changes one of the axial ligands of heme c_1 , shifting the E_m of this heme by more than -300 mV. This introduced a large barrier to electron transfer between 2Fe2S cluster and heme c_1 without affecting the motion of ISP-HD, causing an increase in ROS production. Given that ROS production is also enhanced when electron transfer barrier is introduced at the level of the low potential chain (addition of antimycin A, a mutation disturbing the oxidation of QH_2 at the Q_o site, ^{Sc}E272Q (^{Rh}E295Q)⁵⁹⁹ or mutations to change the axial ligands of hemes b , ^{Rh}H198N and ^{Rh}H111N⁶³⁹), it appears that in general any significant asymmetry in the overall rate of electron flow between the high- and low-potential chains might make the enzyme more prone to generate superoxide. One exception to this is if it is caused by arresting the ISP-HD at the Q_o/Q_p site. Again, these studies could not discriminate between the relative contribution of semiforward or semireverse reactions to ROS generation by the Q_o/Q_p site.

Such discrimination became possible in subsequent studies with the use of the +1Ala mutant and in combination with $Cyt c_1$:^{Rh}M183K (equivalent of ^{Rh}M183L described above). These studies clearly pointed toward the semireverse reaction as the dominant contributor in this process.¹⁰⁷ Mutational studies analyzing the molecular effects of mitochondrial disease-related mutations further substantiated the inclusion of both postulates (i.e. the one related to involvement of the semireverse reaction in SQ^- formation and the other related to the probability of ISP-HD position-dependent interaction of SQ^- with oxygen) in what can be referred to as the “semireverse-Rieske off” model of ROS generation by the Q_o/Q_p site.

The $Cyt b$:^{Rh}G167P mutation in *Rhodobacter capsulatus* is an equivalent of human mitochondrial S151P mutation in *Cyt b*, which was found in patients with exercise intolerance.⁶⁴⁰ This mutant exhibits enhanced production of ROS even without antimycin A.¹²⁰ In contrast to +nAla insertions, ^{Rh}G167P influences the motion of ISP-HD in such a way that it tends to occupy positions more remote from the Q_o site in comparison to WT (see section 3.4). This effect, in agreement with the semireverse-Rieske off model, increases the probability of SQ^- reaction with oxygen (Figure 30). Furthermore, introduction of the +1Ala mutation to the ^{Rh}G167P mutant partially compensated the effect of ^{Rh}G167P, which resulted in diminished ROS production, again consistent with this model. The ^{Rh}G332D mutation, an equivalent of another mitochondrial disease-related mutation G290D (associated with exercise intolerance in humans⁶⁴¹), was also found to influence motion of ISP-HD. However, this influence is less pronounced

compared to ^{Rh}G167P, and accordingly the effects on ROS production are more subtle¹²¹ (Figure 30).

As introduced in section 7.4.1, the kinetic competition between the leaks of electrons and short-circuit reactions, inherent also to the semireverse-Rieske off model, might be of physiological importance. In general, both reactions lead to a drop in the efficiency of electron bifurcation at the Q_o site, but while short-circuits retain electrons within ETC, leaks generate ROS.

Assuming that high production of ROS is deleterious, in some cases, short-circuit reactions may play a beneficial role in lowering of ROS generation. For various enzymes involved in bioenergetics, it has been postulated that such energetic loss, which minimizes ROS-related damage, gives the organism a better chance of survival.⁶⁴² On the other hand, ROS are also postulated to play a redox signaling role,⁶⁴³ thus careful balancing of short-circuits and leaks must be considered as one of the possible elements of the redox signaling/control systems.

When disabled, the Q_i/Q_n site does not completely inhibit the function of the Q_o/Q_p site, and the enzyme can still sustain electron flux through the ETC. This residual flux is presumably possible via short-circuit reactions and electron leaks. In *Cyt b_c1*, that flux is still low, and the enzyme remains nonfunctional at physiologically relevant scale. Interestingly, in *Cyt b_c6f*, a residual flux can sustain the entire photosynthetic chain with the short-circuits that were proposed to act as an “emergency exit” pathway bypassing the Q-cycle and making it dispensable.⁶¹⁷

7.5.3. Other Postulated Reactions Involving Molecular Oxygen. In addition to the reaction of molecular oxygen with SQ^- formed at the Q_o/Q_p site discussed above, it was also proposed that oxygen might act as a redox mediator between QH_2 and heme b_L .⁶⁴⁴ According to this proposal, heme b_L would accept an electron from QH_2 via protonated superoxide (HOO^-) at the Q_o site, which would facilitate electron transfer within the low potential chain. This so far purely hypothetical scenario was introduced to explain the observed enhanced enzymatic activity of *Cyt b_c1* in the presence of oxygen, compared to its activity under anaerobic conditions.

MD simulations showed that O_2 molecules spontaneously diffuse into the Q_o site of *Cyt b_c1* and can react with SQ^- while forming superoxide.⁶⁴⁵ Molecular oxygen may also occasionally get within 5 \AA of the central iron atom of the hemes b_L and b_H . Its presence near the heme b_L raises the question of whether this heme is also an immediate electron donor in the production of superoxide. Indeed, this hypothesis has never been definitively ruled out, and although much less popular compared to models based on SQ^- can also be found in the literature.⁶⁴⁴ It is based on the rationale that the redox potential of heme b_L is sufficiently low to make electron transfer to oxygen theoretically possible.⁶⁴⁶

In this context, an interesting concept concerning the evolutionary adaptation of *Cyt-bc* complexes to the presence of oxygen was proposed by Bergdoll et al.¹⁶⁰ By comparing redox properties of organisms that use different quinones and live in aerobic and anaerobic conditions, they concluded that the Great Oxidation Event occurred about 2.5 billion years ago when the rise of atmospheric oxygen resulted in an upshift of the ambient redox potential of hemes b and the 2Fe2S cluster. The global response of organisms, which included upshift of the redox potential of the $Q(H_2)$ pool by 150 mV (menaquinone versus ubi/plastoquinone) and a commensurable increase in the entire set of redox potentials of the cofactors of *Cytbc* complexes, was aimed to avoid deleterious ROS generation.

A separate question that can be found in the literature is whether the Q_i/Q_m site is also able to produce ROS.⁶⁴⁷ Under high concentrations of QH_2 and in the presence of an inhibitor of the Q_o site, it is possible to generate a stable SQ^- intermediate originating from the reverse reaction at the Q_i site of *Cytc₁* (see section 8.3).^{151,648,649} If Q_i/Q_m -produced ROS have physiological significance, it should be exposed under such conditions. However, measurements conducted in the presence of stigmatellin, a Q_o/Q_p site inhibitor, did not show statistically significant production of radicals in such a system.⁶³⁴ As discussed in section 8, Q_i -derived SQ^- can be stabilized via hydrogen bonding to prevent potential reaction of this SQ^- with molecular oxygen, as was shown for solution-generated SQ^- , which was found to be stabilized through hydrogen bonds with the acceptor solvent.²⁵³

7.5.4. Physiological Considerations. The currently available molecular mechanisms of superoxide generation by *Cytc₁* are derived mostly from analysis of conditions where electron flow through the cofactor chains was severely impeded by various experimentally imposed barriers (inhibitors, mutations). This raises the question whether the natively operating enzyme contributes to ROS generation in living cells, and if so how it does this. There have been reports suggesting that uninhibited *Cytc₁* may produce trace amounts of radicals.^{38,573,650} This was confirmed recently in studies that comprehensively evaluated radical generation in uninhibited *Cytc₁*.⁶⁵¹

It is known that production of ROS is dependent on the respiration rate of mitochondria.^{37,652} Factors enhancing ROS production in mitochondria include high pmf, a high $NADH:NAD^+$ ratio, high QH_2/Q ratio, low local O_2 concentration, and nearly inactive ATPase.^{37,638,652–654} As a rather general rule, the more reduced are the cofactors of ETC, the more prone ETC is to radical formation. Factors lowering production of ROS include high activity of uncoupling proteins which decrease pmf.⁶⁵⁵ High respiration rate also lowers the probability of ROS production.^{37,652}

ROS generation is usually expressed in units of s^{-1} (as the amount of superoxide molecules produced by ETC complex in one second) or as a percentage of ROS production (as % of ETC-derived electrons that pass to oxygen forming superoxide). In state 3 of respiration (upon the addition of ADP) when the rate of oxygen consumption is maximal, the fractional ROS production is negligible. However, in state 4 of respiration (when the ADP levels are depleted) and where respiration chain is slowed down, production of ROS is at the level of 1–2%.⁶²⁵ Interestingly, expressing production in s^{-1} shows that the rate of ROS production in state 3 might be even higher than in state 4.⁶⁵⁶

The possible influence of physiological factors on ROS generation by *Cytc₁* is perhaps best exemplified by the effects of the membrane potential. In its absence, heme b_H is the preferred electron acceptor within the pair of hemes b_L-b_H .⁶⁵⁷ In its presence, the apparent midpoint potentials of these two hemes become similar, leading to a more equal distribution of electrons between them.⁵⁷⁴ Consequently, the reduction level of heme b_L increases, which, as observed experimentally, is expected to lead to ROS production by the Q_o site.⁵⁷⁴

A description of dynamic changes in electron distribution between the b hemes appears to be a more complex issue when possible communication between monomers in the dimer occurring at the level of the heme b_L-b_L bridge is considered (see section 9). Any significant electron transfer between

monomers is expected to decrease the reduction level of the b hemes (including heme b_L), which might decrease the levels of ROS released from the Q_o/Q_p site, in particular if the semireverse-Rieske off mechanism is considered.

The physiological role of superoxide released by the components of ETC remains an open issue, especially in view of the suggestions that it may be one of the components of cellular redox signaling.³⁶ Among four ETC complexes (complex I–complex IV), it is commonly acknowledged that only two of them generate the majority of ROS produced during the operation of the ETC: complex I and complex III (reviewed in refs^{652,658}). These two complexes release superoxide into different compartments of mitochondrion: complex I frees superoxide into the matrix, while complex III releases it into the intermembrane space (IMS). ROS in the IMS are more easily accessible to the cytosol compared to ROS in the matrix, as the former need to cross only the outer mitochondrial membrane while the latter have to cross both inner and outer mitochondrial membranes.⁶⁵⁹

It should be emphasized that consideration of the role of ROS in cellular signaling should always account for the fact that the level of ROS released into the cytosol from mitochondria is the net result of ROS production and its scavenging inside the organelles.

Superoxide generated in the matrix is efficiently converted into H_2O_2 by the highly abundant MnSOD⁶⁶⁰ and H_2O_2 is further consumed by catalase (CAT) and glutathione peroxidase (Gpx). Estimates indicate that H_2O_2 is kept at a low level in the matrix, around 5×10^{-9} M.⁶⁶⁰ Supposedly, matrix-generated superoxide and H_2O_2 from its dismutation do not leave the matrix⁶⁵⁹ and thus any putative signal derived from complex I is probably restricted to this compartment.

ROS signaling communication between the mitochondria and cytosol becomes more plausible for superoxide generated by complex III and released to IMS.^{643,661}

In the IMS, superoxide can be transformed by CuZnSOD to H_2O_2 or, theoretically, scavenged by Cyt_c. The latter reaction, in view of the ratio between superoxide and the high physiological concentration of Cyt_c in the IMS (estimated to be in the range of 1 mM⁶⁶²), raises concern about whether the lifetime of superoxide released to IMS would be sufficient to carry out any meaningful signaling purposes. However, the probability of superoxide oxidation by Cyt_c may actually not be that high considering the rather low ratio of Cyt_c to *Cytc₁* (around 2:1,²⁰⁴ as estimated based on the optical spectrum of reduced mitochondria^{254,663}) and the fact that Cyt_c pool is fully reduced in state 4 of respiration and partially reduced in state 3 of respiration.⁶⁶⁴ While superoxide cannot pass efficiently through the membrane, it can escape mitochondria via voltage-dependent anion channels.⁶⁶⁵ After spontaneous or CuZnSOD-driven dismutation, superoxide is converted into H_2O_2 , and in this form, it can reach cytosol via diffusion much more readily. When overactivity of CuZnSOD in the IMS is observed, this leads to overproduction of H_2O_2 , which in turn may lead to the formation of oxoferryl Cyt_c. This may result in the oxidation of cardiolipin and turn on early pro-apoptotic processes.⁶⁶⁶

Interestingly, until recently no one has succeeded in detecting superoxide evolution from isolated *Cytc₁* by spin-trapping. This seems to stem from the methodological difficulty related to the large difference between rate constants for the superoxide reaction with Cyt_c ($k = 2.5 \times 10^5$ M⁻¹ s⁻¹,⁶⁶⁷) and the EPR spin trap DMPO ($k = 10$ M⁻¹ s⁻¹,⁶⁶⁸). DMPO falls behind oxidized Cyt_c when competing for superoxide. Cyt_c is a substrate for

Cytc₁ and achieving measurable level of radicals requires measurements to be done in the presence of high micromolar concentrations of Cyt_c. For DMPO to be able to trap superoxide before it reacts with Cyt_c, it would need to be in a high molar concentration range, which is unattainable due to its limited solubility. These limitations were recently overcome by the application of a new system in which Cyt_c was constantly oxidized by CcO, which allowed detection of DMPO-OOH radical.⁶⁵¹

7.6. Semiquinone Intermediate at the Q_o/Q_p Site

When discussing the mechanism of QH₂ oxidation at the Q_o/Q_p site, SQ is naturally considered as the transient state of the bifurcation reaction. Over the years the EPR signal related to this state was expected to be typical of a free radical single-line EPR spectrum at a *g* position close to 2. The very first report of detection of a *g* = 2 signal assigned to semiquinone at the Q_o site (SQ_o) in submitochondrial particles from 1981⁶⁶⁹ was invalidated by studies from 1998.⁶⁷⁰ Since that time a notion about SQ_o being highly unstable and therefore undetectable by EPR has been popular in the literature until 2007, when two independent groups reported on detection of SQ_o.^{261,262} In 2013, three additional reports presenting *g* = 2 EPR signals assigned to SQ_o were published.^{263,264,591} All these relatively new reports reopened a discussion on the presence of SQ_o, its properties, and its implications for the mechanism of bifurcation. In general, one would expect the signal to appear under conditions favoring electron transfer reactions at the Q_o/Q_p site and to be sensitive to all specific inhibitors of this site. It should also have paramagnetic properties related to its interactions with other metal cofactors of the site, the heme b_L/b_P or 2Fe2S (such as enhanced paramagnetic relaxation rates compared to a chemically generated SQ in solution). This, however, has not always appeared to be the case. For this reason, in our view, the issue remains debatable and requires further experimental exploration. A detailed discussion of different spectroscopic properties and controversies surrounding the *g* = 2 signals assigned as SQ_o is beyond the scope of this review. The reader is referred to a more detailed review by Pietras et al.²⁵⁸

In one of the reports on SQ_o from 2013, apart from the single-line signal at *g* ≈ 2, measured at 200 K, a new, unexpected transition with the most prominent line at *g* = 1.94 in the region of the spectrum of 2Fe2S was recorded at 20 K²⁶³ (see Figure 31). The new signal was highly sensitive to the inhibitors of the Q_o site and was transient (i.e., was detected only under nonequilibrium conditions before the enzymatic reaction of Cytbc₁ with its substrates reached equilibrium). Furthermore, it was observed that *g* = 1.94 at the X band (~9.5 GHz) shifts to *g* = 1.96 at the Q-band (~33 GHz). These findings, complemented by the simulation analysis of the EPR spectra, led the authors to conclude that the *g* = 1.94 transition belongs to the spectrum originating from SQ_o coupled by spin–spin exchange interaction with the reduced 2Fe2S (SQ-2Fe2S). An isotropic exchange constant of the interaction was estimated at 3.5 GHz. This was all consistent with the theory of exchange interactions, which assume that in the case of spin–spin coupling with an exchange constant of several GHz, the position and shape of EPR transitions of a system of coupled paramagnetic centers will depend on the microwave band used to make the measurements.^{671,672} It is of note that the spin–spin exchange interaction between SQ and the reduced 2Fe2S has already been put forward as an explanation for the failure to detect the *g* = 2 radical signal of SQ_o.⁵⁷⁵ However,

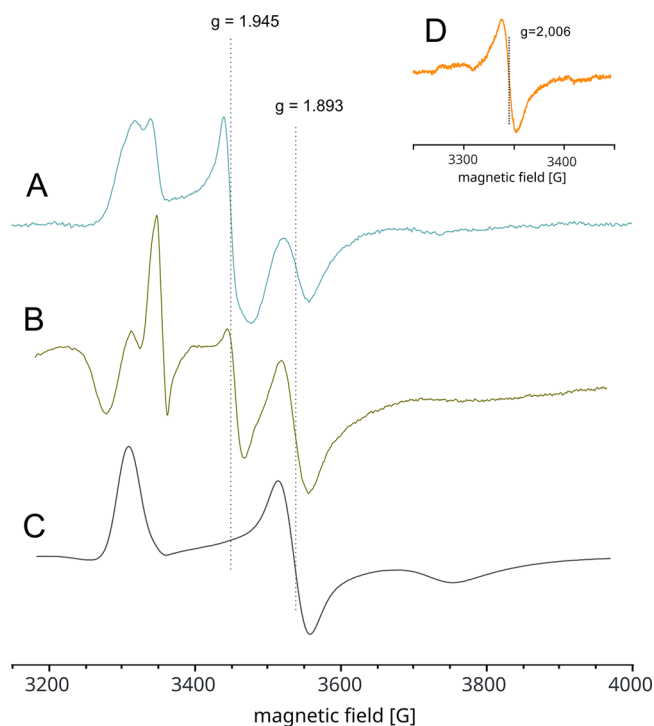


Figure 31. Two forms of SQ detected by EPR for the Q_o/Q_p site of Cytbc₁: the spin coupled SQ-2Fe2S state (with prominent transition at *g* = 1.945) and the “free” SQ_o not coupled to 2Fe2S (with transition at *g* = 2.006). Experimental spectra of (A, C, D) Cytbc₁ and (B) Cytbc_f recorded at the X band. Spectra in A and B contain contributions from the spectrum of SQ-2Fe2S and the spectrum of 2Fe2S. C shows the spectrum of 2Fe2 alone, for comparison. The insert (D) presents the single-line spectrum of the SQ_o.

unlike the original proposal (see section 7.4.3), the more recent data do not result from antiferromagnetic coupling of high energy.

Further research showed that a *g* = 1.94 signal of similar amplitude was observed when the samples were prepared under both aerobic and anaerobic conditions.^{482,673} This dismissed concerns raised by others⁶⁷⁴ that it might have resulted from oxidative damage to the 2Fe2S. This also pointed toward an interesting possibility that the SQ-2Fe2S state is not reactive toward molecular oxygen (see further discussion).

Upon optimization of reagent concentrations, the SQ-2Fe2S signal was detected within the time scale of tens to hundreds of milliseconds, which was comparable to the time of a single turnover of enzyme under the applied conditions (inhibition of the Q_i site with antimycin).⁶⁷³ On the other hand, the time scale of SQ-2Fe2S evolution was slower than the time scale of uninhibited enzyme turnover. Remarkably, so far the SQ-2Fe2S state has been found to coexist exclusively with oxidized heme b_L. All together, these results implicated that the semireverse reaction (heme b_L/b_P to Q electron transfer) at the Q_o/Q_p site is responsible for initiating formation of the SQ-2Fe2S state. This is partly because the semireverse reaction creates SQ_o, which can undergo spin–spin exchange with reduced 2Fe2S provided that the ISP-HD is docked at the site.²⁶³

Further studies revealed that the probability of formation of the SQ-2Fe2S state varies in mutants with decreased motion of ISP-HD.⁶⁷³ It is highest in mutants that have ISP-HD shifted toward the Q_o site (+1Ala and +2Ala). In contrast, the SQ-2Fe2S state was not observed in the ^{Rh}G167P mutant, which has

the oppositely effect to +1Ala or +2Ala and shows impaired docking of ISP-HD into the Q_o site¹²⁰ (^{Rh}G167P mutation).

The various combinations of these mutations have shown that direct interaction between the 2Fe2S and SQ_o is crucial for formation of SQ-2Fe2S state, and even minimal separation of the cluster from SQ_o induced by mutation breaks the spin–spin interaction.

The same family of mutants also revealed a clear negative correlation between superoxide production and the ability to form the SQ-2Fe2S state. On the basis of this observation and the nonreactivity of SQ-2Fe2S center with molecular oxygen discussed earlier, it has been suggested that the SQ-2Fe2S state may be involved in protection against massive release of superoxide under conditions when electron flow through the Q_o site is impeded.⁶⁷³ It should be noted that while the lack of the SQ-2Fe2S state is associated with an increase in the production of superoxide by *Cytc₁*, a high superoxide production may not necessarily imply lack of the SQ-2Fe2S state. This seemingly paradoxical statement is easily explained assuming that the unstable SQ_o is a common substrate for production of superoxide and generation of the SQ-2Fe2S state. An increase in the probability of formation of SQ_o will result in both an increase in superoxide production as well as in more efficient generation of SQ-2Fe2S. Since the SQ-2Fe2S state is non-reactive with oxygen, its formation can be regarded as an alternative route to leaks of electrons on oxygen; thus, it reduces the amount of superoxide production.

The SQ-2Fe2S signal was also detected in enzyme operating with native substrates in membranes of photosynthetic bacteria.⁶⁰⁸ Remarkably, the signal was present only when light-activation of the membranes shifted the redox state of the substrate pools, ubiquinone and *Cytc₂* pools, to a more reduced and oxidized state, respectively.

Under these conditions, SQ-2Fe2S titrated at higher ambient redox potentials compared to the $Q(H_2)$ pool (see section 4.1), which suggests that the SQ-2Fe2S state is somewhat stabilized at the Q_o site. The redox potential at which the SQ-2Fe2S amplitude reaches its maximum increased with decreasing pH indicating that a proton is involved in stabilizing the SQ-2Fe2S state. The interaction of SQ_o through hydrogen bonding with the 2Fe2S coordinating residue ^{Rh}H156, and the role of this interaction in SQ_o stabilization have been postulated many times.^{258,575,597}

Interestingly the SQ-2Fe2S state is not restricted to *Cytc₁* but has as it was also observed in isolated spinach *Cytc_{6f}* exposed to its substrates, PQH₂ and PC.⁴⁸² In this case, however, unlike in *Cytc₁*, inhibition of the Q_n site was not required. This revealed that the probability of SQ-2Fe2S state formation when the enzyme operates without inhibition is higher in the Q_p site of *Cytc_{6f}* compared to the Q_o site *Cytc₁*. The average redox potential of hemes b_n and b_p is probably more negative in *Cytc_{6f}* than respective b hemes in *Cytc₁*, while the redox potential of PQ/PQH₂ couple is higher compared to the potential of the respective UQ/UQH₂ couple. These differences in the redox potentials of b hemes and quinones would foster the semireverse reactions at the Q_p site and thus increase the probability of the SQ-2Fe2S state formation. In addition, electron transfer through heme c_n in *Cytc_{6f}* (not present in *Cytc₁*) might slow electron flow through the low-potential chain, and this could lead to a more favorable semireverse reaction.

The importance of quinone redox potential to SQ-2Fe2S formation is well supported by the observation that the high-potential Q derivative (DBMIB) bound at the Q_p site also

creates the SQ-2Fe2S state with a $g = 1.94$ transition. However, in this case, the state was already observed under equilibrium conditions, without PC present. In fact, its stability is so high that it inhibits the Q_p site. Indeed, the inhibition of *Cytc_{6f}* by DBMIB has long been known, as has its effect on the shape of the EPR spectrum in the region of 2Fe2S.^{84,108,483} This has been interpreted over the years as a structural alteration of the cluster caused by inhibitor binding.¹¹⁰ The frequency-dependent shift in the g value of the signal induced by DBMIB (similar to shifts discussed above) dismisses this interpretation, indicating that the signal must reflect a spin–spin exchange interaction between the SQ form of DBMIB and the reduced 2Fe2S⁴⁸² (see also section 5).

Considering all the details of the formation and properties of SQ-2Fe2S uncovered to date, an energy diagram was proposed for both *Cytc₁* and *Cytc_{6f}*, in which this state represents a local energetic minimum, placed below the state with the reduced heme b_L/b_P (given that SQ-2Fe2S is observed along with oxidized heme b_L/b_P), but above the state with reduced heme b_H/b_n (Figure 32). It has been suggested that SQ-2Fe2S is a

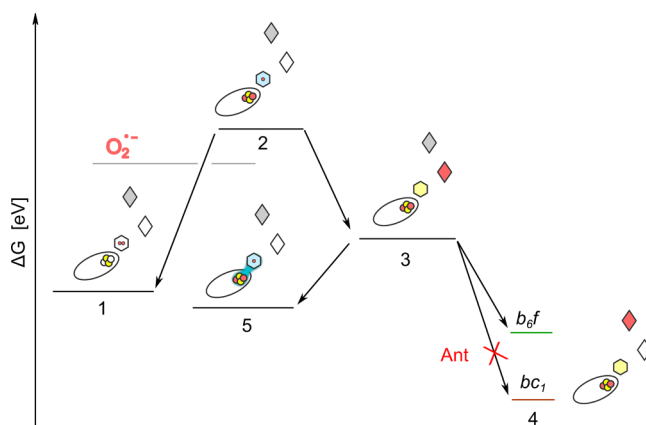


Figure 32. Simplified energy diagram of *Cytc₁* and *b_{6f}*. The diagram shows the states of the catalytic reaction at the Q_o/Q_p site. (1) Conditions before the start of the bifurcation reaction: Q_o/Q_p is occupied by QH₂, 2Fe2S and heme b_L/b_P are oxidized. (2) Transition state: unstable semiquinone and the reduced 2Fe2S, oxidized heme b_L/b_P . (3) Conditions after full oxidation of QH₂: Q_o/Q_p is occupied by Q , cluster 2Fe2S and heme b_L/b_P are reduced. (4) Stage after electron transfer from heme b_L/b_P to heme b_H/b_n . This state has different energy in the *Cytc₁* and *Cytc_{6f}* due to the different potential of heme b_H/b_n in both enzymes and the potential differences between PQ and UQ. (5) Spin-coupled SQ-2Fe2S state with oxidized heme b_L/b_P . The redox state of heme b_H/b_n in all states (1–5) is not considered in the context of the system's energy. The level of the reaction of SQ with oxygen is also indicated as a gray line below state 2.⁴⁸²

metastable state, which may play a role as a buffer for electrons, in particular under conditions when electrons cannot freely leave the low-potential chain through the Q_i/Q_n site. Although the physiological role of this state is not yet known, in view of the observed negative correlation between its presence and superoxide production, and the apparent nonreactivity of this state with molecular oxygen, it was proposed that SQ-2Fe2S may be associated with protection against side reactions at the Q_o/Q_p site. This concept further assumes that the probability of formation of SQ-2Fe2S might be adjusted to the oxygen tension in the cellular environment and varies between different species. This probability depends on the energy difference between SQ-2Fe2S and the states determined by the E_m values of Q/QH_2

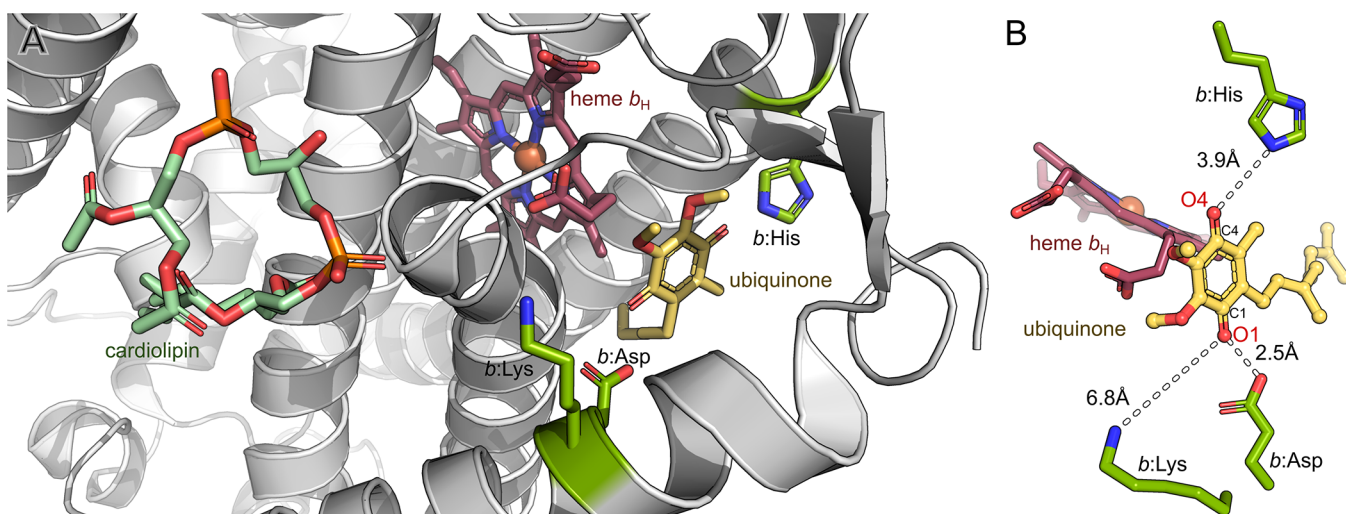


Figure 33. Structural details of the region around the Q_i site. (A) Overall view of the Q binding environment and elements involved in proton transfer to Q . (B) Geometry of the Q binding at the Q_i site. Labels indicate O1, O4, C1, and C4 atoms of the Q molecule and distances between Q and proton donors. Models based on PDB IDs: A206 and 1NTZ, A and B, respectively.

couple and the E_m values of the oxidized/reduced couples of low-potential cofactors of Cyt- bc (Figure 32). This notion was proposed in view of the observation that Cyt bc_1 , which experiences more than an order of magnitude higher levels of oxygen in chloroplasts than does Cyt bc_1 in mitochondria, appears to have a greater tendency to reside in this buffered state.

An intriguing hypothesis was put forward for a possible role of the Cyt bc_1 SQ-2FeS in regulation of the electron transfer pathways in oxygenic photosynthesis. It was proposed that the SQ-2FeS state in Cyt bc_1 might serve as a factor that changes the efficiency of CET versus LET between photosystem I and II. This concept was based on the assumption that transient stabilization of the SQ-2FeS temporarily blocks the oxidation of further PQH $_2$ in the Q_p site, thus creating conditions in which the probability of delivering the second electron needed to complete the reduction of PQ in the Q_n site by Fd/FNR is significantly increased.⁴⁸²

8. MECHANISTIC INSIGHTS INTO THE CATALYTIC Q_i/Q_n SITE

8.1. Overview of Structure of Q_i and Proton Paths

The Q_i site binding pocket is located in the vicinity to heme b_H near the n side of the membrane and its entrance opens toward the membrane core allowing substrate and product molecule to enter and leave the site. The pocket is surrounded by residues from transmembrane helices A, D, E, the amphipatic surface helix a, the DE loop and the N-terminal peptide. The crystal structures identified not only the position of site-specific inhibitor (antimycin A)^{79,123} but also the position of bound substrate (UQ).^{61,63,79,123,675} The binding sites of these compounds were found to significantly overlap with little rearrangements in the protein backbone and side-chains, as compared with the rearrangement of the protein around the Q_o site upon binding inhibitors. This indicates that the Q_i site is structurally more rigid than the Q_o site.

The quinone ring bound at the Q_i site is nearly perpendicular to the plane of heme b_H with the closest distance of 4.2 Å.⁷⁹ It appears to be stabilized by both hydrophobic and polar interactions. The former include interaction with ^{Bt}Phe220/^{Sc}Met221, the latter through formation of hydrogen

bonds with three residues: ^{Bt}Ser205/^{Sc}Ser206, ^{Bt}Asp228/^{Sc}Asp229, and ^{Bt}His201.^{79,675} The His interacts directly with quinone in bovine⁷⁹ and also in bacterial enzyme (His217),⁶³ while in yeast (^{Sc}His202) it interacts indirectly through a water molecule.⁶⁷⁵

As the Asp and His residues interact respectively with O1 and O4 of Q , they are considered to be involved in protonation of Q . In addition to these residues, the crystal structures identified other structural elements that could potentially form proton paths from the protein surface toward the O1 and O4 of Q .

The path toward the O1 (referred to as the D/K path) involves a conserved Lys residue and a bound cardiolipin, which interacts further with a conserved Asp located next to the bound Q (Figure 33). The cardiolipin has been suggested to act as a proton attracting antenna, which transfers protons to the nearby Lys.⁶⁷⁵ The Lys further passes the protons to the conserved Asp through a string of interconnected water molecules,⁶⁷⁶ or alternatively undergoes a rotation toward the Q_i site and directly interacts with the Asp, as suggested by MD simulations.^{79,677}

The path toward the O4 involves a conserved Glu and a conserved Arg that may interact through the water molecules with a conserved His located next to the bound Q .^{675,676} Site-directed mutations of this residue fully inactivated bacterial Cyt bc_1 .⁶⁷⁸ On the other hand the Asp/Lys path was found to be disabled only when both protonable groups were removed. With just one protonable residue from the Asp/Lys pair, the entrance of protons to the catalytic site was sustained, albeit at lower rates, indicating that protons in the Asp/Lys path can travel through parallel routes, possibly involving water molecules.⁶⁷⁹ The Asp/Lys path thus appears to tolerate disruption, as long as all the elements available for functional cooperation secure efficient proton delivery to the catalytic site. In this context, the Q_i site is similar to other Q binding sites, such as the Q_B site of photosynthetic reaction center, for which a multiplicity for proton paths has also been considered.⁶⁸⁰

8.2. Catalytic Electron and Proton Transfers at the Q_i Site of Cytochrome bc_1

The reduction of Q to QH $_2$ at the Q_i site involves two sequential single electron transfer steps in which the electrons are delivered from the same cofactor chain.³⁹ Because the arrival of the

electrons is separated in time, the reaction must involve the formation of an SQ intermediate (SQ_i) that is stabilized within the Q_i binding pocket before the final product (QH_2) is formed and leaves the site. Indeed, a stable radical signal originating from the Q_i site was recognized in early EPR studies on submitochondrial particles⁴⁴⁰ and crude protein extracts^{141,681} and has been explored since then as a key mechanistic element of models proposed for that site.^{151,163,245,648,649,679,682–686}

Considering electron transfer, reduced heme b_H acts as immediate electron donor to Q and then to SQ formed after the first electron transfer (SQ_i). These reactions are favored by the generally lower E_m of the heme compared to the average E_m of the $Q(H_2)$ pool (under physiological pH, E_{m7} of heme b_H is around +50 mV, while that of the pool is around +100 mV).¹⁴⁹ As these reactions leave heme b_H in an oxidized form, the SQ_i associated with the oxidized heme b_H ($SQ_i-b_H^{3+}$) is one of the key intermediate states of the catalytic forward reaction.²

At alkaline pH, the E_m of heme b_H approaches that of the $Q(H_2)$ pool and a partial reversal of the reaction can be observed. In this case, QH_2 bound at the Q_i site reduces heme b_H , resulting in formation of SQ_i at this site.¹⁶³ Such reaction, in which QH_2 (instead of Q) acts as a substrate for the Q_i site, can occur also at high QH_2 to Q ratios.^{648,687} This reaction, unlike the forward reaction, leads to the formation of SQ that is present along with reduced heme b_H ($SQ_i-b_H^{2+}$). For many years, $SQ_i-b_H^{2+}$ has been the dominant form of SQ_i detected and explored experimentally. However, more recent studies indicated that the analysis of both forms of SQ_i (i.e., $SQ_i-b_H^{3+}$ and $SQ_i-b_H^{2+}$) is crucial to advance our understanding of the molecular mechanism of the operation of the Q_i site (see section 8.3).

In addition to the observation of a stable SQ_i radical by EPR, the stability of SQ_i is supported by data from light-induced electron transfer measurements. Under conditions of single-turnover at the Q_o site, the offset in the levels of light-induced heme b_H reduction observed in the absence and presence of antimycin corresponds to the amount of SQ_i that is formed in the forward reaction (electron transfer from heme b_H to Q). On the other hand, when the Q_o site is blocked by an inhibitor, the level of light-induced heme b_H reduction corresponds to the amount of SQ_i formed in the reverse reaction (electron transfer from QH_2 to heme b_H). The extent of the forward reaction reflects the difference between the E_m of heme b_H^{3+}/b_H^{2+} and the E_m of Q/SQ couples, while the extent of the reverse reaction indicates the difference between the E_m of heme b_H^{3+}/b_H^{2+} and the E_m of SQ/ QH_2 couples. Further analysis of such extents might provide estimates of E_m for Q/SQ and E_m for SQ/ QH_2 , which in turn would provide information on the stability constant of SQ ($\log(K_s) = [E_m(Q/SQ) - E_m(SQ/QH_2)]/60$). Using this approach with a specific mutant in which the E_{m7} of heme b_H was elevated to the level of the E_m of the QH_2 pool, the stability constant of SQ_i was estimated to be at the level of 3×10^{-1} .¹⁴⁹

8.3. Fast- and Slow-Relaxing SQ_i as Dominant Intermediates of Forward and Reverse Reactions at the Q_i Site, Respectively

Until recently, EPR-based investigation of the SQ_i intermediate relied on the assumption that the SQ_i interacts antiferromagnetically with the oxidized heme b_H , forming an “EPR-silent exchange couple”. Therefore, only SQ_i present when heme b_H is also reduced ($SQ_i-b_H^{2+}$) was thought to be spectroscopically detectable.^{141,683} This notion is no longer valid in light of the recent studies that identified two distinct populations of SQ_i

differing in the rates of spin–lattice relaxation (Figure 34A).^{151,163} The first population, characterized by a slow relaxation (SQ_{iS}), corresponds to the well-known and extensively examined $SQ_i-b_H^{2+}$ state, whereas the second population, characterized by a significantly faster relaxation time (SQ_{iF}), corresponds to the long-missing $SQ_i-b_H^{3+}$ state. The dipolar interaction between SQ_{iF} and oxidized heme b_H manifests itself in the characteristic properties of SQ_{iF} , including fast spin–lattice relaxation leading to dominant homogeneous line broadening⁶⁸⁸ and unusual behavior of the signal amplitude that does not follow Curie’s law.⁶⁸⁹ These findings established that, contrary to long-standing assumptions, the $SQ_i-b_H^{3+}$ state is not antiferromagnetic and can be separated spectroscopically (as SQ_{iF}) if an appropriate combination of microwave power and temperature is applied during EPR measurements.¹⁵¹

Further studies revealed that SQ_{iS} and SQ_{iF} are separable in equilibrium redox titrations.¹⁶³ Remarkably, over a pH range from 6 to 8, SQ_{iF} represented a large, if not dominant, portion of the whole population of titrated SQ_i , indicating that early titrations²⁴⁵ had indeed missed a significant fraction of SQ in this pH range (Figure 34B). SQ_{iF} was also trapped as a stable intermediate at the Q_i site during steady-state turnover,¹⁶³ which is consistent with the electron transfer reaction scheme predicting $SQ_i-b_H^{3+}$ as the key intermediate state of the catalytic forward reaction (heme b_H to Q electron transfer).² On the other hand, SQ_{iS} appeared as the dominant intermediate state observed under the conditions favoring the reverse reaction (QH_2 to heme b_H electron transfer).

Interestingly, when a single electron gets injected into heme b_H of one monomer through the reverse reaction at the Q_i site, there is a possibility of electron equilibration within all four hemes of the b -chain of the dimer (through the heme b_L – b_L bridge, see Figure 5 and section 9). This way the electron can reach the second Q_i site (reducing Q to SQ_i), which overall will result in a formation of SQ_{iF} in both monomers (Figure 35). The observation that both SQ_{iS} and SQ_{iF} are observed in the native enzyme with an inactivated Q_o site (when only the reverse reaction at Q_i is possible) indicates that electron equilibration within the b -chain of the dimer indeed traps some fraction of the molecules of $Cytc_1$ with the $SQ_i-b_H^{3+}$ state at both Q_i sites.¹⁵¹ This conclusion was further supported by the observation that electron redistribution over b hemes/ Q_i sites taking place within the dimer and monitored by analyzing the change in relative proportions of SQ_{iF}/SQ_{iS} is effectively modulated in mutants that significantly raise the redox midpoint potential of either heme b_L or heme b_H .^{149,151}

8.4. Charge Polarization of SQ_i Facilitates Electron and Proton Reactions at the Q_i Site

The experimental exploration of both states of SQ_i (i.e., SQ_{iS} and SQ_{iF}) complemented by quantum mechanical calculations led to the formulation of a hypothetical mechanism, which places importance on the charge and spin polarization of SQ_i intermediates in the catalytic reactions at the Q_i site.¹⁶³ This polarization is imposed by the local electrostatic field induced by the specific distribution of residue charges within the Q-binding pocket. These are mainly His in the vicinity of the O4 atom and the Asp/Lys pair in the vicinity of the O1 atom.

This “charge polarization” mechanism is schematically presented in Figure 36, right. The evolution of states A to G considers the direction of reduction of Q to QH_2 . The reaction requires initial entry of Q to the Q_i site (states A and B) and heme b_H in reduced state (state C). It starts when the O4 atom of

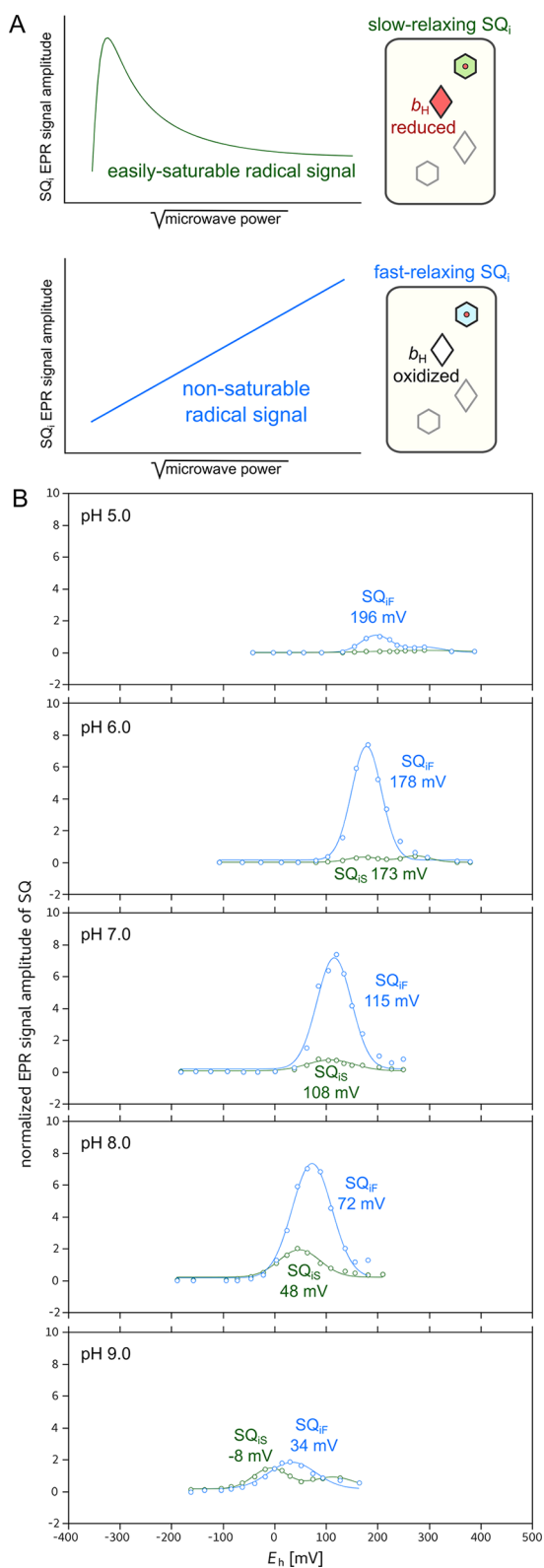


Figure 34. (A) Two populations of SQ_i detected by EPR. Upper: slow-relaxing SQ_i (SQ_{iS}) associated with the presence of reduced (and diamagnetic) heme b_H near the Q_i site. Green line illustrates the expected microwave power saturation profile of SQ_{iS} . Lower: fast-relaxing SQ_i (SQ_{iF}) associated with the presence of oxidized (and paramagnetic) heme b_H near the Q_i site. Blue line illustrates the expected saturation profile of SQ_{iF} . (B) EPR-monitored redox titrations of SQ_{iS} and SQ_{iF} in a range of pH from 5 to 9.¹⁶³

the Q present at the site interacts with the protonated His. The electron is then transferred from this heme to Q resulting in the formation of the SQ_i anion (which is detected by EPR as SQ_{iF} when heme b_H is oxidized) (state D). The anionic SQ_i becomes more negative at the O4 atom than at the O1 atom, while the spin density is larger at the C1 side compared to the C4 side (Figure 36, left). Such polarization and the resulting geometry favor a barrierless exchange of the proton originating from His between the His imidazole ring and the O4 atom of SQ_i . In this state, the SQ_i radical is stabilized and equilibrates between the anionic and neutral forms. This equilibration also takes place after the reduction of heme b_H and is associated with the conversion of SQ_{iF} to SQ_{iS} (conversion of state E to F). This continues until the second electron reduces the neutral SQ_i to unstable QH^- (state F). When this equilibration takes place, the protonation of anionic SQ_i to the neutral form does not influence the spin density but causes an inversion of the direction of charge polarization: the C1 side becomes more negative than the C4 side. This increases the probability that the second proton will be transferred to the O1 atom. Consequently, the reduction of neutral SQ_i to QH^- is accompanied by the spontaneous transfer of a second proton from the Asp/Lys-path to the O1 atom, completing the reduction of Q to QH_2 , followed by dissociation of the product (state G).

The key feature of the proposed mechanism is an initial response of the radical anion to the local electrostatic field, as it triggers progression of the whole catalytic reaction. At the same time, polarized SQ_i exchanging a proton in the absence of barrier with His forms a stable intermediate, which, during enzymatic turnover, safely “waits” for the second electron without the risk of generating other radicals (such as superoxide).

The charge polarization mechanism sheds new light on the protonation states of SQ_i described earlier by the pulse spin-echo-based EPR (ESEEM or HYSCORE),^{648,649,685} which must have referred to just the SQ_{iS} , as the spin-lattice relaxation of SQ_{iF} is fast enough to lead to homogeneous line broadening that precludes the formation of a spin-echo signal. It was proposed that SQ_i (SQ_{iS} in view of the above assumption) is likely to be anionic^{649,684} and ligated by a hydrogen bond from the imidazole-ring nitrogen of the His.^{648,649} It was also suggested that the redox state of heme b_H might influence the protonation state of SQ_i and the His ligand, rendering SQ_i deprotonated at the time when heme is reduced.⁶⁸⁵ This charge polarization mechanism implicates that SQ_i exists as neither an anion nor a neutral radical but should rather be treated as a resonant structure in which the proton undergoes exchange between His and SQ_i . If the frequency of this exchange is much higher than the hyperfine splitting of the radical spectrum caused by the interactions of the proton with unpaired electron spin, then EPR will be unable to detect the presence of protons due to large spectral diffusion effects.

The proposed catalytic role of charge and spin polarization of the SQ_i is likely to be relevant to other sites catalyzing the reduction/oxidation of Q/ QH_2 via stable SQ_i intermediates. Such spin polarization has been noted before for the SQ_i bound at catalytic sites (including SQ_i ,⁶⁸² SQ_H of quinol bo_3 oxidase,⁶⁹⁰ and SQ_A of bacterial reaction center⁶⁹¹) and could be associated with charge polarization induced by the electrostatic field provided by the catalytic site. Further support for this proposal comes from modeling of the effect of the electrostatic field on spin and charge polarization in diboryl monoradical anions.⁶⁹²

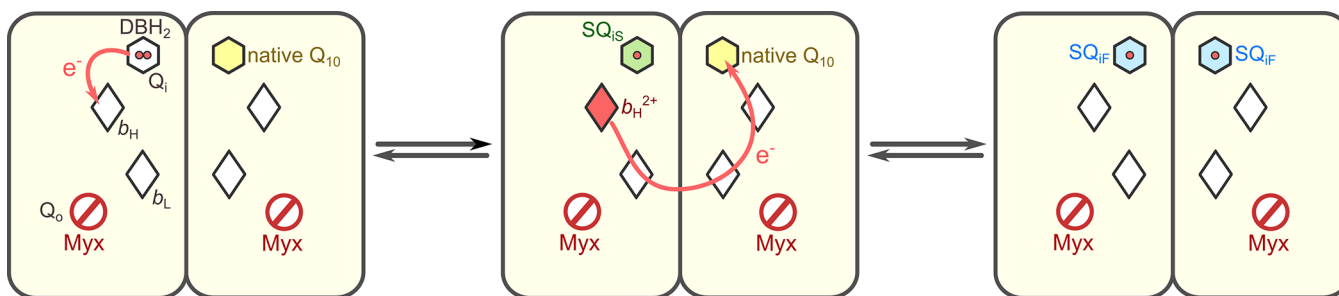


Figure 35. Cross-dimer electron equilibration leading to formation of SQ_{1F} (see details in the text).

8.5. Specific Residues Involved in PQ/QH₂ Binding to the Q_n Site of Cytochrome b₆f

Several attempts have been made in the past to study residues important for Q/QH₂ binding to the Q_n site of Cytochrome b₆f via site directed mutagenesis approaches informed by previous results from work on the Cytbc₁ complex and by structural features of the Cytb₆f. They include residues bG37 and bF41⁶⁹³ because substitutions of the corresponding residues in *Rhodobacter's* Cytb (G48 and A52, respectively) led to impaired redox activity, loss of photosynthetic growth, or failure to assemble a functional complex. The F41V mutant of *Chlamydomonas* displayed a 5-fold decrease in Q_n site activity and became sensitive to antimycin, an inhibitor of the Cytbc₁ Q_i site that is normally not effective against Cytb₆f. Conversely, the bF41G and bF44A mutants did not display any phenotype.⁶⁹⁴ Substitutions of the Gly37 residue did not rescue phototrophic growth, suggesting that mutation of this residue is detrimental to photosynthesis. The same result was found in the case of a C35V mutant, which was unable to grow phototrophically because this substitution (affecting the residue that covalently bonds heme c_n to the Cytb₆) prevents the accumulation of the entire complex in thylakoids.⁶⁹⁵

Other mutants were generated affecting residues in the proximity of the heme: Leu36, Pro41, of SubIV. No clones were recovered after mutagenesis, indicating that these mutations were also detrimental for photosynthesis. On the other hand, a mutant was obtained after the P40T substitution. This mutant showed a significant slowing down of Cytb₆ reoxidation under single turnover flash illumination, consistent with impairment of interaction between the heme and its quinone substrate. The mutant also displayed a downshift of the c_n heme midpoint potential (from +100 mV to -200 mV at pH 7) but conserved WT Cytb₆f turnover rates under a continuous light regime. On the basis of the position of P40 in the Cytb₆f structure, it was proposed that this modified accessibility could originate from the ligation of the heme iron by the phenol(ate) side chain introduced by the mutation.⁴³⁰

A similar approach has been used in cyanobacteria, where a mutant (R214H) was generated to substitute His for a conserved Arg in the Cytb₆ polypeptide of the cyanobacterium *Synechococcus* sp. SPCC 7002. At high light intensity, the R214H mutant grew ~2.5-fold more slowly than the WT, due to inhibition of the Cytb₆f complex turnover. Under single turnover flash illumination the R214H mutation partially blocked electron transfer to the Q_n site, mimicking the effect of the Q_n site inhibitor NQNO. Overall, these data define Pro40 and Arg214 as key residues for catalysis in the Q_n site of the Cytb₆f.⁶⁹⁶

Other mutants were generated to modify the environment of the chlorophyll ring that is located close to the Q_n site.⁶⁹⁷

Residues Val104, Gly136, Tyr124, and Arg125 did not dramatically affect electron transfer in the complex but strongly affected state transitions (see section 10.3 below). This indicates that besides catalysis, the reduction of the PQ at the stromal side Q_n site is also involved in sensing and signaling, two essential functions of the Cytb₆f (see sections 5.2 and 10.3)⁶⁹⁸

9. INTERMONOMER ELECTRON TRANSFER

Crystallographic structures of Cytbc₁ and Cytb₆f revealed a high degree of symmetry between monomers including structural arrangement of the redox active cofactors.^{20–22,48,173} One of the most intriguing structural features of the dimer is the distance between hemes b_L/b_p of different monomers, which theoretically seems to be small enough to allow fast (i.e., ~μs) electron transfer,^{56,195,699,700} in relation to catalytic rates.^{41,68,616,701} For this reason, a discussion began about the possible implications of such an electronic connection between monomers for catalysis and opened the door to construction of models extensively utilizing the heme b_L-b_L bridge.^{86–88,125,329,702,703}

The fundamental question therefore arises as to whether electron transfer between the b_L/b_p hemes of the two monomers can be considered competitive to the intramonomer path: from heme b_L/b_p, through heme b_H/b_n to the Q_i/Q_n site. Alternatively, this is simply a redundancy of the possible electron transfer paths that may be important only under specific and rare conditions.^{206,572,616}

The order of the rates for intermonomer electron transfer can be approximated on the grounds of electron transfer theory⁷⁰⁴ and the phenomenological approximation of the Moser-Dutton ruler (eq 21):^{56,195,699,700}

$$\log(k_{ET}) = 13 - (1.2 - 0.8\rho)(R - 3.6) - 3.1 \frac{(\Delta G + \lambda)^2}{\lambda} \quad (21)$$

where ρ – is packing density (0 for vacuum, 1 for fully packed matrix), ΔG is Gibbs energy associated with electron transfer from donor to acceptor (in the case of electron transfer from heme b_L to b_L this is 0), λ is the reorganization energy, and R is the distance between donor and acceptor (between b_L heme-rings).

Using average values for electron transfer within a protein matrix, ρ and λ in the above equation can be simplified to account only for R (eq 22):⁶⁹⁹

$$\log(k_{ET}) = 12.8 - 0.6R \quad (22)$$

As distances between heme rings are ~13.2–15.2 Å, a crude estimation of the rates gives $k_{ET} \approx 5 \times 10^3 - 8 \times 10^4 \text{ s}^{-1}$. A typical steady-state turnover rate obtained for Cytbc₁ or Cytb₆f does not exceed 10^3 s^{-1} ,^{570,650} meaning that electron transfer between hemes b_L/b_p should not limit the catalytic turnover rate.

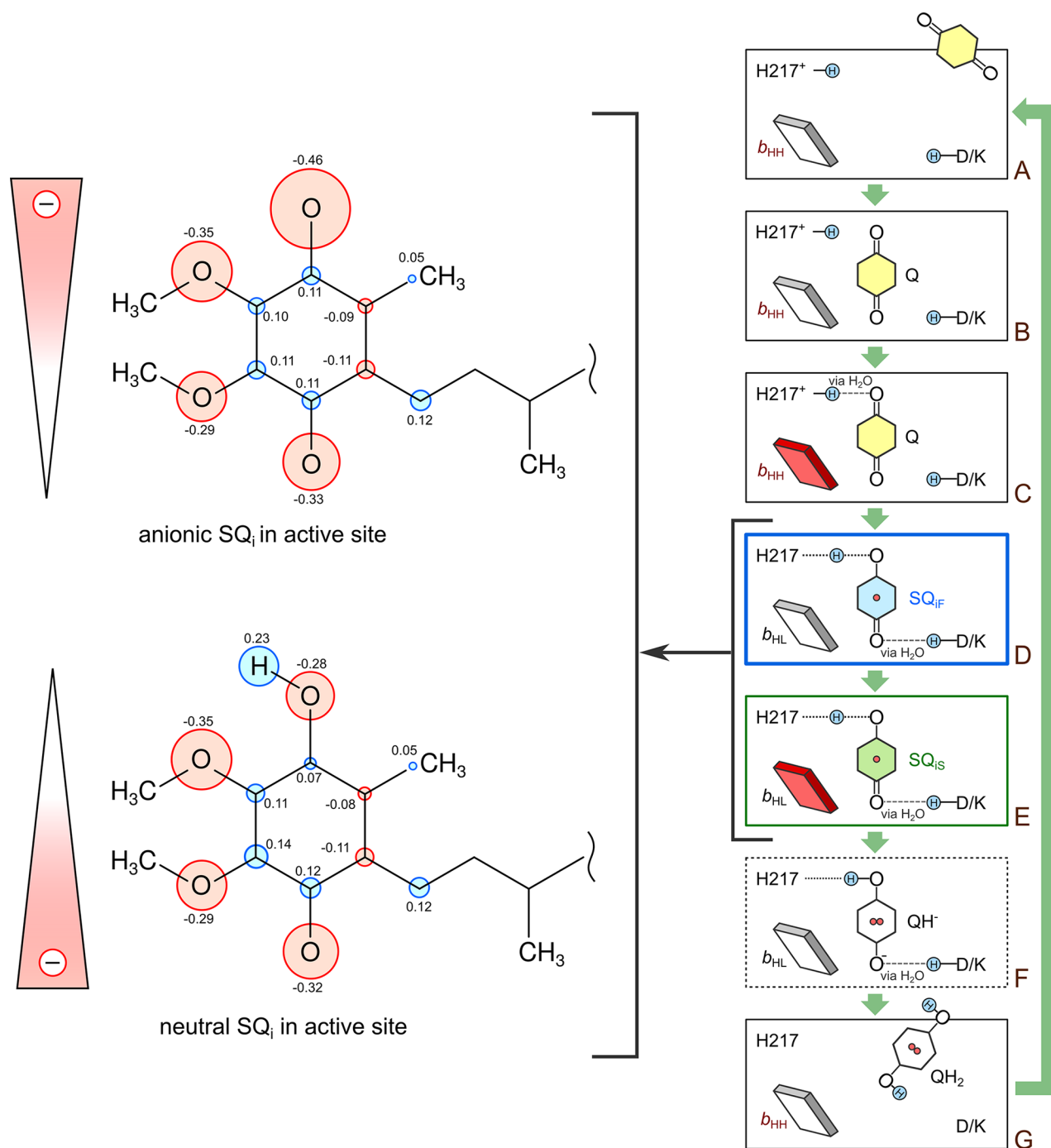


Figure 36. Charge polarization mechanisms of Q reduction at the Q_i site. Boxes on the right represent the reaction steps A to G (see text for details). SQ_i bound at the Q_i site (blue and green boxes refer to the Q_i site occupied by SQ_{iF} and SQ_{iS} , respectively) is stabilized by equilibration between neutral and anionic form of the radical (upper and lower scheme in the left panel, respectively). Red and blue circles denote the negative and positive Mulliken charges, respectively. Radius of each circle is proportional to the charge of the respective atom (the values are shown as black numbers). Spikes on the left indicate the polarization of overall charge on the respective SQ form.¹⁶³

The experimental verification of whether intermonomer electron transfer is indeed as fast as theory predicts, required measuring the electron transfer rate between b_L/b_p hemes in the dimer, which in the native protein is generally difficult considering the structural symmetry of the complex, and the fact that electron transfer between the monomers leads to spectroscopically indistinguishable states. In fact, this has long been out of reach for direct experimental testing due to the lack of a genetic tool to inactivate individual components of the

dimer in an asymmetric manner. This is related to the fact that, in native systems, the genes coding for the subunits do not differentiate between monomers; thus, any mutation is obligatorily introduced to both parts of the homodimer.

New strategies described in 2010 aimed to overcome these limitations.^{47,329,705–709} In these studies, two distinct genetic approaches were used: a fusion duplicating gene or a coexpression of two variants of the gene. Both targeted the *Cytb* subunit of bacterial *Cytc₁*.

The first approach was based on extending the native gene encoding *Cytb* with a short linker followed by a second copy of the same gene.^{47,707–709} As a result, each half of the fusion protein replaced one *Cytb* subunit of the dimer, providing a template for construction of derivatives in which the two halves could be mutated independently. Using such a template, different mutations inactivating key steps of electron transfer were introduced in various combinations to eliminate selected paths and to force electron transfer through other available paths within the dimer (see all forms in Figure 37). This was used to test all possible electron transfer routes for electrons from the Q_o to Q_i site.^{47,709}

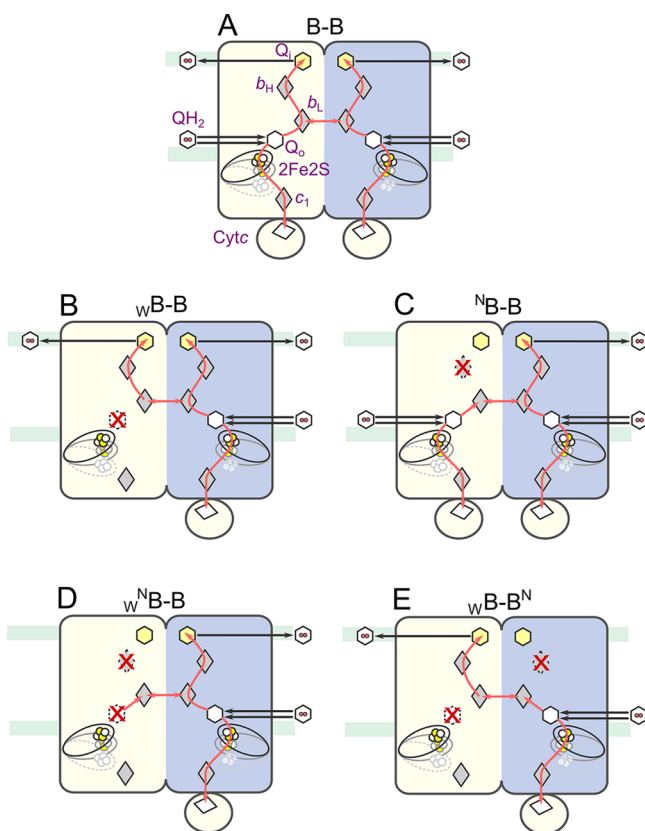


Figure 37. Schematic representation of various forms of *Cytc₁*-like complexes containing *Cytb* fusion protein used to test possible combinations of electron transfer paths. (A) Native-like system with all four branches active (B–B). (B–E) Asymmetric forms containing one or more mutations inactivating either the Q_o site (*Cytc₁*^{Rh}G158W; designated as _wB) or heme b_H (*Cytc₁*^{Rh}H212N; designated as ^NB): _wB–B, one lower branch inactivated; ^NB–B, one upper branch inactivated; _w^NB–B, upper and lower branch on the same side inactivated; _wB–B^N, cross-inactivated enzyme.

Because for a given combination of mutations, only one version of the complex with the fused *Cytc₁* is expressed in the cells, it was possible to monitor the kinetics of light-induced electron transfer in the native membranes. Analysis of the cross-inactivated complex (a variant _wB–B^N in Figure 37), for which electrons derived from the O_o site must have crossed the dimer to reach the Q_i site, revealed that electron transfer between hemes b_L occurs on a millisecond time scale, as theory had predicted. In addition, it was established that the complex remains enzymatically active even if the equivalent of only one monomer (_w^NB–B), or the equivalent of one monomer with a

part of other monomer (_wB–B, ^NB–B) are available. This revealed that any path connecting either or both Q_o sites with either or both Q_i sites is competent in supporting enzymatic turnover at high rates.^{47,706,707} On the basis of these findings, it was proposed that cofactor chains in the native dimer assemble into an H-shaped electron transfer system (two upper, two lower branches and a bridge) connecting the two Q_o sites with the two Q_i sites.

Interestingly, deactivation of only one branch (forms _wB–B, ^NB–B) or both branches of the same monomer (_w^NB–B) decreases V_{max} of the enzyme by approximately 50% when compared to the fusion protein without any disabling mutation (B–B).⁵⁷⁰ This suggests that the two monomers in the dimer contribute equally and independently of each other; thus, any allosteric effect,^{19,87,88,710} if it exists, does not govern the catalytic turnover rate. Forcing electron transfer through the b_L heme “bridge” decreases V_{max} to ~ 70 s^{–1}, which is about 25–40% of the average activity obtained for _wB–B, _w^NB–B, and ^NB–B forms but is still enough to support multiple turnovers at high rates.

When using a fusion gene composed of two copies of the same gene, careful procedures must be employed to maintain high expression of the fusion protein during cell growth and prevent gene recombination.⁷⁰⁸ Without rigorous growth and harvesting protocols, there is a risk of losing the fusion or asymmetry of the mutations, which is especially critical if one wishes to test *Cytc₁*-related support of photosynthetic growth of bacterial cells. Indeed, just such recombination was observed, but incorrectly interpreted by Hong et al.⁷¹¹

To overcome these limitations and gain the possibility to test functionality of the asymmetrically mutated complexes *in vivo*, the original system was modified by constructing a hybrid fusion system, in which the fusion protein was expressed from a gene linking two different genes encoding *Cytc₁* from closely related bacteria *Rhodobacter sphaeroides* and *capsulatus*.^{706,707} Careful analysis of photosynthetic competence of the various complexes containing asymmetrically mutated hybrid fusion proteins (analogous to the ones described above) demonstrated that in agreement with kinetic results, the cross-inactivated form relying exclusively on intermonomer electron transfer is fully functional *in vivo*, as is the form with just one branch inactivated.

A second approach for obtaining asymmetrically mutated variants of *Cytc₁* was based on coexpression of two plasmids, each carrying one copy of the gene encoding for *Cytc₁* with a sequence coding for a different tag attached (His-tag, Flag-tag or Strep-tag).^{329,712,713} The different mutations inactivating either the Q_o or the Q_i sites were placed on different plasmids and the two-step affinity chromatography was used to isolate the cross-inactivated form from the symmetric variants resulting from random assembly of the complexes in the cells.^{705,712} These studies also demonstrated that intermonomer electron transfer through b_L hemes occurs in milliseconds, thus in a catalytically relevant time scale. In addition, some of the kinetic transients were interpreted as resulting from electron equilibration between the two Q_i sites and the four hemes b in the dimer.⁷⁰⁵ The same type of equilibration (see Figure 35) was considered as rationale for the existence of fast-relaxing semiquinone (SQ_{if}) in native *Cytc₁* exposed to conditions favoring one electron reduction of heme b_H by QH_2 bound at the Q_i site (described in section 8.3).¹⁵¹

Although the existence of intermonomer transfer has been confirmed by several studies, its possible physiological meaning and role in the catalysis remain unclear.^{13,701} Electron transfer

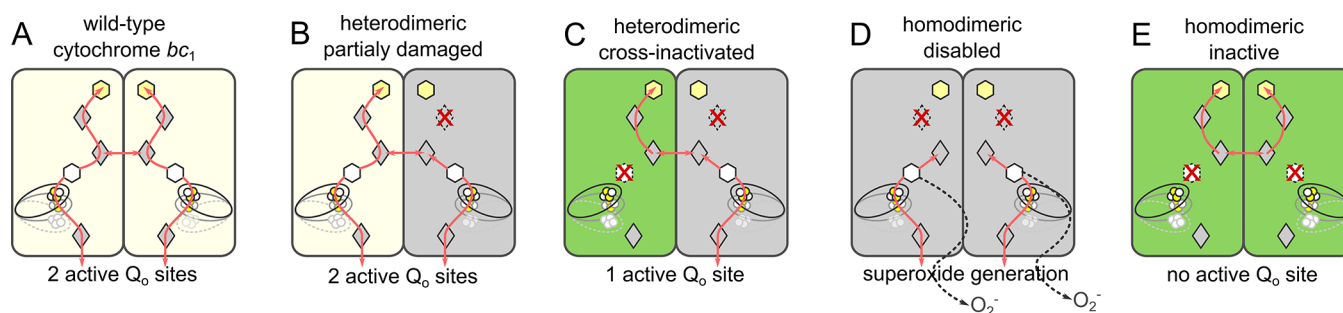


Figure 38. Putative advantage of dimers with possible ET through the hemes b_L . (A) Homodimeric *Cytc_{bc1}* operates normally using two active monomers. (B) Heterodimer in which one monomer has disabled heme b_H and/or Q_i site (gray) is still functional and able to oxidize QH_2 at two Q_o sites. (C) Heterodimer containing two different mutations in each monomer, one with disabled Q_o site (green) and second with heme b_H or Q_i site, still catalyze QH_2 oxidation. (D, E) Homodimers containing mutations are inactive or contribute to elevated superoxide generation. Considering a sum of monomers from B to E, occurrence of intermonomer electron transfer gives 3 active monomers, 3 inactive monomers, and 2 monomers generating O_2^- . If this electron transfer did not exist, we would have 1 active monomer, 3 inactive monomers, and 4 monomers generating O_2^- .

between the b_L hemes could be just a simple coincidence of the conserved structure of the homodimer and as such does not play an important catalytic role, as all structural elements needed to perform catalytic cycle are present in each of the monomers.^{23,206,711}

On the other hand, it has been hypothesized that intermonomer electron transfer to support efficient catalysis may offer some advantage for bioenergetic processes, in particular when unfavorable redox conditions or potential danger of superoxide generation exist. As pointed out by Sarewicz et al.,^{13,701} mitochondria usually possess several copies of genes coding for *Cytc_b*, and the appearance of a mutation in one or more genes is expected to lead to expression of a fraction of the dimers having damage in only one part of the monomer (and thus possibly having a “dead end” for electrons). If this monomer was isolated functionally from undamaged monomer, it would inevitably catalyze only energy-wasting short-circuits or free-radical generating reactions. However, if the damaged monomer is linked functionally with an undamaged one, the existence of the heme b_L – b_L bridge can provide an efficient way to remove electrons from the low-potential chain in the damaged monomer (Figure 38). With such a mechanism, the amount of ROS generated during the QH_2 oxidation will be significantly lowered enabling electron flow through respiratory or photosynthetic chains.

Also, as shown by Pintscher et al.,¹⁵¹ electron exchange between monomers may increase the rate of SQ_i^- reduction to QH_2 by providing electron paths for dismutation of SQ_i^- from two Q_i sites of a dimer, which can be of advantage under shortage of QH_2 .

There are several models presenting more or less elaborate mechanisms of intermonomer allosteric communication in which the role of heme b_L – b_L electron transfer is crucial for catalysis. Most of these were inferred from indirect kinetic measurements or effects of substoichiometric additions of inhibitors. The results of such experiments leave space open for discussion and future experimental exploration. While the existence and potential significance of allosteric effects have never been ruled out, the experiments that exploit the family of fusion proteins suggest the simplest mechanism, in which electrons travel “blindly” using any available path through the H-shaped electron transfer system to complete redox reactions without generation of radicals.

10. HIGHER LEVEL OF ORGANIZATION AND REGULATION (SUPERCOMPLEXES, STATE TRANSITION, KINASE ACTIVATION)

10.1. Role for Cytochrome b_6f in Regulation of Linear versus Cyclic Electron Flow?

Alternative to linear electron transfer (LET), which requires in series PSII and PSI activity, is the cyclic pathway (CET), which involves electron flow via PSI and the P700 reaction center complex via the plastoquinone pool through *Cytc_{b6f}*. It thus produces ATP without generating reducing power, and it is considered as a central element to readjust the ATP/NADPH balance for proper CO_2 assimilation in plants and green algae.²³⁰ Actors involved in CET and CET regulation have been recapitulated in recent reviews.^{374,714–717} Nonetheless, several aspects of this process remain enigmatic. While most of the CET electron carriers (the plastoquinone pool, *Cytc_{b6f}*, plastocyanin, PSI, and ferredoxin and possibly NADPH) are shared with the LET pathway, electron transfer from Fd/NADPH to the quinone pool on the stromal side of the thylakoids may require an additional, CET specific, activity. This activity would be either by the NAD(P)H dehydrogenase (NDH) complex similar (but not identical) to complex I of the mitochondrial respiratory chain,^{715,718} or the FQR (ferredoxin quinone reductase) complex. FQR would correspond either to a PgrL1 and PgrS complex¹⁹⁹ or to the *Cytc_{b6f}* itself either *Cytc_{b6f}* interacting with Fd, most likely via FNR (as discussed section 3.6.5) or possibly PgrL1 and PgrS, although as considered above involvement of the latter components is supported only by very qualitative electron transfer data and stoichiometries are small.

Mutants lacking the NDH complex lack a clear growth phenotype under a variety of environmental conditions,^{718,719} suggesting that the NDH activity, per se, is not essential for CET, since CET is an essential process for plant growth.²³⁵ On the other hand, a mutant with enhanced CET activity, isolated in *Arabidopsis*, displays higher levels of the NDH complex.³⁷⁹ Moreover, *Arabidopsis* photosynthetic embryos, which have a larger CET activity than mature leaves, also display an enhanced NDH activity.⁷²⁰ While the FQR activity was initially identified with the *Cytc_{b6f}*,⁷²¹ this function has later been associated with a complex containing the PgrS, PgrL1 proteins,¹⁹⁹ that is, previously identified as CET actors.⁷¹⁵ Similarly to the NDH, mutants lacking the PgrS:PgrL1 complex show WT like CET rates in *Arabidopsis*³⁸⁶ and *Chlamydomonas*,³⁸⁷ again pointing to a nonessential role of this complex in CET.

Overall, these results can be interpreted assuming that both the NDH and FQR pathways contribute to CET, each activity being compensated by the other when genetically disrupted. Consistent with this conclusion, previous genetic studies have highlighted that severe growth phenotype in *Arabidopsis* can only be observed upon concomitant disruption of the NDH and Pgr5:PgrL1 complexes.⁷²²

What is the role for the Cytb₆f (if any) in a context where the role of the NDH and PgrL1:Pgr5 pathways in CET is still controversial? Interactions of the Cytb₆f with PSI or FNR have been proposed as a mean to trigger CET.^{723,724} This notion has received experimental support by the finding by Cramer and co-workers that Cytb₆f copurified with FNR in plants.¹⁸⁰ Moreover, interactions between subunit of PSI, Cytb₆, FNR, and Pgr5 were reported in a yeast two-hybrid assay using *Arabidopsis* genes.²³⁶ In the green alga *Chlamydomonas reinhardtii*, Minagawa and colleagues¹⁹⁷ were able to isolate a PSI:Cytb₆f, which they considered as a specific component of CET. The existence/function of this complex is still debated. If real, why would a supercomplex be needed for CET? As mentioned earlier, most electron carriers are shared between the CET and LET pathways. Therefore, CET, which is a “circular” process, continually recycling electrons around PSI, would be easily overcompeted by LET every time that a cyclic electron is shunted toward the stromal sinks by LET. Two alternative models have been proposed to explain how LET does not overcompete CET.^{426,725,726}

The first one considers that CET and LET are, to some extent, segregated (“segregated CET”). It is well-known that the photosynthetic complexes are unevenly distributed in the thylakoids: PSII is mainly concentrated in the appressed grana, PSI is mainly found in the non appressed membranes (stroma lamellae, grana margins), while the Cytb₆f is roughly homogeneously distributed.⁷²⁷ Moreover, the diffusion of PQ/PQH₂ in the thylakoid membrane is highly restricted, probably due to the very high protein concentrations that characterize this membrane.^{272,728} The “segregated CET” model assumes that because the physical distance between the different domains is rather large and the PQ diffusion in the thylakoids is restricted, two electron carrier pools would exist with different functions. Photosynthetic complexes present in the grana and grana margins (PSII, Cytb₆f and PSI) would be involved in LET, while those in the stroma lamellae (Cytb₆f and PSI) would be the CET ones. Consistent with this hypothesis, recent affinity-mapping AFM studies have revealed nanodomains of colocalized PSII and Cytb₆f complexes.⁷²⁹ The domains (previously hypothesized by Lavergne and Joliot²⁷²) would provide a structural rationale for the segregation of LET and CET and its regulation. Small changes in the distance between adjacent membranes in stacked grana regions might control the access of Cytb₆f to the grana because of steric hindrance.⁵ Because the width of the stromal gap is variable and light regulated, this model predicts that changes in the lateral distribution of the Cytb₆f should affect CET and LET by modulating the amount of this complex present in the CET and LET compartments. Obviously, the presence of a supercomplex is an extreme case of the “segregated CET” hypothesis, the CET domain becoming the PSI:Cytb₆f supercomplex itself.

Alternative to the “segregated CET” model, a “dynamic” hypothesis to explain CET cyclic flow has been proposed.^{410,426,725,730} According to this model, CET and LET would not be segregated but actually directly compete for electrons. Under most physiological conditions, this competi-

tion would favor LET because of electron leak toward stromal sinks. However, under particular conditions (high light, CO₂ limitation, low oxygen in microalgae), CET would become more efficient because the LET efficiency would be reduced by limitation at the PSI acceptor side. Competition would occur either at the PSI acceptor side (via competition for Fd, likely via the FNR–Cytb₆f complex⁷²⁵) or at the level of the PQ(H₂) pool.³⁷⁴ The model proposed by these authors is particularly interesting from a Cytb₆f perspective, as it postulates that a functional interaction between the two Cytb₆f monomers at the PQ-reducing site would allow a “direct” electron flow from the stromal to the luminal PQ_i in a confined environment not in contact with the photoactive PQ(H₂) pool in the thylakoids, similar to the semiquinone version of the Q cycle proposed earlier.⁷³¹ This hypothesis is therefore somehow in between the “segregated CET” and the redox competition hypotheses previously described.

10.2. The “Elusive” Cytochrome b₆f-PSI CET Supercomplex

As discussed above, the presence of a PSI–Cytb₆f complexes represent the most extreme case of the “segregated CET” hypothesis. In the green alga *Chlamydomonas reinhardtii*, where CET can be a prominent process,^{730,732,733} Iwai and colleagues used a sucrose density gradient to isolate a supercomplex composed of the PSI-LHCI supercomplex with LHCIIs, Cytb₆f, FNR, and PgrL1 in a fraction heavier than that of the single complexes (PSI-LHCI, Cytb₆f) alone.¹⁹⁷ Its formation is enhanced by reducing conditions, which increases CET activity in this alga.^{221,734} Spectroscopic analyses⁷³⁴ indicate that PSI and Cytb₆f are able to exchange electrons within the supercomplex, PSI being able to reduce Cytb₆ in the presence of Fd and NADPH and to oxidize Cytf in the presence of plastocyanin.¹⁹⁷ On the basis of these results, the authors conclude that the PSI–Cytb₆f supercomplex corresponds to the CET supercomplex, the existence of which had been anticipated by theoretical predictions⁷³⁵ and functional studies (e.g., Joliot and Joliot⁷³⁶).

Supercomplex formation in *Chlamydomonas reinhardtii* requires not only reducing conditions (anaerobiosis) but also Ca²⁺ signaling in *Chlamydomonas reinhardtii*.^{197,737} Regulation by anaerobiosis would be mediated by a protein, Anaerobic Response 1 (ANR1). ANR1, as well as the plastid localized Ca²⁺ sensor (CAS), is found in the PSI–Cytb₆f supercomplex, together with PgrL1.⁷³⁷ The Cytb₆f associated subunit PetO cofractionates with other thylakoid proteins involved in CET (ANR1, PgrL1, FNR). The absence of PetO impairs the formation of the supercomplex in anaerobic conditions.

Since its discovery and biochemical characterization, the existence/function of the *Chlamydomonas* CET supercomplex has been debated. The biochemical significance of the green band of high molecular weight in sucrose density gradient that was used to purify this complex has been recently questioned because various PSI complexes can migrate in these sucrose density regions.³⁷⁶ On the other hand, single-particle analysis of the PSI–Cytb₆f complex from *Chlamydomonas*⁷³⁸ has provided a structural support for the existence of a true supercomplexes in this alga.

Until recently, no such supercomplex was found in plants,⁴²⁶ and it was argued that no such supercomplex is required for CET to occur in plants.^{410,716} However, the isolation a PSI–Cytb₆f supercomplex has been reported starting from stroma lamellae of *Arabidopsis*.⁷³⁹ Even in this case, the significance of this complex has been questioned³⁷⁴ because in this preparation

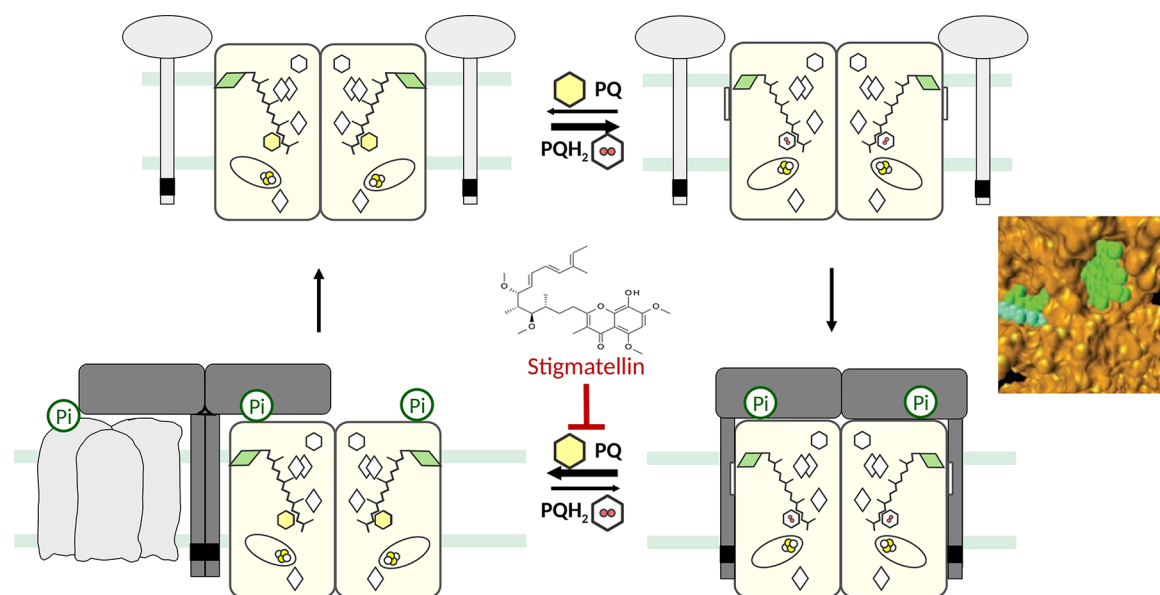


Figure 39. Multistep model for the activation of the state transitions kinase by *Cytb_{6f}* in photosynthetic eukaryotes. The model assumes that PQH_2 interaction with the Q_a/Q_b site leads to conformational changes within the complex, likely mediated by the movement of the ISP-HD.⁵⁵⁵ These changes would promote the association between the cytochrome and the kinase responsible for state transitions (Stt7 in algae, STN7 in plants). *Cytb_{6f}*–kinase interaction would be mediated by residues surrounding the chlorophyll ring, as indicated by mutagenesis studies.⁷⁵⁸ Upon binding, the kinase would become active and phosphorylate the *Cytb_{6f}*-associated subunit PetO. The active kinase would then be released from the cytochrome complex, in a step possibly involving PQH_2 oxidation, PQ release from the Q_a site, and conformational changes of the ISP, as suggested by the inhibitory effect of the PQ analogue stigmatellin on this step.⁷⁵⁷ The active kinase would be in a dimeric state, thanks to the interaction between conserved cysteines present on every monomer (black squares).⁷⁵³ It would interact with LHCII promoting its phosphorylation and migration from PSII to PSI. Alternatively, a ternary binding complex might be formed between LHCII, *Cytb_{6f}*, and the kinase. Finally, monomerization of the kinase would inactivate it, closing the activation cycle. See also Singh et al.⁷⁵⁵ for a further discussion.

Cytb_{6f} complex bound to PSI was not only in its active (dimeric) conformation but also in the inactive (monomeric) one.

At variance with the respiratory chain, where several supercomplexes between different component of the electron flow chain have been characterized, no other photosynthetic supercomplex has been reported so far, besides the PSI-NDH supercomplex that was characterized in *Arabidopsis*.⁷⁴⁰ Formation of the PSI-NDH supercomplex requires the presence of specific forms of the PSI Light Harvesting Complex (LHCI).⁷⁴¹

10.3. Role of Cytochrome *b_{6f}* in State Transitions

In oxygenic photosynthesis, the two photosystems have distinct pigment containing antenna complexes and consequently different spectral absorption features. PSI has an enriched light absorption capacity in the far-red region, while PSII has a slightly higher absorption capacity in the spectral regions where chlorophyll *b* absorbs. Under natural light conditions, where both the quality and quantity fluctuate with time,⁷⁴² light absorption by these two complexes may be unbalanced, with negative consequences on the quantum yield of photosynthesis, which requires a commensurate light utilization by PSI and PSII for optimum photosynthetic yield.

In plants and green algae, balanced light utilization is achieved via a regulatory mechanism called state transitions, which actively adjusts the absorption capacity of PSI and PSII, in response to chromatic changes in the light. Discovered by Murata and Sugahara and Bonaventura and Myers^{743,744} state transitions rely on a redox triggered phosphorylation of the PSII antenna complexes (LHCII), which dissociates from PSII binding to PSI under conditions where absorption of the former is enhanced (e.g., when the light available for photosynthesis enhances light absorption by chlorophyll *b*). This state is called

state 2. Conversely, overexcitation of PSI (e.g., by far red light) leads to the detachment of LHCII from PSI, and its reassociation to PSII, leading to state 1.²³⁰

Pharmacological and genetic experiments have pinpointed the PSII electron acceptors (the plastoquinone, PQ) pool as the sensor triggering LHCII phosphorylation.⁷⁴⁵ This occurs via the activation of a specific kinase,³⁵ mediated by the *Cytb_{6f}*. The plastoquinone can act as the redox sensor because it is functionally “located” between PSII and PSI. Thus, this redox active molecule “senses” the relative imbalance in the light harvesting capacity of the two photosystems, becoming reduced when the PSII activity overcomes that of PSI, and oxidized when PSI is prevailing. The kinase responsible for LHCII phosphorylation has been first identified in *Chlamydomonas*, Stt7⁷⁴⁶ and later in *Arabidopsis*, STN7.⁷⁴⁷ It is as a Ser/Thr kinase located in the thylakoids. A phosphatase (TAP38/PPH1) has also been found, which dephosphorylates LHCII^{748,749} during the state 2 to state 1 transition.

Several pieces of evidence suggest that the $PQ(H_2)$ pool activates the Stt7/STN7 kinase via *Cytb_{6f}*. Wollman and Lemaire⁷⁵⁰ used *Chlamydomonas* lines with mutations in the photosynthetic apparatus to demonstrate that state transitions were missing in mutants lacking the *Cytb_{6f}*. Later, independent spectroscopic⁷⁵¹ and genetic studies⁵⁷⁷ suggested that the *Cytb_{6f}* mediates kinase activation upon PQH_2 binding to its luminal binding pocket via a still largely unknown mechanism.

Several models have been proposed so far to account for the *Cytb_{6f}* mediated activation of the Stt7/STN7 kinase.^{726,752–755} They are summarized in a multistep model proposed in Figure 39. There, PQH_2 binding to the cytochrome luminal pocket would induce conformational changes (via movements of the ISP-HD) making the *Cytb_{6f}*-kinase interaction possible.

Formation of a *Cytb₆f*-kinase complex would activate this protein leading to the phosphorylation of the *Cytb₆f*-associated subunit PetO.^{745,756,757} This step would precede LHCII phosphorylation, implying the existence of an additional step, where the active kinase would be released from *Cytb₆f* to interact with the PSII antenna. The existence of two separate steps for *Cytb₆f* and LHCII phosphorylation is suggested by the finding that PQ analogue stigmatellin, which blocks *Cytb₆f* activity likely by interfering with the movement of the ISP-HD,^{61,555,757} prevents LHCII phosphorylation but not the phosphorylation of PetO.

This model also accounts for additional information concerning the induction of state transitions. The first one is how the signal generated by PQH₂ binding in the luminal part of the complex is transduced to the stromal site where the catalytic domain of Stt7/STN7 is located. Several hypotheses have been conceived to address this point: Vener and colleagues⁷⁵¹ proposed that the putative transmembrane helix of the kinase could directly sense PQH₂ binding to the luminal site, leading to kinase activation. Consistent with this possibility, Shapiguzov and colleagues found that the N terminus moiety of the kinase (which is supposed to be on the luminal side) interacts with the transmembrane part of the ISP based on yeast two hybrid.⁷⁵³ Alternatively, a chlorophyll-based hypothesis has been proposed by Zito and colleagues. These authors analyzed a *Cytb₆f* mutant of *Chlamydomonas*, in which the small subunit PetL was fused to subunit IV to “transform” the *Cytb₆f*, which contains seven helices in its core complex subunits (*Cytb₆*- and sub IV), into a *Cytc₁*-type of complex (which contains eight helices in its unique core complex subunit, *Cytc₁*). They found that while this mutation was not affecting electron flow, it was able to completely abolish state transitions.⁷⁵⁸ They conclude therefore that the mutation was sterically hindering kinase docking to *Cytb₆f*, that is, that the kinase docking site was located in the proximity of the C terminus of subunit IV (where the subunit PetL was fused in the mutant). There, the tetrapyrrole ring of *Cytb₆f* bound chlorophyll is exposed to the lipid solvent. Conversely, the PQ phytol chain goes deeply into the complex structure ending up in the luminal pocket (in *Chlamydomonas*⁴¹) or in proximity of the F helix, which sandwiches the chlorophyll ring in the cyanobacterium *Mastigocladus laminosus*.⁴² There, it could sense PQH₂ binding to its luminal site via a conformational change⁷⁵⁵ and transduce the signal via its chlorophyll ring. The possible involvement of the chlorophyll ring in kinase activation was later supported by the finding that mutants affecting the environment of the chlorophyll ring in the complex were altering the kinetics of state transitions in *Chlamydomonas*.⁶⁹⁷ Hasan and colleagues further developed this concept, proposing that specific lipids located on the surface of *Cytb₆f* close to the chlorophyll could provide an adaptable surface for interaction with Stt7/STN7.¹⁷⁴ This hypothesis has been refined by the finding that several residues in the stromal loop linking helices F and G of *Cytb₆f* subunit IV (where the chlorophyll ring is exposed) are crucial for state transitions. This has led to the idea of an interaction between *Cytb₆f* and the Stt7 kinase mediated by the stromal side of the complex above the chlorophyll ring.⁶⁹⁸

The second information concerns inhibition of state transitions in high-light treated *Chlamydomonas* cells⁷⁵⁹ and plants.^{760,761} It was proposed that this inhibition would stem from redox control by reduced stromal thioredoxins targeting a disulfide bond in the kinase.⁷⁶⁰ Analysis of the Stt7/STN7 protein sequences revealed indeed the presence of two

conserved Cys residues close to the N-terminal end of this kinase, which are highly conserved and essential for kinase activity.^{274,746} However, mutagenesis of the Cys pair of the Stt7/STN7 kinase showed no change in the redox state of these Cys during state transitions and high-light treatment. On the basis of these results, a different role for Cys in kinase activation by the *Cytb₆f* was proposed⁷⁵³ in which these residues would allow the formation of a dimer between two kinases bound to each monomer of the *Cytb₆f* dimer via formation of intermolecular disulfide bridges. Consistent with this idea, while no STN7 dimer was detectable *in vivo*, it could be clearly detected in the *Arabidopsis* STN7-Cys mutants in which C68 or C73 was stabilized.⁷⁶² Such dimer would be rather unstable and revert rapidly to an intramolecular disulfide bridge in each monomer when the luminal site is empty, explaining why the kinase rapidly inactivates upon oxidation of the PQ(H₂) pool.

The molecular description of the Stt7 kinase⁷⁵⁵ and its interaction with *Cytb₆f* are unknown or unclear. The Stt7 kinase has been cloned, expressed, and purified in a heterologous host. The kinase is active *in vitro* in the presence of reductant and has been purified as a tetramer, determined by analytical ultracentrifugation, electron microscopy, and electrospray ionization mass spectrometry, with a molecular weight of 332 kDa, consisting of an 83.41 kDa monomer. Far-UV circular dichroism spectra have shown Stt7 to be mostly α -helical and document a physical interaction with *Cytb₆f* through increased thermal stability of Stt7 secondary structure. The activity of wild-type Stt7 and its Cys-Ser mutant at positions 68 and 73 in the presence of a reductant suggest that the enzyme does not require a disulfide bridge for its activity as suggested elsewhere. Kinase activation *in vivo* could result from direct interaction between Stt7 and *Cytb₆f* or long-range reduction of Stt7 by superoxide, known to be generated in *Cytb₆f* by quinol oxidation. Although kinase activation on the n side of the thylakoid membrane requires a transmembrane configuration of the kinase (Figure 39), the only hydrophobic domain of the kinase, near the N-terminus, contains 3–4 prolines. There is no known precedent for such a transmembrane domain.

11. COMMENTS ON THE NOMENCLATURE USED FOR CYTOCHROME BC₁ AND CYTOCHROME B₆F

In the literature, there are number of differences in naming of similar structural or functional elements of *Cytc₁* and *Cytb₆f*. This section contains short comments on nomenclature to clarify the potentially confusing terms and, when needed, explains how they are used in this review.

11.1. Complexes

The term “Cyt-*bc*” refers to both *Cytc₁* and *Cytb₆f* as enzymes belonging to one group traditionally named cytochromes *bc*. This is how it is used in the review. On the basis of phylogenetic analysis, it has been proposed to rename this group as “Rieske/*b* complexes”, as it would better reflect the key and evolutionary unchanged subunits.⁷⁶³ However, this name, in spite of being scientifically justified, did not gain popularity in the literature.

In mitochondrial electron transport chain, *Cytc₁* is also named “mitochondrial complex III” or in short “complex III”.

11.1.2. Quinone Binding Catalytic Sites

The quinol oxidation site is named the “Q_o site” (in the case of *Cytc₁*, in particular bacterial *Cytc₁*) or “Q_p site” (in the case of *Cytb₆f* and sometimes eukariotic *Cytc₁*/complex III). The same rule applies for the quinone reduction site, which is named either the “Q_i site” (*Cytc₁*) or the “Q_n site” (*Cytb₆f* and *Cytc₁*/

complex III). The subscripts “_o” and “_i” were originally used by Mitchell to indicate “out” and “in”, respectively, as the direction of proton transfers catalyzed by the respective sites. The subscripts “_p” and “_n” refer to “positive” and “negative” side of the membrane. In brief, $Q_o = Q_p$, while $Q_i = Q_n$.

In this review, we use “ Q_o/Q_p ” and “ Q_i/Q_n ” when referring to the sites in both *Cytc₁* and *Cytb_{6f}*; “ Q_o ” and “ Q_i ” when referring specifically to *Cytc₁*; and “ Q_p ” and “ Q_n ” when referring specifically to *Cytb_{6f}*.

11.2. Cofactor Chains

In *Cytc₁*, the “high-potential chain” is alternatively named the “*c*-chain” and the “low-potential chain” is the “*b*-chain”.

11.3. Protein Subunits

In *Cytb_{6f}*, the assembly of two subunits: *Cytb₆* and Subunit IV corresponds to one larger subunit, *Cytc₁*.

11.4. Cofactors

The *b* hemes in *Cytc₁* and *Cytb_{6f}* are often named differently. Hemes *b* in *Cytc₁* are usually named b_H and b_L (to denote higher and lower E_m of the heme, respectively). Their counterparts in *Cytb_{6f}* are named b_n and b_p (to denote proximity of the heme to negative and positive side of the membrane, respectively). In brief, $b_H = b_n$, while $b_L = b_p$.

In this review, we use heme b_H/b_n and b_L/b_p when referring to hemes in *Cytc₁* and *Cytb_{6f}*. Hemes b_H and b_L are used when referring specifically to hemes of *Cytc₁*. Hemes b_n and b_p are used when referring specifically to hemes of *Cytb_{6f}*.

The atypical *c*-type heme present in *Cytb_{6f}* is designated using different symbols such as c_n and c_i and also c_x . All these symbols describe the same heme.

11.5. Other

When describing the motion of ISP-HD, the “ Q_o -position” or “*b*-position” of ISP-HD refers to the same position of ISP-HD (when it is bound at the Q_o site/cytochrome *b* or the Q_p site/cytochrome b_6).

AUTHOR INFORMATION

Corresponding Author

Artur Osyczka – Department of Molecular Biophysics, Faculty of Biochemistry, Biophysics and Biotechnology, Jagiellonian University, 30-387 Kraków, Poland; orcid.org/0000-0002-1637-2365; Email: artur.osyczka@uj.edu.pl

Authors

Marcin Sarewicz – Department of Molecular Biophysics, Faculty of Biochemistry, Biophysics and Biotechnology, Jagiellonian University, 30-387 Kraków, Poland

Sebastian Pintscher – Department of Molecular Biophysics, Faculty of Biochemistry, Biophysics and Biotechnology, Jagiellonian University, 30-387 Kraków, Poland; orcid.org/0000-0001-6356-2607

Rafał Pietras – Department of Molecular Biophysics, Faculty of Biochemistry, Biophysics and Biotechnology, Jagiellonian University, 30-387 Kraków, Poland

Arkadiusz Borek – Department of Molecular Biophysics, Faculty of Biochemistry, Biophysics and Biotechnology, Jagiellonian University, 30-387 Kraków, Poland

Łukasz Bujnowicz – Department of Molecular Biophysics, Faculty of Biochemistry, Biophysics and Biotechnology, Jagiellonian University, 30-387 Kraków, Poland

Guy Hanke – School of Biological and Chemical Sciences, Queen Mary University of London, London E1 4NS, U.K.

William A. Cramer – Department of Biological Sciences, Purdue University, West Lafayette, Indiana 47907, United States

Giovanni Finazzi – Laboratoire de Physiologie Cellulaire et Végétale, Université Grenoble Alpes, Centre National Recherche Scientifique, Commissariat Energie Atomique et Energies Alternatives, Institut National Recherche l'agriculture, l'alimentation et l'environnement, 38054 Grenoble, France

Complete contact information is available at:
<https://pubs.acs.org/10.1021/acs.chemrev.0c00712>

Notes

The authors declare no competing financial interest.

Biographies

Marcin Sarewicz was born in Poland in 1979. In the years 2003–2007, he was a Ph.D. student at the Faculty of Biochemistry, Biophysics, and Biotechnology of the Jagiellonian University in Krakow and his dissertation was awarded by “Prime Minister Award for the Ph.D. thesis”. After postdoctoral studies, he was employed as a lecturer at the same department, where he began working on the study of the molecular mechanisms of cytochrome *bc₁* catalysis. In 2013, he obtained “Scientific Scholarship for an outstanding young scientist” awarded by the Ministry of Science and Higher Education. In 2019, he obtained the degree of habilitated doctor, and currently he is an assistant professor at the Department of Molecular Biophysics. His research program focuses on the use of electron paramagnetic resonance in conjunction with rapid freezing techniques to study the molecular mechanisms of electron transfer processes in enzymes involved in cellular bioenergetics.

Sebastian Pintscher received his Ph.D. from the Jagiellonian University in 2016 for his work on the semiquinone intermediates of the cytochrome *bc₁*. Currently he is a postdoctoral fellow at the Jagiellonian University, pursuing research on the cyclic electron transfer in plant chloroplasts. His research interests include the redox chemistry of quinone oxidoreductases, properties of free-radical intermediates, and evolution of bioenergetic systems.

Rafał Pietras (Kielce, Poland, 1985) graduated from Jagiellonian University in Kraków (Poland) where he also received his Ph.D. in biophysics in 2015. His research activities are focused around interactions between components of bioenergetic systems. In his scientific endeavour, he applies EPR spectroscopy to investigate spin-labelled proteins and metalloenzymes. Currently he is involved in a project on the regulation of cyclic electron transfer in photosynthesis as a postdoc fellow at Jagiellonian University.

Arkadiusz Borek received a Ph.D. degree in biophysics from Jagiellonian University (Poland) in 2015. His Ph.D. research was focused on the understanding of the mechanism of superoxide production by cytochrome *bc₁*. He is a member of Molecular Bioenergetics Group of the Jagiellonian University led by Prof. A. Osyczka. His postdoctoral studies concern the search for a mechanism of regulation of the operation of complex III. He is a grantee of the National Science Center, Poland. The topic of his project is understanding of the molecular effects of human mitochondrial cytochrome *b* mutations.

Łukasz Bujnowicz is currently a postdoc in the Department of Molecular Biophysics at the Faculty of Biochemistry, Biophysics, and Biotechnology of Jagiellonian University in Kraków. He received his M.Sc. (2013) and Ph.D. in biophysics at the same faculty. The Ph.D. thesis written by Łukasz was awarded as the best polish thesis in biochemistry in 2018 by The Polish Biochemical Society. He is interested in molecular mechanisms of electron transfer, development

of methods of kinetic measurements with usage of electron paramagnetic resonance combined with optical spectroscopy, and occasionally image analysis, but his passion is fly fishing.

Guy Hanke received his Ph.D. from the University of Manchester in 1999 after working in the research groups of Professor Mike Emes and Caroline Bowsher. He then worked until 2008 first as a Japan Society of the Promotion of Science Research Fellow and Royal Society Research Fellow, then an Assistant Professor in the group of Professor Toshiharu Hase at Osaka University, before moving to become an assistant in the group of Professor Renate Scheibe at the University of Osnabrueck. In 2015, he was appointed as a Senior Lecturer in Plant Cell and Molecular Biology at Queen Mary University of London. His research interest throughout his career has been how the distribution of energy, in particular electrons, is controlled within photosynthetic cells. This is explored using plant and cyanobacterial genetics, omics approaches, physiology and protein biochemistry to examine the function of proteins at the interface between energy generation in thylakoid membranes, and energy consumption by soluble enzymes.

William A. Cramer received a B.S. and M.S. in Physics from the Massachusetts Institute of Technology (MIT) and the University of Chicago, respectively, the MIT thesis on “anisotropy in the arrival direction of high energy cosmic rays.” Initial studies were published on (a) “ μ meson capture rates” and (b) “optical birefringence of muscle proteins”. The Chicago Doctorate in Biophysics focused on photo-dynamically induced mutagenesis of T4 bacteriophage. As an NSF postdoctoral Fellow with W. L. Butler at the University of California/San Diego, biophysical studies on the photosynthetic electron transport chain provided some of the first quantitative information on *in situ* properties of the cytochrome transport proteins. The latter studies became part of a research program subsequently pursued at Purdue University, where Cramer became Distinguished Professor of Biological Sciences, on structure–function of membrane proteins including membrane-active bactericidal toxins (“colicins”). These studies were recognized by Fellowships from the EMBO, and the Alexander von Humboldt and Guggenheim Foundations, by recognition as a “Fellow” by (i) the American Association for the Advancement of Science (AAAS), (ii) by the Biophysical Society for which Cramer participated in the establishment of the Bioenergetics Sub-Group of the Society and served as Chair, and (iii) by selection as Chair of two international Gordon Conferences on (1) “Biochemical Aspects of Photosynthesis” and (2) “Bioenergetics”.

Giovanni Finazzi obtained his Ph.D. in Cellular and Molecular Biology (specializing in biophysics) at the University of Milano (Italy), under the supervision of Giorgio Forti. After a post doc at the Institut de Biologie Physico Chimique (IBPC) in Paris on the biophysics of photosynthesis under the supervision of Pierre Joliot, he joined the Italian Research Council as a junior research scientist. He pursued his career in the French CNRS, first in Paris (IBPC) and then in the Laboratory of Plant and Cell Physiology of the CEA of Grenoble as a Research Director. His main interest is understanding how photosynthetic organisms manage their energy resources to thrive in different environments. He has studied photosynthetic light harvesting, electron transport, ATP synthesis, and stress acclimation responses using a multidisciplinary approach including biophysics, photophysiology, cell and molecular biology, and 3D imaging.

Artur Osyczka is a professor in the Department of Molecular Biophysics at the Jagiellonian University (JU) in Kraków. His interest in redox-active proteins dates back to his graduate studies. In 1999, he completed his doctoral degree in the group of professor Katsumi Matsuura at Tokyo Metropolitan University working on bacterial photosynthetic reaction center. His postdoctoral work (1999–2006), carried out at the

University of Pennsylvania in the group of professor P. Leslie Dutton, focused on molecular mechanism of energy conservation in cytochrome bc_1 . In 2006, he established the Laboratory of Molecular Bioenergetics, which now constitutes the major part of the Department of Molecular Biophysics at JU. He was twice the recipient of Senior Research Fellowship from the Wellcome Trust (in 2006–2012 and in 2011–2016). His research aims at understanding operation of energy conserving systems from the physicochemical point of view and also in relation to cellular physiology. The topics include enzymatic catalysis and regulation of respiratory and photosynthetic protein complexes, electron and proton transfers, reactive oxygen species, mitochondrial diseases, and dynamics of macromolecular interactions in redox systems.

ACKNOWLEDGMENTS

A.O. acknowledges financial support from National Science Centre, Poland (Grant No. 2015/18/A/NZ1/00046) and from Foundation for Polish Science (programme TEAM, POIR.04.04.00-00-5B54/17-00). W.A.C. acknowledges support for the research studies described in this Review, supported at different times by the U.S. National Institutes of Health/General Medical Sciences (GMS-038323) and the U.S. Dept. of Energy (DOE DE-SC0018238). G.F. acknowledges support by the French national funding agency ANR (“Momix” Projet-ANR-17-CE05-0029), the excellence cluster LabEX GRAL (ANR-10-LABX-49-01 financed within the University Grenoble Alpes graduate school -Ecoles Universitaires de Recherche- CBH-EUR-GS ANR-17-EURE-0003), and the European Research Council (ERC AdG “Chloro-mito”, Grant No. 833184). The open-access publication of this article was funded by the Priority Research Area BioS under the program “Excellence Initiative – Research University” at the Jagiellonian University.

ABBREVIATIONS

$\Delta\tilde{\mu}_H^+$ = transmembrane electrochemical potential gradient
 2Fe2S = Rieske 2Fe-2S cluster
 ADP = adenosine diphosphate
 ATP = adenosine triphosphate
 b_H = high-potential heme *b* of *Cytc₁*
 b_H/b_n = high-potential heme *b* of *Cytc₁* or heme *b* at *n*-side of *Cytc₁*
 b_L = low-potential heme *b* of *Cytc₁*
 b_L/b_p = low-potential heme *b* of *Cytc₁* or heme *b* at *p*-side of *Cytc₁*
 b_n = heme *b* at *n*-side of *Cytc₁*
 b_p = heme *b* at *p*-side of *Cytc₁*
 CcO = cytochrome *c* oxidase
 CET = cyclic electron transfer
 CW = continuous wave
 Cyt-*bc* = enzyme belonging to the family of cytochromes *bc* (*Cytc₁* or *Cytc₁*)
 Cyt*b* = cytochrome *b*
 Cyt*b₆* = cytochrome *b₆*
 Cyt*b₆f* = cytochrome *b₆f* complex
 Cyt*bc₁* = cytochrome *bc₁* complex
 Cyt*c*, Cyt*c₂*, Cyt*c₆* = cytochrome *c*, *c₂*, *c₆*
 Cyt*c₁* = cytochrome *c₁*
 Cyt*f* = cytochrome *f*
 DBMIB = dibromothymoquinone
 DMPO = 5,5-dimethyl-1-pyrroline *N*-oxide (spin trap)
 ECS = electrochromic band shift
 E_m = redox midpoint potential

$E_{m,x}$ = redox midpoint potential at pH = x
 EPR = electron paramagnetic resonance
 ES = enzyme–substrate complex
 ET = electron transfer
 ETC = electron transport chain
 Fd = ferredoxin
 FQR = ferredoxin quinoine reductase
 heme c_1 = type c heme in cytochrome c_1
 IMS = intermembrane space
 ISP = iron–sulfur protein
 ISP-HD = mobile head domain of the iron–sulfur protein
 K_d = dissociation constant
 MD = molecular dynamics
 MK = menaquinone
 NMR = nuclear magnetic resonance
 p, n side = electrochemically positive, negative sides of membrane, respectively
 PC = plastocyanin
 P_f = inhibitor that fixes ISP-HD at b-position
 P_i = phosphate
 P_m = inhibitor that does not fix ISP-HD
 pmf = transmembrane electrochemical potential gradient, $\Delta\mu_{H^+}$
 PQ = plastoquinone
 $PQ(H_2)$ = plastoquinone or plastoquinol
 PQH_2 = plastoquinol
 PSI = photosystem I
 PSII = photosystem II
 PSQ = plastosemiquinone
 PT = proton transfer
 Q = quinone (in general)
 $Q(H_2)$ = quinone or quinol
 QH_2 = quinol
 Q_i = quinone reduction site of $Cytb_{c_1}$
 Q_i/Q_n = quinone reduction site of $Cytb_{c_1}$ or $Cytb_{6f}$
 Q_n = plastoquinone reduction site of $Cytb_{6f}$
 Q_o = quinol oxidation site of $Cytb_{c_1}$
 Q_o/Q_p = quinol oxidation site of $Cytb_{c_1}$ or $Cytb_{6f}$
 Q_{os} = strong-binding niche of the Q_o site
 Q_{ow} = weak-binding niche of the Q_o site
 Q_p = plastoquinol oxidation site of $Cyt b_{6f}$
 RC = photosynthetic reaction center
 R^hA_{xxx} , B^tA_{xxx} , S^cA_{xxx} , M^lA_{xxx} = residue of code “A” at position number xxx from *Rhodobacter capsulatus/sphaeroides*, *Bos taurus*, *Saccharomyces cerevisiae*, *Mastigocladus laminosus* ($Cytb_{6f}$), respectively
 ROS = reactive oxygen species
 SMP = submitochondrial particles
 SQ = general semiquinone
 SQ^- = semiquinone anion
 $SQ-2Fe_2S$ = semiquinone at the Q_o/Q_p site spin-coupled to the reduced $2Fe_2S$ cluster
 SQH = protonated semiquinone
 SQ_i = semiquinone at the Q_i site
 SQ_o = semiquinone at the Q_o site
 TMH = transmembrane helix
 UQ = ubiquinone
 $UQ(H_2)$ = ubiquinone or ubiquinol
 UQH_2 = ubiquinol
 $UQH_2^{Q_{os}}$ = ubiquinol bound at the Q_{os}
 $UQH_2^{Q_{ow}}$ = ubiquinol bound at the Q_{ow}
 $UQ^{Q_{os}}$ = ubiquinone bound at the Q_{os}
 $UQ^{Q_{ow}}$ = ubiquinone bound at the Q_{ow}

USQ = ubisemiquinone

REFERENCES

- Berry, E. A.; Guergova-Kuras, M.; Huang, L.; Crofts, A. R. Structure and Function of Cytochrome Bc Complexes. *Annu. Rev. Biochem.* **2000**, *69*, 1005–1075.
- Crofts, A. R. The Cytochrome Bc_1 Complex: Function in the Context of Structure. *Annu. Rev. Physiol.* **2004**, *66*, 689–733.
- Borek, A.; Ekiert, R.; Osyczka, A. Advances in Understanding Mechanism and Physiology of Cytochromes Bc . In *Mechanisms of primary energy transduction in biology*; Wikström, M., Ed.; Royal Society of Chemistry: London, 2018; pp 192–214.
- Cramer, W. A. Structure–Function of the Cytochrome b_{6f} Lipoprotein Complex: A Scientific Odyssey and Personal Perspective. *Photosynth. Res.* **2019**, *139*, 53–65.
- Kirchhoff, H.; Li, M.; Puthiyaveetil, S. Sublocalization of Cytochrome b_{6f} Complexes in Photosynthetic Membranes. *Trends Plant Sci.* **2017**, *22*, 574–582.
- Schöttler, M. A.; Tóth, S. Z.; Boulouis, A.; Kahlau, S. Photosynthetic Complex Stoichiometry Dynamics in Higher Plants: Biogenesis, Function, and Turnover of ATP Synthase and the Cytochrome b_{6f} Complex. *J. Exp. Bot.* **2015**, *66*, 2373–2400.
- Tikhonov, A. N. The Cytochrome b_{6f} Complex at the Crossroad of Photosynthetic Electron Transport Pathways. *Plant Physiol. Biochem.* **2014**, *81*, 163–183.
- Tikkanen, M.; Grieco, M.; Nurmi, M.; Rantala, M.; Suorsa, M.; Aro, E. M. Regulation of the Photosynthetic Apparatus under Fluctuating Growth Light. *Philos. Trans. R. Soc., B* **2012**, *367*, 3486–3493.
- Cruz-Gallardo, I.; Díaz-Moreno, I.; Díaz-Quintana, A.; De La Rosa, M. A. The Cytochrome F-Plastocyanin Complex as a Model to Study Transient Interactions between Redox Proteins. *FEBS Lett.* **2012**, *586*, 646–652.
- Nelson, N. Photosystems and Global Effects of Oxygenic Photosynthesis. *Biochim. Biophys. Acta, Bioenerg.* **2011**, *1807*, 856–863.
- Nowaczyk, M. M.; Sander, J.; Grasse, N.; Cormann, K. U.; Rexroth, D.; Bernát, G.; Rögner, M. Dynamics of the Cyanobacterial Photosynthetic Network: Communication and Modification of Membrane Protein Complexes. *Eur. J. Cell Biol.* **2010**, *89*, 974–982.
- Trebst, A. Inhibitors in the Functional Dissection of the Photosynthetic Electron Transport System. *Photosynth. Res.* **2007**, *92*, 217–224.
- Sarewicz, M.; Osyczka, A. Electronic Connection between the Quinone and Cytochrome c Redox Pools and Its Role in Regulation of Mitochondrial Electron Transport and Redox Signaling. *Physiol. Rev.* **2015**, *95*, 219–243.
- Allen, J. F. Cytochrome b_{6f} : Structure for Signalling and Vectorial Metabolism. *Trends Plant Sci.* **2004**, *9*, 130–137.
- Choquet, Y.; Wostrikoff, K.; Girard-Bascou, J.; Wollman, F.-A. Assembly-Controlled Regulation of Chloroplast Gene Translation. *Biochem. Soc. Trans.* **2001**, *29*, A51–A51.
- Nelson, N.; Ben-Shem, A. The Complex Architecture of Oxygenic Photosynthesis. *Nat. Rev. Mol. Cell Biol.* **2004**, *5*, 971–982.
- Cramer, W. A.; Hasan, S. S. Structure-Function of the Cytochrome b_{6f} Lipoprotein Complex. In *Cytochrome Complexes: Evolution, Structures, Energy Transduction, and Signaling*; Cramer, W. A., Kallas, T., Eds.; Springer: Dordrecht, 2016; pp 177–207.
- Cramer, W. A.; Zhang, H.; Yan, J.; Kurisu, G.; Smith, J. L. Transmembrane Traffic in the Cytochrome b_{6f} Complex. *Annu. Rev. Biochem.* **2006**, *75*, 769–790.
- Mulki-Janian, A. Y. Activated Q-Cycle as a Common Mechanism for Cytochrome Bc_1 and Cytochrome b_{6f} Complexes. *Biochim. Biophys. Acta, Bioenerg.* **2010**, *1797*, 1858–1868.
- Berry, E. A.; De Bari, H.; Huang, L.-S. Unanswered Questions about the Structure of Cytochrome Bc_1 Complexes. *Biochim. Biophys. Acta, Bioenerg.* **2013**, *1827*, 1258–1277.
- Xia, D.; Esser, L.; Tang, W.-K.; Zhou, F.; Zhou, Y.; Yu, L.; Yu, C.-A. Structural Analysis of Cytochrome Bc_1 Complexes: Implications to

the Mechanism of Function. *Biochim. Biophys. Acta, Bioenerg.* **2013**, *1827*, 1278–1294.

(22) Hasan, S. S.; Yamashita, E.; Cramer, W. A. Transmembrane Signaling and Assembly of the Cytochrome *b₆f*-Lipidic Charge Transfer Complex. *Biochim. Biophys. Acta, Bioenerg.* **2013**, *1827*, 1295–1308.

(23) Crofts, A. R.; Hong, S.; Wilson, C.; Burton, R.; Victoria, D.; Harrison, C.; Schulten, K. The Mechanism of Ubihydroquinone Oxidation at the Q_o-Site of the Cytochrome *Bc₁* Complex. *Biochim. Biophys. Acta, Bioenerg.* **2013**, *1827*, 1362–1377.

(24) Berry, E. A.; Lee, D.-W.; Huang, L.-S.; Daldal, F. Structural and Mutational Studies of the Cytochrome *bc₁* Complex. In *The Purple Phototrophic Bacteria*; Hunter, C. N., Daldal, F., Thurnauer, M. C., Beatty, J. T., Eds.; Springer Science, 2009; pp 425–450.

(25) Kramer, D. M.; Nitschke, W.; Cooley, J. W. The Cytochrome *bc₁* and Related Bc Complexes: The Rieske/Cytochrome *b* Complex as the Functional Core of a Central Electron/Proton Transfer Complex. *Adv. Photosynth. Respir.* **2009**, *28*, 451–473.

(26) Crofts, A. R.; Wilson, C. A.; Rose, S. W.; Dikanov, S. A.; Burton, R. L. The *bc₁* Complex: A Physicochemical Retrospective and a Atomistic Perspective. In *Mechanisms of primary energy transduction in biology*; 2018; pp 161–191.

(27) Mitchell, P. Possible Molecular Mechanisms of the Protonmotive Function of Cytochrome Systems. *J. Theor. Biol.* **1976**, *62*, 327–367.

(28) Mitchell, P. Coupling of Phosphorylation to Electron and Hydrogen Transfer by a Chemi-Osmotic Type of Mechanism. *Nature* **1961**, *191*, 144–148.

(29) Al-Attar, S.; de Vries, S. Energy Transduction by Respiratory Metallo-Enzymes: From Molecular Mechanism to Cell Physiology. *Coord. Chem. Rev.* **2013**, *257*, 64–80.

(30) Nicholls, D. G.; Ferguson, S. J. *Bioenergetics* 4, 4th ed.; Kim, C. H., Ozawa, T., Eds.; Academic Press: Amsterdam, 2013.

(31) Cramer, W. A.; Kallas, T. *Cytochrome Complexes: Evolution, Structures, Energy Transduction, and Signaling*; Cramer, W. A., Kallas, T., Eds.; Springer Science: Dordrecht, 2016.

(32) Mitchell, P. The Protonmotive Q Cycle: A General Formulation. *FEBS Lett.* **1975**, *59*, 137–139.

(33) Mitchell, P. Protonmotive Redox Mechanism of the Cytochrome B-C₁ Complex in the Respiratory Chain: Protonmotive Ubiquinone Cycle. *FEBS Lett.* **1975**, *56*, 1–6.

(34) *The Purple Phototrophic Bacteria*; Hunter, C. N., Daldal, F., Thurnauer, M. C., Beatty, J. T., Eds.; Springer, 2009.

(35) Rochaix, J. D.; Lemeille, S.; Shapiguzov, A.; Samol, I.; Fucile, G.; Willig, A.; Goldschmidt-Clermont, M. Protein Kinases and Phosphatases Involved in the Acclimation of the Photosynthetic Apparatus to a Changing Light Environment. *Philos. Trans. R. Soc., B* **2012**, *367*, 3466–3474.

(36) Sena, L. A.; Chandel, N. S. Physiological Roles of Mitochondrial Reactive Oxygen Species. *Mol. Cell* **2012**, *48*, 158–167.

(37) Adam-Vizi, V.; Chinopoulos, C. Bioenergetics and the Formation of Mitochondrial Reactive Oxygen Species. *Trends Pharmacol. Sci.* **2006**, *27*, 639–645.

(38) Baniulis, D.; Hasan, S. S.; Stofleth, J. T.; Cramer, W. A. Mechanism of Enhanced Superoxide Production in the Cytochrome *b₆f* Complex of Oxygenic Photosynthesis. *Biochemistry* **2013**, *52*, 8975–8983.

(39) Crofts, A. R.; Meinhardt, S. W.; Jones, K. R.; Snozzi, M. The Role of the Quinone Pool in the Cyclic Electron-Transfer Chain of *Rhodospseudomonas Sphaeroides*: A Modified Q₂-Cycle Mechanism. *Biochim. Biophys. Acta, Bioenerg.* **1983**, *723*, 202–218.

(40) Furbacher, P. N.; Girvin, M. E.; Cramer, W. A. On the Question of Interheme Electron Transfer in the Chloroplast Cytochrome *b₆f* in Situ. *Biochemistry* **1989**, *28*, 8990–8998.

(41) Stroebel, D.; Choquet, Y.; Popot, J.-L.; Picot, D. An Atypical Haem in the Cytochrome *b₆f* Complex. *Nature* **2003**, *426*, 413–418.

(42) Kurisu, G.; Zhang, H.; Smith, J. L.; Cramer, W. A. Structure of the Cytochrome *b₆f* Complex of Oxygenic Photosynthesis: Tuning the Cavity. *Science* **2003**, *302*, 1009–1014.

(43) Zatsman, A. I.; Zhang, H.; Gunderson, W. A.; Cramer, W. A.; Hendrich, M. P. Heme-Heme Interactions in the Cytochrome *b₆f*

Complex: EPR Spectroscopy and Correlation with Structure. *J. Am. Chem. Soc.* **2006**, *128*, 14246–14247.

(44) Buckel, W.; Thauer, R. K. Flavin-Based Electron Bifurcation, A New Mechanism of Biological Energy Coupling. *Chem. Rev.* **2018**, *118*, 3862–3886.

(45) Baniulis, D.; Hasan, S. S.; Miliute, I.; Cramer, W. A. Mechanisms of Superoxide Generation and Signaling in Cytochrome Bc Complexes. In *Cytochrome Complexes: Evolution, Structures, Energy Transduction, and Signaling*; Cramer, W., Kallas, T., Eds.; Springer: Dordrecht, 2016; pp 397–417.

(46) Agarwal, R.; Hasan, S. S.; Jones, L. M.; Stofleth, J. T.; Ryan, C. M.; Whitelegge, J. P.; Kehoe, D. M.; Cramer, W. A. Role of Domain Swapping in the Hetero-Oligomeric Cytochrome B6 f Lipoprotein Complex. *Biochemistry* **2015**, *54*, 3151–3163.

(47) Swierczek, M.; Cieluch, E.; Sarewicz, M.; Borek, A.; Moser, C. C.; Dutton, P. L.; Osyczka, A. An Electronic Bus Bar Lies in the Core of Cytochrome *Bc₁*. *Science* **2010**, *329*, 451–454.

(48) Berry, E. A.; Huang, L.-S.; Saechao, L. K.; Pon, N. G.; Valkova-Valchanova, M.; Daldal, F. X-Ray Structure of *Rhodobacter Capsulatus* Cytochrome *Bc₁*: Comparison with Its Mitochondrial and Chloroplast Counterparts. *Photosynth. Res.* **2004**, *81*, 251–275.

(49) Tian, H.; White, S.; Yu, L.; Yu, C.-A. Evidence for the Head Domain Movement of the Rieske Iron-Sulfur Protein in Electron Transfer Reaction of the Cytochrome *Bc₁* Complex. *J. Biol. Chem.* **1999**, *274*, 7146–7152.

(50) Darrouzet, E.; Valkova-Valchanova, M.; Daldal, F. Probing the Role of the Fe-S Subunit Hinge Region during Q_o Site Catalysis in *Rhodobacter Capsulatus* *Bc₁* Complex. *Biochemistry* **2000**, *39*, 15475–15483.

(51) Darrouzet, E.; Valkova-Valchanova, M.; Moser, C. C.; Dutton, P. L.; Daldal, F. Uncovering the [2Fe2S] Domain Movement in Cytochrome *Bc₁* and Its Implications for Energy Conversion. *Proc. Natl. Acad. Sci. U. S. A.* **2000**, *97*, 4567–4572.

(52) Darrouzet, E.; Moser, C. C.; Dutton, P. L.; Daldal, F. Large Scale Domain Movement in Cytochrome *Bc₁*: A New Device for Electron Transfer in Proteins. *Trends Biochem. Sci.* **2001**, *26*, 445–451.

(53) Darrouzet, E.; Daldal, F. Movement of the Iron-Sulfur Subunit beyond the *Ef* Loop of Cytochrome *b* Is Required for Multiple Turnovers of the *Bc₁* Complex but Not for Single Turnover Q_o Site Catalysis. *J. Biol. Chem.* **2002**, *277*, 3471–3476.

(54) Sadoski, R. C.; Engstrom, G.; Tian, H.; Zhang, L.; Yu, C.-A.; Yu, L.; Durham, B.; Millett, F. Use of a Photoactivated Ruthenium Dimer Complex to Measure Electron Transfer between the Rieske Iron-Sulfur Protein and Cytochrome C1 in the Cytochrome *bc₁* Complex. *Biochemistry* **2000**, *39*, 4231–4236.

(55) Rajagukguk, S.; Yang, S.; Yu, C.-A.; Yu, L.; Durham, B.; Millett, F. Effect of Mutations in the Cytochrome *b* *Ef* Loop on the Electron-Transfer Reactions of the Rieske Iron-Sulfur Protein in the Cytochrome *bc₁* Complex. *Biochemistry* **2007**, *46*, 1791–1798.

(56) Page, C. C.; Moser, C. C.; Chen, X.; Dutton, P. L. Natural Engineering Principles of Electron Tunneling in Biological Oxidation-Reduction. *Nature* **1999**, *402*, 47–52.

(57) Brandt, U.; von Jagow, G. Analysis of Inhibitor Binding to the Mitochondrial Cytochrome *c* Reductase by Fluorescence Quench Titration. Evidence for a “catalytic Switch” at the Q_o Center. *Eur. J. Biochem.* **1991**, *195*, 163–170.

(58) Brandt, U.; Haase, U.; Schagger, H.; von Jagow, G. Significance of the “Rieske” Iron-Sulfur Protein for Formation and Function of the Ubiquinol-Oxidation Pocket of Mitochondrial Cytochrome *c* Reductase (*bc₁* Complex). *J. Biol. Chem.* **1991**, *266*, 19958–19964.

(59) Xia, D.; Yu, C.-A.; Kim, H.; Xia, J.-Z.; Kachurin, A. M.; Zhang, L.; Yu, L.; Deisenhofer, J. Crystal Structure of the Cytochrome *bc₁* Complex from Bovine Heart Mitochondria. *Science* **1997**, *277*, 60–66.

(60) Iwata, S.; Lee, J. W.; Okada, K.; Lee, J. K.; Iwata, M.; Rasmussen, B.; Link, T. A.; Ramaswamy, S.; Jap, B. K. Complete Structure of the 11-Subunit Bovine Mitochondrial Cytochrome *Bc₁* Complex. *Science* **1998**, *281*, 64–71.

(61) Zhang, Z.; Huang, L.-S.; Shulmeister, V. M.; Chi, Y.-I.; Kim, K. K.; Hung, L.-W.; Crofts, A. R.; Berry, E. A.; Kim, S.-H. Electron

Transfer by Domain Movement in Cytochrome Bc_1 . *Nature* **1998**, *392*, 677–684.

(62) Kleinschroth, T.; Castellani, M.; Trinh, C. H.; Morgner, N.; Brutschy, B.; Ludwig, B.; Hunte, C. X-Ray Structure of the Dimeric Cytochrome Bc_1 Complex from the Soil Bacterium *Paracoccus Denitrificans* at 2.7-Å Resolution. *Biochim. Biophys. Acta, Bioenerg.* **2011**, *1807*, 1606–1615.

(63) Esser, L.; Elberry, M.; Zhou, F.; Yu, C.-A. A.; Yu, L.; Xia, D. Inhibitor-Complexed Structures of the Cytochrome b_{c1} from the Photosynthetic Bacterium *Rhodospira rubra*. *J. Biol. Chem.* **2008**, *283*, 2846–2857.

(64) Esser, L.; Zhou, F.; Yu, C. A.; Xia, D. Crystal Structure of Bacterial Cytochrome b_{c1} in Complex with Azoxystrobin Reveals a Conformational Switch of the Rieske Iron–Sulfur Protein Subunit. *J. Biol. Chem.* **2019**, *294*, 12007–12019.

(65) Baniulis, D.; Yamashita, E.; Whitelegge, J. P.; Zatsman, A. I.; Hendrich, M. P.; Hasan, S. S.; Ryan, C. M.; Cramer, W. A. Structure-Function, Stability, and Chemical Modification of the Cyanobacterial Cytochrome b_{6f} Complex from *Nostoc* Sp. PCC 7120. *J. Biol. Chem.* **2009**, *284*, 9861–9869.

(66) Hasan, S. S.; Yamashita, E.; Baniulis, D.; Cramer, W. A. Quinone-Dependent Proton Transfer Pathways in the Photosynthetic Cytochrome b_{6f} Complex. *Proc. Natl. Acad. Sci. U. S. A.* **2013**, *110*, 4297–4302.

(67) Yan, J.; Kurisu, G.; Cramer, W. A. Intraprotein Transfer of the Quinone Analogue Inhibitor 2,5-Dibromo-3-Methyl-6-Isopropyl-p-Benzoquinone in the Cytochrome b_{6f} Complex. *Proc. Natl. Acad. Sci. U. S. A.* **2006**, *103*, 69–74.

(68) Hunte, C.; Koepke, J.; Lange, C.; Roßmanith, T.; Michel, H. Structure at 2.3 Å Resolution of the Cytochrome Bc_1 Complex from the Yeast *Saccharomyces cerevisiae* Co-Crystallized with an Antibody Fv Fragment. *Structure* **2000**, *8*, 669–684.

(69) Lange, C.; Hunte, C. Crystal Structure of the Yeast Cytochrome Bc_1 Complex with Its Bound Substrate Cytochrome C. *Proc. Natl. Acad. Sci. U. S. A.* **2002**, *99*, 2800–2805.

(70) Palsdottir, H.; Lojero, C. G.; Trumpower, B. L.; Hunte, C. Structure of the Yeast Cytochrome Bc_1 Complex with a Hydroxyquinone Anion Q_0 Site Inhibitor Bound. *J. Biol. Chem.* **2003**, *278*, 31303–31311.

(71) Birth, D.; Kao, W.-C.; Hunte, C. Structural Analysis of Atovaquone-Inhibited Cytochrome Bc_1 Complex Reveals the Molecular Basis of Antimalarial Drug Action. *Nat. Commun.* **2014**, *5*, 1–11.

(72) Solmaz, S. R. N.; Hunte, C. Structure of Complex III with Bound Cytochrome C in Reduced State and Definition of a Minimal Core Interface for Electron Transfer. *J. Biol. Chem.* **2008**, *283*, 17542–17549.

(73) Malone, L. A.; Qian, P.; Mayneord, G. E.; Hitchcock, A.; Farmer, D. A.; Thompson, R. F.; Swainsbury, D. J. K.; Ranson, N. A.; Hunter, C. N.; Johnson, M. P. Cryo-EM Structure of the Spinach Cytochrome b_{6f} Complex at 3.6 Å Resolution. *Nature* **2019**, *575*, 535–539.

(74) Berry, E. A.; Huang, L. S.; Zhang, Z.; Kim, S. H. Structure of the Avian Mitochondrial Cytochrome b_{c1} Complex. *J. Bioenerg. Biomembr.* **1999**, *31*, 177–190.

(75) Crowley, P. J.; Berry, E. A.; Cromartie, T.; Daldal, F.; Godfrey, C. R. A. A.; Lee, D.-W. W.; Phillips, J. E.; Taylor, A.; Viner, R. The Role of Molecular Modeling in the Design of Analogues of the Fungicidal Natural Products Crocins A and D. *Bioorg. Med. Chem.* **2008**, *16*, 10345–10355.

(76) Berry, E. A.; Zhang, Z.; Bellamy, H. D.; Huang, L. Crystallographic Location of Two Zn^{2+} -Binding Sites in the Avian Cytochrome Bc_1 Complex. *Biochim. Biophys. Acta, Bioenerg.* **2000**, *1459*, 440–448.

(77) Esser, L.; Quinn, B.; Li, Y.-F.; Zhang, M.; Elberry, M.; Yu, L.; Yu, C.-A.; Xia, D. Crystallographic Studies of Quinol Oxidation Site Inhibitors: A Modified Classification of Inhibitors for the Cytochrome b_{c1} Complex. *J. Mol. Biol.* **2004**, *341*, 281–302.

(78) Esser, L.; Gong, X.; Yang, S.; Yu, L.; Yu, C.-A.; Xia, D. Surface-Modulated Motion Switch: Capture and Release of Iron–Sulfur Protein in the Cytochrome b_{c1} Complex. *Proc. Natl. Acad. Sci. U. S. A.* **2006**, *103*, 13045–13050.

(79) Gao, X.; Wen, X.; Esser, L.; Quinn, B.; Yu, L.; Yu, C.-A.; Xia, D. Structural Basis for the Quinone Reduction in the Bc_1 Complex: A Comparative Analysis of Crystal Structures of Mitochondrial Cytochrome Bc_1 with Bound Substrate and Inhibitors at the Q_0 Site. *Biochemistry* **2003**, *42*, 9067–9080.

(80) Guo, R.; Zong, S.; Wu, M.; Gu, J.; Yang, M. Architecture of Human Mitochondrial Respiratory Megacomplex I2III2IV2. *Cell* **2017**, *170*, 1247–1257.

(81) Gong, H.; Li, J.; Xu, A.; Tang, Y.; Ji, W.; Gao, R.; Wang, S.; Yu, L.; Tian, C.; Li, J.; Yen, H. Y.; Lam, S. M.; Shui, G.; Yang, X.; Sun, Y.; Li, X.; Jia, M.; Yang, C.; Jiang, B.; Lou, Z.; Robinson, C. V.; Wong, L. L.; Guddat, L. W.; Sun, F.; Wang, Q.; Rao, Z. An Electron Transfer Path Connects Subunits of a Mycobacterial Respiratory Supercomplex. *Science (Washington, DC, U. S.)* **2018**, *362*, eaat8923.

(82) Wiseman, B.; Nitharwal, R. G.; Fedotovskaya, O.; Schäfer, J.; Guo, H.; Kuang, Q.; Benlekbir, S.; Sjöstrand, D.; Adelroth, P.; Rubinstein, J. L.; Brzezinski, P.; Högbom, M. Structure of a Functional Obligate Complex III2IV2 Respiratory Supercomplex from *Mycobacterium smegmatis*. *Nat. Struct. Mol. Biol.* **2018**, *25*, 1128–1136.

(83) Kim, H.; Xia, D.; Yu, C.-A.; Xia, J.-Z.; Kachurin, A. M.; Zhang, L.; Yu, L.; Deisenhofer, J. Inhibitor Binding Changes Domain Mobility in the Iron-Sulfur Protein of the Mitochondrial b_{c1} Complex from Bovine Heart. *Proc. Natl. Acad. Sci. U. S. A.* **1998**, *95*, 8026–8033.

(84) Schoepp, B.; Brugna, M.; Riedel, A.; Nitschke, W.; Kramer, D. M. The Q_0 -Site Inhibitor DBMIB Favours the Proximal Position of the Chloroplast Rieske Protein and Induces a pK-Shift of the Redox-Linked Proton. *FEBS Lett.* **1999**, *450*, 245–250.

(85) Berry, E. A.; Huang, L. Observations Concerning the Quinol Oxidation Site of the Cytochrome Bc_1 Complex. *FEBS Lett.* **2003**, *555*, 13–20.

(86) Cooley, J. W. Protein Conformational Changes Involved in the Cytochrome b_{c1} Complex Catalytic Cycle. *Biochim. Biophys. Acta, Bioenerg.* **2013**, *1827*, 1340–1345.

(87) Covian, R.; Trumpower, B. L. Regulatory Interactions in the Dimeric Cytochrome b_{c1} Complex: The Advantages of Being a Twin. *Biochimica et Biophysica Acta - Bioenergetics*; Elsevier, 2008; pp 1079–1091.

(88) Cooley, J. W.; Lee, D.-W.; Daldal, F. Across Membrane Communication between the Q_0 and Q_i Active Sites of Cytochrome b_{c1} . *Biochemistry* **2009**, *48*, 1888–1899.

(89) Cen, X.; Yu, L.; Yu, C.-A. Domain Movement of Iron Sulfur Protein in Cytochrome Bc_1 Complex Is Facilitated by the Electron Transfer from Cytochrome b_L to b_H . *FEBS Lett.* **2008**, *582*, 523–526.

(90) Sarewicz, M.; Dutka, M.; Froncisz, W.; Osyczka, A. Magnetic Interactions Sense Changes in Distance between Heme b_L and the Iron-Sulfur Cluster in Cytochrome Bc_1 . *Biochemistry* **2009**, *48*, 5708–5720.

(91) Crofts, A. R.; Guergova-Kuras, M.; Huang, L.; Kuras, R.; Zhang, Z.; Berry, E. A. Mechanism of Ubiquinol Oxidation by the Bc_1 Complex: Different Domains of the Quinol Binding Pocket and Their Role in the Mechanism and Binding of Inhibitors. *Biochemistry* **1999**, *38*, 15791–15806.

(92) Crofts, A. R.; Hong, S.; Zhang, Z.; Berry, E. A. Physicochemical Aspects of the Movement of the Rieske Iron Sulfur Protein during Quinol Oxidation by the Bc_1 Complex from Mitochondria and Photosynthetic Bacteria. *Biochemistry* **1999**, *38*, 15827–15839.

(93) Millett, F.; Durham, B. Kinetics of Electron Transfer within Cytochrome Bc_1 and between Cytochrome Bc_1 and Cytochrome C. *Photosynth. Res.* **2004**, *82*, 1–16.

(94) Crofts, A. R.; Shinkarev, V. P.; Kolling, D. R. J.; Hong, S. The Modified Q-Cycle Explains the Apparent Mismatch between the Kinetics of Reduction of Cytochromes c_1 and b_H in the Bc_1 Complex. *J. Biol. Chem.* **2003**, *278*, 36191–36201.

(95) Postila, P. A.; Kaszuba, K.; Sarewicz, M.; Osyczka, A.; Vattulainen, I.; Róg, T. Key Role of Water in Proton Transfer at the Q_0 -Site of the Cytochrome Bc_1 Complex Predicted by Atomistic Molecular Dynamics Simulations. *Biochim. Biophys. Acta, Bioenerg.* **2013**, *1827*, 761–768.

- (96) Barragan, A. M.; Crofts, A. R.; Schulten, K.; Solov'yov, I. A. Identification of Ubiquinol Binding Motifs at the Q_b -Site of the Cytochrome Bc_1 Complex. *J. Phys. Chem. B* **2015**, *119*, 433–447.
- (97) Barragan, A. M.; Schulten, K.; Solov'yov, I. A. Mechanism of the Primary Charge Transfer Reaction in the Cytochrome Bc_1 Complex. *J. Phys. Chem. B* **2016**, *120*, 11369–11380.
- (98) Darrouzet, E.; Valkova-Valchanova, M.; Ohnishi, T.; Daldal, F. Structure and Function of the Bacterial Bc_1 Complex: Domain Movement, Subunit Interactions, and Emerging Rationale Engineering Attempts. *J. Bioenerg. Biomembr.* **1999**, *31*, 275–288.
- (99) Tian, H.; Yu, L.; Mather, M. W.; Yu, C.-A. Flexibility of the Neck Region of the Rieske Iron-Sulfur Protein Is Functionally Important in the Cytochrome Bc_1 Complex. *J. Biol. Chem.* **1998**, *273*, 27953–27959.
- (100) Brugna, M.; Rodgers, S.; Schricker, A.; Montoya, G.; Kazmeier, M.; Nitschke, W.; Sinning, I. A Spectroscopic Method for Observing the Domain Movement of the Rieske Iron-Sulfur Protein. *Proc. Natl. Acad. Sci. U. S. A.* **2000**, *97*, 2069–2074.
- (101) Liebl, U.; Sled, V.; Brasseur, G.; Ohnishi, T.; Daldal, F. Conserved Nonliganding Residues of the *Rhodobacter Capsulatus* Rieske Iron-Sulfur Protein of the Bc_1 Complex Are Essential for Protein Structure, Properties of the [2Fe-2S] Cluster, and Communication with the Quinone Pool. *Biochemistry* **1997**, *36*, 11675–11684.
- (102) Brasseur, G.; Sled, V.; Liebl, U.; Ohnishi, T.; Daldal, F. The Amino-Terminal Portion of the Rieske Iron-Sulfur Protein Contributes to the Ubiquinol Oxidation Site Catalysis of the *Rhodobacter Capsulatus* Bc_1 Complex. *Biochemistry* **1997**, *36*, 11685–11696.
- (103) Xiao, K.; Engstrom, G.; Rajagukguk, S.; Yu, C.-A.; Yu, L.; Durham, B.; Millett, F. Effect of Fomoxadone on Photoinduced Electron Transfer between the Iron-Sulfur Center and Cytochrome c_1 in the Cytochrome Bc_1 Complex. *J. Biol. Chem.* **2003**, *278*, 11419–11426.
- (104) Cieluch, E.; Pietryga, K.; Sarewicz, M.; Osyczka, A. Visualizing Changes in Electron Distribution in Coupled Chains of Cytochrome bc_1 by Modifying Barrier for Electron Transfer between the FeS Cluster and Heme C1. *Biochim. Biophys. Acta, Bioenerg.* **2010**, *1797*, 296–303.
- (105) Nett, J. H.; Hunte, C.; Trumpower, B. L. Changes to the Length of the Flexible Linker Region of the Rieske Protein Impair the Interaction of Ubiquinol with the Cytochrome Bc_1 Complex. *Eur. J. Biochem.* **2000**, *267*, 5777–5782.
- (106) Darrouzet, E.; Valkova-Valchanova, M.; Daldal, F. The [2Fe-2S] Cluster E_m as an Indicator of the Iron-Sulfur Subunit Position in the Ubiquinol Oxidation Site of the Cytochrome Bc_1 Complex. *J. Biol. Chem.* **2002**, *277*, 3464–3470.
- (107) Sarewicz, M.; Borek, A.; Cieluch, E.; Swierczek, M.; Osyczka, A. Discrimination between Two Possible Reaction Sequences That Create Potential Risk of Generation of Deleterious Radicals by Cytochrome Bc_1 . Implications for the Mechanism of Superoxide Production. *Biochim. Biophys. Acta, Bioenerg.* **2010**, *1797*, 1820–1827.
- (108) Roberts, A. G.; Bowman, M. K.; Kramer, D. M. Certain Metal Ions Are Inhibitors of Cytochrome b_6f Complex “Rieske” Iron-Sulfur Protein Domain Movements. *Biochemistry* **2002**, *41*, 4070–4079.
- (109) Cooley, J. W.; Roberts, A. G.; Bowman, M. K.; Kramer, D. M.; Daldal, F. The Raised Midpoint Potential of the [2Fe2S] Cluster of Cytochrome Bc_1 Is Mediated by Both the Q_b Site Occupants and the Head Domain Position of the Fe-S Protein Subunit. *Biochemistry* **2004**, *43*, 2217–2227.
- (110) Roberts, A. G.; Bowman, M. K.; Kramer, D. M. The Inhibitor DBMIB Provides Insight into the Functional Architecture of the Q_b Site in the Cytochrome b_6f Complex. *Biochemistry* **2004**, *43*, 7707–7716.
- (111) Cooley, J. W.; Ohnishi, T.; Daldal, F. Binding Dynamics at the Quinone Reduction (Q_i) Site Influence the Equilibrium Interactions of the Iron Sulfur Protein and Hydroquinone Oxidation (Q_o) Site of the Cytochrome bc_1 Complex. *Biochemistry* **2005**, *44*, 10520–10532.
- (112) Rao, S.; Tyryshkin, A. M.; Roberts, A. G.; Bowman, M. K.; Kramer, D. M. Inhibitory Copper Binding Site on the Spinach Cytochrome b_6f Complex: Implications for Q_o Site Catalysis. *Biochemistry* **2000**, *39*, 3285–3296.
- (113) Sarewicz, M.; Dutka, M.; Pietras, R.; Borek, A.; Osyczka, A. Effect of H Bond Removal and Changes in the Position of the Iron-Sulphur Head Domain on the Spin-Lattice Relaxation Properties of the [2Fe-2S] $^{2+}$ Rieske Cluster in Cytochrome bc_1 . *Phys. Chem. Chem. Phys.* **2015**, *17*, 25297–25308.
- (114) von Jagow, G.; Ohnishi, T. The Chromone Inhibitor Stigmatellin-Binding to the Ubiquinol Oxidation Center at the C-Side of the Mitochondrial Membrane. *FEBS Lett.* **1985**, *185*, 311–315.
- (115) Gurung, B.; Yu, L.; Yu, C. A. Stigmatellin Induces Reduction of Iron-Sulfur Protein in the Oxidized Cytochrome bc_1 Complex. *J. Biol. Chem.* **2008**, *283*, 28087–28094.
- (116) Bowyer, J. R.; Edwards, C. A.; Ohnishi, T.; Trumpower, B. L. An Analogue of Ubiquinone Which Inhibits Respiration by Binding to the Iron-Sulfur Protein of the Cytochrome b -C1 Segment of the Mitochondrial Respiratory Chain. *J. Biol. Chem.* **1982**, *257*, 3705–3713.
- (117) Berry, E. A.; Huang, L.-S. Conformationally Linked Interaction in the Cytochrome Bc_1 Complex between Inhibitors of the Q_b Site and the Rieske Iron-Sulfur Protein. *Biochim. Biophys. Acta, Bioenerg.* **2011**, *1807*, 1349–1363.
- (118) Kao, W.-C.; Hunte, C. The Molecular Evolution of the Q_b Motif. *Genome Biol. Evol.* **2014**, *6*, 1894–1910.
- (119) Crofts, A. R.; Shinkarev, V. P.; Dikanov, S. A.; Samoilova, R. I.; Kolling, D. Interactions of Quinone with the Iron-Sulfur Protein of the bc_1 Complex: Is the Mechanism Spring-Loaded? *Biochim. Biophys. Acta, Bioenerg.* **2002**, *1555*, 48–53.
- (120) Borek, A.; Kuleta, P.; Ekiert, R.; Pietras, R.; Sarewicz, M.; Osyczka, A. Mitochondrial Disease-Related Mutation G167P in Cytochrome b of *Rhodobacter Capsulatus* Cytochrome Bc_1 (S151P in Human) Affects the Equilibrium Distribution of [2Fe-2S] Cluster and Generation of Superoxide. *J. Biol. Chem.* **2015**, *290*, 23781–23792.
- (121) Ekiert, R.; Borek, A.; Kuleta, P.; Czernek, J.; Osyczka, A. Mitochondrial Disease-Related Mutations at the Cytochrome b -Iron-Sulfur Protein (ISP) Interface: Molecular Effects on the Large-Scale Motion of ISP and Superoxide Generation Studied in *Rhodobacter Capsulatus* Cytochrome Bc_1 . *Biochim. Biophys. Acta, Bioenerg.* **2016**, *1857*, 1102–1110.
- (122) Darrouzet, E.; Daldal, F. Protein-Protein Interactions between Cytochrome b and the Fe-S Protein Subunits during QH_2 Oxidation and Large-Scale Domain Movement in the Bc_1 Complex. *Biochemistry* **2003**, *42*, 1499–1507.
- (123) Huang, L.-S.; Cobessi, D.; Tung, E. Y.; Berry, E. A. Binding of the Respiratory Chain Inhibitor Antimycin to the Mitochondrial Bc_1 Complex: A New Crystal Structure Reveals an Altered Intramolecular Hydrogen-Bonding Pattern. *J. Mol. Biol.* **2005**, *351*, 573–597.
- (124) Valkova-Valchanova, M.; Darrouzet, E.; Moomaw, C. R.; Slaughter, C. A.; Daldal, F. Proteolytic Cleavage of the Fe-S Subunit Hinge Region of *Rhodobacter Capsulatus* Bc_1 Complex: Effects of Inhibitors and Mutations. *Biochemistry* **2000**, *39*, 15484–15492.
- (125) Covian, R.; Trumpower, B. L. Regulatory Interactions between Ubiquinol Oxidation and Ubiquinone Reduction Sites in the Dimeric Cytochrome bc_1 Complex. *J. Biol. Chem.* **2006**, *281*, 30925–30932.
- (126) Covian, R.; Trumpower, B. L. The Dimeric Structure of the Cytochrome bc_1 Complex Prevents Center P Inhibition by Reverse Reactions at Center N. *Biochim. Biophys. Acta, Bioenerg.* **2008**, *1777*, 1044–1052.
- (127) Robertson, D. E.; Ding, H.; Chelminski, P. R.; Slaughter, C.; Hsu, J.; Moomaw, C.; Tokito, M.; Daldal, F.; Dutton, P. L. Hydrobiquinone-Cytochrome C2 Oxidoreductase from *Rhodobacter Capsulatus*: Definition of a Minimal, Functional Isolated Preparation. *Biochemistry* **1993**, *32*, 1310–1317.
- (128) Shinkarev, V. P.; Kolling, D. R. J.; Miller, T. J.; Crofts, A. R. Modulation of the Midpoint Potential of the [2Fe-2S] Rieske Iron Sulfur Center by Q_b Occupants in the Bc_1 Complex. *Biochemistry* **2002**, *41*, 14372–14382.
- (129) Tso, S.-C.; Shenoy, S. K.; Quinn, B. N.; Yu, L. Subunit IV of Cytochrome Bc_1 Complex from *Rhodobacter Sphaeroides*. *J. Biol. Chem.* **2000**, *275*, 15287–15294.
- (130) Koch, H.-G.; Schneider, D. Folding, Assembly, and Stability of Transmembrane Cytochromes. *Curr. Chem. Biol.* **2007**, *1*, 59–74.
- (131) Volkmer, T.; Becker, C.; Prodöhl, A.; Finger, C.; Schneider, D. Assembly of a Transmembrane B-Type Cytochrome Is Mainly Driven

by Transmembrane Helix Interactions. *Biochim. Biophys. Acta, Biomembr.* **2006**, *1758*, 1815–1822.

(132) Berry, E. A.; Walker, F. A. Bis-Histidine-Coordinated Hemes in Four-Helix Bundles: How the Geometry of the Bundle Controls the Axial Imidazole Plane Orientations in Transmembrane Cytochromes of Mitochondrial Complexes II and III and Related Proteins. *JBC, J. Biol. Inorg. Chem.* **2008**, *13*, 481–498.

(133) Yun, C.-H.; Crofts, A. R.; Gennis, R. B. Assignment of the Histidine Axial Ligands to the Cytochrome BH and Cytochrome BL Components of the bc_1 Complex from *Rhodobacter Sphaeroides* by Site-Directed Mutagenesis. *Biochemistry* **1991**, *30*, 6747–6754.

(134) Bertini, I.; Cavallaro, G.; Rosato, A. Cytochrome *c*: Occurrence and Functions. *Chem. Rev.* **2006**, *106*, 90–115.

(135) Osyczka, A.; Dutton, P. L.; Moser, C. C.; Darrouzet, E.; Daldal, F. Controlling the Functionality of Cytochrome c_1 Redox Potentials in the *Rhodobacter Capsulatus* Bc_1 Complex through Disulfide Anchoring of a Loop and a β -Branched Amino Acid near the Heme-Ligating Methionine. *Biochemistry* **2001**, *40*, 14547–14556.

(136) Osyczka, A.; Moser, C. C.; Dutton, P. L. Novel Cyanide Inhibition at Cytochrome c_1 of *Rhodobacter Capsulatus* Cytochrome Bc_1 . *Biochim. Biophys. Acta, Bioenerg.* **2004**, *1655*, 71–76.

(137) Zhang, H.; Osyczka, A.; Moser, C. C.; Dutton, P. L. Resilience of *Rhodobacter Sphaeroides* Cytochrome bc_1 to Heme C1 Ligation Changes. *Biochemistry* **2006**, *45*, 14247–14255.

(138) Davidson, E.; Ohnishi, T.; Atta-Asafo-Adjei, E.; Daldal, F. Potential Ligands to the [2Fe-2S] Rieske Cluster of the Cytochrome Bc_1 of *Rhodobacter Capsulatus* Probed by Site-Directed Mutagenesis. *Biochemistry* **1992**, *31*, 3342–3351.

(139) Mason, J. R.; Cammack, R. The Electron-Transport Proteins of Hydroxylating Bacterial Dioxygenases. *Annu. Rev. Microbiol.* **1992**, *46*, 277–305.

(140) Gurbiel, R. J.; Doan, P. E.; Gassner, G. T.; Macke, T. J.; Case, D. A.; Ohnishi, T.; Fee, J. A.; Ballou, D. P.; Hoffman, B. M. Active Site Structure of Rieske-Type Proteins: Electron Nuclear Double Resonance Studies of Isotopically Labeled Phthalate Dioxygenase from *Pseudomonas Cepacia* and Rieske Protein from *Rhodobacter Capsulatus* and Molecular Modeling Studies of a Rieske Cente. *Biochemistry* **1996**, *35*, 7834–7845.

(141) Siedow, J. N.; Power, S.; de la Rosa, F. F.; Palmer, G. The Preparation and Characterization of Highly Purified, Enzymically Active Complex III from Baker's Yeast. *J. Biol. Chem.* **1978**, *253*, 2392–2399.

(142) Kriauciunas, A.; Yu, L.; Yu, C. A.; Wynn, R. M.; Knaff, D. B. The Rhodospirillum Rubrum Cytochrome bc_1 Complex: Pep Tide Composition, Prosthetic Group Content and Quinone Binding. *Biochim. Biophys. Acta, Bioenerg.* **1989**, *976*, 70–76.

(143) Andrews, K. M.; Crofts, A. R.; Gennis, R. B. Large-Scale Purification and Characterization of a Highly Active Four-Subunit Cytochrome bc_1 Complex from *Rhodobacter Sphaeroides*. *Biochemistry* **1990**, *29*, 2645–2651.

(144) Ljungdahl, P. O.; Pennoyer, J. D.; Robertson, D. E.; Trumpower, B. L. Purification of Highly Active Cytochrome bc_1 Complexes from Phylogenetically Diverse Species by a Single Chromatographic Procedure. *Biochim. Biophys. Acta, Bioenerg.* **1987**, *891*, 227–241.

(145) Shinkarev, V. P.; Crofts, A. R.; Wraight, C. A. Spectral Analysis of the bc_1 Complex Components in Situ: Beyond the Traditional Difference Approach. *Biochim. Biophys. Acta, Bioenerg.* **2006**, *1757*, 67–77.

(146) Baymann, F.; Robertson, D. E.; Dutton, P. L.; Mantele, W. Electrochemical and Spectroscopic Investigations of the Cytochrome bc_1 Complex from *Rhodobacter Capsulatus*. *Biochemistry* **1999**, *38*, 13188–13199.

(147) Palmer, G. The Electron Paramagnetic Resonance of Metalloproteins. *Biochem. Soc. Trans.* **1985**, *13*, 548–560.

(148) Zoppellaro, G.; Bren, K. L.; Ensign, A. A.; Harbitz, E.; Kaur, R.; Hersleth, H.-P. P.; Ryde, U.; Hederstedt, L.; Andersson, K. K. Studies of Ferric Heme Proteins with Highly Anisotropic/Highly Axial Low Spin ($S = 1/2$) Electron Paramagnetic Resonance Signals with Bis-Histidine

and Histidine-Methionine Axial Iron Coordination. *Biopolymers* **2009**, *91*, 1064–1082.

(149) Pintscher, S.; Kuleta, P.; Cieluch, E.; Borek, A.; Sarewicz, M.; Osyczka, A. Tuning of Hemes *b* Equilibrium Redox Potential Is Not Required for Cross-Membrane Electron Transfer. *J. Biol. Chem.* **2016**, *291*, 6872–6881.

(150) Valkova-Valchanova, M.; Saribas, A. S.; Gibney, B. R.; Dutton, P. L.; Daldal, F. Isolation and Characterization of a Two-Subunit Cytochrome $b-c_1$ Subcomplex from *Rhodobacter Capsulatus* and Reconstitution of Its Ubihydroquinone Oxidation (Q_u) Site with Purified Fe-S Protein Subunit. *Biochemistry* **1998**, *37*, 16242–16251.

(151) Pintscher, S.; Pietras, R. R.; Sarewicz, M.; Osyczka, A. Electron Sweep across Four B-Hemes of Cytochrome Bc_1 Revealed by Unusual Paramagnetic Properties of the Q_i Semiquinone Intermediate. *Biochim. Biophys. Acta, Bioenerg.* **2018**, *1859*, 459–469.

(152) Li, J.; Darrouzet, E.; Dhawan, I. K.; Johnson, M. K.; Osyczka, A.; Daldal, F.; Knaff, D. B. Spectroscopic and Oxidation–Reduction Properties of *Rhodobacter Capsulatus* Cytochrome c_1 and Its M183K and M183H Variants. *Biochim. Biophys. Acta, Bioenerg.* **2002**, *1556*, 175–186.

(153) Finnegan, M. G.; Knaff, D. B.; Qin, H.; Gray, K. A.; Daldal, F.; Yu, L.; Yu, C.-A.; Kleis-San Francisco, S.; Johnson, M. K. Axial Heme Ligation in the Cytochrome Bc_1 Complexes of Mitochondrial and Photosynthetic Membranes. A near-Infrared Magnetic Circular Dichroism and Electron Paramagnetic Resonance Study. *Biochim. Biophys. Acta, Bioenerg.* **1996**, *1274*, 9–20.

(154) Link, T. A.; Schägger, H.; von Jagow, G. Analysis of the Structures of the Subunits of the Cytochrome bc_1 Complex from Beef Heart Mitochondria. *FEBS Lett.* **1986**, *204*, 9–15.

(155) Zhu, J.; Egawa, T.; Yeh, S.-R.; Yu, L.; Yu, C.-A. Simultaneous Reduction of Iron-Sulfur Protein and Cytochrome b_L during Ubiquinol Oxidation in Cytochrome Bc_1 Complex. *Proc. Natl. Acad. Sci. U. S. A.* **2007**, *104*, 4864–4869.

(156) Schütz, M.; Schoepp-Cothenet, B.; Lojou, E.; Woodstra, M.; Lexa, D.; Tron, P.; Dolla, A.; Durand, M. C.; Stetter, K. O.; Baymann, F. The Naphthoquinol Oxidizing Cytochrome bc_1 Complex of the Hyperthermophilic Knallgasbacterium *Aquifex Aeolicus*: Properties and Phylogenetic Relationships. *Biochemistry* **2003**, *42*, 10800–10808.

(157) Link, T. A. The Structures of Rieske and Rieske-Type Proteins. *Adv. Inorg. Chem.* **1999**, *47*, 83–157.

(158) Hagen, W. R. EPR Spectroscopy of Iron-Sulfur Proteins. In *Advances in Inorganic Chemistry, Iron-Sulfur Proteins*; Academic Press, Inc.: San Diego, 1992; pp 165–222.

(159) de Vries, S.; Albracht, S. P. J.; Leeuwerik, F. J. The Multiplicity and Stoichiometry of the Prosthetic Groups in QH₂:Cytochrome *c* Oxidoreductase as Studied by EPR. *Biochim. Biophys. Acta, Bioenerg.* **1979**, *546*, 316–333.

(160) Bergdoll, L.; ten Brink, F.; Nitschke, W.; Picot, D.; Baymann, F. From Low- to High-Potential Bioenergetic Chains: Thermodynamic Constraints of Q-Cycle Function. *Biochim. Biophys. Acta, Bioenerg.* **2016**, *1857*, 1569–1579.

(161) Shinkarev, V. P.; Crofts, A. R.; Wraight, C. A. The Electric Field Generated by Photosynthetic Reaction Center Induces Rapid Reversed Electron Transfer in the Bc_1 Complex. *Biochemistry* **2001**, *40*, 12584–12590.

(162) Nicholls, D. G.; Ferguson, S. *Bioenergetics*; Elsevier, 2013.

(163) Pintscher, S.; Wójcik-Augustyn, A.; Sarewicz, M.; Osyczka, A. Charge Polarization Imposed by the Binding Site Facilitates Enzymatic Redox Reactions of Quinone. *Biochim. Biophys. Acta, Bioenerg.* **2020**, *1861*, 148216.

(164) Rich, P. R.; Jeal, A. E.; Madgwick, S. A.; Moody, A. J. Inhibitor Effects on Redox-Linked Protonations of the *b* Haems of the Mitochondrial Bc_1 Complex. *Biochim. Biophys. Acta, Bioenerg.* **1990**, *1018*, 29–40.

(165) Trumpower, B. L. Cytochrome Bc_1 Complexes of Microorganisms. *Microbiol. Rev.* **1990**, *54*, 101–129.

(166) Denke, E.; Merbitz-Zahradnik, T.; Hatzfeld, O. M.; Snyder, C. H.; Link, T. A.; Trumpower, B. L. Alteration of the Midpoint Potential and Catalytic Activity of the Rieske Iron-Sulfur Protein by Changes of

Amino Acids Forming Hydrogen Bonds to the Iron-Sulfur Cluster. *J. Biol. Chem.* **1998**, *273*, 9085–9093.

(167) Rotsaert, F. A. J.; Covian, R.; Trumpower, B. L. Mutations in Cytochrome *b* That Affect Kinetics of the Electron Transfer Reactions at Center N in the Yeast Cytochrome *Bc₁* Complex. *Biochim. Biophys. Acta, Bioenerg.* **2008**, *1777*, 239–249.

(168) T'Sai, A. L.; Palmer, G. Potentiometric Studies on Yeast Complex III. *Biochim. Biophys. Acta, Bioenerg.* **1983**, *722*, 349–363.

(169) Van Wielink, J. E.; Oltmann, L. F.; Leeuwerik, F. J.; De Hollander, J. A.; Stouthamer, A. H. A Method for in Situ Characterization of *b*- and *c*-Type Cytochromes in *Escherichia Coli* and in Complex III from Beef Heart Mitochondria by Combined Spectrum Deconvolution and Potentiometric Analysis. *Biochim. Biophys. Acta, Bioenerg.* **1982**, *681*, 177–190.

(170) Liu, X.; Yu, C. A.; Yu, L. The Role of Extra Fragment at the C-Terminal of Cytochrome *b* (Residues 421–445) in the Cytochrome *bc₁* Complex from *Rhodobacter Sphaeroides*. *J. Biol. Chem.* **2004**, *279*, 47363–47371.

(171) Martinez, S. E.; Huang, D.; Szczepaniak, A.; Cramer, W. A.; Smith, J. L. Crystal Structure of Chloroplast Cytochrome *f* Reveals a Novel Cytochrome Fold and Unexpected Heme Ligation. *Structure* **1994**, *2*, 95–105.

(172) Martinez, S. E.; Huang, D.; Ponomarev, M.; Cramer, W. A.; Smith, J. L. The Heme Redox Center of Chloroplast Cytochrome *f* Is Linked to a Buried Five-Water Chain. *Protein Sci.* **1996**, *5*, 1081–1092.

(173) Yamashita, E.; Zhang, H.; Cramer, W. A. Structure of the Cytochrome *b₆f* Complex: Quinone Analogue Inhibitors as Ligands of Heme C_n. *J. Mol. Biol.* **2007**, *370*, 39–52.

(174) Hasan, S. S.; Cramer, W. A. Internal Lipid Architecture of the Hetero-Oligomeric Cytochrome *b₆f* Complex. *Structure* **2014**, *22*, 1008–1015.

(175) Widger, W. R.; Cramer, W. A.; Herrmann, R. G.; Trebst, A. Sequence Homology and Structural Similarity between Cytochrome *b* of Mitochondrial Complex III and the Chloroplast *B6-f* Complex: Position of the Cytochrome *b* Hemes in the Membrane. *Proc. Natl. Acad. Sci. U. S. A.* **1984**, *81*, 674–678.

(176) Rieske, J. S.; Hansen, R. E.; Zuagg, W. S. Studies on the Electron Transfer System. 58. Properties of a New Oxidation-Reduction Component of the Respiratory Chain As Studied By Electron Paramagnetic Resonance Spectroscopy. *J. Biol. Chem.* **1964**, *239*, 3017–3022.

(177) Schwenkert, S.; Legen, J.; Takami, T.; Shikanai, T.; Herrmann, R. G.; Meurer, J. Role of the Low-Molecular-Weight Subunits PetL, PetG, and PetN in Assembly, Stability, and Dimerization of the Cytochrome *b₆f* Complex in Tobacco. *Plant Physiol.* **2007**, *144*, 1924–1935.

(178) Carrell, C. J.; Zhang, H.; Cramer, W. A.; Smith, J. L. Biological Identity and Diversity in Photosynthesis and Respiration: Structure of the Lumen-Side Domain of the Chloroplast Rieske Protein. *Structure* **1997**, *5*, 1613–1625.

(179) Pierre, Y.; Breyton, C.; Kramer, D.; Popot, J. L. Purification and Characterization of the Cytochrome *B6 f* Complex from *Chlamydomonas Reinhardtii*. *J. Biol. Chem.* **1995**, *270*, 29342–29349.

(180) Zhang, H.; Whitelegge, J. P.; Cramer, W. A. Ferredoxin:NADP⁺ Oxidoreductase Is a Subunit of the Chloroplast Cytochrome *b₆f* Complex. *J. Biol. Chem.* **2001**, *276*, 38159–38165.

(181) Rexroth, S.; Rexroth, D.; Veit, S.; Plohnke, N.; Cormann, K. U.; Nowaczyk, M. M.; Rögner, M. Functional Characterization of the Small Regulatory Subunit PetP from the Cytochrome *b₆f* Complex in *Thermosynechococcus Elongatus*. *Plant Cell* **2014**, *26*, 3435–3448.

(182) Huang, D.; Everly, R. M.; Cheng, R. H.; Heymann, J. B.; Baker, T. S.; Cramer, W. A.; Schägger, H.; Sled, V.; Ohnishi, T. Characterization of the Chloroplast Cytochrome *b₆f* Complex as a Structural and Functional Dimer. *Biochemistry* **1994**, *33*, 4401–4409.

(183) Zhang, H.; Huang, D.; Cramer, W. A. Stochiometrically Bound β -Carotene in the Cytochrome *b₆f* Complex of Oxygenic Photosynthesis Protects against Oxygen Damage. *J. Biol. Chem.* **1999**, *274*, 1581–1587.

(184) Hasan, S. S.; Zakharov, S. D.; Chauvet, A.; Stadnytskiy, V.; Savikhin, S.; Cramer, W. A. A Map of Dielectric Heterogeneity in a

Membrane Protein: The Hetero-Oligomeric Cytochrome *B6 f* Complex. *J. Phys. Chem. B* **2014**, *118*, 6614–6625.

(185) Baymann, F.; Giusti, F.; Picot, D.; Nitschke, W. The *c_i/b_H* Moiety in the *b₆f* Complex Studied by EPR: A Pair of Strongly Interacting Hemes. *Proc. Natl. Acad. Sci. U. S. A.* **2007**, *104*, 519–524.

(186) Twigg, A. I.; Baniulis, D.; Cramer, W. A.; Hendrich, M. P. EPR Detection of an O₂ Surrogate to Heme *c_n* of the Cytochrome *b₆f* Complex. *J. Am. Chem. Soc.* **2009**, *131*, 12536–12537.

(187) Pierre, Y.; Breyton, C.; Lemoine, Y.; Robert, B.; Vernotte, C.; Popot, J. L. On the Presence and Role of a Molecule of Chlorophyll *a* in the Cytochrome *b₆f* Complex. *J. Biol. Chem.* **1997**, *272*, 21901–21908.

(188) Dashdorj, N.; Zhang, H.; Kim, H.; Yan, J.; Cramer, W. A.; Savikhin, S. The Single Chlorophyll *a* Molecule in the Cytochrome *B6 f* Complex: Unusual Optical Properties Protect the Complex against Singlet Oxygen. *Biophys. J.* **2005**, *88*, 4178–4187.

(189) Kim, H.; Dashdorj, N.; Zhang, H.; Yan, J.; Cramer, W. A.; Savikhin, S. An Anomalous Distance Dependence of Intraprotein Chlorophyll-Carotenoid Triplet Energy Transfer. *Biophys. J.* **2005**, *89*, L28–L30.

(190) Zhang, H.; Primak, A.; Cape, J.; Bowman, M. K.; Kramer, D. M.; Cramer, W. A. Characterization of the High-Spin Heme *x* in the Cytochrome *b₆f* Complex of Oxygenic Photosynthesis. *Biochemistry* **2004**, *43*, 16329–16336.

(191) Alric, J.; Pierre, Y.; Picot, D.; Lavergne, J.; Rappaport, F. Spectral and Redox Characterization of the Heme *Ci* of the Cytochrome *b₆f* Complex. *Proc. Natl. Acad. Sci. U. S. A.* **2005**, *102*, 15860–15865.

(192) Girvin, M. E.; Cramer, W. A. A Redox Study of the Electron Transport Pathway Responsible for Generation of the Slow Electrochromic Phase in Chloroplasts. *Biochim. Biophys. Acta, Bioenerg.* **1984**, *767*, 29–38.

(193) Palmer, G.; Esposti, M. D. Application of Exciton Coupling Theory to the Structure of Mitochondrial Cytochrome *B*. *Biochemistry* **1994**, *33*, 176–185.

(194) Schoepp, B.; Chabaud, E.; Breyton, C.; Verméglio, A.; Popot, J. L. On the Spatial Organization of Hemes and Chlorophyll in Cytochrome *b₆f*: A Linear and Circular Dichroism Study. *J. Biol. Chem.* **2000**, *275*, 5275–5283.

(195) Moser, C. C.; Keske, J. M.; Warncke, K.; Farid, R. S.; Dutton, P. L. Nature of Biological Electron Transfer. *Nature* **1992**, *355*, 796–802.

(196) Gray, H. B.; Winkler, J. R. Electron Transfer in Proteins. *Annu. Rev. Biochem.* **1996**, *65*, 537–561.

(197) Iwai, M.; Takizawa, K.; Tokutsu, R.; Okamura, A.; Takahashi, Y.; Minagawa, J. Isolation of the Elusive Supercomplex That Drives Cyclic Electron Flow in Photosynthesis. *Nature* **2010**, *464*, 1210–1213.

(198) Bhaduri, S.; Zhang, H.; Erramilli, S.; Cramer, W. A. Structural and Functional Contributions of Lipids to the Stability and Activity of the Photosynthetic Cytochrome *b₆f* Lipoprotein Complex. *J. Biol. Chem.* **2019**, *294*, 17758–17767.

(199) Hertle, A. P.; Blunder, T.; Wunder, T.; Pesaresi, P.; Pribil, M.; Armbruster, U.; Leister, D. PGRL1 Is the Elusive Ferredoxin-Plastoquinone Reductase in Photosynthetic Cyclic Electron Flow. *Mol. Cell* **2013**, *49*, 511–523.

(200) Whitelegge, J. P.; Zhang, H.; Aguilera, R.; Taylor, R. M.; Cramer, W. A. Full Subunit Coverage Liquid Chromatography Electrospray Ionization Mass Spectrometry (LCMS+) of an Oligomeric Membrane Protein: Cytochrome *b(6)f* Complex from Spinach and the Cyanobacterium *Mastigocladus Laminosus*. *Mol. Cell. Proteomics* **2002**, *1*, 816–827.

(201) McKenzie, S. D.; Ibrahim, I. M.; Aryal, U. K.; Puthiyaveetil, S. Stoichiometry of Protein Complexes in Plant Photosynthetic Membranes. *Biochim. Biophys. Acta, Bioenerg.* **2020**, *1861*, 148141 DOI: 10.1016/j.bbabi.2019.148141.

(202) Wikström, M. K. F.; Berden, J. A. Oxidoreduction of Cytochrome *b* in the Presence of Antimycin. *Biochim. Biophys. Acta, Bioenerg.* **1972**, *283*, 403–420.

(203) Trumpower, B. L. Function of the Iron-Sulfur Protein of the Cytochrome *b-C1* Segment in Electron-Transfer and Energy-Conserving Reactions of the Mitochondrial Respiratory Chain. *Biochim. Biophys. Acta, Rev. Bioenerg.* **1981**, *639*, 129–155.

- (204) Wikstrom, M. K.; Saraste, M. The Mitochondrial Respiratory Chain. In *New comprehensive biochemistry*; Elsevier, 1984; pp 49–94.
- (205) Rich, P. R. Mechanisms of Quinol Oxidation in Photosynthesis. *Photosynth. Res.* **1985**, *6*, 335–348.
- (206) Crofts, A. R.; Holland, J. T.; Victoria, D.; Kolling, D. R. J.; Dikanov, S. A.; Gilbreth, R.; Lhee, S.; Kuras, R.; Guergova-Kuras, M. The Q-Cycle Reviewed: How Well Does a Monomeric Mechanism of the Bc_1 Complex Account for the Function of a Dimeric Complex? *Biochim. Biophys. Acta, Bioenerg.* **2008**, *1777*, 1001–1019.
- (207) Crofts, A. R.; Berry, E. A. Structure and Function of the Cytochrome Bc_1 Complex of Mitochondria and Photosynthetic Bacteria. *Curr. Opin. Struct. Biol.* **1998**, *8*, 501–509.
- (208) Iwaki, M.; Yakovlev, G.; Hirst, J.; Osyczka, A.; Dutton, P. L.; Marshall, D.; Rich, P. R. Direct Observation of Redox-Linked Histidine Protonation Changes in the Iron–sulfur Protein of the Cytochrome Bc_1 Complex by ATR-FTIR Spectroscopy. *Biochemistry* **2005**, *44*, 4230–4237.
- (209) Cramer, W. A.; Savikhin, S.; Yan, J.; Yamashita, E. The Enigmatic Chlorophyll a Molecule in the Cytochrome b_6f Complex. In *The Chloroplast*; Springer: Dordrecht, 2010; pp 89–94.
- (210) Cramer, W. A.; Baniulis, D.; Yamashita, E.; Zhang, H.; Zatsman, A. I.; Hendrich, M. P. Cytochrome b_6f Complex, Core Structure, Spectroscopy, and Function of Heme Cn n-Side Electron and Proton Transfer Reactions. *Photosynth. Protein Complexes A Struct. Approach* **2008**, 155–179.
- (211) Baniulis, D.; Yamashita, E.; Zhang, H.; Hasan, S. S.; Cramer, W. A. Structure-Function of the Cytochrome b_6f Complex. *Photochem. Photobiol.* **2008**, *84*, 1349–1358.
- (212) Nitschke, W.; van Lis, R.; Schoepp-Cothenet, B.; Baymann, F. The “Green” Phylogenetic Clade of Rieske/Cytb Complexes. *Photosynth. Res.* **2010**, *104*, 347–355.
- (213) Kallas, T. Cytochrome b_6f Complex at the Heart of Energy Transduction and Redox Signaling. In *Photosynthesis*; Springer: Dordrecht, 2012; pp 501–560.
- (214) Dibrova, D. V.; Cherepanov, D. A.; Galperin, M. Y.; Skulachev, V. P.; Mulkidjanian, A. Y. Evolution of Cytochrome Bc Complexes: From Membrane-Anchored Dehydrogenases of Ancient Bacteria to Triggers of Apoptosis in Vertebrates. *Biochim. Biophys. Acta, Bioenerg.* **2013**, *1827*, 1407–1427.
- (215) Ten Brink, F.; Schoepp-Cothenet, B.; Van Lis, R.; Nitschke, W.; Baymann, F. Multiple Rieske/Cytb Complexes in a Single Organism. *Biochim. Biophys. Acta, Bioenerg.* **2013**, *1827*, 1392–1406.
- (216) Cramer, W. A.; Hasan, S. S.; Yamashita, E. The Q Cycle of Cytochrome Bc Complexes: A Structure Perspective. *Biochim. Biophys. Acta, Bioenerg.* **2011**, *1807*, 788–802.
- (217) Joliot, P.; Joliot, A. Mechanism of Electron Transfer in the Cytochrome b/f Complex of Algae: Evidence for a Semiquinone Cycle. *Proc. Natl. Acad. Sci. U. S. A.* **1994**, *91*, 1034–1038.
- (218) Kramer, D. M.; Crofts, A. R. Re-Examination of the Properties and Function of the b Cytochromes of the Thylakoid Cytochrome Bf Complex. *Biochim. Biophys. Acta, Bioenerg.* **1994**, *1184*, 193–201.
- (219) Deniau, C.; Rappaport, F. New Insights on the Proton Pump Associated with Cytochrome b_6f Turnovers from the Study of H/D Substitution Effects on the Electrostaticity and Electron Transfer Reactions. *Biochemistry* **2000**, *39*, 3304–3310.
- (220) Kramer, D. M.; Crofts, A. R. The Concerted Reduction of the High- and Low-Potential Chains of the Bf Complex by Plastoquinol. *Biochim. Biophys. Acta, Bioenerg.* **1993**, *1183*, 72–84.
- (221) Finazzi, G.; Rappaport, F.; Furia, A.; Fleischmann, M.; Rochaix, J.-D.; Zito, F.; Forti, G. Involvement of State Transitions in the Switch between Linear and Cyclic Electron Flow in *Chlamydomonas Reinhardtii*. *EMBO Rep.* **2002**, *3*, 280–285.
- (222) Böhme, H.; Cramer, W. A. Uncoupler-Dependent Decrease in Midpoint Potential of the Chloroplast Cytochrome B6. *Biochim. Biophys. Acta, Bioenerg.* **1973**, *325*, 275–283.
- (223) Sacksteder, C. A.; Kanazawa, A.; Jacoby, M. E.; Kramer, D. M. The Proton to Electron Stoichiometry of Steady-State Photosynthesis in Living Plants: A Proton-Pumping Q Cycle Is Continuously Engaged. *Proc. Natl. Acad. Sci. U. S. A.* **2000**, *97*, 14283–14288.
- (224) Cape, J. L.; Bowman, M. K.; Kramer, D. M. Understanding the Cytochrome Bc Complexes by What They Don't Do. The Q-Cycle at 30. *Trends Plant Sci.* **2006**, *11*, 46–55.
- (225) Schobert, B.; Brown, L. S.; Lanyi, J. K. Crystallographic Structures of the M and N Intermediates of Bacteriorhodopsin: Assembly of a Hydrogen-Bonded Chain of Water Molecules between Asp-96 and the Retinal Schiff Base. *J. Mol. Biol.* **2003**, *330*, 553–570.
- (226) Capitanio, G.; Martino, P. L.; Capitanio, N.; Papa, S. Redox Bohr Effects and the Role of Heme a in the Proton Pump of Bovine Heart Cytochrome c Oxidase. *Biochim. Biophys. Acta, Bioenerg.* **2011**, *1807*, 1287–1294.
- (227) Arnon, D. I.; Allen, M. B.; Whatley, F. R. Photosynthesis by Isolated Chloroplasts. *Nature* **1954**, *174*, 394–396.
- (228) Johnson, G. N. Cyclic Electron Transport in C3 Plants: Fact or Artefact? *J. Exp. Bot.* **2004**, *56*, 407–416.
- (229) Steigmiller, S.; Turina, P.; Gräber, P. The Thermodynamic H⁺/ATP Ratios of the H⁺-ATPsynthases from Chloroplasts and *Escherichia Coli*. *Proc. Natl. Acad. Sci. U. S. A.* **2008**, *105*, 3745–3750.
- (230) Allen, J. F. Photosynthesis of ATP-Electrons, Proton Pumps, Rotors, and Poise. *Cell* **2002**, *110*, 273–276.
- (231) Peltier, G.; Aro, E.-M.; Shikanai, T. NDH-1 and NDH-2 Plastoquinone Reductases in Oxygenic Photosynthesis. *Annu. Rev. Plant Biol.* **2016**, *67*, 55–80.
- (232) Desplats, C.; Mus, F.; Cuiné, S.; Billon, E.; Cournac, L.; Peltier, G. Characterization of Nda2, a Plastoquinone-Reducing Type II NAD(P) H Dehydrogenase in *Chlamydomonas Chloroplasts*. *J. Biol. Chem.* **2009**, *284*, 4148–4157.
- (233) Bendall, D. S.; Manasse, R. S. Cyclic Photophosphorylation and Electron Transport. *Biochim. Biophys. Acta, Bioenerg.* **1995**, *1229*, 23–38.
- (234) Sugimoto, K.; Okegawa, Y.; Tohri, A.; Long, T. A.; Covert, S. F.; Hisabori, T.; Shikanai, T. A Single Amino Acid Alteration in PGR5 Confers Resistance to Antimycin a in Cyclic Electron Transport around PSI. *Plant Cell Physiol.* **2013**, *54*, 1525–1534.
- (235) Munekage, Y.; Hojo, M.; Meurer, J.; Endo, T.; Tasaka, M.; Shikanai, T. PGR5 Is Involved in Cyclic Electron Flow around Photosystem I and Is Essential for Photoprotection in Arabidopsis. *Cell* **2002**, *110*, 361–371.
- (236) DalCorso, G.; Pesaresi, P.; Masiero, S.; Aseeva, E.; Schünemann, D.; Finazzi, G.; Joliot, P.; Barbato, R.; Leister, D. A Complex Containing PGRL1 and PGR5 Is Involved in the Switch between Linear and Cyclic Electron Flow in Arabidopsis. *Cell* **2008**, *132*, 273–285.
- (237) Crane, F. L.; Hatefi, Y.; Lester, R. L.; Widmer, C. Isolation of a Quinone from Beef Heart Mitochondria. *Biochim. Biophys. Acta* **1957**, *25*, 220–221.
- (238) Crane, F. L. Discovery of Ubiquinone (Coenzyme Q) and an Overview of Function. *Mitochondrion* **2007**, *7*, S2–S7.
- (239) Ernster, L.; Lee, I.-Y.; Norling, B.; Persson, B. Studies with Ubiquinone-Depleted Submitochondrial Particles. Essentiality of Ubiquinone for the Interaction of Succinate Dehydrogenase, NADH Dehydrogenase, and Cytochrome B. *Eur. J. Biochem.* **1969**, *9*, 299–310.
- (240) Schoepp-Cothenet, B.; Lieutaud, C.; Baymann, F.; Verméglio, A.; Friedrich, T.; Kramer, D. M.; Nitschke, W. Menaquinone as Pool Quinone in a Purple Bacterium. *Proc. Natl. Acad. Sci. U. S. A.* **2009**, *106*, 8549–8554.
- (241) Nowicka, B.; Kruk, J. Occurrence, Biosynthesis and Function of Isoprenoid Quinones. *Biochim. Biophys. Acta, Bioenerg.* **2010**, *1797*, 1587–1605.
- (242) Rich, P. R.; Harper, R. Partition Coefficients of Quinones and Hydroquinones and Their Relation to Biochemical Reactivity. *FEBS Lett.* **1990**, *269*, 139–144.
- (243) Rich, P. R. Electron and Proton Transfers in Chemical and Biological Quinone Systems. *Faraday Discuss. Chem. Soc.* **1982**, *74*, 349–364.
- (244) Zhu, Z.; Gunner, M. R. Energetics of Quinone-Dependent Electron and Proton Transfers in *Rhodobacter Sphaeroides* Photosynthetic Reaction Centers. *Biochemistry* **2005**, *44*, 82–96.

- (245) Robertson, D. E.; Prince, R. C.; Bowyer, J. R.; Matsuura, K.; Dutton, P. L.; Ohnishi, T. Thermodynamic Properties of the Semiquinone and Its Binding Site in the Ubiquinol-Cytochrome *c* (C2) Oxidoreductase of Respiratory and Photosynthetic Systems. *J. Biol. Chem.* **1984**, *259*, 1758–1763.
- (246) Song, Y.; Buettner, G. R. Thermodynamic and Kinetic Considerations for the Reaction of Semiquinone Radicals to Form Superoxide and Hydrogen Peroxide. *Free Radical Biol. Med.* **2010**, *49*, 919–962.
- (247) Song, Y.; Buettner, G. R.; Parkin, S.; Wagner, B. A.; Robertson, L. W.; Lehmler, H.-J. Chlorination Increases the Persistence of Semiquinone Free Radicals Derived from Polychlorinated Biphenyl Hydroquinones and Quinones. *J. Org. Chem.* **2008**, *73*, 8296–8304.
- (248) Cape, J. L.; Aidasani, D.; Kramer, D. M.; Bowman, M. K. Substrate Redox Potential Controls Superoxide Production Kinetics in the Cytochrome *Bc* Complex. *Biochemistry* **2009**, *48*, 10716–10723.
- (249) Gunner, M. R.; Madeo, J.; Zhu, Z. Modification of Quinone Electrochemistry by the Proteins in the Biological Electron Transfer Chains: Examples from Photosynthetic Reaction Centers. *J. Bioenerg. Biomembr.* **2008**, *40*, 509–519.
- (250) Roginsky, V.; Barsukova, T. Kinetics of Oxidation of Hydroquinones by Molecular Oxygen. Effect of Superoxide Dismutase. *J. Chem. Soc. Perkin Trans. 2* **2000**, *7*, 1575–1582.
- (251) Butler, J.; Hoey, B. M.; Swallow, A. J. Reactions of the Semiquinone Free Radicals of Anti-Tumour Agents with Oxygen and Iron Complexes. *FEBS Lett.* **1985**, *182*, 95–98.
- (252) Dohrmann, J. K.; Bergmann, B. Equilibria and Rates of Redox Reactions Involving the 2-Tert-Butyl-1,4-Benzosemiquinone Radical in Aqueous Solution: An Investigation by Potentiometry, ESR, and Pulse Radiolysis. *J. Phys. Chem.* **1995**, *99*, 1218–1227.
- (253) Valgimigli, L.; Amorati, R.; Funo, M. G.; DiLabio, G. A.; Pedulli, G. F.; Ingold, K. U.; Pratt, D. A. The Unusual Reaction of Semiquinone Radicals with Molecular Oxygen. *J. Org. Chem.* **2008**, *73*, 1830–1841.
- (254) Turrens, J. F.; Alexandre, A.; Lehninger, A. L. Ubisemiquinone Is the Electron Donor for Superoxide Formation by Complex III of Heart Mitochondria. *Arch. Biochem. Biophys.* **1985**, *237*, 408–414.
- (255) Pereverzev, M. O.; Vygodina, T. V.; Konstantinov, A. A.; Skulachev, V. P. Cytochrome *c*, an Ideal Antioxidant. *Biochem. Soc. Trans.* **2003**, *31*, 1312–1315.
- (256) Takahashi, M. A.; Kono, Y.; Asada, K. Reduction of Plastocyanin with O₂⁻ and Superoxide Dismutase-Dependent Oxidation of Plastocyanin by H₂O₂. *Plant Cell Physiol.* **1980**, *21*, 1431–1438.
- (257) Wikström, M.; Krab, K.; Sharma, V. Oxygen Activation and Energy Conservation by Cytochrome *c* Oxidase. *Chem. Rev.* **2018**, *118*, 2469–2490.
- (258) Pietras, R.; Sarewicz, M.; Osyczka, A. Distinct Properties of Semiquinone Species Detected at the Ubiquinol Oxidation Q_o Site of Cytochrome *bc₁* and Their Mechanistic Implications. *J. R. Soc., Interface* **2016**, *13*, 1–11.
- (259) Osyczka, A.; Moser, C. C.; Dutton, P. L. Fixing the Q Cycle. *Trends Biochem. Sci.* **2005**, *30*, 176–182.
- (260) Ding, H.; Moser, C. C.; Robertson, D. E.; Tokito, M. K.; Daldal, F.; Dutton, P. L. Ubiquinone Pair in the Q_o Site Central to the Primary Energy Conversion Reactions of Cytochrome *Bc₁* Complex. *Biochemistry* **1995**, *34*, 15979–15996.
- (261) Cape, J. L.; Bowman, M. K.; Kramer, D. M. A Semiquinone Intermediate Generated at the Q_o Site of the Cytochrome *Bc₁* Complex: Importance for the Q-Cycle and Superoxide Production. *Proc. Natl. Acad. Sci. U. S. A.* **2007**, *104*, 7887–7892.
- (262) Zhang, H.; Osyczka, A.; Dutton, P. L.; Moser, C. C. Exposing the Complex III Q_o Semiquinone Radical. *Biochim. Biophys. Acta, Bioenerg.* **2007**, *1767*, 883–887.
- (263) Sarewicz, M.; Dutka, M.; Pintscher, S.; Osyczka, A. Triplet State of the Semiquinone-Rieske Cluster as an Intermediate of Electronic Bifurcation Catalyzed by Cytochrome *Bc₁*. *Biochemistry* **2013**, *52*, 6388–6395.
- (264) Vennam, P. R.; Fisher, N.; Krzyaniak, M. D.; Kramer, D. M.; Bowman, M. K. A Caged, Destabilized, Free Radical Intermediate in the Q-Cycle. *ChemBioChem* **2013**, *14*, 1745–1753.
- (265) Rich, P. R. Electron Transfer Reactions between Quinols and Quinones in Aqueous and Aprotic Media. *Biochim. Biophys. Acta, Bioenerg.* **1981**, *637*, 28–33.
- (266) Kruk, J.; Karpinski, S. An HPLC-Based Method of Estimation of the Total Redox State of Plastoquinone in Chloroplasts, the Size of the Photochemically Active Plastoquinone-Pool and Its Redox State in Thylakoids of Arabidopsis. *Biochim. Biophys. Acta, Bioenerg.* **2006**, *1757*, 1669–1675.
- (267) Block, A.; Fristedt, R.; Rogers, S.; Kumar, J.; Barnes, B.; Barnes, J.; Elowsky, C. G.; Wamboldt, Y.; Mackenzie, S. A.; Redding, K.; Merchant, S. S.; Basset, G. J. Functional Modeling Identifies Paralogous Solanesyl-Diphosphate Synthases That Assemble the Side Chain of Plastoquinone-9 in Plastids. *J. Biol. Chem.* **2013**, *288*, 27594–27606.
- (268) Ksas, B.; Légeret, B.; Ferretti, U.; Chevalier, A.; Pospíšil, P.; Alric, J.; Havaux, M. The Plastoquinone Pool Outside the Thylakoid Membrane Serves in Plant Photoprotection as a Reservoir of Singlet Oxygen Scavengers. *Plant, Cell Environ.* **2018**, *41*, 2277–2287.
- (269) Zbierzak, A. M.; Kanwischer, M.; Wille, C.; Vidi, P. A.; Giavalisco, P.; Lohmann, A.; Briesen, I.; Porfirova, S.; Bréhélin, C.; Kessler, F.; Dörmann, P. Intersection of the Tocopherol and Plastoquinol Metabolic Pathways at the Plastoglobule. *Biochem. J.* **2010**, *425*, 389–399.
- (270) Ksas, B.; Becuwe, N.; Chevalier, A.; Havaux, M. Plant Tolerance to Excess Light Energy and Photooxidative Damage Relies on Plastoquinone Biosynthesis. *Sci. Rep.* **2015**, *5*, 10919.
- (271) Blackwell, M.; Gibas, C.; Gygas, S.; Roman, D.; Wagner, B. The Plastoquinone Diffusion Coefficient in Chloroplasts and Its Mechanistic Implications. *Biochim. Biophys. Acta, Bioenerg.* **1994**, *1183*, 533–543.
- (272) Lavergne, J.; Joliot, P. Restricted Diffusion in Photosynthetic Membranes. *Trends Biochem. Sci.* **1991**, *16*, 129–134.
- (273) Kirchhoff, H. Diffusion of Molecules and Macromolecules in Thylakoid Membranes. *Biochim. Biophys. Acta, Bioenerg.* **2014**, *1837*, 495–502.
- (274) Lemeille, S.; Rochaix, J. D. State Transitions at the Crossroad of Thylakoid Signalling Pathways. *Photosynth. Res.* **2010**, *106*, 33–46.
- (275) Pfannschmidt, T. Chloroplast Redox Signals: How Photosynthesis Controls Its Own Genes. *Trends Plant Sci.* **2003**, *8*, 33–41.
- (276) Lundquist, P. K.; Poliakov, A.; Bhuiyan, N. H.; Zybailov, B.; Sun, Q.; van Wijk, K. J. The Functional Network of the Arabidopsis Plastoglobule Proteome Based on Quantitative Proteomics and Genome-Wide Coexpression Analysis. *Plant Physiol.* **2012**, *158*, 1172–1192.
- (277) Shikanai, T.; Munekage, Y.; Shimizu, K.; Endo, T.; Hashimoto, T. Identification and Characterization of Arabidopsis Mutants with Reduced Quenching of Chlorophyll Fluorescence. *Plant Cell Physiol.* **1999**, *40*, 1134–1142.
- (278) Pralon, T.; Shanmugabalaji, V.; Longoni, P.; Glauser, G.; Ksas, B.; Collombat, J.; Desmeules, S.; Havaux, M.; Finazzi, G.; Kessler, F. Plastoquinone Homeostasis by Arabidopsis Proton Gradient Regulation 6 Is Essential for Photosynthetic Efficiency. *Commun. Biol.* **2019**, *2*, 220.
- (279) Pralon, T.; Collombat, J.; Pipitone, R.; Ksas, B.; Shanmugabalaji, V.; Havaux, M.; Finazzi, G.; Longoni, P.; Kessler, F. Mutation of the Atypical Kinase ABC1K3 Partially Rescues the PROTON GRADIENT REGULATION 6 Phenotype in Arabidopsis Thaliana. *Front. Plant Sci.* **2020**, *11*, 337.
- (280) Lefebvre-Legendre, L.; Rappaport, F.; Finazzi, G.; Ceol, M.; Grivet, C.; Hopfgartner, G.; Rochaix, J. D. Loss of Phylloquinone in Chlamydomonas Affects Plastoquinone Pool Size and Photosystem II Synthesis. *J. Biol. Chem.* **2007**, *282*, 13250–13263.
- (281) Wikstrom, M. K. Proton Pump Coupled to Cytochrome *c* Oxidase in Mitochondria. *Nature* **1977**, *266*, 673–678.
- (282) Haehnel, W.; Pröpper, A.; Krause, H. Evidence for Complexed Plastocyanin as the Immediate Electron Donor of P-700. *Biochim. Biophys. Acta, Bioenerg.* **1980**, *593*, 384–399.

- (283) Hatefi, Y.; Haavik, A. G.; Griffiths, D. E. Studies on the Electron Transfer System: XLI. Reduced Coenzyme Q (QH₂)-Cytochrome c Reductase. *J. Biol. Chem.* **1962**, *237*, 1681–1685.
- (284) Myllykallio, H.; Drepper, F.; Mathis, P.; Daldal, F. Membrane-Anchored Cytochrome *c*₂ Mediated Microsecond Time Range Electron Transfer from the Cytochrome *Bc*₁ Complex to the Reaction Center in *Rhodobacter Capsulatus*. *Biochemistry* **1998**, *37*, 5501–5510.
- (285) Myllykallio, H.; Zannoni, D.; Daldal, F. The Membrane-Attached Electron Carrier Cytochrome *c*₂ from *Rhodobacter Sphaeroides* Is Functional in Respiratory but Not in Photosynthetic Electron Transfer. *Proc. Natl. Acad. Sci. U. S. A.* **1999**, *96*, 4348–4353.
- (286) Cartron, M. L.; Olsen, J. D.; Sener, M.; Jackson, P. J.; Brindley, A. A.; Qian, P.; Dickman, M. J.; Leggett, G. J.; Schulten, K.; Hunter, C. N. Integration of Energy and Electron Transfer Processes in the Photosynthetic Membrane of *Rhodobacter Sphaeroides*. *Biochim. Biophys. Acta, Bioenerg.* **2014**, *1837*, No. e118.
- (287) Ki Ho, K.; Krogmann, D. W. Cytochrome *f* from Spinach and Cyanobacteria. Purification and Characterization. *J. Biol. Chem.* **1980**, *255*, 3855–3861.
- (288) Niwa, S.; Ishikawa, H.; Nikai, S.; Takabe, T. Electron Transfer Reactions between Cytochrome *f* and Plastocyanin from *Brassica Komatsuna*. *J. Biochem.* **1980**, *88*, 1177–1183.
- (289) De La Rosa, M. A.; Navarro, J. A.; Díaz-Quintana, A.; De La Cerda, B.; Molina-Heredia, F. P.; Balme, A.; Murdoch, P. D. S.; Díaz-Moreno, I.; Durán, R. V.; Hervás, M. An Evolutionary Analysis of the Reaction Mechanisms of Photosystem I Reduction by Cytochrome C6 and Plastocyanin. *Bioelectrochemistry* **2002**, *55*, 41–45.
- (290) Molina-Heredia, F. P.; Balme, A.; Hervás, M.; Navarro, J. A.; De la Rosa, M. A. A Comparative Structural and Functional Analysis of Cytochrome CM, Cytochrome C6 and Plastocyanin from the Cyanobacterium *Synechocystis* Sp. PCC 6803. *FEBS Lett.* **2002**, *517*, 50–54.
- (291) Merchant, S.; Bogorad, L. Rapid Degradation of Apoplastocyanin in Cu(II)-Deficient Cells of *Chlamydomonas Reinhardtii*. *J. Biol. Chem.* **1986**, *261*, 15850–15853.
- (292) Gupta, R.; He, Z.; Luan, S. Functional Relationship of Cytochrome C6 and Plastocyanin in *Arabidopsis*. *Nature* **2002**, *417*, 567–571.
- (293) Díaz-Quintana, A.; Navarro, J. A.; Hervás, M.; Molina-Heredia, F. P.; De La Cerda, B.; De La Rosa, M. A. A Comparative Structural and Functional Analysis of Cyanobacterial Plastocyanin and Cytochrome C6 as Alternative Electron Donors to Photosystem I: Photosystem I Reduction in Cyanobacteria. *Photosynth. Res.* **2003**, *75*, 97–110.
- (294) Liu, J.; Chakraborty, S.; Hosseinzadeh, P.; Yu, Y.; Tian, S.; Petrik, I.; Bhagi, A.; Lu, Y. Metalloproteins Containing Cytochrome, Iron-Sulfur, or Copper Redox Centers. *Chem. Rev.* **2014**, *114*, 4366–4369.
- (295) Alvarez-Paggi, D.; Hannibal, L.; Castro, M. A.; Oviedo-Rouco, S.; Demicheli, V.; Tórtora, V.; Tomasina, F.; Radi, R.; Murgida, D. H. Multifunctional Cytochrome *c*: Learning New Tricks from an Old Dog. *Chem. Rev.* **2017**, *117*, 13382–13460.
- (296) Barker, P. D.; Ferguson, S. J. Still a Puzzle: Why Is Haem Covalently Attached in *c*-Type Cytochromes? *Structure* **1999**, *7*, R281.
- (297) Dolla, A.; Blanchard, L.; Guerlesquin, F.; Bruschi, M. The Protein Moiety Modulates the Redox Potential in Cytochromes C. *Biochimie* **1994**, *76*, 471–479.
- (298) Margalit, R.; Schejter, A. Cytochrome *c*: A Thermodynamic Study of the Relationships among Oxidation State, Ion-Binding and Structural Parameters: 1. The Effects of Temperature, PH and Electrostatic Media on the Standard Redox Potential of Cytochrome C. *Eur. J. Biochem.* **1973**, *32*, 492–499.
- (299) Moore, G. R.; Harris, D. E.; Leitch, F. A.; Pettigrew, G. W. Characterisation of Ionisations That Influence the Redox Potential of Mitochondrial Cytochrome *c* and Photosynthetic Bacterial Cytochromes C2. *Biochim. Biophys. Acta, Bioenerg.* **1984**, *764*, 331–342.
- (300) Daldal, F.; Mandaci, S.; Winterstein, C.; Myllykallio, H.; Duyck, K.; Zannoni, D. Mobile Cytochrome C2 and Membrane-Anchored Cytochrome Cy Are Both Efficient Electron Donors to the Cbb3- and Aa3-Type Cytochrome *c* Oxidases during Respiratory Growth of *Rhodobacter Sphaeroides*. *J. Bacteriol.* **2001**, *183*, 2013–2024.
- (301) Howe, C. J.; Schlarb-Ridley, B. G.; Wastl, J.; Purton, S.; Bendall, D. S. The Novel Cytochrome C6 of Chloroplasts: A Case of Evolutionary Bricolage? *J. Exp. Bot.* **2006**, *57*, 13–22.
- (302) D'Arcy, S.; Cell Death, M. A Review of the Major Forms of Apoptosis, Necrosis and Autophagy. *Cell Biol. Int.* **2019**, *43*, 582–592.
- (303) Margoliash, E. Primary Structure and Evolution of Cytochrome C. *Proc. Natl. Acad. Sci. U. S. A.* **1963**, *50*, 672–679.
- (304) Ambler, R. P. Sequence Variability in Bacterial Cytochromes C. *Biochim. Biophys. Acta, Bioenerg.* **1991**, *1058*, 42–47.
- (305) Dickerson, R. E.; Timkovich, R.; Almassy, R. J. The Cytochrome Fold and the Evolution of Bacterial Energy Metabolism. *J. Mol. Biol.* **1976**, *100*, 473–491.
- (306) Latypov, R. F.; Maki, K.; Cheng, H.; Luck, S. D.; Roder, H. Folding Mechanism of Reduced Cytochrome *c*: Equilibrium and Kinetic Properties in the Presence of Carbon Monoxide. *J. Mol. Biol.* **2008**, *383*, 437–453.
- (307) Droghetti, E.; Oellerich, S.; Hildebrandt, P.; Smulevich, G. Heme Coordination States of Unfolded Ferrous Cytochrome C. *Biophys. J.* **2006**, *91*, 3022–3031.
- (308) Urry, D. W. The Heme Chromophore in the Ultraviolet. *J. Biol. Chem.* **1967**, *242*, 4441–4448.
- (309) Brautigam, D. L.; Feinberg, B. A.; Hoffman, B. M.; Margoliash, E.; Peisach, J.; Blumberg, W. E.; Peisach, J.; Blumberg, W. E. Multiple Low Spin Forms of the Cytochrome *c* Ferrihemochrome. *J. Biol. Chem.* **1977**, *252*, 574–582.
- (310) Harbitz, E.; Andersson, K. K. Cytochrome C-554 from *Methylosinus Trichosporium* OB3b; a Protein That Belongs to the Cytochrome C2 Family and Exhibits a HALS-Type EPR Signal. *PLoS One* **2011**, *6*, e22014.
- (311) Tomášková, N.; Varhač, R.; Lysáková, V.; Musatov, A.; Sedláč, E. Peroxidase Activity of Cytochrome *c* in Its Compact State Depends on Dynamics of the Heme Region. *Biochim. Biophys. Acta, Proteins Proteomics* **2018**, *1866*, 1073–1083.
- (312) Ranieri, A.; Bernini, F.; Bortolotti, C. A.; Bonifacio, A.; Sergio, V.; Castellini, E. PH-Dependent Peroxidase Activity of Yeast Cytochrome *c* and Its Triple Mutant Adsorbed on Kaolinite. *Langmuir* **2011**, *27*, 10683–10690.
- (313) Muenzner, J.; Pletneva, E. V. Structural Transformations of Cytochrome *c* upon Interaction with Cardiolipin. *Chem. Phys. Lipids* **2014**, *179*, 57–63.
- (314) Engstrom, G.; Rajagukguk, R.; Saunders, A. J.; Patel, C. N.; Rajagukguk, S.; Merbitz-Zahradnik, T.; Xiao, K.; Pielak, G. J.; Trumpower, B.; Yu, C.-A.; Yu, L.; Durham, B.; Millett, F. Design of a Ruthenium-Labeled Cytochrome *c* Derivative to Study Electron Transfer with the Cytochrome *Bc*₁ Complex. *Biochemistry* **2003**, *42*, 2816–2824.
- (315) Hall, J.; Kriacionas, A.; Knaff, D. B.; Millett, F. The Reaction Domain on *Rhodospirillum Rubrum* Cytochrome *c*₂ and Horse Cytochrome *c* for the *Rhodospirillum Rubrum* Cytochrome *Bc*₁ Complex. *J. Biol. Chem.* **1987**, *262*, 14005–14009.
- (316) Speck, S. H.; Dye, D.; Margoliash, E. Single Catalytic Site Model for the Oxidation of Ferrocycytochrome *c* by Mitochondrial Cytochrome *c* Oxidase. *Proc. Natl. Acad. Sci. U. S. A.* **1984**, *81*, 347–351.
- (317) Yu, C. A.; Yu, L.; King, T. E. Kinetics of Electron Transfer between Cardiac Cytochrome C1 and C. *J. Biol. Chem.* **1973**, *248*, 528–533.
- (318) Güner, S.; Willie, A.; Millett, F.; Caffrey, M. S.; Cusanovich, M. A.; Robertson, D. E.; Knaff, D. B. The Interaction between Cytochrome C2 and the Cytochrome *bc*₁ Complex in the Photosynthetic Purple Bacteria *Rhodobacter Capsulatus* and *Rhodospseudomonas Viridis*. *Biochemistry* **1993**, *32*, 4793–4800.
- (319) Janzon, J.; Eichhorn, A. C.; Ludwig, B.; Malatesta, F. Electron Transfer Kinetics between Soluble Modules of *Paracoccus Denitrificans* Cytochrome C1 and Its Physiological Redox Partners. *Biochim. Biophys. Acta, Bioenerg.* **2008**, *1777*, 250–259.

- (320) Bosshard, H. R.; Wynn, R. M.; Knaff, D. B. Binding Site on *Rhodospirillum Rubrum* Cytochrome c_2 for the *Rhodospirillum Rubrum* Cytochrome Bc_1 Complex. *Biochemistry* **1987**, *26*, 7688–7693.
- (321) Li, J.; Osyczka, A.; Conover, R. C.; Johnson, M. K.; Qin, H.; Daldal, F.; Knaff, D. B. Role of Acidic and Aromatic Amino Acids in *Rhodobacter Capsulatus* Cytochrome c_1 . A Site-Directed Mutagenesis Study. *Biochemistry* **2003**, *42*, 8818–8830.
- (322) Stonehuerner, J.; O'Brien, P.; Geren, L.; Millett, F.; Steidl, J.; Yu, L.; Yun, C.-A. Identification of the Binding Site on Cytochrome c_1 for Cytochrome C. *J. Biol. Chem.* **1985**, *260*, 5392–5398.
- (323) Tian, H.; Sadoski, R.; Zhang, L.; Yu, C.-A.; Yu, L.; Durham, B.; Millett, F. Definition of the Interaction Domain for Cytochrome c on the Cytochrome Bc_1 Complex. *J. Biol. Chem.* **2000**, *275*, 9587–9595.
- (324) Rieder, R.; Bosshard, H. R. Comparison of the Binding Sites on Cytochrome c for Cytochrome c Oxidase, Cytochrome bc_1 , and Cytochrome C1. Differential Acetylation of Lysyl Residues in Free and Complexed Cytochrome C. *J. Biol. Chem.* **1980**, *255*, 4732–4739.
- (325) Ahmed, A. J.; Smith, H. T.; Smith, M. B.; Millett, F. S. Effect of Specific Lysine Modification on the Reduction of Cytochrome c by Succinate-Cytochrome c Reductase. *Biochemistry* **1978**, *17*, 2479–2483.
- (326) Sarewicz, M.; Pietras, R.; Froncisz, W.; Osyczka, A. Reorientation of Cytochrome c_2 upon Interaction with Oppositely Charged Macromolecules Probed by SR EPR: Implications for the Role of Dipole Moment to Facilitate Collisions in Proper Configuration for Electron Transfer. *Metallomics* **2011**, *3*, 404–409.
- (327) Hunte, C.; Solmaz, S.; Lange, C. Electron Transfer between Yeast Cytochrome Bc_1 Complex and Cytochrome c : A Structural Analysis. *Biochim. Biophys. Acta, Bioenerg.* **2002**, *1555*, 21–28.
- (328) Kokhan, O.; Wraight, C. A.; Tajkhorshid, E. The Binding Interface of Cytochrome c and Cytochrome C1 in the bc_1 Complex: Rationalizing the Role of Key Residues. *Biophys. J.* **2010**, *99*, 2647–2656.
- (329) Castellani, M.; Covian, R.; Kleinschroth, T.; Anderka, O.; Ludwig, B.; Trumppower, B. L. Direct Demonstration of Half-of-the-Sites Reactivity in the Dimeric Cytochrome Bc_1 Complex. *J. Biol. Chem.* **2010**, *285*, 502–510.
- (330) Devanathan, S.; Salamon, Z.; Tollin, G.; Fitch, J. C.; Meyer, T. E.; Berry, E. A.; Cusanovich, M. A. Plasmon Waveguide Resonance Spectroscopic Evidence for Differential Binding of Oxidized and Reduced *Rhodobacter Capsulatus* Cytochrome C2 to the Cytochrome bc_1 Complex Mediated by the Conformation of the Rieske Ir. *Biochemistry* **2007**, *46*, 7138–7145.
- (331) Moreno-Beltrán, B.; Díaz-Quintana, A.; González-Arzola, K.; Velázquez-Campoy, A.; De La Rosa, M. A.; Díaz-Moreno, I. Cytochrome C1 Exhibits Two Binding Sites for Cytochrome c in Plants. *Biochim. Biophys. Acta, Bioenerg.* **2014**, *1837*, 1717–1729.
- (332) Pietras, R.; Sarewicz, M.; Osyczka, A. Molecular Organization of Cytochrome c_2 near the Binding Domain of Cytochrome Bc_1 Studied by Electron Spin-Lattice Relaxation Enhancement. *J. Phys. Chem. B* **2014**, *118*, 6634–6643.
- (333) Moreno-Beltrán, B.; Díaz-Moreno, I.; González-Arzola, K.; Guerra-Castellano, A.; Velázquez-Campoy, A.; De La Rosa, M. A.; Díaz-Quintana, A. Respiratory Complexes III and IV Can Each Bind Two Molecules of Cytochrome c at Low Ionic Strength. *FEBS Lett.* **2015**, *589*, 476–483.
- (334) Sarewicz, M.; Borek, A.; Daldal, F.; Froncisz, W.; Osyczka, A. Demonstration of Short-Lived Complexes of Cytochrome c with Cytochrome Bc_1 by EPR Spectroscopy: Implications for the Mechanism of Interprotein Electron Transfer. *J. Biol. Chem.* **2008**, *283*, 24826–24836.
- (335) Carrell, C. J.; Schlarb, B. G.; Bendall, D. S.; Howe, C. J.; Cramer, W. A.; Smith, J. L. Structure of the Soluble Domain of Cytochrome f from the Cyanobacterium *Phormidium Laminosum*. *Biochemistry* **1999**, *38*, 9590–9599.
- (336) Chi, Y.-I.; Huang, L.-S.; Zhang, Z.; Fernández-Velasco, J. G.; Berry, E. A. X-Ray Structure of a Truncated Form of Cytochrome f from *Chlamydomonas Reinhardtii* †, ‡. *Biochemistry* **2000**, *39*, 7689–7701.
- (337) Cramer, W. A.; Martinez, S. E.; Huang, D.; Tae, G. S.; Everly, R. M.; Heymann, J. B.; Cheng, R. H.; Baker, T. S.; Smith, J. L. Structural Aspects of the Cytochrome b_6f Complex; Structure of the Lumen-Side Domain of Cytochrome f . *J. Bioenerg. Biomembr.* **1994**, *26*, 31–47.
- (338) Gong, X. S.; Wen, J. Q.; Fisher, N. E.; Young, S.; Howe, C. J.; Bendall, D. S.; Gray, J. C. The Role of Individual Lysine Residues in the Basic Patch on Turnip Cytochrome f for Electrostatic Interactions with Plastocyanin in Vitro. *Eur. J. Biochem.* **2000**, *267*, 3461–3468.
- (339) Soriano, G. M.; Ponamarev, M. V.; Piskorowski, R. A.; Cramer, W. A. Identification of the Basic Residues of Cytochrome f Responsible for Electrostatic Docking Interactions with Plastocyanin in Vitro: Relevance to the Electron Transfer Reaction in Vivo. *Biochemistry* **1998**, *37*, 15120–15128.
- (340) Soriano, G. M.; Ponamarev, M. V.; Tae, G. S.; Cramer, W. A. Effect of the Interdomain Basic Region of Cytochrome f on Its Redox Reactions in Vivo. *Biochemistry* **1996**, *35*, 14590–14598.
- (341) Albarrán, C.; Navarro, J. A.; De La Rosa, M. A.; Hervás, M. The Specificity in the Interaction between Cytochrome f and Plastocyanin from the Cyanobacterium *Nostoc Sp. PCC 7119* Is Mainly Determined by the Copper Protein. *Biochemistry* **2007**, *46*, 997–1003.
- (342) Schlarb-Ridley, B. G.; Bendall, D. S.; Howe, C. J. Role of Electrostatics in the Interaction between Cytochrome f and Plastocyanin of the Cyanobacterium *Phormidium Laminosum*. *Biochemistry* **2002**, *41*, 3279–3285.
- (343) Bond, C. S.; Bendall, D. S.; Freeman, H. C.; Mitchell Guss, J.; Howe, C. J.; Wagner, M. J.; Wilce, M. C. J. The Structure of Plastocyanin from the Cyanobacterium *Phormidium Laminosum*. *Acta Crystallogr., Sect. D: Biol. Crystallogr.* **1999**, *55*, 414–421.
- (344) Collyer, C. A.; Guss, J. M.; Sugimura, Y.; Yoshizaki, F.; Freeman, H. C. Crystal Structure of Plastocyanin from a Green Alga, *Enteromorpha Prolifera*. *J. Mol. Biol.* **1990**, *211*, 617–632.
- (345) Mitchell Guss, J.; Freeman, H. C. Structure of Oxidized Poplar Plastocyanin at 1.6 Å Resolution. *J. Mol. Biol.* **1983**, *169*, 521–563.
- (346) Schmidt, L.; Christensen, H. E. M.; Harris, P. Structure of Plastocyanin from the Cyanobacterium *Anabaena Variabilis*. *Acta Crystallogr., Sect. D: Biol. Crystallogr.* **2006**, *62*, 1022–1029.
- (347) Díaz-Moreno, I.; Díaz-Quintana, A.; De La Rosa, M. A.; Crowley, P. B.; Ubbink, M. Different Modes of Interaction in Cyanobacterial Complexes of Plastocyanin and Cytochrome f . *Biochemistry* **2005**, *44*, 3176–3183.
- (348) Crowley, P. B.; Otting, G.; Schlarb-Ridley, B. G.; Canters, G. W.; Ubbink, M. Hydrophobic Interactions in a Cyanobacterial Plastocyanin - Cytochrome f Complex. *J. Am. Chem. Soc.* **2001**, *123*, 10444–10453.
- (349) Ubbink, M.; Ejdebäck, M.; Karlsson, B. G.; Bendall, D. S. The Structure of the Complex of Plastocyanin and Cytochrome f , Determined by Paramagnetic NMR and Restrained Rigid-Body Molecular Dynamics. *Structure* **1998**, *6*, 323–335.
- (350) Ueda, T.; Nomoto, N.; Koga, M.; Ogasa, H.; Ogawa, Y.; Matsumoto, M.; Stampoulis, P.; Sode, K.; Terasawa, H.; Shimada, I. Structural Basis of Efficient Electron Transport between Photosynthetic Membrane Proteins and Plastocyanin in Spinach Revealed Using Nuclear Magnetic Resonance. *Plant Cell* **2012**, *24*, 4173–4186.
- (351) Lange, C.; Cornvik, T.; Díaz-Moreno, I.; Ubbink, M. The Transient Complex of Poplar Plastocyanin with Cytochrome f : Effects of Ionic Strength and PH. *Biochim. Biophys. Acta, Bioenerg.* **2005**, *1707*, 179–188.
- (352) Mayneord, G. E.; Vasilev, C.; Malone, L. A.; Swainsbury, D. J. K.; Hunter, C. N.; Johnson, M. P. Single-Molecule Study of Redox Control Involved in Establishing the Spinach Plastocyanin-Cytochrome b_6f Electron Transfer Complex. *Biochim. Biophys. Acta, Bioenerg.* **2019**, *1860*, 591–599.
- (353) Fedorov, V. A.; Kovalenko, I. B.; Khruschev, S. S.; Ustinin, D. M.; Antal, T. K.; Rizinchenko, G. Y.; Rubin, A. B. Comparative Analysis of Plastocyanin–Cytochrome f Complex Formation in Higher Plants, Green Algae and Cyanobacteria. *Physiol. Plant.* **2019**, *166*, 320–335.
- (354) Ramos, S.; Le Sueur, A. L.; Horness, R. E.; Specker, J. T.; Collins, J. A.; Thibodeau, K. E.; Thielges, M. C. Heterogeneous and Highly Dynamic Interface in Plastocyanin-Cytochrome f Complex

Revealed by Site-Specific 2D-IR Spectroscopy. *J. Phys. Chem. B* **2019**, *123*, 2114–2122.

(355) Díaz-Moreno, I.; Díaz-Quintana, A.; De la Rosa, M. A.; Ubbink, M. Structure of the Complex between Plastocyanin and Cytochrome *f* from the Cyanobacterium *Nostoc* Sp. PCC 7119 as Determined by Paramagnetic NMR. The Balance between Electrostatic and Hydrophobic Interactions within the Transient Complex Determines the Relati. *J. Biol. Chem.* **2005**, *280*, 18908–18915.

(356) Crowley, P. B.; Hunter, D. M.; Sato, K.; McFarlane, W.; Dennison, C. The Parsley Plastocyanin-Turnip Cytochrome *f* Complex: A Structurally Distorted but Kinetically Functional Acidic Patch. *Biochem. J.* **2004**, *378*, 45–51.

(357) Gross, E. L.; Rosenberg, I. A Brownian Dynamics Study of the Interaction of Phormidium Cytochrome *f* with Various Cyanobacterial Plastocyanins. *Biophys. J.* **2006**, *90*, 366–380.

(358) Hulsker, R.; Baranova, M. V.; Bullerjahn, G. S.; Ubbink, M. Dynamics in the Transient Complex of Plastocyanin-Cytochrome *f* from *Prochlorothrix Hollandica*. *J. Am. Chem. Soc.* **2008**, *130*, 1985–1991.

(359) Díaz-Moreno, I.; Díaz-Quintana, A.; Díaz-Moreno, S.; Subías, G.; De la Rosa, M. A. Transient Binding of Plastocyanin to Its Physiological Redox Partners Modifies the Copper Site Geometry. *FEBS Lett.* **2006**, *580*, 6187–6194.

(360) Malkin, R.; Knaff, D. B.; Bearden, A. J. The Oxidation-Reduction Potential of Membrane-Bound Chloroplast Plastocyanin and Cytochrome *F*. *Biochim. Biophys. Acta, Bioenerg.* **1973**, *305*, 675–678.

(361) Albarrán, C.; Navarro, J. A.; Molina-Heredia, F. P.; Murdoch, P. D. S.; De La Rosa, M. A.; Hervás, M. Laser Flash-Induced Kinetic Analysis of Cytochrome *f* Oxidation by Wild-Type and Mutant Plastocyanin from the Cyanobacterium *Nostoc* Sp. PCC 7119. *Biochemistry* **2005**, *44*, 11601–11607.

(362) Hope, A. B. Electron Transfers amongst Cytochrome *f*, Plastocyanin and Photosystem I: Kinetics and Mechanisms. *Biochim. Biophys. Acta, Bioenerg.* **2000**, *1456*, 5–26.

(363) Torrado, A.; Ramírez-Moncayo, C.; Navarro, J. A.; Mariscal, V.; Molina-Heredia, F. P. Cytochrome *C6* Is the Main Respiratory and Photosynthetic Soluble Electron Donor in Heterocysts of the Cyanobacterium *Anabaena* Sp. PCC 7120. *Biochim. Biophys. Acta, Bioenerg.* **2019**, *1860*, 60–68.

(364) Magnuson, A.; Cardona, T. Thylakoid Membrane Function in Heterocysts. *Biochim. Biophys. Acta, Bioenerg.* **2016**, *1857*, 309–319.

(365) Beißinger, M.; Sticht, H.; Sutter, M.; Ejchart, A.; Haehnel, W.; Rösch, P. Solution Structure of Cytochrome *C6* from the Thermophilic Cyanobacterium *Synechococcus elongatus*. *EMBO J.* **1998**, *17*, 27–36.

(366) Molina-Heredia, F. P.; Hervás, M.; Navarro, J. A.; De La Rosa, M. A. Cloning and Correct Expression in *Escherichia coli* of the *PetE* and *PetJ* Genes Respectively Encoding Plastocyanin and Cytochrome *C6* from the Cyanobacterium *Anabaena* Sp. PCC 7119. *Biochem. Biophys. Res. Commun.* **1998**, *243*, 302–306.

(367) Crowley, P. B.; Rabe, K. S.; Worrall, J. A. R.; Canters, G. W.; Ubbink, M. The Ternary Complex of Cytochrome *f* and Cytochrome *c*: Identification of a Second Binding Site and Competition for Plastocyanin Binding. *ChemBioChem* **2002**, *3*, 526–533.

(368) Gross, E. L.; Pearson, D. C. Brownian Dynamics Simulations of the Interaction of *Chlamydomonas* Cytochrome *f* with Plastocyanin and Cytochrome *C6*. *Biophys. J.* **2003**, *85*, 2055–2068.

(369) Díaz-Moreno, I.; Hulsker, R.; Skubak, P.; Foerster, J. M.; Cavazzini, D.; Finiguerra, M. G.; Díaz-Quintana, A.; Moreno-Beltrán, B.; Rossi, G. L.; Ullmann, G. M.; Pannu, N. S.; De La Rosa, M. A.; Ubbink, M. The Dynamic Complex of Cytochrome *C6* and Cytochrome *f* Studied with Paramagnetic NMR Spectroscopy. *Biochim. Biophys. Acta, Bioenerg.* **2014**, *1837*, 1305–1315.

(370) Shin, M.; Tagawa, K.; Arnon, D. I. Crystallization of Ferredoxin-Tpn Reductase and Its Role in the Photosynthetic Apparatus of Chloroplasts. *Biochem. Z.* **1963**, *338*, 84–96.

(371) Carrillo, N.; Ceccarelli, E. A. Open Questions in Ferredoxin-NADP⁺ Reductase Catalytic Mechanism. *Eur. J. Biochem.* **2003**, *270*, 1900–1915.

(372) Cassan, N.; Lagoutte, B.; Sétif, P. Ferredoxin-NADP⁺ Reductase: Kinetics of Electron Transfer, Transient Intermediates, and Catalytic Activities Studied by Flash-Absorption Spectroscopy with Isolated Photosystem I and Ferredoxin. *J. Biol. Chem.* **2005**, *280*, 25960–25972.

(373) Moss, D. A.; Bendall, D. S. Cyclic Electron Transport in Chloroplasts. The Q-Cycle and the Site of Action of Antimycin. *Biochim. Biophys. Acta, Bioenerg.* **1984**, *767*, 389–395.

(374) Nawrocki, W. J.; Bailleul, B.; Picot, D.; Cardol, P.; Rappaport, F.; Wollman, F. A.; Joliot, P. The Mechanism of Cyclic Electron Flow. *Biochim. Biophys. Acta, Bioenerg.* **2019**, *1860*, 433–438.

(375) Ravenel, J.; Peltier, G.; Havaux, M. The Cyclic Electron Pathways around Photosystem I in *Chlamydomonas Reinhardtii* as Determined in Vivo by Photoacoustic Measurements of Energy Storage. *Planta* **1994**, *193*, 251–259.

(376) Buchert, F.; Hamon, M.; Gäbelein, P.; Scholz, M.; Hippler, M.; Wollman, F. A. The Labile Interactions of Cyclic Electron Flow Effector Proteins. *J. Biol. Chem.* **2018**, *293*, 17559–17573.

(377) Avenson, T. J.; Cruz, J. A.; Kanazawa, A.; Kramer, D. M. Regulating the Proton Budget of Higher Plant Photosynthesis. *Proc. Natl. Acad. Sci. U. S. A.* **2005**, *102*, 9709–9713.

(378) Kanazawa, A.; Ostendorf, E.; Kohzuma, K.; Hoh, D.; Strand, D. D.; Sato-Cruz, M.; Savage, L.; Cruz, J. A.; Fisher, N.; Froehlich, J. E.; Kramer, D. M. Chloroplast ATP Synthase Modulation of the Thylakoid Proton Motive Force: Implications for Photosystem I and Photosystem II Photoprotection. *Front. Plant Sci.* **2017**, *8*, 1–12.

(379) Livingston, A. K.; Cruz, J. A.; Kohzuma, K.; Dhingra, A.; Kramer, D. M. An Arabidopsis Mutant with High Cyclic Electron Flow around Photosystem I (Hcef) Involving the NADPH dehydrogenase Complex. *Plant Cell* **2010**, *22*, 221–233.

(380) Wang, C.; Takahashi, H.; Shikanai, T. PROTON GRADIENT REGULATION 5 Contributes to Ferredoxin-Dependent Cyclic Phosphorylation in Ruptured Chloroplasts. *Biochim. Biophys. Acta, Bioenerg.* **2018**, *1859*, 1173–1179.

(381) Labs, M.; Rühle, T.; Leister, D. The Antimycin A-Sensitive Pathway of Cyclic Electron Flow: From 1963 to 2015. *Photosynth. Res.* **2016**, *129*, 231–238.

(382) Storti, M.; Alboresi, A.; Gerotto, C.; Aro, E. M.; Finazzi, G.; Morosinotto, T. Role of Cyclic and Pseudo-Cyclic Electron Transport in Response to Dynamic Light Changes in *Physcomitrella patens*. *Plant, Cell Environ.* **2019**, *42*, 1590–1602.

(383) Suorsa, M.; Järvi, S.; Grieco, M.; Nurmi, M.; Pietrzykowska, M.; Rantala, M.; Kangasjärvi, S.; Paakkarinen, V.; Tikkanen, M.; Jansson, S.; Aro, E. M. PROTON GRADIENT REGULATIONS 5 Is Essential for Proper Acclimation of Arabidopsis Photosystem I to Naturally and Artificially Fluctuating Light Conditions. *Plant Cell* **2012**, *24*, 2934–2948.

(384) Suorsa, M.; Rossi, F.; Tadini, L.; Labs, M.; Colombo, M.; Jahns, P.; Kater, M. M. M.; Leister, D.; Finazzi, G.; Aro, E. M.; Barbato, R.; Pesaresi, P. PGR5-PGRL1-Dependent Cyclic Electron Transport Modulates Linear Electron Transport Rate in Arabidopsis *Thaliana*. *Mol. Plant* **2016**, *9*, 271–288.

(385) Yamamoto, H.; Shikanai, T. PGR5-Dependent Cyclic Electron Flow Protects Photosystem I under Fluctuating Light at Donor and Acceptor Sides. *Plant Physiol.* **2019**, *179*, 588–600.

(386) Nandha, B.; Finazzi, G.; Joliot, P.; Hald, S.; Johnson, G. N. The Role of PGR5 in the Redox Poising of Photosynthetic Electron Transport. *Biochim. Biophys. Acta, Bioenerg.* **2007**, *1767*, 1252–1259.

(387) Nawrocki, W. J.; Bailleul, B.; Cardol, P.; Rappaport, F.; Wollman, F. A.; Joliot, P. Maximal Cyclic Electron Flow Rate Is Independent of PGRL1 in *Chlamydomonas*. *Biochim. Biophys. Acta, Bioenerg.* **2019**, *1860*, 425–432.

(388) Buchert, F.; Hippler, M. Cytochrome *b₆f* Complex Inhibition by Antimycin-A Requires Stt7 Kinase Activation but Not PGR5. *bioRxiv* **2020**, 1.

(389) Hanke, G.; Mulo, P. Plant Type Ferredoxins and Ferredoxin-Dependent Metabolism. *Plant, Cell Environ.* **2013**, *36*, 1071–1084.

- (390) Cassier-Chauvat, C.; Chauvat, F. Function and Regulation of Ferredoxins in the Cyanobacterium, *Synechocystis* PCC6803: Recent Advances. *Life* **2014**, *4*, 666–680.
- (391) Hanke, G. T.; Kimata-Arigo, Y.; Taniguchi, I.; Hase, T. A Post Genomic Characterization of Arabidopsis Ferredoxins. *Plant Physiol.* **2004**, *134*, 255–264.
- (392) Hase, T.; Kimata, Y.; Yonekura, K.; Matsumura, T.; Sakakibara, H. Molecular Cloning and Differential Expression of the Maize Ferredoxin Gene Family. *Plant Physiol.* **1991**, *96*, 77–83.
- (393) Matsumura, T.; Sakakibara, H.; Nakano, R.; Kimata, Y.; Sugiyama, T.; Hase, T. A Nitrate-Inducible Ferredoxin in Maize Roots: Genomic Organization and Differential Expression of Two Non-photosynthetic Ferredoxin Isoforms. *Plant Physiol.* **1997**, *114*, 653–660.
- (394) Razquin, P.; Schmitz, S.; Peleato, M. L.; Fillat, M. F.; Gómez-Moreno, C.; Böhme, H. Differential Activities of Heterocyst Ferredoxin, Vegetative Cell Ferredoxin, and Flavodoxin as Electron Carriers in Nitrogen Fixation and Photosynthesis in *Anabaena* Sp. *Photosynth. Res.* **1995**, *43*, 35–40.
- (395) Terauchi, A. M.; Lu, S. F.; Zaffagnini, M.; Tappa, S.; Hirasawa, M.; Tripathy, J. N.; Knaff, D. B.; Farmer, P. J.; Lemaire, S. D.; Hase, T.; Merchant, S. S. Pattern of Expression and Substrate Specificity of Chloroplast Ferredoxins from *Chlamydomonas Reinhardtii*. *J. Biol. Chem.* **2009**, *284*, 25867–25878.
- (396) Goss, T.; Hanke, G. The End of the Line: Can Ferredoxin and Ferredoxin NADP(H) Oxidoreductase Determine the Fate of Photosynthetic Electrons? *Curr. Protein Pept. Sci.* **2014**, *15*, 385–393.
- (397) Matsumura, T.; Kimata-Arigo, Y.; Sakakibara, H.; Sugiyama, T.; Murata, H.; Takao, T.; Shimonishi, Y.; Hase, T. Complementary DNA Cloning and Characterization of Ferredoxin Localized in Bundle-Sheath Cells of Maize Leaves. *Plant Physiol.* **1999**, *119*, 481–488.
- (398) Kimata-Arigo, Y.; Matsumura, T.; Kada, S.; Fujimoto, H.; Fujita, Y.; Endo, T.; Mano, J.; Sato, F.; Hase, T. Differential Electron Flow around Photosystem I by Two C₄-Photosynthetic-Cell-Specific Ferredoxins. *EMBO J.* **2000**, *19*, 5041–5050.
- (399) Dutton, J. E.; Rogers, L. J.; Haslett, B. G.; Takruri, I. A. H.; Gleaves, J. T.; Boulter, D. Comparative Studies on the Properties of Two Ferredoxins from *Pisum Sativum* L. *J. Exp. Bot.* **1980**, *31*, 379–391.
- (400) Kristin, M. S.; Akulova, E. A. Two Forms of Pea Leaf Ferredoxin. *Biokhimiia* **1976**, *41*, 500–505.
- (401) Peltier, J.-B.; Friso, G.; Kalume, D. E.; Roepstorff, P.; Nilsson, F.; Adamska, I.; van Wijk, K. J. Proteomics of the Chloroplast: Systematic Identification and Targeting Analysis of Lumenal and Peripheral Thylakoid Proteins. *Plant Cell* **2000**, *12*, 319–341.
- (402) Blanco, N. E.; Ceccoli, R. D.; Dalla Via, M. V.; Voss, I.; Segretin, M. E.; Bravo-Almonacid, F. F.; Melzer, M.; Hajirezaei, M. R.; Scheibe, R.; Hanke, G. T. Expression of the Minor Isoform Pea Ferredoxin in Tobacco Alters Photosynthetic Electron Partitioning and Enhances Cyclic Electron Flow. *Plant Physiol.* **2013**, *161*, 866–879.
- (403) Arnon, D. I.; Chain, R. K. Regulation of Ferredoxin-Catalyzed Photosynthetic Phosphorylations (Photophosphorylation/Photosynthesis/Energy Conversion). *Proc. Natl. Acad. Sci. U. S. A.* **1975**, *72*, 4961–4965.
- (404) Cox, R. P. Chloroplast Cytochrome B-563, Hydrophobic Environment and Lack of Direct Reaction with Ferredoxin. *Biochem. J.* **1979**, *184*, 39–44.
- (405) Hase, T.; Schürmann, P.; Knaff, D. B. The Interaction of Ferredoxin with Ferredoxin-Dependent Enzymes. In *Photosystem I*; Golbeck, J., Ed.; Springer Netherlands: Dordrecht, 2007; pp 477–498.
- (406) Hurley, J. K.; Hazzard, J. T.; Martínez-Júlvez, M.; Medina, M.; Gómez-Moreno, C.; Tollin, G. Electrostatic Forces Involved in Orienting *Anabaena* Ferredoxin during Binding to *Anabaena* Ferredoxin:NADP + Reductase: Site-Specific Mutagenesis, Transient Kinetic Measurements, and Electrostatic Surface Potentials. *Protein Sci.* **1999**, *8*, 1614–1622.
- (407) Schmitz, S.; Martínez-Júlvez, M.; Gómez-Moreno, C.; Böhme, H. Interaction of Positively Charged Amino Acid Residues of Recombinant, Cyanobacterial Ferredoxin:NADP+ Reductase with Ferredoxin Probed by Site Directed Mutagenesis. *Biochim. Biophys. Acta, Bioenerg.* **1998**, *1363*, 85–93.
- (408) Van Thor, J. J.; Jeanjean, R.; Havaux, M.; Sjollem, K. A.; Joset, F.; Hellingwerf, K. J.; Matthijs, H. C. P. Salt Shock-Inducible Photosystem I Cyclic Electron Transfer in *Synechocystis* PCC6803 Relies on Binding of Ferredoxin:NADP+ Reductase to the Thylakoid Membranes via Its CpcD Phycobilisome-Linker Homologous N-Terminal Domain. *Biochim. Biophys. Acta, Bioenerg.* **2000**, *1457*, 129–144.
- (409) Twachtman, M.; Altmann, B.; Muraki, N.; Voss, I.; Okutani, S.; Kurisu, G.; Hase, T.; Hanke, G. T. N-Terminal Structure of Maize Ferredoxin:NADP+ Reductase Determines Recruitment into Different Thylakoid Membrane Complexes. *Plant Cell* **2012**, *24*, 2979–2991.
- (410) Joliot, P.; Johnson, G. N. Regulation of Cyclic and Linear Electron Flow in Higher Plants. *Proc. Natl. Acad. Sci. U. S. A.* **2011**, *108*, 13317–13322.
- (411) Mosebach, L.; Heilmann, C.; Mutoh, R.; Gäbelein, P.; Steinbeck, J.; Happe, T.; Ikegami, T.; Hanke, G.; Kurisu, G.; Hippler, M. Association of Ferredoxin:NADP+ Oxidoreductase with the Photosynthetic Apparatus Modulates Electron Transfer in *Chlamydomonas Reinhardtii*. *Photosynth. Res.* **2017**, *134*, 291–306.
- (412) Cleland, R. E.; Bendall, D. S. Photosystem I Cyclic Electron Transport: Measurement of Ferredoxin-Plastoquinone Reductase Activity. *Photosynth. Res.* **1992**, *34*, 409–418.
- (413) Mills, J. D.; Crowther, D.; Slovacek, R. E.; Hind, G.; McCarty, R. E. Electron Transport Pathways in Spinach Chloroplasts. Reduction of the Primary Acceptor of Photosystem II by Reduced Nicotinamide Adenine Dinucleotide Phosphate in the Dark. *Biochim. Biophys. Acta, Bioenerg.* **1979**, *547*, 127–137.
- (414) Shahak, Y.; Crowther, D.; Hind, G. The Involvement of Ferredoxin-NADP+ Reductase in Cyclic Electron Transport in Chloroplasts. *Biochim. Biophys. Acta, Bioenerg.* **1981**, *636*, 234–243.
- (415) Ye, J. Y.; Wang, Y. J. The Involvement of Ferredoxin-NADP Reductase in the Photosynthetic Cyclic Electron Transport. *Sheng Wu Hua Xue Yu Sheng Wu Wu Li Xue Bao (Shanghai)* **1997**, *29*, 40–45.
- (416) Hosler, J. P.; Yocum, C. F. Evidence for Two Cyclic Photophosphorylation Reactions Concurrent with Ferredoxin-Catalyzed Non-Cyclic Electron Transport. *Biochim. Biophys. Acta, Bioenerg.* **1985**, *808*, 21–31.
- (417) Hosler, J. P.; Yocum, C. F. Heparin Inhibition of Ferredoxin-NADP Reductase in Chloroplast Thylakoid Membranes. *Arch. Biochem. Biophys.* **1985**, *236*, 473–478.
- (418) Böhme, H. On the Role of Ferredoxin and Ferredoxin-NADP+ Reductase in Cyclic Electron Transport of Spinach Chloroplasts. *Eur. J. Biochem.* **1977**, *72*, 283–289.
- (419) Szymańska, R.; Dłuzewska, J.; Slesak, I.; Kruk, J. Ferredoxin:NADP + Oxidoreductase Bound to Cytochrome *b₆f* Complex Is Active in Plastoquinone Reduction: Implications for Cyclic Electron Transport. *Physiol. Plant.* **2011**, *141*, 289–298.
- (420) Lintala, M.; Lehtimäki, N.; Benz, J. P.; Jungfer, A.; Soll, J.; Aro, E. M.; Bölder, B.; Mulo, P. Depletion of Leaf-Type Ferredoxin-NADP + Oxidoreductase Results in the Permanent Induction of Photoprotective Mechanisms in Arabidopsis Chloroplasts. *Plant J.* **2012**, *70*, 809–817.
- (421) Clark, R. D.; Hawkesford, M. J.; Coughlan, S. J.; Bennett, J.; Hind, G. Association of Ferredoxin-NADP+ Oxidoreductase with the Chloroplast Cytochrome *b₆f* Complex. *FEBS Lett.* **1984**, *174*, 137–142.
- (422) Okutani, S.; Hanke, G. T.; Satomi, Y.; Takao, T.; Kurisu, G.; Suzuki, A.; Hase, T. Three Maize Leaf Ferredoxin:NADPH Oxidoreductases Vary in Subchloroplast Location, Expression, and Interaction with Ferredoxin. *Plant Physiol.* **2005**, *139*, 1451–1459.
- (423) Benz, J. P.; Stengel, A.; Lintala, M.; Lee, Y. H.; Weber, A.; Philipp, K.; Gügel, I. L.; Kaieda, S.; Ikegami, T.; Mulo, P.; Soll, J.; Bölder, B. Arabidopsis Tic62 and Ferredoxin-NADP(H) Oxidoreductase Form Light-Regulated Complexes That Are Integrated into the Chloroplast Redox Poise. *Plant Cell* **2009**, *21*, 3965–3983.
- (424) Jurić, S.; Hazler-Pilepić, K.; Tomašić, A.; Lepeduš, H.; Jeličić, B.; Puthiyaveetil, S.; Bionda, T.; Vojta, L.; Allen, J. F.; Schleiff, E.; Fulgosi, H. Tethering of Ferredoxin:NADP+ Oxidoreductase to

Thylakoid Membranes Is Mediated by Novel Chloroplast Protein TROL. *Plant J.* **2009**, *60*, 783–794.

(425) Benz, J. P.; Lintala, M.; Soll, J.; Mulo, P.; Bölter, B. A New Concept for Ferredoxin-NADP(H) Oxidoreductase Binding to Plant Thylakoids. *Trends Plant Sci.* **2010**, *15*, 608–613.

(426) Breyton, C.; Nandha, B.; Johnson, G. N.; Joliot, P.; Finazzi, G. Redox Modulation of Cyclic Electron Flow around Photosystem I in C3 Plants. *Biochemistry* **2006**, *45*, 13465–13475.

(427) Faro, M.; Gomez-Moreno, C.; Stankovich, M.; Medina, M. Role of Critical Charged Residues in Reduction Potential Modulation of Ferredoxin-NADP+ Reductase. *Eur. J. Biochem.* **2002**, *269*, 2656–2661.

(428) Corrado, M. E.; Aliverti, A.; Zanetti, G.; Mayhew, S. G. Analysis of the Oxidation-Reduction Potentials of Recombinant Ferredoxin-NADP+ Reductase from Spinach Chloroplasts. *Eur. J. Biochem.* **1996**, *239*, 662–667.

(429) Pueyo, J. J.; Gomez-Moreno, C.; Mayhew, S. G. Oxidation-reduction Potentials of Ferredoxin-NADP+ Reductase and Flavodoxin from Anabaena PCC 7119 and Their Electrostatic and Covalent Complexes. *Eur. J. Biochem.* **1991**, *202*, 1065–1071.

(430) de Lacroix de Lavalette, A.; Barucq, L.; Alric, J.; Rappaport, F.; Zito, F. Is the Redox State of the Ci Heme of the Cytochrome *b₆f* Complex Dependent on the Occupation and Structure of the Qi Site and Vice Versa? *J. Biol. Chem.* **2009**, *284*, 20822–20829.

(431) Joliot, P.; Béal, D.; Joliot, A. Cyclic Electron Flow under Saturating Excitation of Dark-Adapted Arabidopsis Leaves. *Biochim. Biophys. Acta, Bioenerg.* **2004**, *1656*, 166–176.

(432) Deul, D. H.; Thorn, M. B. Effects of 2,3-Dimercaptopropanol and Antimycin on Absorption Spectra of Heart-Muscle Preparations. *Biochim. Biophys. Acta* **1962**, *59*, 426–436.

(433) Slater, E. C.; de Vries, S. Identification of the BAL-Labile Factor. *Nature* **1980**, *288*, 717–718.

(434) Liu, J.; Zhu, X.; Kim, S. J.; Zhang, W. Antimycin-Type Depsipeptides: Discovery, Biosynthesis, Chemical Synthesis, and Bioactivities. *Nat. Prod. Rep.* **2016**, *33*, 1146–1165.

(435) Leben, C.; Keitt, G. W. An Antibiotic Substance Active against Certain Phytopathogens. *Phytopathology* **1948**, *38*, 899–906.

(436) Dunshee, B. R.; Leben, C.; Keitt, G. W.; Strong, F. M. The Isolation and Properties of Antimycin A1. *J. Am. Chem. Soc.* **1949**, *71*, 2436–2437.

(437) Li, H.; Zhu, X. L.; Yang, W. C.; Yang, G. F. Comparative Kinetics of Qi Site Inhibitors of Cytochrome *b_c1* Complex: Picomolar Antimycin and Micromolar Cyazofamid. *Chem. Biol. Drug Des.* **2014**, *83*, 71–80.

(438) Van Ark, G.; Berden, J. A. Binding of HQNO to Beef-Heart Sub-Mitochondrial Particles. *Biochim. Biophys. Acta, Bioenerg.* **1977**, *459*, 119–137.

(439) Gutierrez-Cirlos, E. B.; Merbitz-Zahradnik, T.; Trumpower, B. L. Inhibition of the Yeast Cytochrome *b_c1* Complex by Ilicicolin H, a Novel Inhibitor That Acts at the Qn Site of the *b_c1* Complex. *J. Biol. Chem.* **2004**, *279*, 8708–8714.

(440) de Vries, S.; Berden, J. A.; Slater, E. C. Properties of a Semiquinone Anion Located in the QH2: Cytochrome *c* Oxidoreductase Segment of the Mitochondrial Respiratory Chain. *FEBS Lett.* **1980**, *122*, 143–148.

(441) Rodrigues, T.; Lopes, F.; Moreira, R. Inhibitors of the Mitochondrial Electron Transport Chain and de Novo Pyrimidine Biosynthesis as Antimalarials: The Present Status. *Curr. Med. Chem.* **2010**, *17*, 929–956.

(442) Bolgunas, S.; Clark, D. A.; Hanna, W. S.; Mauvais, P. A.; Pember, S. O. Potent Inhibitors of the Qi Site of the Mitochondrial Respiratory Complex III. *J. Med. Chem.* **2006**, *49*, 4762–4766.

(443) Dickie, J. P.; Loomans, M. E.; Farley, T. M.; Strong, F. M. The Chemistry of Antimycin A. XI. N-Substituted 3-Formamidosalicylic Amides. *J. Med. Chem.* **1963**, *6*, 424–427.

(444) Tokutake, N.; Miyoshi, H.; Nakazato, H.; Iwamura, H. Inhibition of Electron Transport of Rat-Liver Mitochondria by Synthesized Antimycin A Analogs. *Biochim. Biophys. Acta, Bioenerg.* **1993**, *1142*, 262–268.

(445) Hanafi, M.; Shibata, K.; Ueki, M.; Taniguchi, M. UK-2A, B, C and D, Novel Antifungal Antibiotics From *Streptomyces* Sp. 517–02. II. Structural Elucidation. *J. Antibiot.* **1996**, *49*, 1226–1231.

(446) Ueki, M.; Taniguchi, M. The Mode of Action of UK-2A and UK-3A, Novel Antifungal Antibiotics from *Streptomyces* Sp. 517–02. *J. Antibiot.* **1997**, *50*, 1052–1057.

(447) Young, D. H.; Wang, N. X.; Meyer, S. T.; Avila-Adame, C. Characterization of the Mechanism of Action of the Fungicide Fenpicoxamid and Its Metabolite UK-2A. *Pest Manage. Sci.* **2018**, *74*, 489–498.

(448) Machida, K.; Takimoto, H.; Miyoshi, H.; Taniguchi, M. UK-2A, B, C and D, Novel Antifungal Antibiotics from *Streptomyces* Sp. 517–02 V. Inhibition Mechanism of Bovine Heart Mitochondrial Cytochrome *b_c1*, by the Novel Antibiotic UK-2A. *J. Antibiot.* **1999**, *52*, 748–753.

(449) Ando, K.; Saeki, T.; Tamura, G.; Arima, K.; Suzuki, S. Funiculosin, a New Antibiotic. I Isolation, Biological and Chemical Properties. *J. Antibiot.* **1969**, *22*, 189–194.

(450) Ando, K.; Matsuura, I.; Nawata, Y.; Endo, H.; Sasaki, H.; Okyotomi, T.; Saehi, T.; Tamura, G. Funiculosin, a New Antibiotic. II: Structure Elucidation and Antifungal Activity. *J. Antibiot.* **1978**, *31*, 533–538.

(451) Nelson, B. D.; Walter, P.; Ernster, L. Funiculosin: An Antibiotic with Antimycin-like Inhibitory Properties. *Biochim. Biophys. Acta, Bioenerg.* **1977**, *460*, 157–162.

(452) Brasseur, G.; Brivet-Chevillotte, P. Specificities of the Two Center N Inhibitors of Mitochondrial *b_c1* Complex, Antimycin and Funiculosin: Strong Involvement of Cytochrome *b*-Asparagine-208 in Funiculosin Binding. *FEBS Lett.* **1994**, *354*, 23–29.

(453) Ohsumi, K.; Watanabe, M.; Fujie, A. AS2077715 Is a Selective Inhibitor of Fungal Mitochondrial Cytochrome *b_c1* Complex. *J. Antibiot.* **2014**, *67*, 713–716.

(454) Hayakawa, S.; Minato, H.; Katagiri, K. The Ilicicolins, Antibiotics from *Cylindrocladium Ilicicola*. *J. Antibiot.* **1971**, *24*, 653–654.

(455) Junker, B.; Zhang, J.; Mann, Z.; Reddy, J.; Greasham, R. Scale-up Studies on a Defined Medium Process for Pilot Plant Production of Ilicicolin by *Gliocladium Roseum*. *Biotechnol. Prog.* **2001**, *17*, 278–286.

(456) Singh, S. B.; Liu, W.; Li, X.; Chen, T.; Shafiee, A.; Dreikorn, S.; Hornak, V.; Meinz, M.; Onishi, J. C. Structure-Activity Relationship of Cytochrome *b_c1* Reductase Inhibitor Broad Spectrum Antifungal Ilicicolin H. *Bioorg. Med. Chem. Lett.* **2013**, *23*, 3018–3022.

(457) Rotsaert, F. A. J.; Ding, M. G.; Trumpower, B. L. Differential Efficacy of Inhibition of Mitochondrial and Bacterial Cytochrome *b_c1* Complexes by Center N Inhibitors Antimycin, Ilicicolin H and Funiculosin. *Biochim. Biophys. Acta, Bioenerg.* **2008**, *1777*, 211–219.

(458) Kim, J. C.; Lee, Y. W.; Tamura, H.; Yoshizawa, T. Sambutoxin: A New Mycotoxin Isolated from *Fusarium Sambucinum*. *Tetrahedron Lett.* **1995**, *36*, 1047–1050.

(459) Kawai, K.; Suzuki, T.; Kitagawa, A.; Kim, J. C.; Lee, Y. W. A Novel Respiratory Chain Inhibitor, Sambutoxin from *Fusarium Sambucinum*. In *Cereal Research Communications*; 1997; pp 325–326.

(460) Kim, J. C.; Lee, Y. W.; Yu, S. H. Sambutoxin-Producing Isolates of *Fusarium* Species and Occurrence of Sambutoxin in Rotten Potato Tubers. *Appl. Environ. Microbiol.* **1995**, *61*, 3750–3751.

(461) Sakai, K.; Unten, Y.; Iwatsuki, M.; Matsuo, H.; Fukasawa, W.; Hirose, T.; Chinen, T.; Nonaka, K.; Nakashima, T.; Sunazuka, T.; Usui, T.; Murai, M.; Miyoshi, H.; Asami, Y.; Omura, S.; Shiomi, K. Fusaramin, an Antimitochondrial Compound Produced by *Fusarium* Sp., Discovered Using Multidrug-Sensitive *Saccharomyces Cerevisiae*. *J. Antibiot.* **2019**, *72*, 645–652.

(462) Capper, M. J.; O'Neill, P. M.; Fisher, N.; Strange, R. W.; Moss, D.; Ward, S. A.; Berry, N. G.; Lawrenson, A. S.; Hasnain, S. S.; Biagini, G. A.; Antonyuk, S. V. Antimalarial 4(1H)-Pyridones Bind to the Qi Site of Cytochrome *b_c1*. *Proc. Natl. Acad. Sci. U. S. A.* **2015**, *112*, 755–760.

(463) McPhillie, M.; Zhou, Y.; El Bissati, K.; Dubey, J.; Lorenzi, H.; Capper, M.; Lukens, A. K.; Hickman, M.; Muench, S.; Verma, S. K.; Weber, C. R.; Wheeler, K.; Gordon, J.; Sanders, J.; Moulton, H.; Wang,

- K.; Kim, T. K.; He, Y.; Santos, T.; Woods, S.; Lee, P.; Donkin, D.; Kim, E.; Fraczek, L.; Lykins, J.; Esaa, F.; Alibana-Clouser, F.; Dovgin, S.; Weiss, L.; Brasseur, G.; Wirth, D.; Kent, M.; Hood, L.; Meunier, B.; Roberts, C. W.; Hasnain, S. S.; Antonyuk, S. V.; Fishwick, C.; McLeod, R. New Paradigms for Understanding and Step Changes in Treating Active and Chronic, Persistent Apicomplexan Infections. *Sci. Rep.* **2016**, *6*, 1–23.
- (464) Inoue, Y.; Ishizuka, K.; Mitsui, S. Inhibition of Respiration of Yeast by Photosynthesis Inhibiting Herbicides. *Agric. Biol. Chem.* **1967**, *31*, 422–427.
- (465) di Rago, J. P.; Colson, A.-M. Molecular Basis for Resistance to Antimycin and Diuron, Q₂-Cycle Inhibitors Acting at the Q_i Site in the Mitochondrial Ubiquinol-Cytochrome c Reductase in *Saccharomyces Cerevisiae*. *J. Biol. Chem.* **1988**, *263*, 12564–12570.
- (466) Weber, S.; Wolf, K. Two Changes of the Same Nucleotide Confer Resistance to Diuron and Antimycin in the Mitochondrial Cytochrome *b* Gene of *Schizosaccharomyces Pombe*. *FEBS Lett.* **1988**, *237*, 31–34.
- (467) Convent, B.; Briquet, M. Properties of 3-(3,4-Dichlorophenyl)-1,1-Dimethylurea and Other Inhibitors of the Cytochrome *b_e* Segment of the Mitochondrial Respiratory Chain in *Saccharomyces Cerevisiae*. *Eur. J. Biochem.* **1978**, *82*, 473–481.
- (468) Zhu, X.; Zhang, M.; Liu, J.; Ge, J.; Yang, G. Ametocetradin Is a Potent Q_o Site Inhibitor of the Mitochondrial Respiration Complex III. *J. Agric. Food Chem.* **2015**, *63*, 3377–3386.
- (469) Fontaine, S.; Remuson, F.; Caddoux, L.; Barrès, B. Investigation of the Sensitivity of *Plasmopara Viticola* to Amisulbrom and Ametocetradin in French Vineyards Using Bioassays and Molecular Tools. *Pest Manage. Sci.* **2019**, *75*, 2115–2123.
- (470) Mitani, S.; Araki, S.; Takii, Y.; Ohshima, T.; Matsuo, N.; Miyoshi, H. The Biochemical Mode of Action of the Novel Selective Fungicide Cyazofamid: Specific Inhibition of Mitochondrial Complex III in *Phythium Spinosum*. *Pestic. Biochem. Physiol.* **2001**, *71*, 107–115.
- (471) Kunze, B.; Kemmer, T.; Höfle, G.; Reichenbach, H. Stigmatellin, a New Antibiotic from *Stigmatella Aurantiaca* (Myxobacteriales): I. Production, Physico-Chemical and Biological Properties. *J. Antibiot.* **1984**, *37*, 454–461.
- (472) Ohnishi, T.; Brandt, U.; von Jagow, G. Studies on the Effect of Stigmatellin Derivative on Cytochrome Band the Rieske Iron-sulfur Cluster of Cytochrome *c* Reductase from Bovine Heart Mitochondria. *Eur. J. Biochem.* **1988**, *176*, 385–389.
- (473) Lancaster, C. R. D.; Hunte, C.; Kelley, J., III; Trumpower, B. L.; Ditchfield, R. A Comparison of Stigmatellin Conformations, Free and Bound to the Photosynthetic Reaction Center and the Cytochrome *B_{c1}* Complex. *J. Mol. Biol.* **2007**, *368*, 197–208.
- (474) Esser, L.; Yu, C.-A.; Xia, D. Structural Basis of Resistance to Anti-Cytochrome *B_{c1}* Complex Inhibitors: Implication for Drug Improvement. *Curr. Pharm. Des.* **2014**, *20*, 704–724.
- (475) Hope, A. B.; Valente, P. Inhibitor Binding to Isolated Chloroplast Cytochrome *B_f* Complex. *Photosynth. Res.* **1996**, *49*, 37–48.
- (476) Fry, M.; Pudney, M. Site of Action of the Antimalarial Hydroxynaphthoquinone, 2-[Trans-4-(4'-Chlorophenyl) Cyclohexyl]-3-Hydroxy-1,4-Naphthoquinone (566C80). *Biochem. Pharmacol.* **1992**, *43*, 1545–1553.
- (477) Dike, S. Y.; Singh, D.; Thankachen, B. N.; Sharma, B.; Mathur, P. K.; Kore, S.; Kumar, A. A Single-Pot Synthesis of Atovaquone: An Antiparasitic Drug of Choice. *Org. Process Res. Dev.* **2014**, *18*, 618–625.
- (478) Siregar, J. E.; Kurisu, G.; Kobayashi, T.; Matsuzaki, M.; Sakamoto, K.; Mi-ichi, F.; Watanabe, Y.; Hirai, M.; Matsuo, H.; Syafruddin, D.; Marzuki, S.; Kita, K. Direct Evidence for the Atovaquone Action on the Plasmodium Cytochrome *b_{c1}* Complex. *Parasitol. Int.* **2015**, *64*, 295–300.
- (479) Kessel, J. J.; Lange, B. B.; Merbitz-Zahradnik, T.; Zwicker, K.; Hill, P.; Meunier, B.; Pálsdóttir, H.; Hunte, C.; Meshnick, S.; Trumpower, B. L. Molecular Basis for Atovaquone Binding to the Cytochrome *B_{c1}* Complex. *J. Biol. Chem.* **2003**, *278*, 31312–31318.
- (480) Nilsen, A.; LaCrue, A. N.; White, K. L.; Forquer, I. P.; Cross, R. M.; Marfurt, J.; Mather, M. W.; Delves, M. J.; Shackelford, D. M.; Saenz, F. E.; Morrisey, J. M.; Steuten, J.; Mutka, T.; Li, Y.; Wirjanata, G.; Ryan, E.; Duffy, S.; Kelly, J. X.; Sebayang, B. F.; Zeeman, A. M.; Noviyanti, R.; Sinden, R. E.; Kocken, C. H. M.; Price, R. N.; Avery, V. M.; Angulo-Barturen, I.; Jiménez-Díaz, M. B.; Ferrer, S.; Herreros, E.; Sanz, L. M.; Gamo, F. J.; Bathurst, I.; Burrows, J. N.; Siegl, P.; Guy, R. K.; Winter, R. W.; Vaidya, A. B.; Charman, S. A.; Kyle, D. E.; Manetsch, R.; Riscoe, M. K. Quinolone-3-Diarylethers: A New Class of Antimalarial Drug. *Sci. Transl. Med.* **2013**, *5*, 177ra37.
- (481) Esposti, M. D.; Rotilio, G.; Lenaz, G. Effects of Dibromothymoquinone on the Structure and Function of the Mitochondrial *b_{c1}* Complex. *Biochim. Biophys. Acta, Bioenerg.* **1984**, *767*, 10–20.
- (482) Sarewicz, M.; Bujnowicz, L.; Bhaduri, S.; Singh, S. K.; Cramer, W. A.; Osyczka, A. Metastable Radical State, Nonreactive with Oxygen, Is Inherent to Catalysis by Respiratory and Photosynthetic Cytochromes *B_{c1}/b₆F*. *Proc. Natl. Acad. Sci. U. S. A.* **2017**, *114*, 1323–1328.
- (483) Malkin, R. Redox Properties of the DBMIB-Rieske Iron-Sulfur Complex in Spinach Chloroplast Membranes. *FEBS Lett.* **1981**, *131*, 169–172.
- (484) Yang, F. D.; Yu, L.; Yu, C. A. The Nature of the Inhibition of 4,7-Dioxobenzothiazole Derivatives on Mitochondrial Ubiquinol-Cytochrome *c* Reductase. *J. Biol. Chem.* **1989**, *264*, 891–898.
- (485) Zhang, L.; Snyder, C.; Trumpower, B. L.; Yu, L.; Yu, C. A. Determination of the Binding Rate Constants of Stigmatellin and UHDBT to Bovine Cytochrome *b_{c1}* Complex by Cytochrome C1 Oxidation. *FEBS Lett.* **1999**, *460*, 349–352.
- (486) Trumpower, B. L.; Haggerty, J. G. Inhibition of Electron Transfer in the Cytochrome *B-C1* Segment of the Mitochondrial Respiratory Chain by a Synthetic Analogue of Ubiquinone. *J. Bioenerg. Biomembr.* **1980**, *12*, 151–164.
- (487) Takamiya, K.-I.; Dutton, P. L. Ubiquinone in *Rhodospseudomonas Sphaeroides*. Some Thermodynamic Properties. *Biochim. Biophys. Acta, Bioenerg.* **1979**, *546*, 1–16.
- (488) Zhang, H.; Chobot, S. E.; Osyczka, A.; Wraight, C. A.; Dutton, P. L.; Moser, C. C. Quinone and Non-Quinone Redox Couples in Complex III. *J. Bioenerg. Biomembr.* **2008**, *40*, 493–499.
- (489) Kunze, B.; Jansen, R.; Höfle, G.; Reichenbach, H. Crocacin, a New Electron Transport Inhibitor from *Chondromyces Crocatus* (Myxobacteria). Production, Isolation, Physico-Chemical and Biological Properties. *J. Antibiot.* **1994**, *47*, 881–886.
- (490) Jansen, R.; Washausen, P.; Kunze, B.; Reichenbach, H.; Höfle, G. The Crocacin, Novel Antifungal and Cytotoxic Antibiotics from *Chondromyces Crocatus* and *Chondromyces Pediculatus* (Myxobacteria): Isolation and Structure Elucidation. *Eur. J. Org. Chem.* **1999**, *1999*, 10850–11089.
- (491) Dias, L. C.; De Oliveira, L. G.; Vilcachagua, J. D.; Nigsch, F. Total Synthesis of (+)-Crocacin D. *J. Org. Chem.* **2005**, *70*, 2225–2234.
- (492) Chakraborty, T. K.; Laxman, P. Total Synthesis of (+)-Crocacin A. *Tetrahedron Lett.* **2003**, *44*, 4989–4992.
- (493) Pasqua, A. E.; Ferrari, F. D.; Crawford, J. J.; Whittingham, W. G.; Marquez, R. Synthesis of (+)-Crocacin D and Simplified Bioactive Analogues. *Bioorg. Med. Chem.* **2015**, *23*, 1062–1068.
- (494) Sternberg, J. A.; Geffken, D.; Adams, J. B.; Pöstages, R.; Sternberg, C. G.; Campbell, C. L.; Moberg, W. K. Famoxadone: The Discovery and Optimisation of a New Agricultural Fungicide. *Pest Manage. Sci.* **2001**, *57*, 143–152.
- (495) Esser, L.; Zhou, F.; Zhou, Y.; Xiao, Y.; Tang, W. K.; Yu, C. A.; Qin, Z.; Xia, D. Hydrogen Bonding to the Substrate Is Not Required for Rieske Iron-Sulfur Protein Docking to the Quinol Oxidation Site of Complex III. *J. Biol. Chem.* **2016**, *291*, 25019–25031.
- (496) Zheng, Y. J.; Shapiro, R.; Marshall, W. J.; Jordan, D. B. Synthesis and Structural Analysis of the Active Enantiomer of Famoxadone, a Potent Inhibitor of Cytochrome *b_{c1}*. *Bioorg. Med. Chem. Lett.* **2000**, *10*, 1059–1062.
- (497) Gerth, K.; Irschik, H.; Reichenbach, H.; Trowitzsch, W. Myxothiazol, an Antibiotic from *Myxococcus Fulvus* (Myxobacteriales): I. Cultivation, Isolation, Physico-Chemical and Biological Properties. *J. Antibiot.* **1980**, *33*, 1474–1479.

- (498) Thierbach, G.; Reichenbach, H. Myxothiazol, a New Inhibitor of the Cytochrome b-C1 Segment of the Respiratory Chain. *Biochim. Biophys. Acta, Bioenerg.* **1981**, *638*, 282–289.
- (499) Becker, W. F.; von Jagow, G.; Anke, T.; Steglich, W. Oudemansin, Strobilurin A, Strobilurin B, and Myxothiazol: New Inhibitors of the bc_1 Segment of the Respiratory Chain with an ϵ - β -Methoxyacrylate System as Common Structural Element. *FEBS Lett.* **1981**, *132*, 329–333.
- (500) von Jagow, G.; Ljungdahl, P. O.; Graf, P.; Ohnishi, T.; Trumpower, B. L. An Inhibitor of Mitochondrial Respiration Which Binds to Cytochrome- b and Displaces Quinone from the Iron-Sulfur Protein of the Cytochrome- Bc_1 Complex. *J. Biol. Chem.* **1984**, *259*, 6318–6326.
- (501) Schieferdecker, S.; Exner, T. E.; Gross, H.; Roth, M.; Nett, M. New Myxothiazols from the Predatory Bacterium *Myxococcus Fulvus*. *J. Antibiot.* **2014**, *67*, 519–525.
- (502) Sasse, F.; Böhlendorf, B.; Hermann, M.; Kunze, B.; Forche, E.; Steinmetz, H.; Höfle, G.; Reichenbach, H. Melithiazols, New β -Methoxyacrylate Inhibitors of the Respiratory Chain Isolated from Myxobacteria. Production, Isolation, Physico-Chemical and Biological Properties. *J. Antibiot.* **1999**, *52*, 721–729.
- (503) Ojika, M.; Suzuki, Y.; Tsukamoto, A.; Sakagami, Y.; Fudou, R.; Yoshimura, T.; Yamanaka, S. Cystothiazoles A and B, New Bithiazole-Type Antibiotics from the Myxobacterium *Cystobacter Fuscus*. *J. Antibiot.* **1998**, *51*, 275–281.
- (504) Sasse, F.; Leibold, T.; Kunze, B.; Höfle, G.; Reichenbach, H. Cyrmensins, New β -Methoxyacrylate Inhibitors of the Electron Transport. Production, Isolation, Physico-Chemical and Biological Properties. *J. Antibiot.* **2003**, *56*, 827–831.
- (505) Chakor, N. S.; Dallavalle, S.; Musso, L.; Sardi, P. Synthesis and Evaluation of Structural Requirements for Antifungal Activity of Cyrmensin B₁ Analogues. *Tetrahedron Lett.* **2012**, *53*, 228–231.
- (506) Von Jagow, G.; Gribble, G. W.; Trumpower, B. L. Mucidin and Strobilurin A Are Identical and Inhibit Electron Transfer in the Cytochrome bc_1 Complex of the Mitochondrial Respiratory Chain at the Same Site as Myxothiazol. *Biochemistry* **1986**, *25*, 775–780.
- (507) Anke, T.; Oberwinkler, F.; Steglich, W.; Schramm, G. The Strobilurins - New Antifungal Antibiotics from the Basidiomycete *Strobilurus Tenacellus* (Pers. Ex Fr.) Sing. *J. Antibiot.* **1977**, *30*, 806–810.
- (508) Anke, T.; Hecht, H. J.; Schramm, G.; Steglich, W. Antibiotics from Basidiomycetes. IX Oudemansin, an Antifungal Antibiotic from *Oudemansiella Mucida* (Schradler Ex Fr.) Hoehnel (Agaricales). *J. Antibiot.* **1979**, *32*, 1112–1117.
- (509) Fredenhagen, A.; Kuhn, A.; Cuomo, V.; Giuliano, U.; Strobilurins F, G, H. Three New Antifungal Metabolites from *Bolinea Lutea*: I. Fermentation, Isolation and Biological Activity. *J. Antibiot. (Tokyo)*. **1990**, *43*, 655–660.
- (510) Balba, H. Review of Strobilurin Fungicide Chemicals. *J. Environ. Sci. Health, Part B* **2007**, *42*, 441–451.
- (511) Brandt, U.; Schagger, H.; von Jagow, G. Characterisation of Binding of the Methoxyacrylate Inhibitors to Mitochondrial Cytochrome c Reductase. *Eur. J. Biochem.* **1988**, *173*, 499–506.
- (512) Brandt, U.; Djafarzadeh-Andabili, R. Binding of MOA-Stilbene to the Mitochondrial Cytochrome bc_1 Complex Is Affected by the Protonation State of a Redox-Bohr Group of the “Rieske” Iron-Sulfur Protein. *Biochim. Biophys. Acta, Bioenerg.* **1997**, *1321*, 238–242.
- (513) Nofiani, R.; de Mattos-Shiple, K.; Lebe, K. E.; Han, L. C.; Iqbal, Z.; Bailey, A. M.; Willis, C. L.; Simpson, T. J.; Cox, R. J. Strobilurin Biosynthesis in Basidiomycete Fungi. *Nat. Commun.* **2018**, *9*, 1–11.
- (514) Bartlett, D. W.; Clough, J. M.; Godwin, J. R.; Hall, A. A.; Hamer, M.; Parr-Dobrzanski, B. Review: The Strobilurin Fungicides. *Pest Manage. Sci.* **2002**, *58*, 649–662.
- (515) Arakawa, A.; Kasai, Y.; Yamazaki, K.; Iwahashi, F. Features of Interactions Responsible for Antifungal Activity against Resistant Type Cytochrome bc_1 : A Data-Driven Analysis Based on the Binding Free Energy at the Atomic Level. *PLoS One* **2018**, *13*, 1–16.
- (516) Brown, R. J.; Annis, G.; Casalnuovo, A.; Chan, D.; Shapiro, R.; Marshall, W. J. Synthesis and Properties of Axially-Chiral N-(2,6-Disubstituted)Phenyl Triazolones. *Tetrahedron* **2004**, *60*, 4361–4375.
- (517) Matsuzaki, Y.; Yoshimoto, Y.; Arimori, S.; Kiguchi, S.; Harada, T.; Iwahashi, F. Discovery of Metyltetraprole: Identification of Tetrazolinone Pharmacophore to Overcome QoI Resistance. *Bioorg. Med. Chem.* **2020**, *28*, 115211.
- (518) Takagaki, M.; Ozaki, M.; Fujimoto, S.; Fukumoto, S. Development of a Novel Fungicide, Pyribencarb. *J. Pestic. Sci.* **2014**, *39*, 177–178.
- (519) Huang, L.; Berry, E. A. Famoxadone and Related Inhibitors Bind like Methoxy Acrylate Inhibitors in the Q_o Site of the BC1 Compl and Fix the Rieske Iron-Sulfur Protein in a Position Close to but Distinct from That Seen with Stigmatellin and Other “DISTAL” Q_o Inhibitors, to be published.
- (520) Gallon, J.; Reymond, S.; Cossy, J. Neopeltolide, a New Promising Antitumoral Agent. *C. R. Chim.* **2008**, *11*, 1463–1476.
- (521) Wright, A. E.; Botelho, J. C.; Guzmán, E.; Harmody, D.; Linley, P.; McCarthy, P. J.; Pitts, T. P.; Pomponi, S. A.; Reed, J. K. Neopeltolide, a Macrolide from a Lithistid Sponge of the Family Neopeltidae. *J. Nat. Prod.* **2007**, *70*, 412–416.
- (522) D’Ambrosio, M.; Guerriero, A.; Debitus, C.; Pietra, F. Leucascandrolide A, a New Type of Macrolide: The First Powerfully Bioactive Metabolite of Calcareous Sponges (*Leucascandra Caveolata*, a New Genus from the Coral Sea). *Helv. Chim. Acta* **1996**, *79*, 51–60.
- (523) Ulanovskaya, O. A.; Janjic, J.; Suzuki, M.; Sabharwal, S. S.; Schumacker, P. T.; Kron, S. J.; Kozmin, S. A. Synthesis Enables Identification of the Cellular Target of Leucascandrolide A and Neopeltolide. *Nat. Chem. Biol.* **2008**, *4*, 418–424.
- (524) Zhu, X. L.; Zhang, R.; Wu, Q. Y.; Song, Y. J.; Wang, Y. X.; Yang, J. F.; Yang, G. F. Natural Product Neopeltolide as a Cytochrome bc_1 Complex Inhibitor: Mechanism of Action and Structural Modification. *J. Agric. Food Chem.* **2019**, *67*, 2774–2781.
- (525) Yan, X.; Qin, W.; Sun, L.; Qi, S.; Yang, D.; Qin, Z.; Yuan, H. Study of Inhibitory Effects and Action Mechanism of the Novel Fungicide Pyrimorph against *Phytophthora Capsici*. *J. Agric. Food Chem.* **2010**, *58*, 2720–2725.
- (526) Pang, Z.; Shao, J.; Chen, L.; Lu, X.; Hu, J.; Qin, Z.; Liu, X. Resistance to the Novel Fungicide Pyrimorph in *Phytophthora Capsici*: Risk Assessment and Detection of Point Mutations in Cesa3 That Confer Resistance. *PLoS One* **2013**, *8*, e6513.
- (527) Xiao, Y. M.; Esser, L.; Zhou, F.; Li, C.; Zhou, Y. H.; Yu, C. A.; Qin, Z. H.; Xia, D. Studies on Inhibition of Respiratory Cytochrome bc_1 Complex by the Fungicide Pyrimorph Suggest a Novel Inhibitory Mechanism. *PLoS One* **2014**, *9*, 1–12.
- (528) Vallières, C.; Fisher, N.; Antoine, T.; Al-Helal, M.; Stocks, P.; Berry, N. G.; Lawrenson, A. S.; Ward, S. A.; O’Neill, P. M.; Biagini, G. A.; Meunier, B. HDQ, a Potent Inhibitor of Plasmodium Falciparum Proliferation, Binds to the Quinone Reduction Site of the Cytochrome bc_1 Complex. *Antimicrob. Agents Chemother.* **2012**, *56*, 3739–3747.
- (529) Papa, S.; Izzo, G.; Guerrieri, F. On the Inhibition of the bc_1 Segment on the Mitochondrial Respiratory Chain by Quinone Analogues and Hydroxyquinoline Derivatives. *FEBS Lett.* **1982**, *145*, 93–98.
- (530) Riccio, P.; Bobba, A.; Quagliariello, E. Characterization of [³H]NoHQNo Binding to Purified Complex III. *FEBS Lett.* **1982**, *137*, 222–226.
- (531) Doggett, J. S.; Nilsen, A.; Forquer, I.; Wegmann, K. W.; Jones-Brando, L.; Yolken, R. H.; Bordón, C.; Charman, S. A.; Katneni, K.; Schultz, T.; Burrows, J. N.; Hinrichs, D. J.; Meunier, B.; Carruthers, V. B.; Riscoe, M. K. Endochin-like Quinolones Are Highly Efficacious against Acute and Latent Experimental Toxoplasmosis. *Proc. Natl. Acad. Sci. U. S. A.* **2012**, *109*, 15936–15941.
- (532) Stickle, A. M.; Smilkstein, M. J.; Morrisey, J. M.; Li, Y.; Forquer, I. P.; Kelly, J. X.; Pou, S.; Winter, R. W.; Nilsen, A.; Vaidya, A. B.; Riscoe, M. K. Atovaquone and ELQ-300 Combination Therapy as a Novel Dual-Site Cytochrome bc_1 Inhibition Strategy for Malaria. *Antimicrob. Agents Chemother.* **2016**, *60*, 4853–4859.

- (533) Song, Z.; Iorga, B. I.; Mounkoro, P.; Fisher, N.; Meunier, B. The Antimalarial Compound ELQ-400 Is an Unusual Inhibitor of the bc_1 Complex, Targeting Both Qo and Qi Sites. *FEBS Lett.* **2018**, *592*, 1346–1356.
- (534) Merk, M.; Frechen, T.; Gold, R. E.; Schiffer, H.; Levy, T.; Saramago, J. INITIUM®: A New Innovative Fungicide of a New Chemical Class for the Control of Late Blight and Downy Mildew Diseases. *Acta Hort.* **2011**, *917*, 143–148.
- (535) Fehr, M.; Wolf, A.; Stammler, G. Binding of the Respiratory Chain Inhibitor Ametocradin to the Mitochondrial bc_1 Complex. *Pest Manage. Sci.* **2016**, *72*, 591–602.
- (536) Dreiner, A.; Wolf, A.; Mentzel, T.; Meunier, B.; Fehr, M. The Cytochrome bc_1 Complex Inhibitor Ametocradin Has an Unusual Binding Mode. *Biochim. Biophys. Acta, Bioenerg.* **2018**, *1859*, 567–576.
- (537) Tamura, G.; Takatsuki, A.; Ando, K.; Arima, K.; Suzuki, S. Ascochlorin, A New Antibiotic, Found by Paper-Disc Agar-Diffusion Method. *J. Antibiot.* **1968**, *21*, 539–544.
- (538) Sasaki, H.; Hosokawa, T.; Nawata, Y.; Ando, K. Isolation and Structure of Ascochlorin and Its Analogs. *Agric. Biol. Chem.* **1974**, *38*, 1463–1466.
- (539) Ellestad, G. A.; Evans, R. H.; Kunstmann, M. P. Some New Terpenoid Metabolites from an Unidentified Fusarium Species. *Tetrahedron* **1969**, *25*, 1323–1334.
- (540) Cagnoli-Bellavita, N.; Ceccherelli, P.; Fringuelli, R.; Ribaldi, M. Ascochlorin: A Terpenoid Metabolite from *Acremonium Luzulae*. *Phytochemistry* **1975**, *14*, 807.
- (541) Minato, H.; Katayama, T.; Katagiri, K.; Hayakawa, S. Identification of Illicicolins with Ascochlorin and LL-Z 1272. *J. Antibiot.* **1972**, *25*, 315–316.
- (542) Berry, E. A.; Huang, L.; Lee, D. W.; Daldal, F.; Nagai, K.; Minagawa, N. Ascochlorin Is a Novel, Specific Inhibitor of the Mitochondrial Cytochrome bc_1 Complex. *Biochim. Biophys. Acta, Bioenerg.* **2010**, *1797*, 360–370.
- (543) Mogi, T.; Ui, H.; Shiomi, K.; Omura, S.; Miyoshi, H.; Kita, K. Antibiotics LL-Z1272 Identified as Novel Inhibitors Discriminating Bacterial and Mitochondrial Quinol Oxidases. *Biochim. Biophys. Acta, Bioenerg.* **2009**, *1787*, 129–133.
- (544) Hao, G. F.; Wang, F.; Li, H.; Zhu, X. L.; Yang, W. C.; Huang, L. S.; Wu, J. W.; Berry, E. A.; Yang, G. F. Computational Discovery of Picomolar Qo Site Inhibitors of Cytochrome Bc 1 Complex. *J. Am. Chem. Soc.* **2012**, *134*, 11168–11176.
- (545) Flematti, G. R.; Scaffidi, A.; Dixon, K. W.; Smith, S. M.; Ghisalberti, E. L. Production of the Seed Germination Stimulant Karrikinolide from Combustion of Simple Carbohydrates. *J. Agric. Food Chem.* **2011**, *59*, 1195–1198.
- (546) Chen, C.; Wu, Q. Y.; Shan, L. Y.; Zhang, B.; Verpoort, F.; Yang, G. F. Discovery of Cytochrome bc_1 Complex Inhibitors Inspired by the Natural Product Karrikinolide. *RSC Adv.* **2016**, *6*, 97580–97586.
- (547) Trebst, A. [65] Inhibitors in Electron Flow: Tools for the Functional and Structural Localization of Carriers and Energy Conservation Sites. *Methods Enzymol.* **1980**, *69*, 675–715.
- (548) Delosme, R.; Joliot, P.; Trebst, A. Flash-Induced Oxidation of Cytochrome b-563 in Algae under Anaerobic Conditions: Effect of Dinitrophenylether of Iodonitrothymol. *Biochim. Biophys. Acta, Bioenerg.* **1987**, *893*, 1–6.
- (549) Witt, H. T. Energy Conversion in the Functional Membrane of Photosynthesis. Analysis by Light Pulse and Electric Pulse Methods. The Central Role of the Electric Field. *Biochim. Biophys. Acta, Rev. Bioenerg.* **1979**, *505*, 355–427.
- (550) Bailleul, B.; Cardol, P.; Breyton, C.; Finazzi, G. Electrochromism: A Useful Probe to Study Algal Photosynthesis. *Photosynth. Res.* **2010**, *106*, 179–189.
- (551) Fitzpatrick, D.; Aro, E. M.; Tiwari, A. A commonly used photosynthetic inhibitor fails to block electron flow to photosystem I in intact systems. *Front. Plant Sci.* **2020**, *11*, 382.
- (552) Barbagallo, R. P.; Finazzi, G.; Forti, G. Effects of Inhibitors on the Activity of the Cytochrome b_6/f Complex: Evidence for the Existence of Two Binding Pockets in the Luminal Site. *Biochemistry* **1999**, *38*, 12814–12821.
- (553) Oettmeier, W.; Godde, D.; Kunze, B.; Höfle, G. Stigmatellin. A Dual Type Inhibitor of Photosynthetic Electron Transport. *Biochim. Biophys. Acta, Bioenerg.* **1985**, *807*, 216–219.
- (554) Nitschke, W.; Hauska, G.; Rutherford, A. W. The Inhibition of Quinol Oxidation by Stigmatellin Is Similar in Cytochrome bc_1 and b_6/f Complexes. *Biochim. Biophys. Acta, Bioenerg.* **1989**, *974*, 223–226.
- (555) Breyton, C. Conformational Changes in the Cytochrome b_6/f Complex Induced by Inhibitor Binding. *J. Biol. Chem.* **2000**, *275*, 13195–13201.
- (556) Haehnel, W. In *Bioenergetics of Membranes*; Elsevier: Amsterdam, 1977.
- (557) Roberts, A. G.; Kramer, D. M. Inhibitor “Double Occupancy” in the Qo Pocket of the Chloroplast Cytochrome b_6/f Complex. *Biochemistry* **2001**, *40*, 13407–13412.
- (558) Rich, P. R.; Madgwick, S. A.; Moss, D. A. The Interactions of Duroquinol, DBMIB and NQNO with the Chloroplast Cytochrome Bf Complex. *Biochim. Biophys. Acta, Bioenerg.* **1991**, *1058*, 312–328.
- (559) Surpin, M.; Larkin, R. M.; Chory, J. Signal Transduction between the Chloroplast and the Nucleus. *Plant Cell* **2002**, *14*, S327.
- (560) Nott, A.; Jung, H.-S.; Koussevitzky, S.; Chory, J. Plastid-To-Nucleus Retrograde Signaling. *Annu. Rev. Plant Biol.* **2006**, *57*, 739–759.
- (561) Chi, W.; Sun, X.; Zhang, L. Intracellular Signaling from Plastid to Nucleus. *Annu. Rev. Plant Biol.* **2013**, *64*, 559–582.
- (562) Pfannschmidt, T. Plastidial Retrograde Signalling - a True “Plastid Factor” or Just Metabolite Signatures? *Trends Plant Sci.* **2010**, *15*, 427–435.
- (563) Chan, K. X.; Phua, S. Y.; Crisp, P.; McQuinn, R.; Pogson, B. J. Learning the Languages of the Chloroplast: Retrograde Signaling and Beyond. *Annu. Rev. Plant Biol.* **2016**, *67*, 25–53.
- (564) Jones, R. W.; Whitmarsh, J. Origin of the Electrogenic Reaction in the Chloroplast Cytochrome b/f Complex. *Photobiochem. Photobiophys.* **1985**, *9*, 119–127.
- (565) Joliot, P.; Joliot, A. Proton Pumping and Electron Transfer in the Cytochrome bf Complex of Algae. *Biochim. Biophys. Acta, Bioenerg.* **1986**, *849*, 211–222.
- (566) Jones, R. W.; Whitmarsh, J. Inhibition of Electron Transfer and the Electrogenic Reaction in the Cytochrome bf Complex by 2-n-Nonyl-4-Hydroxyquinoline-N-Oxide (NQNO) and 2,5-Dibromo-3-Methyl-6-Isopropyl-p-Benzoquinone (DBMIB). *Biochim. Biophys. Acta, Bioenerg.* **1988**, *933*, 258–268.
- (567) Rich, P. R.; Madgwick, S. A.; Brown, S.; von Jagow, G.; Brandt, U. MOA-Stilbene: A New Tool for Investigation of the Reactions of the Chloroplast Cytochrome Bf Complex. *Photosynth. Res.* **1992**, *34*, 465–477.
- (568) Brandt, U.; Trumpower, B. The Protonmotive Q Cycle in Mitochondria and Bacteria. *Crit. Rev. Biochem. Mol. Biol.* **1994**, *29*, 165–197.
- (569) Dutton, P. L. Redox Potentiometry: Determination of Midpoint Potentials of Oxidation-Reduction Components of Biological Electron-Transfer Systems. *Methods Enzymol.* **1978**, *54*, 411–435.
- (570) Czaplá, M.; Borek, A.; Sarewicz, M.; Osyczka, A. Enzymatic Activities of Isolated Cytochrome Bc_1 -like Complexes Containing Fused Cytochrome b Subunits with Asymmetrically Inactivated Segments of Electron Transfer Chains. *Biochemistry* **2012**, *51*, 829–835.
- (571) Eddowes, M. J.; Hill, H. A. O. Electrochemistry of Horse Heart Cytochrome C. *J. Am. Chem. Soc.* **1979**, *101*, 4461–4464.
- (572) Shinkarev, V. P.; Wraight, C. A. Intermonomer Electron Transfer in the Bc_1 Complex Dimer Is Controlled by the Energized State and by Impaired Electron Transfer between Low and High Potential Hemes. *FEBS Lett.* **2007**, *581*, 1535–1541.
- (573) Rottenberg, H.; Covian, R.; Trumpower, B. L. Membrane Potential Greatly Enhances Superoxide Generation by the Cytochrome Bc_1 Complex Reconstituted into Phospholipid Vesicles. *J. Biol. Chem.* **2009**, *284*, 19203–19210.
- (574) Quinlan, C. L.; Gerencser, A. A.; Treberg, J. R.; Brand, M. D. The Mechanism of Superoxide Production by the Antimycin-Inhibited Mitochondrial Q-Cycle. *J. Biol. Chem.* **2011**, *286*, 31361–31372.

- (575) Link, T. A. The Role of the “Rieske” Iron Sulfur Protein in the Hydroquinone Oxidation (QP) Site of the Cytochrome b_{c_1} Complex. *FEBS Lett.* **1997**, *412*, 257–264.
- (576) Crofts, A. R.; Hong, S.; Ugulava, N.; Barquera, B.; Gennis, R.; Guergova-Kuras, M.; Berry, E. A. Pathways for Proton Release during Ubihydroquinone Oxidation by the b_{c_1} Complex. *Proc. Natl. Acad. Sci. U. S. A.* **1999**, *96*, 10021–10026.
- (577) Zito, F.; Finazzi, G.; Delosme, R.; Nitschke, W.; Picot, D.; Wollman, F. A. The Q_o Site of Cytochrome b_{c_1} Complexes Controls the Activation of the LHCII Kinase. *EMBO J.* **1999**, *18*, 2961–2969.
- (578) Hagen, W. R.; Hearshen, D. O.; Harding, L. J.; Dunham, W. R. Quantitative Numerical Analysis of g Strain in the EPR of Distributed Systems and Its Importance for Multicenter Metalloproteins. *J. Magn. Reson.* **1985**, *61*, 233–244.
- (579) Ding, H.; Robertson, D. E.; Daldal, F.; Dutton, P. L. Cytochrome B_{c_1} Complex [2Fe-2S] Cluster and Its Interaction with Ubiquinone and Ubihydroquinone at the Q_o Site: A Double-Occupancy Q_o Site Model. *Biochemistry* **1992**, *31*, 3144–3158.
- (580) Osyczka, A.; Zhang, H.; Mathe, C.; Rich, P. R.; Moser, C. C.; Dutton, P. L. Role of the PEWY Glutamate in Hydroquinone-Quinone Oxidation-Reduction Catalysis in the Q_o Site of Cytochrome B_{c_1} . *Biochemistry* **2006**, *45*, 10492–10503.
- (581) Sharp, R. E.; Moser, C. C.; Gibney, B. R.; Dutton, P. L. Primary Steps in the Energy Conversion Reaction of the Cytochrome B_{c_1} Complex Q_o Site. *J. Bioenerg. Biomembr.* **1999**, *31*, 225–234.
- (582) Bowman, M. K.; Berry, E. A.; Roberts, A. G.; Kramer, D. M. Orientation of the G-Tensor Axes of the Rieske Subunit in the Cytochrome B_{c_1} Complex. *Biochemistry* **2004**, *43*, 430–436.
- (583) Sharp, R. E.; Palmitessa, A.; Gibney, B. R.; Moser, C. C.; Daldal, F.; Dutton, P. L. Non-Inhibiting Perturbation of the Primary Energy Conversion Site (Q_o Site) in *Rhodobacter Capsulatus* Ubihydroquinone: Cytochrome c Oxidoreductase (Cytochrome B_{c_1} Complex). *FEBS Lett.* **1998**, *431*, 423–426.
- (584) Bizzarri, A. R.; Cannistraro, S. Solvent Modulation of the Structural Heterogeneity in Fe^{III} Myoglobin Samples: A Low Temperature EPR Investigation. *Eur. Biophys. J.* **1993**, *22*, 259–267.
- (585) Sharp, R. E.; Gibney, B. R.; Palmitessa, A.; White, J. L.; Dixon, J. A.; Moser, C. C.; Daldal, F.; Dutton, P. L. Effect of Inhibitors on the Ubiquinone Binding Capacity of the Primary Energy Conversion Site in the *Rhodobacter Capsulatus* Cytochrome B_{c_1} Complex. *Biochemistry* **1999**, *38*, 14973–14980.
- (586) Bartoschek, S.; Johansson, M.; Geierstanger, B. H.; Okun, J. G.; Lancaster, C. R. D.; Humpfer, E.; Yu, L.; Yu, C.-A.; Griesinger, C.; Brandt, U. Three Molecules of Ubiquinone Bind Specifically to Mitochondrial Cytochrome B_{c_1} Complex. *J. Biol. Chem.* **2001**, *276*, 35231–35234.
- (587) Brandt, U. Bifurcated Ubihydroquinone Oxidation in the Cytochrome B_{c_1} Complex by Proton-Gated Charge Transfer. *FEBS Lett.* **1996**, *387*, 1–6.
- (588) Urban, P. F.; Klingenberg, M. On the Redox Potentials of Ubiquinone and Cytochrome b in the Respiratory Chain. *Eur. J. Biochem.* **1969**, *9*, 519–525.
- (589) Fisher, N.; Rich, P. R. A Motif for Quinone Binding Sites in Respiratory and Photosynthetic Systems. *J. Mol. Biol.* **2000**, *296*, 1153–1162.
- (590) Crofts, A. R.; Guergova-Kuras, M.; Kuras, R.; Ugulava, N.; Li, J.; Hong, S. Proton-Coupled Electron Transfer at the Q_o Site: What Type of Mechanism Can Account for the High Activation Barrier? *Biochim. Biophys. Acta, Bioenerg.* **2000**, *1459*, 456–466.
- (591) Victoria, D.; Burton, R.; Crofts, A. R. Role of the -PEWY-Glutamate in Catalysis at the Q_o -Site of the Cyt b_{c_1} Complex. *Biochim. Biophys. Acta, Bioenerg.* **2013**, *1827*, 365–386.
- (592) Lübben, M. Cytochromes of Archaeal Electron Transfer Chains. *Biochim. Biophys. Acta, Bioenerg.* **1995**, *1229*, 1–22.
- (593) Gurbiel, R. J.; Ohnishi, T.; Robertson, D. E.; Daldal, F.; Hoffman, B. M. Q-Band ENDOR Spectra of the Rieske Protein from *Rhodobacter Capsulatus* Ubiquinol-Cytochrome c Oxidoreductase Show Two Histidines Coordinated to the [2Fe-2S] Cluster. *Biochemistry* **1991**, *30*, 11579–11584.
- (594) Link, T. A.; Iwata, S. Functional Implications of the Structure of the “Rieske” Iron-Sulfur Protein of Bovine Heart Mitochondrial Cytochrome b_{c_1} Complex. *Biochim. Biophys. Acta, Bioenerg.* **1996**, *1275*, 54–60.
- (595) Link, T. A.; Hagen, W. R.; Pierik, A. J.; Assmann, C.; von Jagow, G. Determination of the Redox Properties of the Rieske [2Fe-2S] Cluster of Bovine Heart B_{c_1} Complex by Direct Electrochemistry of a Water-soluble Fragment. *Eur. J. Biochem.* **1992**, *208*, 685–691.
- (596) Hong, S.; Ugulava, N.; Guergova-Kuras, M.; Crofts, A. R. The Energy Landscape for Ubihydroquinone Oxidation at the Q_o Site of the B_{c_1} Complex in *Rhodobacter Sphaeroides*. *J. Biol. Chem.* **1999**, *274*, 33931–33944.
- (597) Crofts, A. R.; Lhee, S.; Crofts, S. B.; Cheng, J.; Rose, S. Proton Pumping in the B_{c_1} Complex: A New Gating Mechanism That Prevents Short Circuits. *Biochim. Biophys. Acta, Bioenerg.* **2006**, *1757*, 1019–1034.
- (598) Rich, P. R. The Quinone Chemistry of B_c Complexes. *Biochim. Biophys. Acta, Bioenerg.* **2004**, *1658*, 165–171.
- (599) Wenz, T.; Hellwig, P.; MacMillan, F.; Meunier, B.; Hunte, C. Probing the Role of E272 in Quinol Oxidation of Mitochondrial Complex III. *Biochemistry* **2006**, *45*, 9042–9052.
- (600) Saribas, A. S.; Ding, H.; Dutton, P. L.; Daldal, F. Tyrosine 147 of Cytochrome b Is Required for Efficient Electron Transfer at the Ubihydroquinone Oxidase Site (Q_o) of the Cytochrome b_{c_1} Complex. *Biochemistry* **1995**, *34*, 16004–16012.
- (601) Fisher, N.; Castleden, C. K.; Bourges, I.; Brasseur, G.; Dujardin, G.; Meunier, B. Human Disease-Related Mutations in Cytochrome b Studied in Yeast. *J. Biol. Chem.* **2004**, *279*, 12951–12958.
- (602) Lee, D.-W.; Selamoglu, N.; Lanciano, P.; Cooley, J. W.; Forquer, I.; Kramer, D. M.; Daldal, F. Loss of a Conserved Tyrosine Residue of Cytochrome b Induces Reactive Oxygen Species Production by Cytochrome B_{c_1} . *J. Biol. Chem.* **2011**, *286*, 18139–18148.
- (603) Ghelli, A.; Tropeano, C. V.; Calvaruso, M. A.; Marchesini, A.; Iommarini, L.; Porcelli, A. M.; Zanna, C.; De Nardo, V.; Martinuzzi, A.; Wibrand, F.; Vissing, J.; Kurelac, I.; Gasparre, G.; Selamoglu, N.; Daldal, F.; Rugolo, M. The Cytochrome b p.278Y > C Mutation Causative of a Multisystem Disorder Enhances Superoxide Production and Alters Supramolecular Interactions of Respiratory Chain Complexes. *Hum. Mol. Genet.* **2013**, *22*, 2141–2151.
- (604) Lanciano, P.; Khalfaoui-Hassani, B.; Selamoglu, N.; Ghelli, A.; Rugolo, M.; Daldal, F. Molecular Mechanisms of Superoxide Production by Complex III: A Bacterial versus Human Mitochondrial Comparative Case Study. *Biochim. Biophys. Acta, Bioenerg.* **2013**, *1827*, 1332–1339.
- (605) Hughes, L. M.; Lanteri, C. A.; O’Neil, M. T.; Johnson, J. D.; Gribble, G. W.; Trumpower, B. L. Design of Anti-Parasitic and Anti-Fungal Hydroxy-Naphthoquinones That Are Less Susceptible to Drug Resistance. *Mol. Biochem. Parasitol.* **2011**, *177*, 12–19.
- (606) Barton, V.; Fisher, N.; Biagini, G. A.; Ward, S. A.; O’Neill, P. M. Inhibiting *Plasmodium* Cytochrome B_{c_1} : A Complex Issue. *Curr. Opin. Chem. Biol.* **2010**, *14*, 440–446.
- (607) Nayak, S. K.; Mallik, S. B.; Kanaujia, S. P.; Sekar, K.; Ranganathan, K. R.; Ananthlakshmi, V.; Jeyaraman, G.; Saralaya, S. S.; Rao, K. S.; Shridhara, K.; Nagarajan, K.; Row, T. N. G. Crystal Structures and Binding Studies of Atovaquone and Its Derivatives with Cytochrome B_{c_1} : A Molecular Basis for Drug Design. *CrystEngComm* **2013**, *15*, 4871–4884.
- (608) Sarewicz, M.; Bujnowicz, L.; Osyczka, A. Generation of Semiquinone-[2Fe-2S]⁺ Spin-Coupled Center at the Q_o Site of Cytochrome B_{c_1} in Redox-Poised, Illuminated Photosynthetic Membranes from *Rhodobacter Capsulatus*. *Biochim. Biophys. Acta, Bioenerg.* **2018**, *1859*, 145–153.
- (609) Finazzi, G.; Büschlen, S.; De Vitry, C.; Rappaport, F.; Joliot, P.; Wollman, F. A. Function-Directed Mutagenesis of the Cytochrome b_{c_1} Complex in *Chlamydomonas Reinhardtii*: Involvement of the Cd Loop of Cytochrome B_6 in Quinol Binding to the Q_o Site. *Biochemistry* **1997**, *36*, 2867–2874.
- (610) De Vitry, C.; Ouyang, Y.; Finazzi, G.; Wollman, F. A.; Kallas, T. The Chloroplast Rieske Iron-Sulfur Protein. At the Crossroad of

Electron Transport and Signal Transduction. *J. Biol. Chem.* **2004**, *279*, 44621–44627.

(611) Munekage, Y.; Takeda, S.; Endo, T.; Jahns, P.; Hashimoto, T.; Shikanai, T. Cytochrome *b₆f* Mutation Specifically Affects Thermal Dissipation of Absorbed Light Energy in Arabidopsis. *Plant J.* **2001**, *28*, 351–359.

(612) Lee, T. X.; Metzger, S. U.; Cho, Y. S.; Whitmarsh, J.; Kallas, T. Modification of Inhibitor Binding Sites in the Cytochrome *b₆f* Complex by Directed Mutagenesis of Cytochrome *b₆* in *Synechococcus* Sp. PCC 7002. *Biochim. Biophys. Acta, Bioenerg.* **2001**, *1504*, 235–247.

(613) Erecinska, M.; Chance, B.; Wilson, D. F.; Dutton, P. L. Aerobic Reduction of Cytochrome *b₅₅₆* in Pigeon-Heart Mitochondria. *Proc. Natl. Acad. Sci. U. S. A.* **1972**, *69*, 50–54.

(614) Miki, T.; Miki, M.; Orii, Y. Membrane Potential-Linked Reversed Electron Transfer in the Beef Heart Cytochrome *Bc₁* Complex Reconstituted into Potassium-Loaded Phospholipid Vesicles. *J. Biol. Chem.* **1994**, *269*, 1827–1833.

(615) Elbehti, A.; Brasseur, G.; Lemesle-Meunier, D. First Evidence for Existence of an Uphill Electron Transfer through the *bc₁* and NADH-Q Oxidoreductase Complexes of the Acidophilic Obligate Chemolithotrophic Ferrous Ion-Oxidizing Bacterium *Thiobacillus Ferrooxidans*. *J. Bacteriol.* **2000**, *182*, 3602–3606.

(616) Osyczka, A.; Moser, C. C.; Daldal, F.; Dutton, P. L. Reversible Redox Energy Coupling in Electron Transfer Chains. *Nature* **2004**, *427*, 607–612.

(617) Malnoë, A.; Wollman, F.-A.; de Vitry, C.; Rappaport, F. Photosynthetic Growth despite a Broken Q-Cycle. *Nat. Commun.* **2011**, *2*, 1–6.

(618) Ransac, S.; Mazat, J.-P. How Does Antimycin Inhibit the *bc₁* Complex? A Part-Time Twin. *Biochim. Biophys. Acta, Bioenerg.* **2010**, *1797*, 1849–1857.

(619) Ransac, S.; Parisey, N.; Mazat, J.-P. The Loneliness of the Electrons in the *bc₁* Complex. *Biochim. Biophys. Acta, Bioenerg.* **2008**, *1777*, 1053–1059.

(620) Snyder, C. H.; Gutierrez-Cirlos, E. B.; Trumpower, B. L. Evidence for a Concerted Mechanism of Ubiquinol Oxidation by the Cytochrome *Bc₁* Complex. *J. Biol. Chem.* **2000**, *275*, 13535–13541.

(621) Trumpower, B. L. A Concerted, Alternating Sites Mechanism of Ubiquinol Oxidation by the Dimeric Cytochrome *Bc₁* Complex. *Biochim. Biophys. Acta, Bioenerg.* **2002**, *1555*, 166–173.

(622) Boman, P.; Eliasson, B.; Grimm, R. A.; Martin, G. S.; Strnad, J. T.; Staley, S. W. Kinetics of Bond Shift and Charge Transfer in Dialkynylphenylene- Bridged Dicyclooctatetraenes and Their Dianions. *J. Am. Chem. Soc.* **1999**, *121*, 1558–1564.

(623) Lambert, C. Concerted Two-Electron-Transfer Processes in Mixed-Valence Species with Square Topology. *ChemPhysChem* **2003**, *4*, 877–880.

(624) Yu, C.-A.; Wen, X.; Xiao, K.; Xia, D.; Yu, L. Inter- and Intra-Molecular Electron Transfer in the Cytochrome *bc₁* Complex. *Biochim. Biophys. Acta, Bioenerg.* **2002**, *1555*, 65–70.

(625) Chance, B.; Williams, G. R. The Respiratory Chain and Oxidative Phosphorylation. In *Adv. Enzymol. Relat. Subj. Biochem.*; Wiley, 1956; Vol. 17, pp 65–134.

(626) Boveris, A.; Oshino, N.; Chance, B. The Cellular Production of Hydrogen Peroxide. *Biochem. J.* **1972**, *128*, 617–630.

(627) Loschen, G.; Azzi, A.; Richter, C.; Flohé, L. Superoxide Radicals as Precursors Mitochondrial Hydrogen Peroxide. *FEBS Lett.* **1974**, *42*, 68–72.

(628) Boveris, A.; Chance, B. The Mitochondrial Generation of Hydrogen Peroxide. General Properties and Effect of Hyperbaric Oxygen. *Biochem. J.* **1973**, *134*, 707–716.

(629) Boveris, A.; Cadenas, E. Mitochondrial Production of Superoxide Anions and Its Relationship to the Antimycin Insensitive Respiration. *FEBS Lett.* **1975**, *54*, 311–314.

(630) Boveris, A.; Cadenas, E.; Stoppani, A. O. M. Role of Ubiquinone in the Mitochondrial Generation of Hydrogen Peroxide. *Biochem. J.* **1976**, *156*, 435–444.

(631) Nohl, H.; Hegner, D. Do Mitochondria Produce Oxygen Radicals *In Vivo*? *Eur. J. Biochem.* **1978**, *82*, 563–567.

(632) Ksenzenko, M.; Konstantinov, A. A.; Khomutov, G. B.; Tikhonov, A. N.; Ruuge, E. K. Effect of Electron Transfer Inhibitors on Superoxide Generation in the Cytochrome *Bc₁* Site of the Mitochondrial Respiratory Chain. *FEBS Lett.* **1983**, *155*, 19–24.

(633) Muller, F.; Crofts, A. R.; Kramer, D. M. Multiple Q-Cycle Bypass Reactions at the *Q_o* Site of the Cytochrome *Bc₁* Complex. *Biochemistry* **2002**, *41*, 7866–7874.

(634) Muller, F. L.; Roberts, A. G.; Bowman, M. K.; Kramer, D. M. Architecture of the *Q_o* Site of the Cytochrome *Bc₁* Complex Probed by Superoxide Production. *Biochemistry* **2003**, *42*, 6493–6499.

(635) Kramer, D. M.; Roberts, A. G.; Muller, F.; Cape, J. L.; Bowman, M. K. Q-Cycle Bypass Reactions at the *Q_o* Site of the Cytochrome *Bc₁* (and Related) Complexes. *Methods Enzymol.* **2004**, *382*, 21–45.

(636) Borek, A.; Sarewicz, M.; Osyczka, A. Movement of the Iron-Sulfur Head Domain of Cytochrome *Bc₁* Transiently Opens the Catalytic *Q_o* Site for Reaction with Oxygen. *Biochemistry* **2008**, *47*, 12365–12370.

(637) Dröse, S.; Brandt, U. The Mechanism of Mitochondrial Superoxide Production by the Cytochrome *bc₁* Complex. *J. Biol. Chem.* **2008**, *283*, 21649–21654.

(638) Korshunov, S. S.; Skulachev, V. P.; Starkov, A. A. High Protonic Potential Actuates a Mechanism of Production of Reactive Oxygen Species in Mitochondria. *FEBS Lett.* **1997**, *416*, 15–18.

(639) Yang, S.; Ma, H.-W.; Yu, L.; Yu, C.-A. On the Mechanism of Quinol Oxidation at the Q_P Site in the Cytochrome *Bc₁* Complex. *J. Biol. Chem.* **2008**, *283*, 28767–28776.

(640) Legros, F.; Chatzoglou, E.; Frachon, P.; Ogie De Baulny, H.; Laforêt, P.; Jardel, C.; Godinot, C.; Lombès, A. Functional Characterization of Novel Mutations in the Human Cytochrome *b* Gene. *Eur. J. Hum. Genet.* **2001**, *9*, 510–518.

(641) Dumoulin, R.; Sagnol, I.; Ferlin, T.; Bozon, D.; Stepien, G.; Mousson, B. A Novel Gly290asp Mitochondrial Cytochrome *b* Mutation Linked to a Complex III Deficiency in Progressive Exercise Intolerance. *Mol. Cell. Probes* **1996**, *10*, 389–391.

(642) Rutherford, A. W.; Osyczka, A.; Rappaport, F. Back-Reactions, Short-Circuits, Leaks and Other Energy Wasteful Reactions in Biological Electron Transfer: Redox Tuning to Survive Life in O₂. *FEBS Lett.* **2012**, *586*, 603–616.

(643) Bleier, L.; Dröse, S. Superoxide Generation by Complex III: From Mechanistic Rationales to Functional Consequences. *Biochim. Biophys. Acta, Bioenerg.* **2013**, *1827*, 1320–1331.

(644) Zhou, F.; Yin, Y.; Su, T.; Yu, L.; Yu, C.-A. Oxygen Dependent Electron Transfer in the Cytochrome *Bc₁* Complex. *Biochim. Biophys. Acta, Bioenerg.* **2012**, *1817*, 2103–2109.

(645) Husen, P.; Solov'yov, I. A. Spontaneous Binding of Molecular Oxygen at the *Q_o*-Site of the *Bc₁* Complex Could Stimulate Superoxide Formation. *J. Am. Chem. Soc.* **2016**, *138*, 12150–12158.

(646) Nohl, H.; Jordan, W. The Mitochondrial Site of Superoxide Formation. *Biochem. Biophys. Res. Commun.* **1986**, *138*, 533–539.

(647) Raha, S.; McEachern, G. E.; Myint, A. T.; Robinson, B. H. Superoxides from Mitochondrial Complex III: The Role of Manganese Superoxide Dismutase. *Free Radical Biol. Med.* **2000**, *29*, 170–180.

(648) Kolling, D. R. J.; Samoilova, R. I.; Holland, J. T.; Berry, E. A.; Dikanov, S. A.; Crofts, A. R. Exploration of Ligands to the *Q_o* Site Semiquinone in the *Bc₁* Complex Using High-Resolution EPR. *J. Biol. Chem.* **2003**, *278*, 39747–39754.

(649) Dikanov, S. A.; Holland, J. T.; Endeward, B.; Kolling, D. R. J.; Samoilova, R. I.; Prisner, T. F.; Crofts, A. R. Hydrogen Bonds between Nitrogen Donors and the Semiquinone in the *Q_o*-Site of the *Bc₁* Complex. *J. Biol. Chem.* **2007**, *282*, 25831–25841.

(650) Sun, J.; Trumpower, B. L. Superoxide Anion Generation by the Cytochrome *Bc₁* Complex. *Arch. Biochem. Biophys.* **2003**, *419*, 198–206.

(651) Pagacz, J.; Broniec, A.; Wolska, M.; Osyczka, A.; Borek, A. ROS signaling capacity of cytochrome *bc₁*: Opposing effects of adaptive and pathogenic mitochondrial mutations. *Free Radical Biol. Med.* **2021**, *163*, 243–254.

(652) Murphy, M. P. How Mitochondria Produce Reactive Oxygen Species. *Biochem. J.* **2009**, *417*, 1–13.

- (653) Guzy, R. D.; Schumacker, P. T. Oxygen Sensing by Mitochondria at Complex III: The Paradox of Increased Reactive Oxygen Species during Hypoxia. *Exp. Physiol.* **2006**, *91*, 807–819.
- (654) Solaini, G.; Baracca, A.; Lenaz, G.; Sgarbi, G. Hypoxia and Mitochondrial Oxidative Metabolism. *Biochim. Biophys. Acta, Bioenerg.* **2010**, *1797*, 1171–1177.
- (655) Berry, B. J.; Trewin, A. J.; Amitrano, A. M.; Kim, M.; Wojtovich, A. P. Use the Protonmotive Force: Mitochondrial Uncoupling and Reactive Oxygen Species. *J. Mol. Biol.* **2018**, *430*, 3873–3891.
- (656) Saborido, A.; Soblechero, L.; Megias, A. Isolated Respiring Heart Mitochondria Release Oxygen Species in States 4 and 3. *Free Radical Res.* **2005**, *39*, 921–931.
- (657) West, I. C.; Mitchell, P.; Rich, P. R. Electron Conduction between *b* Cytochromes of the Mitochondrial Respiratory Chain in the Presence of Antimycin plus Myxothiazol. *Biochim. Biophys. Acta, Bioenerg.* **1988**, *933*, 35–41.
- (658) Zorov, D. B.; Juhaszova, M.; Sollott, S. J. Mitochondrial Reactive Oxygen Species (ROS) and ROS-Induced ROS Release. *Physiol. Rev.* **2014**, *94*, 909–950.
- (659) Muller, F. L.; Liu, Y.; Van Remmen, H. Complex III Releases Superoxide to Both Sides of the Inner Mitochondrial Membrane. *J. Biol. Chem.* **2004**, *279*, 49064–49073.
- (660) Boveris, A.; Cadenas, E. Mitochondrial Production of Hydrogen Peroxide Regulation by Nitric Oxide and the Role of Ubisemiquinone. *IUBMB Life* **2001**, *50*, 245–250.
- (661) Dröse, S.; Hanley, P. J.; Brandt, U. Ambivalent Effects of Diazoxide on Mitochondrial ROS Production at Respiratory Chain Complexes I and III. *Biochim. Biophys. Acta, Gen. Subj.* **2009**, *1790*, 558–565.
- (662) Forman, H. J.; Azzi, A. On the Virtual Existence of Superoxide Anions in Mitochondria: Thoughts Regarding Its Role in Pathophysiology. *FASEB J.* **1997**, *11*, 374–375.
- (663) Hollis, V. S.; Palacios-Callender, M.; Springett, R. J.; Delpy, D. T.; Moncada, S. Monitoring Cytochrome Redox Changes in the Mitochondria of Intact Cells Using Multi-Wavelength Visible Light Spectroscopy. *Biochim. Biophys. Acta, Bioenerg.* **2003**, *1607*, 191–202.
- (664) Benard, G.; Faustin, B.; Galinier, A.; Rocher, C.; Bellance, N.; Smolkova, K.; Casteilla, L.; Rossignol, R.; Letellier, T. Functional Dynamic Compartmentalization of Respiratory Chain Intermediate Substrates: Implications for the Control of Energy Production and Mitochondrial Diseases. *Int. J. Biochem. Cell Biol.* **2008**, *40*, 1543–1554.
- (665) Han, D.; Antunes, F.; Canali, R.; Rettori, D.; Cadenas, E. Voltage-Dependent Anion Channels Control the Release of the Superoxide Anion from Mitochondria to Cytosol. *J. Biol. Chem.* **2003**, *278*, 5557–5563.
- (666) Goldsteins, G.; Keksa-Goldsteine, V.; Ahtoniemi, T.; Jaronen, M.; Arens, E.; Åkerman, K.; Chan, P. H.; Koistinaho, J. Deleterious Role of Superoxide Dismutase in the Mitochondrial Intermembrane Space. *J. Biol. Chem.* **2008**, *283*, 8446–8452.
- (667) Butler, J.; Koppenol, W. H.; Margoliash, E. Kinetics and Mechanism of the Reduction of Ferricytochrome *c* by the Superoxide Anion. *J. Biol. Chem.* **1982**, *257*, 10747–10750.
- (668) Finkelstein, E.; Rosen, G. M.; Rauckman, E. J. Spin Trapping. Kinetics of the Reaction of Superoxide and Hydroxyl Radicals with Nitrones. *J. Am. Chem. Soc.* **1980**, *102*, 4994–4999.
- (669) de Vries, S.; Albracht, S. P.; Berden, J. A.; Slater, E. C. A New Species of Bound Ubisemiquinone Anion in QH₂: Cytochrome *c* Oxidoreductase. *J. Biol. Chem.* **1981**, *256*, 11996–11998.
- (670) Jünemann, S.; Heathcote, P.; Rich, P. R. On the Mechanism of Quinol Oxidation in the Bc₁ Complex. *J. Biol. Chem.* **1998**, *273*, 21603–21607.
- (671) Fournel, A.; Gambarelli, S.; Guigliarelli, B.; More, C.; Asso, M.; Chouteau, G.; Hille, R.; Bertrand, P. Magnetic Interactions between a [4Fe–4S]¹⁺ Cluster and a Flavin Mononucleotide Radical in the Enzyme Trimethylamine Dehydrogenase: A High-Field Electron Paramagnetic Resonance Study. *J. Chem. Phys.* **1998**, *109*, 10905–10913.
- (672) Calvo, R. EPR Measurements of Weak Exchange Interactions Coupling Unpaired Spins in Model Compounds. *Appl. Magn. Reson.* **2007**, *31*, 271–299.
- (673) Bujnowicz, L.; Sarewicz, M.; Borek, A.; Kuleta, P.; Osyczka, A. Suppression of Superoxide Production by a Spin-Spin Coupling between Semiquinone and the Rieske Cluster in Cytochrome Bc₁. *FEBS Lett.* **2019**, *593*, 3–12.
- (674) Fisher, N.; Bowman, M. K.; Kramer, D. M. Electron Transfer Reactions at the Qo Site of the Cytochrome bc₁ Complex: The Good, the Bad, and the Ugly. *Cytochrome Complexes Evolution, Structure, Energy Transduction, and Signaling*; Springer, 2016; 419–434.
- (675) Lange, C.; Nett, J. H.; Trumpower, B. L.; Hunte, C. Specific Roles of Protein-Phospholipid Interactions in the Yeast Cytochrome bc₁ Complex Structure. *EMBO J.* **2001**, *20*, 6591–6600.
- (676) Hunte, C.; Palsdottir, H.; Trumpower, B. L. Protonmotive Pathways and Mechanisms in the Cytochrome Bc₁ Complex. *FEBS Lett.* **2003**, *545*, 39–46.
- (677) Postila, P. A.; Kaszuba, K.; Kuleta, P.; Vattulainen, I.; Sarewicz, M.; Osyczka, A.; Róg, T. Atomistic Determinants of Co-Enzyme Q Reduction at the Qi-Site of the Cytochrome bc₁ Complex. *Sci. Rep.* **2016**, *6*, 33607.
- (678) Gray, K. A.; Dutton, P. L.; Daldal, F. Requirement of Histidine 217 for Ubiquinone Reductase Activity (Q_i Site) in the Cytochrome Bc₁ Complex. *Biochemistry* **1994**, *33*, 723–733.
- (679) Kuleta, P.; Sarewicz, M.; Postila, P. A.; Róg, T.; Osyczka, A. Identifying Involvement of Lys251/Asp252 Pair in Electron Transfer and Associated Proton Transfer at the Quinone Reduction Site of *Rhodobacter Capsulatus* Cytochrome Bc₁. *Biochim. Biophys. Acta, Bioenerg.* **2016**, *1857*, 1661–1668.
- (680) Hanson, D. K.; Tiede, D. M.; Nance, S. L.; Chang, C. H.; Schiffer, M. Site-Specific and Compensatory Mutations Imply Unexpected Pathways for Proton Delivery to the QB Binding Site of the Photosynthetic Reaction Center. *Proc. Natl. Acad. Sci. U. S. A.* **1993**, *90*, 8929–8933.
- (681) Ohnishi, T.; Trumpower, B. L. Differential Effects of Antimycin on Ubisemiquinone Bound in Different Environments in Isolated Succinate-Cytochrome *c* Reductase Complex. *J. Biol. Chem.* **1980**, *255*, 3278–3284.
- (682) Hong, S.; de Almeida, W. B.; Taguchi, A. T.; Samoilova, R. I.; Gennis, R. B.; O'Malley, P. J.; Dikanov, S. A.; Crofts, A. R. The Semiquinone at the Qi Site of the bc₁ Complex Explored Using HYSCORE Spectroscopy and Specific Isotopic Labeling of Ubiquinone in *Rhodobacter Sphaeroides* via 13C Methionine and Construction of a Methionine Auxotroph. *Biochemistry* **2014**, *53*, 6022–6631.
- (683) de la Rosa, F. F.; Palmer, G. Reductive Titration of CoQ-Depleted Complex III from Baker's Yeast: Evidence for an Exchange-Coupled Complex between QH₂ and Low-Spin Ferricytochrome B. *FEBS Lett.* **1983**, *163*, 140–143.
- (684) Salerno, J. C.; Osgood, M.; Liu, Y.; Taylor, H.; Scholes, C. P. Electron Nuclear Double Resonance (ENDOR) of the Q_i⁻ Ubisemiquinone Radical in the Mitochondrial Electron Transport Chain. *Biochemistry* **1990**, *29*, 6987–6993.
- (685) Dikanov, S. A.; Samoilova, R. I.; Kolling, D. R. J.; Holland, J. T.; Crofts, A. R. Hydrogen Bonds Involved in Binding the Qi-Site Semiquinone in the bc₁ Complex, Identified through Deuterium Exchange Using Pulsed EPR. *J. Biol. Chem.* **2004**, *279*, 15814–15823.
- (686) MacMillan, F.; Lange, C.; Bawn, M.; Hunte, C. Resolving the EPR Spectra in the Cytochrome Bc₁ Complex from *Saccharomyces Cerevisiae*. *Appl. Magn. Reson.* **2010**, *37*, 305–316.
- (687) de Vries, S.; Albracht, S. P. J.; Berden, J. A.; Marres, C. A. M.; Slater, E. C. The Effect of PH, Ubiquinone Depletion and Myxothiazol on the Reduction Kinetics of the Prosthetic Groups of Ubiquinol: Cytochrome *c* Oxidoreductase. *Biochim. Biophys. Acta, Bioenerg.* **1983**, *723*, 91–103.
- (688) Leigh, J. S. ESR Rigid-Lattice Line Shape in a System of Two Interacting Spins. *J. Chem. Phys.* **1970**, *52*, 2608–2612.
- (689) Hagen, W. R. *Biomolecular EPR Spectroscopy*; CRC Press Taylor & Francis Group: Boca Raton, 2009.

- (690) Lin, M. T.; Baldansuren, A.; Hart, R.; Samoilova, R. I.; Narasimhulu, K. V.; Yap, L. L.; Choi, S. K.; O'Malley, P. J.; Gennis, R. B.; Dikanov, S. A. Interactions of Intermediate Semiquinone with Surrounding Protein Residues at the QH Site of Wild-Type and D75H Mutant Cytochrome B₆ from *Escherichia Coli*. *Biochemistry* **2012**, *51*, 3827–3838.
- (691) Martin, E.; Samoilova, R. I.; Narasimhulu, K. V.; Lin, T. J.; O'Malley, P. J.; Wraight, C. A.; Dikanov, S. A. Hydrogen Bonding and Spin Density Distribution in the QB Semiquinone of Bacterial Reaction Centers and Comparison with the QA Site. *J. Am. Chem. Soc.* **2011**, *133*, 5525–5537.
- (692) Wang, X.; Yu, L.; Inakollu, V. S. S.; Pan, X.; Ma, J.; Yu, H. Molecular Quantum Dot Cellular Automata Based on Diboryl Monoradical Anions. *J. Phys. Chem. C* **2018**, *122*, 2454–2460.
- (693) de Lacroix de Lavalette, A.; Barbagallo, R. P.; Zito, F. Why Is It so Difficult to Construct Qi Site Mutants in *Chlamydomonas Reinhardtii*? *C. R. Biol.* **2008**, *331*, 510–517.
- (694) Ondarroat, M.; Zito, F.; Finazzi, G.; Joliot, P.; Wollman, F. A.; Rich, P. R. Characterization and Electron Transfer Kinetics of Wild Type and Mutant Strains of *Chlamydomonas Reinhardtii*. *Biochem. Soc. Trans.* **1996**, *24*, 398.
- (695) Kuras, R.; De Vitry, C.; Choquet, Y.; Girard-Bascou, J.; Culler, D.; Büschlen, S.; Merchant, S.; Wollman, F. A. Molecular Genetic Identification of a Pathway for Heme Binding to Cytochrome B₆. *J. Biol. Chem.* **1997**, *272*, 32427–32435.
- (696) Nelson, M. E.; Finazzi, G.; Qing, J. W.; Middleton-Zarka, K. A.; Whitmarsh, J.; Kallas, T. Cytochrome *b₆* Arginine 214 of *Synechococcus Sp. PCC 7002*, a Key Residue for Quinone-Reductase Site Function and Turnover of the Cytochrome *bf* Complex. *J. Biol. Chem.* **2005**, *280*, 10395–10402.
- (697) de Lacroix de Lavalette, A.; Finazzi, G.; Zito, F. *b₆f*-Associated Chlorophyll: Structural and Dynamic Contribution to the Different Cytochrome Functions. *Biochemistry* **2008**, *47*, 5259–5265.
- (698) Dumas, L.; Zito, F.; Blangy, S.; Auroy, P.; Johnson, X.; Peltier, G.; Alric, J. A Stromal Region of Cytochrome *b₆f* Subunit IV Is Involved in the Activation of the Stt7 Kinase in *Chlamydomonas*. *Proc. Natl. Acad. Sci. U. S. A.* **2017**, *114*, 12063–12068.
- (699) Moser, C. C.; Farid, T. A.; Chobot, S. E.; Dutton, P. L. Electron Tunneling Chains of Mitochondria. *Biochim. Biophys. Acta, Bioenerg.* **2006**, *1757*, 1096–1109.
- (700) Moser, C. C.; Chobot, S. E.; Page, C. C.; Dutton, P. L. Distance Metrics for Heme Protein Electron Tunneling. *Biochim. Biophys. Acta, Bioenerg.* **2008**, *1777*, 1032–1037.
- (701) Sarewicz, M.; Ekiert, R.; Osyczka, A. Inter-Monomer Electron Transfer in Cytochrome *Bc* Complexes. In *Cytochrome complexes: Evolution, structures, energy transduction, and signaling*; Cramer, W. A., Kallas, T., Eds.; Springer: Dordrecht, 2016; pp 281–294.
- (702) Gopta, O. A.; Feniouk, B. A.; Junge, W.; Mulikidjanian, A. Y. The Cytochrome *Bc₁* Complex of *Rhodobacter Capsulatus*: Ubiquinol Oxidation in a Dimeric Q-Cycle? *FEBS Lett.* **1998**, *431*, 291–296.
- (703) Covian, R.; Trumpower, B. L. Rapid Electron Transfer between Monomers When the Cytochrome *bc₁* Complex Dimer Is Reduced through Center N. *J. Biol. Chem.* **2005**, *280*, 22732–22740.
- (704) Marcus, R. A.; Sutin, N. Electron Transfers in Chemistry and Biology. *Biochim. Biophys. Acta, Rev. Bioenerg.* **1985**, *811*, 265–322.
- (705) Lanciano, P.; Khalfaoui-Hassani, B.; Selamoglu, N.; Daldal, F. Intermonomer Electron Transfer between the *b* Hemes of Heterodimeric Cytochrome *Bc₁*. *Biochemistry* **2013**, *52*, 7196–7206.
- (706) Czaplá, M.; Cieluch, E.; Borek, A.; Sarewicz, M.; Osyczka, A. Catalytically-Relevant Electron Transfer between Two Hemes *b_L* in the Hybrid Cytochrome *Bc₁*-like Complex Containing a Fusion of *Rhodobacter Sphaeroides* and *Capsulatus* Cytochromes B. *Biochim. Biophys. Acta, Bioenerg.* **2013**, *1827*, 751–760.
- (707) Ekiert, R.; Czaplá, M.; Sarewicz, M.; Osyczka, A. Hybrid Fusions Show That Inter-Monomer Electron Transfer Robustly Supports Cytochrome *Bc₁* Function in Vivo. *Biochem. Biophys. Res. Commun.* **2014**, *451*, 270–275.
- (708) Czaplá, M.; Borek, A.; Sarewicz, M.; Osyczka, A. Fusing Two Cytochromes *b* of *Rhodobacter Capsulatus* Cytochrome *Bc₁* Using Various Linkers Defines a Set of Protein Templates for Asymmetric Mutagenesis. *Protein Eng., Des. Sel.* **2012**, *25*, 15–25.
- (709) Czaplá, M.; Sarewicz, M.; Osyczka, A. Fusing Proteins as an Approach to Study Bioenergetic Enzymes and Processes. In *Biochimica et Biophysica Acta - Bioenergetics*; Elsevier, 2012; Vol. 1817, pp 1847–1851.
- (710) Mulikidjanian, A. Y. Proton Translocation by the Cytochrome *bc₁* Complexes of Phototrophic Bacteria: Introducing the Activated Q-Cycle. *Photochem. Photobiol. Sci.* **2007**, *6*, 19–34.
- (711) Hong, S.; Victoria, D.; Crofts, A. R. Inter-Monomer Electron Transfer Is Too Slow to Compete with Monomeric Turnover in *Bc₁* Complex. *Biochim. Biophys. Acta, Bioenerg.* **2012**, *1817*, 1053–1062.
- (712) Lanciano, P.; Lee, D.-W.; Yang, H.; Darrouzet, E.; Daldal, F. Intermonomer Electron Transfer between the Low-Potential *b* Hemes of Cytochrome *Bc₁*. *Biochemistry* **2011**, *50*, 1651–1663.
- (713) Khalfaoui-Hassani, B.; Lanciano, P.; Daldal, F. A Robust Genetic System for Producing Heterodimeric Native and Mutant Cytochrome *Bc₁*. *Biochemistry* **2013**, *52*, 7184–7195.
- (714) Kramer, D. M.; Avenson, T. J.; Edwards, G. E. Dynamic Flexibility in the Light Reactions of Photosynthesis Governed by Both Electron and Proton Transfer Reactions. *Trends Plant Sci.* **2004**, *9*, 349–357.
- (715) Shikanai, T. Cyclic Electron Transport Around Photosystem I: Genetic Approaches. *Annu. Rev. Plant Biol.* **2007**, *58*, 199–217.
- (716) Johnson, G. N. Physiology of PSI Cyclic Electron Transport in Higher Plants. *Biochim. Biophys. Acta, Bioenerg.* **2011**, *1807*, 384–389.
- (717) Alric, J.; Johnson, X. Alternative Electron Transport Pathways in Photosynthesis: A Confluence of Regulation. *Curr. Opin. Plant Biol.* **2017**, *37*, 78–86.
- (718) Rumeau, D.; Peltier, G.; Cournac, L. Chlororespiration and Cyclic Electron Flow around PSI during Photosynthesis and Plant Stress Response. *Plant, Cell Environ.* **2007**, *30*, 1041–1051.
- (719) Lehtimäki, N.; Lintala, M.; Allahverdiyeva, Y.; Aro, E. M.; Mulo, P. Drought Stress-Induced Upregulation of Components Involved in Ferredoxin-Dependent Cyclic Electron Transfer. *J. Plant Physiol.* **2010**, *167*, 1018–1022.
- (720) Allorete, G.; Osorio, S.; Ly Vu, J.; Falconet, D.; Jouhet, J.; Kuntz, M.; Fernie, A. R.; Lerbs-Mache, S.; Macherel, D.; Courtois, F.; Finazzi, G. Adjustments of Embryonic Photosynthetic Activity Modulate Seed Fitness in Arabidopsis Thaliana. *New Phytol.* **2015**, *205*, 707–719.
- (721) Tagawa, K.; Tsujimoto, H. Y.; Arnon, D. I. Role of Chloroplast Ferredoxin in the Energy Conversion Process of Photosynthesis. *Proc. Natl. Acad. Sci. U. S. A.* **1963**, *49*, 567–572.
- (722) Munekage, Y.; Hashimoto, M.; Miyake, C.; Tomizawa, K. I.; Endo, T.; Tasaka, M.; Shikanai, T. Cyclic Electron Flow around Photosystem I Is Essential for Photosynthesis. *Nature* **2004**, *429*, 579–582.
- (723) Carrillo, N.; Vallejos, R. H. The Light-Dependent Modulation of Photosynthetic Electron Transport. *Trends Biochem. Sci.* **1983**, *8*, 52–56.
- (724) Arnon, D. I. Divergent Pathways of Photosynthetic Electron Transfer: The Autonomous Oxygenic and Anoxygenic Photosystems. *Photosynth. Res.* **1995**, *46*, 47–71.
- (725) Joliot, P.; Joliot, A. Cyclic Electron Flow in C3 Plants. *Biochim. Biophys. Acta, Bioenerg.* **2006**, *1757*, 362–368.
- (726) Dumas, L.; Chazaux, M.; Peltier, G.; Johnson, X.; Alric, J. Cytochrome *b₆f* Function and Localization, Phosphorylation State of Thylakoid Membrane Proteins and Consequences on Cyclic Electron Flow. *Photosynth. Res.* **2016**, *129*, 307–320.
- (727) Dekker, J. P.; Boekema, E. J. Supramolecular Organization of Thylakoid Membrane Proteins in Green Plants. *Biochim. Biophys. Acta, Bioenerg.* **2005**, *1706*, 12–39.
- (728) Tremmel, I. G.; Kirchhoff, H.; Weis, E.; Farquhar, G. D. Dependence of Plastoquinol Diffusion on the Shape, Size, and Density of Integral Thylakoid Proteins. *Biochim. Biophys. Acta, Bioenerg.* **2003**, *1607*, 97–109.
- (729) Johnson, M. P.; Vasilev, C.; Olsen, J. D.; Hunter, C. N. Nanodomains of Cytochrome *b₆f* and Photosystem II Complexes in

Spinach Grana Thylakoid Membranes. *Plant Cell* **2014**, *26*, 3051–3061.

(730) Alric, J.; Lavergne, J.; Rappaport, F. Redox and ATP Control of Photosynthetic Cyclic Electron Flow in *Chlamydomonas Reinhardtii* (I) Aerobic Conditions. *Biochim. Biophys. Acta, Bioenerg.* **2010**, *1797*, 44–51.

(731) Wikström, M.; Krab, K. The Semiquinone Cycle. A Hypothesis of Electron Transfer and Proton Translocation in Cytochrome Bc-Type Complexes. *J. Bioenerg. Biomembr.* **1986**, *18*, 181–193.

(732) Finazzi, G.; Furia, A.; Barbagallo, R. P.; Forti, G. State Transitions, Cyclic and Linear Electron Transport and Photophosphorylation in *Chlamydomonas Reinhardtii*. *Biochim. Biophys. Acta, Bioenerg.* **1999**, *1413*, 117–129.

(733) Alric, J. Redox and ATP Control of Photosynthetic Cyclic Electron Flow in *Chlamydomonas Reinhardtii*: (II) Involvement of the PGR5-PGRL1 Pathway under Anaerobic Conditions. *Biochim. Biophys. Acta, Bioenerg.* **2014**, *1837*, 825–834.

(734) Takahashi, H.; Clowez, S.; Wollman, F. A.; Vallon, O.; Rappaport, F. Cyclic Electron Flow Is Redox-Controlled but Independent of State Transition. *Nat. Commun.* **2013**, *4*, 1954.

(735) Laisk, A. Mathematical Modelling of Free-Pool and Channelled Electron Transport in Photosynthesis: Evidence for a Functional Supercomplex around Photosystem I. *Proc. R. Soc. London, Ser. B* **1993**, *251*, 243–251.

(736) Joliot, P.; Joliot, A. Cyclic Electron Transfer in Plant Leaf. *Proc. Natl. Acad. Sci. U. S. A.* **2002**, *99*, 10209–10214.

(737) Terashima, M.; Petroustos, D.; Hüdig, M.; Tolstygina, I.; Trompelt, K.; Gäbelein, P.; Fufezan, C.; Kudla, J.; Weinl, S.; Finazzi, G.; Hippler, M. Calcium-Dependent Regulation of Cyclic Photosynthetic Electron Transfer by a CAS, ANRI, and PGRL1 Complex. *Proc. Natl. Acad. Sci. U. S. A.* **2012**, *109*, 17717–17722.

(738) Steinbeck, J.; Ross, I. L.; Rothnagel, R.; Gäbelein, P.; Schulze, S.; Giles, N.; Ali, R.; Drysdale, R.; Sieracki, E.; Gambin, Y.; Stahlberg, H.; Takahashi, Y.; Hippler, M.; Hankamer, B. Structure of a PSI-LHCI-Cyt *b₆f* Supercomplex in *Chlamydomonas Reinhardtii* Promoting Cyclic Electron Flow under Anaerobic Conditions. *Proc. Natl. Acad. Sci. U. S. A.* **2018**, *115*, 10517–10522.

(739) Yadav, K. N. S.; Semchonok, D. A.; Nosek, L.; Kouřil, R.; Fucile, G.; Boekema, E. J.; Eichacker, L. A. Supercomplexes of Plant Photosystem I with Cytochrome *b₆f*, Light-Harvesting Complex II and NDH. *Biochim. Biophys. Acta, Bioenerg.* **2017**, *1858*, 12–20.

(740) Peng, L.; Shimizu, H.; Shikanai, T. The Chloroplast NAD(P)H Dehydrogenase Complex Interacts with Photosystem I in Arabidopsis. *J. Biol. Chem.* **2008**, *283*, 34873–34879.

(741) Otani, T.; Yamamoto, H.; Shikanai, T. Stromal Loop of Lhca6 Is Responsible for the Linker Function Required for the NDH-PSI Supercomplex Formation. *Plant Cell Physiol.* **2017**, *58*, 851–861.

(742) Allen, J. F. Protein-Phosphorylation in Regulation of Photosynthesis. *Biochim. Biophys. Acta, Bioenerg.* **1992**, *1098*, 275–335.

(743) Murata, N.; Sugahara, K. Control of Excitation Transfer in Photosynthesis. III. Light-Induced Decrease of Chlorophyll a Fluorescence Related to Photophosphorylation System in Spinach Chloroplasts. *Biochim. Biophys. Acta, Bioenerg.* **1969**, *189*, 182–192.

(744) Bonaventura, C.; Myers, J. Fluorescence and Oxygen Evolution from *Chlorella Pyrenoidosa*. *Biochim. Biophys. Acta, Bioenerg.* **1969**, *189*, 366–383.

(745) Wollman, F. A. State Transitions Reveal the Dynamics and Flexibility of the Photosynthetic Apparatus. *EMBO J.* **2001**, *20*, 3623–3630.

(746) Depège, N.; Bellafiore, S.; Rochaix, J. D. Role of Chloroplast Protein Kinase Stt7 in LHCII Phosphorylation and State Transition in *Chlamydomonas*. *Science (Washington, DC, U. S.)* **2003**, *299*, 1572–1575.

(747) Bellafiore, S.; Barneche, F.; Peltier, G.; Rochaix, J.-D. State Transitions and Light Adaptation Require Chloroplast Thylakoid Protein Kinase STN7. *Nature* **2005**, *433*, 892–895.

(748) Pribil, M.; Pesaresi, P.; Hertle, A.; Barbato, R.; Leister, D. Role of Plastid Protein Phosphatase TAP38 in LHCII Dephosphorylation and Thylakoid Electron Flow. *PLoS Biol.* **2010**, *8*, No. e1000288.

(749) Shapiguzov, A.; Ingelsson, B.; Samol, I.; Andres, C.; Kessler, F.; Rochaix, J. D.; Vener, A. V.; Goldschmidt-Clermont, M. The PPH1 Phosphatase Is Specifically Involved in LHCII Dephosphorylation and State Transitions in Arabidopsis. *Proc. Natl. Acad. Sci. U. S. A.* **2010**, *107*, 4782–4787.

(750) Wollman, F. A.; Lemaire, C. Studies on Kinase-Controlled State Transitions in Photosystem II and *b₆f* Mutants from *Chlamydomonas Reinhardtii* Which Lack Quinone-Binding Proteins. *Biochim. Biophys. Acta, Bioenerg.* **1988**, *933*, 85–94.

(751) Vener, A. V.; van Kan, P. J. M. M.; Rich, P. R.; Ohad, I.; Andersson, B. Plastoquinol at the Quinol Oxidation Site of Reduced Cytochrome Bf Mediates Signal Transduction between Light and Protein Phosphorylation: Thylakoid Protein Kinase Deactivation by a Single-Turnover Flash. *Proc. Natl. Acad. Sci. U. S. A.* **1997**, *94*, 1585–1590.

(752) Finazzi, G. The Central Role of the Green Alga *Chlamydomonas Reinhardtii* in Revealing the Mechanism of State Transitions. *J. Exp. Bot.* **2004**, *56*, 383–388.

(753) Shapiguzov, A.; Chai, X.; Fucile, G.; Longoni, P.; Zhang, L.; Rochaix, J. D. Activation of the Stt7/STN7 Kinase through Dynamic Interactions with the Cytochrome B6 f Complex. *Plant Physiol.* **2016**, *171*, 82–92.

(754) Finazzi, G.; Minagawa, J.; Johnson, G. N. The Cytochrome *b₆f* Complex: A Regulatory Hub Controlling Electron Flow and the Dynamics of Photosynthesis? In *Cytochrome Complexes: Evolution, Structures, Energy Transduction, and Signaling*; Springer, 2016; pp 437–452.

(755) Singh, S. K.; Hasan, S. S.; Zakharov, S. D.; Naurin, S.; Cohn, W.; Ma, J.; Whitelegge, J. P.; Cramer, W. A. Trans-Membrane Signaling in Photosynthetic State Transitions: Redox- and Structure-Dependent Interaction *In Vitro* between Stt7 Kinase and the Cytochrome *b₆f* Complex. *J. Biol. Chem.* **2016**, *291*, 21740–21750.

(756) Hamel, P.; Olive, J.; Pierre, Y.; Wollman, F. A.; De Vitry, C. A New Subunit of Cytochrome *b₆f* Complex Undergoes Reversible Phosphorylation upon State Transition. *J. Biol. Chem.* **2000**, *275*, 17072–17079.

(757) Finazzi, G.; Zito, F.; Barbagallo, R. P.; Wollman, F. A. Contrasted Effects of Inhibitors of Cytochrome *b₆f* Complex on State Transitions in *Chlamydomonas Reinhardtii*: The Role of Q_o Site Occupancy in LHCII Kinase Activation. *J. Biol. Chem.* **2001**, *276*, 9770–9774.

(758) Zito, F.; Vinh, J.; Popot, J. L.; Finazzi, G. Chimeric Fusions of Subunit IV and PetL in the *b₆f* Complex of *Chlamydomonas Reinhardtii*: Structural Implications and Consequences on State Transitions. *J. Biol. Chem.* **2002**, *277*, 12446–12455.

(759) Schuster, G.; Dewit, M.; Staehelin, L. A.; Ohad, I. Transient Inactivation of the Thylakoid Photosystem II Light-Harvesting Protein Kinase System and Concomitant Changes in Intramembrane Particle Size during Photoinhibition of *Chlamydomonas Reinhardtii*. *J. Cell Biol.* **1986**, *103*, 71–80.

(760) Rintamäki, E.; Martinsuo, P.; Pursiheimo, S.; Aro, E. M. Cooperative Regulation of Light-Harvesting Complex II Phosphorylation via the Plastoquinol and Ferredoxin-Thioredoxin System in Chloroplasts. *Proc. Natl. Acad. Sci. U. S. A.* **2000**, *97*, 11644–11649.

(761) Hou, C. X.; Pursiheimo, S.; Rintamäki, E.; Aro, E. M. Environmental and Metabolic Control of LHCII Protein Phosphorylation: Revealing the Mechanisms for Dual Regulation of the LHCII Kinase. *Plant, Cell Environ.* **2002**, *25*, 1515–1525.

(762) Wunder, T.; Xu, W.; Liu, Q.; Wanner, G.; Leister, D.; Pribil, M. The Major Thylakoid Protein Kinases STN7 and STN8 Revisited: Effects of Altered STN8 Levels and Regulatory Specificities of the STN Kinases. *Front. Plant Sci.* **2013**, *4*, 417.

(763) Schütz, M.; Brugna, M.; Lebrun, E.; Baymann, F.; Huber, R.; Stetter, K. O.; Hauska, G.; Toci, R.; Lemesle-Meunier, D.; Tron, P.; Schmidt, C.; Nitschke, W. Early Evolution of Cytochrome Bc Complexes. *J. Mol. Biol.* **2000**, *300*, 663–675.